

✓
STUDIES ON FLUX AND RETENTION
CHARACTERISTICS DURING
ULTRAFILTRATION: DESIGN AND APPLIED
ASPECTS

A Thesis Submitted
in Partial Fulfillment of the Requirements
for the Degree of
Doctor of Philosophy

by
SIRSHENDU DE

to the
DEPARTMENT OF CHEMICAL ENGINEERING
INDIAN INSTITUTE OF TECHNOLOGY, KANPUR
October, 1996

10 JUL 1997 / Che Engg

CENTRAL LIBRARY
I. I. T., KANPUR

No. A. 123605

CHE-1996-D-DE-FLUX

03/10/96

CERTIFICATE

It is certified that the work contained in this thesis entitled *Studies on Flux and Retention Characteristics During Ultrafiltration: Design and Applied Aspects* by Sirshendu De has been carried out under my supervision and that this work has not been submitted elsewhere for a degree.

P. K. Bhattacharya

Dr. P. K. Bhattacharya
Professor
Department of Chemical Engineering
Indian Institute of Technology, Kanpur
Kanpur-208016 (INDIA)

3rd October, 1996

Synopsis

The major phenomenon which still restricts the pressure driven membrane processes from replacing the conventional separation processes on an industrial scale is concentration polarization (build-up of a concentration boundary layer on the membrane surface). This leads to the decline of permeate flux and may consequently also foul the membrane. The various possible consequences of concentration polarization, namely, osmotic pressure build-up near the membrane-solution interface, formation of a gel type layer near the membrane surface, changes in physical properties of the solute and solution in the polarized layer, irreversible fouling of the membrane due to solute adsorption, pore clogging, etc. can act individually or in concert to cause a decline in permeate flux. Few of the existing ultrafiltration (UF) models for prediction of flux and retention include some of these features in the theoretical framework whereas, most of the models resort to empiricism involving one or more adjustable parameters. These simple models lack physical significance and may vary with the operating conditions and with the nature of solutes and membranes.

With the increase of practical applications of pressure driven membrane processes (pulp and paper, sugar, petroleum industry, micellar enhanced ultrafiltration, etc.), particularly with UF, analysis of the nature of limiting flux and rejection have become extremely important. Several attempts are being made in this regard for better understanding of the processes, case-by-case. They would further help the study of the effect of the parameters that influence UF and would help to design the unit operation efficiently. The general objective of the present work was, therefore, to study the fundamental characterization of membrane flux and retention for different

types of hydrophilic membranes and solute combinations under different process conditions using different module configurations.

The present work analyses the mass transfer phenomena in an UF process under the framework of boundary layer theory for osmotic pressure controlled UF, for both cross flow and stirred conditions. Long term flux decline in a stirred UF, was modeled by analyzing the polarized layer resistance for different solutes. Variation of properties in the mass transfer boundary layer was systematically incorporated in the Sherwood number correlations. Performance of UF for two components, one high molecular weight (gel forming) and the other low molecular weight solute is also modeled using a combination of filtration and osmotic pressure theories. Different existing solution techniques (using boundary layer theory) for osmotic pressure controlled UF have been discussed and some approximate solutions are developed. Inaccuracies owing to each approximation have been compared and a generalized integral solution technique is formulated which predicts permeate flux and solute retention as accurately as detailed numerical solution schemes with much less computational efforts.

Film theory is often utilized as tailor-made tool to evaluate the performance of UF systems using mass transfer coefficient. The effect of suction on mass transfer coefficient is qualitative or at best empirical in the present day literature. This aspect has been looked in two different approaches. The first approach was to obtain correlations through semi-empirical routes in terms of modified Sherwood number correlations; whereas, the second approach was to derive the modified Sherwood correlations including the effects of suction, from first principles. Further, the industrial effluent (black liquor, from paper industry), in general was taken for comparing the developed predictive models in the course of present work. Treatment and separation of black liquor was also looked into in terms of technology development. The main purpose of this applied work was to recover water as well as inorganic chemicals from BL. Another case study was also undertaken to remove phenol from aqueous streams using micellar enhanced UF.

Boundary layer treatment was adopted to predict permeate flux and quality (in terms of solute retention) for osmotic pressure controlled UF. A similarity solution technique was developed to solve the convective-diffusive mass balance equation in the mass transfer boundary layer for cross flow UF (CFUF). This method provides the concentration profile in the boundary layer. Coupling this solution with the phenomenological equation for transport through the membrane (based on Darcy's law) and simultaneous solution using an iterative scheme resulted in estimation of membrane surface concentration and permeate flux, provided the operating conditions, solution properties and membrane characteristics were known. Experiments were conducted using polyethylene glycol (PEG 6000), dextran (T 20) and black liquor. Predicted values of flux agreed well with the experimental results. Further, for BL, the rejection was found to be low with 1K membrane (low rejecting UF); hence, to increase rejection of BL solids, permeate of low rejecting UF was subjected to a high rejecting membrane which substantially increased the rejection of BL. Comparisons were made for the performance of treatment of BL by two different schemes. The first scheme used high rejecting UF and the second scheme started with low rejecting followed by high rejecting UF. It was observed that the second scheme yielded better results.

Mechanisms of flux decline in a stirred UF, for PEG, polyvinyl pyrrolidone (PVP) and BL were also studied. It was observed that short terms flux decline could be ascribed to osmotic pressure build up of solution adjacent to the membrane surface which was very rapid (typically within a few seconds). Long term flux decline was quite gradual and it might be attributed to sluggish growth of polarized layer resistance until the steady state was attained. The variations of physical properties in the polarized layer was incorporated in the mass transfer coefficient. Long term flux decline was modeled semi-empirically using the concept of growth of polarized layer resistance. This involved two parameters; one parameter indicated the rate of growth of polarized layer and the other was related to the steady state value of this resistance. It was observed that the parameter associated with the rate of growth of

polarized layer was constant for a particular solute under all the operating conditions and the parameter for steady state resistance was a function of operating conditions. The experimental observations showed that decline in flux with PEG to be the most rapid compared to PVP and that for BL, was to be the slowest. This elucidates that for BL a slow fouling mechanism was prevailing.

UF of two components, high molecular weight (gel forming) and the other a low molecular weight solute is quite common in industrial practices e.g. UF of clarified sugar cane juice, if permeating and non-permeating solutes are categorized into two separate entities. This system was simulated in the laboratory, using a mixture of polyvinyl alcohol (PVA 52K), as gel forming and sucrose, as low molecular weight permeating solutes. UF of such a system was carried out in a stirred cell with 1K and 10K membranes. An unsteady state model for this two component system was formulated using a combination of filtration theory and osmotic pressure model. The model comprised of several parameters; all of which were estimated independently from separate sets of experiments. Using these estimates, the model predicted the values of flux and sucrose retention which matched closely with the experimental observations.

Boundary layer treatment of polarized layer is essential to get the concentration profile at the membrane surface and consequently, permeate flux. Therefore, different solution techniques with different approximations were investigated in detail for both CFUF and unstirred UF. These solution techniques basically involve similarity and integral methods. In a realistic UF operation, membrane surface concentration should vary with channel length (for CFUF) or time (for unstirred UF). Several approximations are suggested in the literature in terms of velocity gradient adjacent to the membrane surface, surface concentration, etc. Based on these, available approximate solutions were revisited as well as a number of new solution techniques were developed. Inaccuracies incurred due to the inherent assumptions were highlighted and compared. Further, to simulate the actual physics of the system, a generalized integral solution technique was formulated for prediction of both flux and retention.

This simple technique was general enough to accommodate variation of diffusivity with concentration in the boundary layer. Being less computation intensive, generalized integral model was as accurate as the detailed numerical solution of the governing boundary layer equations. Using this model, prediction of flux for both PEG and dextran were found to be in excellent agreement with the experimental results. The method was shown to be remarkably useful to estimate various transport parameters like osmotic pressure resistance, variation of solute diffusivity with concentration, etc.

Film theory is the most widely used model to design UF systems. An accurate estimation of mass transfer coefficient is essential for the purpose. Mass transfer coefficients used till now are based on the standard correlations which are obtained from heat-mass transfer analogies, developed for impervious conduits. It is well accepted that such correlations are inadequate to estimate the mass transfer coefficient, in situations where suction effects are present, as in the case of UF. The effects of suction are generally two fold. Firstly, it enhances the mass transfer and secondly, it stabilizes the flow by delaying the transition from laminar to turbulent region. Sherwood number relations were developed based on first principles for laminar flow regime in cross flow through a rectangular channel, tubular and radial flow modules. Using these relations of mass transfer coefficients, osmotic pressure governed UF was attempted for the development of model to predict flux and retention. It was found that the predictions agreed excellently with the experimental results. Further, effects of suction was also incorporated in the mass transfer coefficient via a semi-analytical route in terms of modified wall Peclet number. Several Sherwood number correlations were proposed using extensive laboratory data as well as the data from the literature. This approach was also extended to the turbulent flow regimes using again the three different module configurations.

Final chapter of the thesis devotes to the process development for membrane based treatment of industrial effluent. Process was developed to recover water as well as inorganic chemicals from BL. First, the BL was carbonated to convert all the

inorganics (free as well as bound to alkali lignin) into carbonate salts. The resulting solution was treated by different schemes, namely, direct UF, direct nanofiltration (NF) and UF followed by NF. The last scheme was observed to be the most effective in terms of permeate flux, rejection of dissolved solids and recovery of inorganics.

In a different attempt, a case study was performed to remove phenol from aqueous stream using micellar enhanced UF. Cetyl pyridinium chloride (CPC) surfactants were used to form the micelles. Permeate flux and retention of CPC as well as separation of phenol for various operating conditions were studied. An optimal surfactant loading (with respect to phenol concentration) was investigated. Further, a design criteria indicating the efficacy of phenol removal by surfactant micelles was also suggested. The present work, therefore, is an attempt to look into details of UF process, particularly its design and some of its applied aspects.

Acknowledgments

During past four years, I came in contact with a number of persons who stretched their kind help without hesitation in different phases of my work. In this context, I would like to express my sincerest thanks to all of them. In particular, I like to acknowledge some persons for whom my doctoral work was completed.

I really don't know how to express my heartiest thanks to Prof. P. K. Bhattacharya, my thesis supervisor. Apart from academics, he provided all out help in non-academic affairs also. I am grateful to him for introducing me in the world of research in membrane science and technology. I really enjoyed working with him.

I am also grateful to Prof. Ashutosh Sharma for valuable discussions on several aspects of my work.

A special note of thanks goes to my Lab mate (ex) Dr. Subir Bhattacharjee who helped me out in a sizable portion of my thesis with his deep insight and constant inspirations. I also like to thank my friends, especially, Rajesh Khanna and others (G.K. Singh, Pandeyji, Gautam, Abir and so on) for their encouragements and support in several academic, non-academic and even personal problems.

I am thankful to Mr. J. S. Virdi for his kind help in designing and fabrication of several experimental set-ups.

Mr. R. Chandra, Mr. N. K. Metia, Mr. S. Singh, Mr. Y. Sharma and the other staffs of the department also provided support whenever needed.

Finally, I express my gratitude to my family members, my mother, brothers, my wife and kid for their unflinching support and endless patience in the most trying situations.

Singhendra D.

Contents

Synopsis	iii
Acknowledgments	ix
List of Tables	xiv
List of Figures	xxiv
Nomenclature	xxv
1 Introduction	1
1.1 UF and other pressure driven membrane separation processes	1
1.2 Decline of flux	2
1.2.1 Concentration polarization and membrane fouling	3
1.3 Control of concentration polarization	4
1.4 Prediction of permeate flux	4
1.5 Mass transfer coefficient	5
1.6 Applications of membrane technologies	6
1.7 Organization of the thesis	6
2 Literature review	9
2.1 Introduction	9
2.2 Decline in flux and attainment of limiting flux	10
2.3 Causes of flux decline	11

2.4	Mass transfer analysis in membrane modules	11
2.5	Reduction of concentration polarization	13
2.5.1	Chemical methods	16
2.5.2	Hydrodynamic methods	16
2.5.3	Physical methods	18
2.6	Theories of concentration polarization and flux decline	19
2.6.1	Boundary layer theory	19
2.6.2	Filtration theory	26
2.6.3	Resistance in series model	28
2.6.4	Effects of solute-solute and solute-membrane interactions . . .	29
2.6.5	Flux paradox for colloidal suspensions and possible explanations	30
2.6.6	Typical applications: Treatment of black liquor (BL)and micellar enhanced UF	32
3	Prediction of flux and retention	35
3.1	Flux prediction for black liquor in a cross flow ultrafiltration	35
3.1.1	Introduction	35
3.1.2	Theory	38
3.1.3	Experimental	42
3.1.4	Results and Discussions	49
3.1.5	Conclusions	67
3.2	Short and long term flux decline analysis in ultrafiltration	68
3.2.1	Introduction	68
3.2.2	Theory	69
3.2.3	Experimental	73
3.2.4	Results and Discussion	77
3.2.5	Conclusions	90
3.3	Modeling of Ultrafiltration Process for a Two Component Aqueous Solution of Low and High (Gel-Forming) Molecular Weight Solutes .	91
3.3.1	Introduction	91

3.3.2	Theory	94
3.3.3	Experimental	98
3.3.4	Results and discussions	101
3.3.5	Conclusions	119
3.4	Generalized Integral and Similarity Solutions of The Concentration Profiles for Osmotic Pressure Controlled Ultrafiltration	121
3.4.1	Introduction	121
3.4.2	Theory	124
3.4.3	Experimental	138
3.4.4	Results and discussion	141
3.4.5	Conclusions	167
4	Estimation of Mass Transfer Coefficient with Suction	168
4.1	Theoretical estimation of mass transfer coefficient for laminar flow	169
4.1.1	Introduction	169
4.1.2	Theory	171
4.1.3	Results and Discussions	183
4.1.4	Conclusions	196
4.2	Development of Correlations for Mass Transfer Coefficient in Ultrafiltration Systems	197
4.2.1	Introduction	197
4.2.2	Theory	197
4.2.3	Experimental Data	200
4.2.4	Results and Discussion	201
4.2.5	Conclusions	214
5	Applied aspects	215
5.1	Recovery of Water with Inorganic Chemicals from Kraft Black Liquor by Pressure Carbonation in Combination with Membrane Separation Processes	215

5.1.1	Introduction	215
5.1.2	Experimental	218
5.1.3	Results and discussions	221
5.1.4	Conclusions	241
5.2	Removal of phenol by micelle enhanced ultrafiltration	242
5.2.1	Introduction	242
5.2.2	Experimental	245
5.2.3	Results and Discussions:	247
5.2.4	Conclusions	261
6	General conclusions and recommendations	262
	Appendices	265
A	Membrane characteristics	265
B	Physical properties of the solutes	267
B.1	Viscosity	267
B.2	Density	267
B.3	Diffusivity	268
B.4	Osmotic pressure	268
	Bibliography	270
	List of Publications	298

List of Tables

3.1	Analysis of black liquor	44
3.2	Results for scheme A (Direct LRUF of BL)	48
3.3	Results for scheme B (Direct HRUF runs)	48
3.4	Results for scheme C (LRUF followed by HRUF)	48
3.5	Durations required for c_m to reach osmotic pressure limited value for different solutes at $\Delta P = 550$ kPa and $c_0 = 90$ kg/m ³	82
3.6	Gel porosity and equivalent spherical solute diameter for different pressures	107
3.7	Comparison of various resistances for typical operating conditions . .	113
4.1	The characteristic features of the experimental data.	202
4.2	Hydraulic resistances for different membranes.	203
4.3	Mass transfer coefficients for PEG 6K in a stirred cell under turbulent flow condition using different techniques.	204
4.4	Estimation and statistical results for the different correlations developed.	208
B.1	Diffusion coefficients of different solutes	269

List of Figures

1.1	Hierarchy of the present work	7
2.1	Possible outcomes of concentration polarization	12
2.2	Steps of mass transfer analysis	14
2.3	Methods for controlling concentration polarization	15
3.1	Schematic diagram of a cross flow unit	39
3.2	Cross section view of the cross flow cell	46
3.3	Line diagram of the experimental set up	47
3.4	Effect of pressure on experimental flux for PEG and dextran at $Q = 2.80 \times 10^{-5} \text{ m}^3/\text{s}$. Solid line is for water flux, long dashed lines are for dextran and small dashed lines are for PEG.	50
3.5	Effect of pressure on experimental flux for BL at $Q = 2.22 \times 10^{-5} \text{ m}^3/\text{s}$. Curve with diamonds is for water flux.	51
3.6	Effect of pressure on observed rejection for BL at $Q = 2.22 \times 10^{-5} \text{ m}^3/\text{s}$. Solid curves are for BL and dashed curves are for PEG.	53
3.7	Development of concentration boundary layer at $\Delta P = 415 \text{ kPa}$, $c_0 = 50 \text{ kg/m}^3$ and $Q = 2.22 \times 10^{-5} \text{ m}^3/\text{s}$. Solid line is for black liquor, dashed line is for dextran and dotted line is for PEG.	56
3.8	Effect of cross flow on concentration boundary layer at $\Delta P = 415 \text{ kPa}$, $c_0 = 50 \text{ kg/m}^3$. 1: $Q = 2.22 \times 10^{-5}$; 2: $Q = 2.80 \times 10^{-5}$; 3: $Q = 3.33 \times 10^{-5} \text{ m}^3/\text{s}$. Solid lines are for BL and dashed lines are for PEG.	57

3.9	Concentration profile for black liquor at $\Delta P = 415$ kPa, $c_0 = 50$ kg/m ³ and $Q = 3.33 \times 10^{-5}$ m ³ /s.	58
3.10	Comparison of predicted and experimental flux for LRUF under all operating conditions. Δ - BL; \circ - PEG; + - Dextran.	60
3.11	Variation of real rejection (theoretical) with pressure for LRUF at $Q = 3.33 \times 10^{-5}$ m ³ /s. Solid lines are for BL and dotted lines are for PEG.	61
3.12	Variation of c_m with c_0 for LRUF	64
3.13	Flux versus concentration for HRUF at $\Delta P = 1722$ kPa and $Q = 2.22 \times 10^{-5}$ m ³ /s. \bullet - scheme B; + - scheme C. Solid lines are for theoretical predictions	65
3.14	Real rejection (predicted) versus concentration for HRUF at $\Delta P = 1722$ kPa and $Q = 2.22 \times 10^{-5}$ m ³ /s. Solid line is for scheme C and dashed line is for scheme B.	66
3.15	Block diagram for algorithm of successive substitution	71
3.16	Line diagram of the experimental set up	76
3.17	Variation of membrane resistance over successive runs. $c_0 = 90$ kg/m ³ ; \circ (BL); Δ (PEG); \square (PVP)	78
3.18	Variation of Sh_m/Sh with Sc/Sc_m for all the solutes under all the operating conditions. \circ (BL); Δ (PEG); \square (PVP).	80
3.19	Concentration profiles across the boundary layer for different solutes at different points of time at $\Delta P = 830$ kPa, $c_0 = 90$ kg/m ³ and 545 rpm. Solid lines are for $t = 0.1$ sec; long dashed lines are for $t = 0.3$ sec and short dashed lines are for $t = 0.5$ sec.	83
3.20	Concentration profiles for different solutes under different stirrer speeds at the end of short term flux decline. $\Delta P = 830$ kPa; $c_0 = 90$ kg/m ³ . Solid lines are for $\omega = 325$ rpm and dashed lines are for $\omega = 525$ rpm.	84
3.21	Variation of the dimensionless steady state polarized layer resistance with Reynolds number at $\Delta P = 690$ kPa and $c_0 = 90$ kg/m ³ . \circ (BL); Δ (PEG); \square (PVP).	86

3.22	Variation of the dimensionless steady state polarized layer resistance with the group $\left(\frac{c_m - c_p}{c_0 - c_p} \times \frac{\Delta\pi}{\Delta P}\right)$ at $\omega = 325$ rpm and $c_0 = 90$ kg/m ³ . \circ (BL); Δ (PEG); \square (PVP).	87
3.23	Long term flux decline profiles for different solutes at $\Delta P = 550$ kPa; $c_0 = 90$ kg/m ³ and $\omega = 425$ rpm. The solid lines are for predicted profiles and symbols are for the experimental data. \circ (BL); Δ (PEG); \square (PVP).	88
3.24	Comparison of the predicted and experimental fluxes for all the solutes under all the operating conditions at different points of time.	89
3.25	Schematic of gel polarized UF of two components	95
3.26	Steady state flux versus concentration of PVA solution	102
3.27	Steady state flux versus stirrer speed of PVA solution	104
3.28	$1/v_p^2$ versus time plot for PVA in unstirred UF. Specific cake resistance versus pressure (inset)	105
3.29	Concentration profiles of PVA and sucrose with distance for a typical operating condition. Concentration profile of sucrose (inset)	109
3.30	Variation of gel and boundary layer thicknesses with stirrer speed	111
3.31	Permeate flux of the mixed feed UF with time, for 1K membrane. (a) $\Delta P = 482$ kPa; (b) $\Delta P = 620$ kPa	112
3.32	Observed rejection of sucrose with time, for 1K membrane. (a) $\Delta P = 482$ kPa; (b) $\Delta P = 620$ kPa	115
3.33	Permeate flux of the mixed feed UF with time, for 10K membrane. (a) $\Delta P = 482$ kPa; (b) $\Delta P = 792$ kPa	116
3.34	Observed rejection of sucrose with time, for 10K membrane. (a) $\Delta P = 482$ kPa; (b) $\Delta P = 792$ kPa	117
3.35	Observed rejection of sucrose versus pressure	118

- 3.36 Comparison of the detailed numerical simulation results with different simplified solutions of the boundary layer – osmotic pressure model for unstirred batch cell UF of (a) Dextran (T-40); (b) PEG 6000. The detailed simulation (DS) and GIM results are represented by solid lines which virtually overlap. \square IMCC; \times QSSM1. $c_0 = 10 \text{ kg/m}^3$; $L_p = 2.4 \times 10^{-11} \text{ m/Pa.s}$. Upper curves in each figure represent $\Delta P = 450 \text{ kPa}$ while lower curves are drawn for $\Delta P = 600 \text{ kPa}$ 144
- 3.37 Variation of permeate flux with axial distance in a cross flow UF cell at a cross flow velocity $u_0 = 0.31 \text{ m/s}$ using DS and different simplified models proposed in the present work. $L_p = 2.46 \times 10^{-11} \text{ m/Pa.s}$ 1: $c_0=10 \text{ kg/m}^3$, $\Delta P - 550 \text{ kPa}$; 2: $c_0=10 \text{ kg/m}^3$, $\Delta P - 275 \text{ kPa}$; 3: $c_0=50 \text{ kg/m}^3$, $\Delta P - 550 \text{ kPa}$; Solid lines represent the solution obtained by GIM. DS; QSSM1; – – – QSIM; + + + IMCC. 147
- 3.38 Concentration profiles of dextran (T-20) during laminar cross flow UF cell. Curves represented by 1, 2, 3 are generated using conditions specified in Fig. (3.37). Solid lines represent the solution obtained by GIM. DS; QSSM1; – – – QSIM; 149
- 3.39 Comparison of average flux (Eq. (3.113)) of dextran (T-20) in a cross flow cell predicted by different simplified models with the predictions of DS. Filled symbols correspond to the operating conditions $\Delta P=275 \text{ kPa}$, $c_0 = 10 \text{ kg/m}^3$, $u_0=0.46 \text{ m/s}$ and open symbols correspond to $\Delta P = 550 \text{ kPa}$, $c_0 = 10 \text{ kg/m}^3$, $u_0 = 0.31 \text{ m/s}$. \circ IMCC; \square SMCC; \star GIM; \times QSSM1; \diamond QSIM; \triangle QSSM2. 151

- 3.40 Variation of dimensionless permeate flux (solid lines) and observed rejection (discontinuous lines and symbol) with time in an unstirred batch cell. The variation of diffusivity, when considered is assumed to be linear, $D = D_{\infty}(1 + Kc)$, with K varying from 0 to $2 \times 10^{-3} \text{ m}^3/\text{kg}$. Osmotic pressure and other solution properties correspond to Dextran T-20. $c_0 = 10 \text{ kg/m}^3$; $\Delta P = 600 \text{ kPa}$. Curve1: $R_r = 1.0, K = 2 \times 10^{-3} \text{ m}^3/\text{kg}$; 2: $R_r = 0.99, K = 0.0$; 3: $R_r = 0.99, K = 2 \times 10^{-3} \text{ m}^3/\text{kg}$; 4: $R_r = 0.98, K = 2 \times 10^{-3} \text{ m}^3/\text{kg}$; 5: $R_r = 0.97, K = 2 \times 10^{-3} \text{ m}^3/\text{kg}$; $K = 2.0 \times 10^{-3} \text{ m}^3/\text{kg}$ for curves 6 to 8 Curve 6: $R_r = 0.99$; 7: $R_r = 0.98$; 8: $R_r = 0.97$; symbols (\square): $K = 0.0, R_r = 0.99$ 155
- 3.41 Variation of dimensionless membrane surface concentration with channel length in a cross flow ultrafiltration system for constant diffusivity. Simulations are performed using solution properties of Dextran T-20 with $L_p = 2.46 \times 10^{-11} \text{ m/Pa.s}$. $\Delta P = 550 \text{ kPa}$; $Re = 1000$; $c_0 = 10 \text{ kg/m}^3$. Curve 1: $R_r = 1.0$; 2: $R_r = 0.99$; 3: $R_r = 0.95$; 4: $R_r = 0.90$; 156
- 3.42 Variation of dimensionless membrane surface concentration with channel length in a cross flow system at constant R_r (1.0). Simulations are performed using solution properties of Dextran T-20. Operating conditions and membrane properties are same as Fig. (3.41). Variation of diffusivity is assumed to be linear. $K = 0$ for curves 1–3. Curve 1: $D_{\infty} = 6.75 \times 10^{-11} \text{ m}^2/\text{s}$; 2: $D_{\infty} = 8 \times 10^{-11} \text{ m}^2/\text{s}$; 3: $D_{\infty} = 10.34 \times 10^{-11} \text{ m}^2/\text{s}$; K is varied for curves 4–6. Curve 4: $K = 0.5 \times 10^{-3} \text{ m}^3/\text{kg}$; 5: $K = 1.0 \times 10^{-3} \text{ m}^3/\text{kg}$; 6: $K = 2 \times 10^{-3} \text{ m}^3/\text{kg}$; 157
- 3.43 Variation of dimensionless permeate flux with channel length at constant diffusivity in a cross flow system. Simulations are performed using solution properties of Dextran T-20. Operating conditions and membrane properties are same as Fig (3.41). Curve 1: $R_r = 1.0$; 2: $R_r = 0.99$; 3: $R_r = 0.95$; $R_r = 0.90$ 160

- 3.44 Variation of dimensionless flux with channel length in a cross flow system at constant ($R_r=1.0$). Simulations are done with the solution properties of Dextran T-20. Operating conditions and membrane properties correspond to those of Fig. (3.41). For curves 1 to 3, $K = 0$. Curve 1: $D_\infty = 6.75 \times 10^{-11} \text{m}^2/\text{s}$; 2: $D_\infty = 8.00 \times 10^{-11} \text{m}^2/\text{s}$; 3: $D_\infty = 10.34 \times 10^{-11} \text{m}^2/\text{s}$; K is varied for curves 4 to 6. Curve 4: $K = 0.5 \times 10^{-3} \text{m}^3/\text{kg}$; 5: $K = 1.0 \times 10^{-3} \text{m}^3/\text{kg}$; 6: $K = 2.0 \times 10^{-3} \text{m}^3/\text{kg}$. 161
- 3.45 Variation of observed rejection with channel length in a cross flow system. Simulations are carried out using the solution properties of Dextran T-20. Operating conditions and membrane properties correspond to those of Fig. (3.41). Curves 1 to 4 are drawn at constant R_r (1.0) and 5 to 7 are drawn at constant value of D_∞ (10.34×10^{-11}). Curve 1: $D_\infty = 6.75 \times 10^{-11} \text{m}^2/\text{s}$; 2: $D_\infty = 8.00 \times 10^{-11} \text{m}^2/\text{s}$; 3: $D_\infty = 10.34 \times 10^{-11} \text{m}^2/\text{s}$ and $K = 0$; 4: $D_\infty = 10.34 \times 10^{-11} \text{m}^2/\text{s}$ and $K = 2.0 \times 10^{-3} \text{m}^3/\text{kg}$; 5: $R_r = 0.99$; 6: $R_r = 0.95$; 7: $R_r = 0.90$ 162
- 3.46 Variation of observed rejection with channel length in a cross flow system. Simulations are performed using the solution properties of Dextran T-20. Operating conditions and membrane properties correspond to those of Fig. (3.41). Curve 1: $Re = 2000$; 2: $Re = 1500$; 3: $Re = 1000$; 4: $Re = 500$ 163

- 3.47 Variation of osmotic pressure resistance with channel length in a cross flow UF system. Simulations are performed with the solution properties of Dextran T-20. Operating conditions and membrane properties correspond to those of Fig. (3.41). Solid lines are for constant R_r (1.0) and discontinuous lines are for constant D_∞ ($10.34 \times 10^{-11} \text{m}^2/\text{s}$). $K = 0$ for curves 1 to 3 and K is varied for curves 4 to 6. Curve 1: $D_\infty = 6.75 \times 10^{-11} \text{m}^2/\text{s}$; 2: $D_\infty = 8.00 \times 10^{-11} \text{m}^2/\text{s}$; 3: $D_\infty = 10.34 \times 10^{-11} \text{m}^2/\text{s}$. $D_\infty = 10.34 \times 10^{-11} \text{m}^2/\text{s}$ for curves 4 to 9. Curve 4: $K = 0.5 \times 10^{-3} \text{m}^3/\text{kg}$; 5: $K = 1.0 \times 10^{-3} \text{m}^3/\text{kg}$; 6: $K = 2.0 \times 10^{-3} \text{m}^3/\text{kg}$; 7: $R_r = 0.99$; 8: $R_r = 0.95$; 9: $R_r = 0.90$ 164
- 3.48 Variation of average permeate flux with ΔP during UF of dextran (T-20) in a cross flow cell. The curves represent the predictions using GLM and symbols represent the experimental fluxes. 1: $c_0 = 10 \text{ kg/m}^3$; 2: $c_0 = 30 \text{ kg/m}^3$; 3: $c_0 = 50 \text{ kg/m}^3$. For each set, the three curves from top to bottom correspond to the cross flow velocities 0.46, 0.38, 0.31 m/s, respectively. $\Delta - u_0 = 0.46 \text{ m/s}$; $\circ - u_0 = 0.38 \text{ m/s}$; $\square - u_0 = 0.31 \text{ m/s}$. 166
- 4.1 Schematic of the flow configuration in a radial cross flow cell 172
- 4.2 Variation of $1/I_{1,2,3}$ with $\lambda_{1,2,3}$. Solid line is for rectangular cell (Eq. (4.54)), dotted line is for tubular module (Eq. (4.55)) and long dashed line is for radial cross flow cell (Eq.(4.56)). Symbols represent the numerically integrated values, obtained from Eq.(4.16) (circle), Eq.(4.34) (box) and Eq.(4.47) (triangle) 181
- 4.3 Variation of local Sherwood number along the channel length for different values of suction, for a rectangular cross flow cell. 1: $Pe_w = 0$; 2: $Pe_w = 50$; 3: $Pe_w = 100$; 4: $Pe_w = 200$; 5: $Pe_w = 300$. Solid lines are for $ReScd_e/L = 10^3$ and dashed lines are for $ReScd_e/L = 10^5$. . . 184

- 4.4 Variation of local Sherwood number along the module length for different values of suction, for a tubular module. 1: $Pe_w = 0$; 2: $Pe_w = 50$; 3: $Pe_w = 100$; 4: $Pe_w = 200$; 5: $Pe_w = 300$. Solid lines are for $ReScd/L = 10^3$ and dashed lines are for $ReScd/L = 10^5$ 185
- 4.5 Variation of local Sherwood number along the channel radius for different values of suction, for a radial cross flow cell. 1: $Pe_w = 0$; 2: $Pe_w = 50$; 3: $Pe_w = 100$; 4: $Pe_w = 200$; 5: $Pe_w = 300$. Solid lines are for $ReSch/R = 10^3$ and dashed lines are for $ReSch/R = 10^5$ 186
- 4.6 Variation of $\overline{Sh}/\overline{Sh}_{no\ suction}$ with Pe_w for different $ReScd_e/L$ in a rectangular cell. 1: $ReScd_e/L = 10^3$; 2: $ReScd_e/L = 10^4$; 3: $ReScd_e/L = 10^5$; 4: $ReScd_e/L = 10^6$ 188
- 4.7 Variation of $\overline{Sh}/\overline{Sh}_{no\ suction}$ with Pe_w for different $ReScd_e/L$ in a tubular module. 1: $ReScd/L = 10^3$; 2: $ReScd/L = 10^4$; 3: $ReScd/L = 10^5$; 4: $ReScd/L = 10^6$ 189
- 4.8 Variation of $\overline{Sh}/\overline{Sh}_{no\ suction}$ with Pe_w for different $ReScd_e/L$ in a radial cross flow cell. 1: $ReSch/R = 10^3$; 2: $ReSch/R = 10^4$; 3: $ReSch/R = 10^5$; 4: $ReSch/R = 10^6$ 190
- 4.9 Variation of dimensionless flux (Pe_w) with Re for RO system. Solid lines are predicted flux and symbols are the experimental data of Merten et al. [266]. 1: $L/d_e = 5.0$; 2: $L/d_e = 16.56$; 3: $L/d_e = 30.0$; 4: $L/d_e = 60.0$; 5: $L/d_e = 150.0$; 6: $L/d_e = 300.0$ 191
- 4.10 Variation of permeate flux with pressure for UF of dextran (T-20). 1: $c_0 = 10\text{ kg/m}^3$; 2: $c_0 = 30\text{ kg/m}^3$; 3: $c_0 = 50\text{ kg/m}^3$. Symbols represent as, open circle, $u_0 = 0.44\text{ m/s}$; box, $u_0 = 0.38\text{ m/s}$ and triangle, $u_0 = 0.30\text{ m/s}$. Curves are the predicted values of permeate flux. . . . 193
- 4.11 Fitting between predicted and experimental permeate flux for UF of PEG 6K in a rectangular channel. Dashed lines are for $\pm 10\%$ deviations. 194

4.12	Fitting between predicted and experimental permeate flux for UF of PEG 6K in a radial cross flow cell. Dashed lines are for $\pm 10\%$ deviations.	195
4.13	Variation of Sh_{exp} with Pe_{test} under laminar and turbulent (inset) flow domain in a rectangular channel. \circ PEG 6K (this work); \square Dextran T20 [122]; \triangle Dextran T20; \diamond BSA [9]; \circ dextran T70 [115] (inset); Solid lines are Eq. (4.67) and Eq. (4.69) (inset).	206
4.14	Variation of Sh_{exp} with Pe_{test} under turbulent flow domain in a stirred cell. \circ PEG 6K [220]; \triangle PVP 10K [242]; solid line is Eq. (4.70).	210
4.15	Variation of Pe_{test} for BL under laminar flow in a rectangular channel and turbulent flow in a stirred cell (inset). \circ experimental data; Solid lines are Eqs. (4.67) and (4.70) (inset) for BL.	211
4.16	Variation of Sh_{std}/Sh_{corr} with Pe for different solutes and flow regimes. Solid lines are for standard solutes and dashed lines are for BL. Curve 1: BL under laminar conditions in a rectangular channel, $Re = 500$. 2: Standard solutes under laminar conditions in a rectangular channel, $Re = 500$. 3: Standard solutes in a radial cross flow cell, $Re = 500$. 4: BL under turbulent conditions in a stirred cell, $Re = 50,000$. 5: Standard solutes under turbulent conditions in a stirred cell, $Re = 50,000$. 6: Standard solutes under turbulent conditions in a rectangular channel, $Re = 5,000$	213
5.1	Basic Units of lignin	223
5.2	Variation of pH with time	224
5.3	Variation of activity with time	225
5.4	Change of concentration of active alkali and sodium carbonate with time	227
5.5	Different schemes which were studied	229
5.6	Variation of inorganic recovery with time	230
5.7	Steady state NF permeate flux for different schemes versus feed concentration	232

5.8	Flux decline with time for 55 kg/m ³ BL for different schemes	235
5.9	Flux decline with time for 73 kg/m ³ BL for different schemes	236
5.10	Flux decline with time for 90 kg/m ³ BL for different schemes	237
5.11	Variation of tds rejection with feed concentration for different schemes	238
5.12	Performance of different schemes	240
5.13	Schematic of a typical MEUF process	244
5.14	Variation of permeate flux with time for CPC solution in unstirred batch cell for $c_0 = 10.2 \text{ kg/m}^3$; 1: $\Delta P = 207 \text{ kPa}$; 2: $\Delta P = 345 \text{ kPa}$; 3: $\Delta P = 483 \text{ kPa}$; symbols are for experimental data.	249
5.15	Variation of permeate flux with stirrer speed for CPC solution in stirred batch cell. 1: $c_0 = 10.2 \text{ kg/m}^3$; 2: $c_0 = 20.4 \text{ kg/m}^3$; 3: $c_0 = 30.6 \text{ kg/m}^3$; symbols are for experimental data.	250
5.16	Comparison of permeate flux with concentration between stirred and unstirred batch UF; symbols are for experimental data.	252
5.17	Comparison of permeate concentration with feed concentration between stirred and unstirred batch UF ; symbols are for experimental data.	253
5.18	Schematic of micelle deposition on the membrane surface. (a): Unstirred cell; (b): Stirred cell.	254
5.19	Variation of phenol consumption with CPC to phenol ratio in the bulk. 1: $\Delta P = 207 \text{ kPa}$; 2: $\Delta P = 345 \text{ kPa}$; 3: $\Delta P = 483 \text{ kPa}$; symbols are for experimental data.	256
5.20	Distribution of organic solute in the micelle phase.	258
5.21	Variation of equilibrium parameter with CPC to phenol ratio for different pressure in unstirred batch cell. 1: $\Delta P = 207 \text{ kPa}$; 2: $\Delta P = 345 \text{ kPa}$; 3: $\Delta P = 483 \text{ kPa}$; symbols are for experimental data.	260
A.1	Rejection curves for the membranes	266

Nomenclature

List of symbols

$A_{1,2,3}, A_{12}$	Constants
a	Constant
c	Concentration (kg/m ³)
c_0, c_b	Bulk concentration (kg/m ³)
c_s	Solute concentration in the micelle phase
c^*	Non-dimensional concentration (c/c_0)
D	Diffusivity (m ² /s)
D_∞	Diffusivity at infinite dilution (m ² /s)
d_p	Particle diameter (m)
d	Tube diameter (m)
H	Equilibrium parameter
h	Channel half height (m)
$I_{1,2,3}$	Integrals
J_w	Pure water flux (m ³ /m ² .s)
j	Mass flux (kg/m ² .s)
$K_{1,2,3}$	Integration constants
k	Mass transfer coefficient (m/s)
k_C	Mass transfer coefficient based on Colton's correlation (m/s)
k_{corr}	Correlated mass transfer coefficient (m/s)
k_{exp}	Experimental mass transfer coefficient (m/s)
k_{vv}	Mass transfer coefficient from velocity variation technique (m/s)

k_0	Constant in Eq. (3.33) (s^{-1})
L	Channel Length (m)
L_g	Gel layer thickness (m)
L_p	Membrane Permeability (m/Pa.s)
M_w	Molecular weight
N_A	Avogadro number
n_1, n_2	Constants
Pe	Peclet number
Pe_w	Wall Peclet number
Pe_{test}	Peclet number based on test rig data
Q	Flow rate (m^3/s)
R	Radius (m)
R_a	Adsorption resistance (m^{-1})
Re	Reynolds number
R_g	Gel layer resistance (m^{-1})
R_m	Membrane resistance (m^{-1})
R_p	Polarized layer resistance (m^{-1})
R_T	Total Resistance (m^{-1})
R_0	Observed rejection
R_r	Real rejection
R_{ad}	Resistance due to solute adsorption (m^{-1})
R_{bl}	Boundary layer resistance (m^{-1})
R_{ma}	Membrane resistance including irreversible adsorption (m^{-1})
R_{osm}	Osmotic pressure resistance (m^{-1})
R_{ps}^*	Steady state polarized layer resistance (m^{-1})
r	Radial position (m)
Sc	Schmidt number
Sh	Sherwood number
Sh_{r^*}	Local Sherwood number for radial cell

Sh_x	Local Sherwood number
\overline{Sh}	Average Sherwood number
Sh_{std}	Standard Sherwood number
$Sh_{nosuction}$	Sherwood number without suction
T	Temperature ($^{\circ}$ K)
t	Time (sec)
u	Axial velocity (m/s)
V_p	Average permeate flux ($\text{m}^3/\text{m}^2 \text{ s}$)
v	Transverse velocity (m/s)
v_p	Permeate flux ($\text{m}^3/\text{m}^2 \text{ s}$)
v_p^0	Initial flux for long term decline ($\text{m}^3/\text{m}^2.\text{s}$)
x	Axial distance (m)
y	Normal distance (m)

Greek symbols

α	Specific cake resistance (m/kg)
$\beta_{1,2,3}$	Constants
δ	Boundary layer thickness (m)
ΔP	Pressure difference (kPa)
η	Similarity parameter for rectangular cell
ϵ	Porosity
γ	Partition coefficient
$\lambda_{1,2,3}$	Constants
μ	Viscosity (Pa.s)
ω	Stirrer speed (rpm)
π	Osmotic pressure (kPa)
ϕ	Similarity parameter for tubular module
Φ_s	Micelle mole fraction in the bulk
ρ	Density (kg/m^3)

σ_f	Osmotic reflection coefficient
ξ	Similarity parameter for radial cell

Subscripts

g	Gel
m	Membrane
p	Permeate
0	Bulk
w	Water
1	High molecular weight solute
2	Low molecular weight solute

Superscripts

*	Non-dimensional
—	Average

Chapter 1

Introduction

Technological advances developed over the last thirty years enabled engineers to economically purify water or perform other separation/purification/concentration processes via pressure driven membrane processes i.e. reverse osmosis (RO), nanofiltration (NF), ultrafiltration (UF), microfiltration (MF), etc. Decline of permeate flux over time is the major limitation of such separation processes. Therefore, a detailed theoretical understanding, experimental observations and interpretation of flux decline and retention characteristics are necessary for the process design and development. In this context, a series of experimental studies, development of pertinent theories and various aspects of some of the applications of membrane based separation processes for the treatment of industrial effluent were undertaken. In the present thesis, before going into details, the subject is introduced in this chapter. The preliminary concepts of the topic starting from the definition of the process are revisited in the following sections.

1.1 UF and other pressure driven membrane separation processes

UF is a pressure driven, rate governed membrane separation process in which components of a mixture is separated by preferential transport of solutes through a porous barrier, called membrane. Obviously, higher molecular weight solutes are

retained and lower molecular weight solutes permeate through the membrane.

Classification of the membrane separation processes are broadly based on the domains of operating conditions [1–3]. Operating pressures of 25 atmosphere and more are encountered in RO and that for UF is generally between 2 to 10 atmospheres; whereas, for microfiltration, even less pressure (1 to 4 atmosphere) is required. In terms of solute size, there is no sharp boundary of identification of the processes. Among these, UF is generally considered to be the most versatile and can be employed for separation of solutes having a wide range of molecular sizes, from nm to microns.

The major applications of ultrafiltration process include concentration, purification and fractionation of various process streams. The process is widely applicable for protein recovery from cheese whey. Recovery of enzyme as well as its acceptability in electroplating industries, etc. [1, 2, 4] are reported. Apart from this, recently UF was found to be suitable in effluent treatment of several industries like, textile, leather, pulp and paper, etc. [1, 2]. The process is also gaining acceptability in biomedical, food and beverages, environmental applications. The advantages of UF over other conventional separation processes are mainly: (i) generally less energy intensive; (ii) operable under ambient temperature; (iii) no phase change and, (iv) almost no damage to the species under processing. Therefore, UF can play a major role in replacing many of the conventional separation processes, looking into these advantages. However, the pressure driven membrane separation processes could not fulfill their earlier promises. If today, the industrial applications of UF are not that successful, it may be due to the inherent limitation of the processes, which is the decline of permeate flux and product quality over time.

1.2 Decline of flux

In any membrane separation processes, permeate flux which defines the throughput of the process per unit time, declines during the operation time [5]. This decline is

a direct consequence of change in membrane permeability. The decline in flux is extremely rapid initially and becomes gradual later on. This decline can be reversible or irreversible in nature. In the former, initial permeate flux can be restored once the process is stopped; the membrane is washed meticulously and the process is restarted. In the latter, the membrane gets damaged permanently and initial flux cannot be recovered even after thorough washing of the membrane. For any such change in the membrane permeability, the retention characteristics of the membrane also change, affecting the quality of the product.

1.2.1 Concentration polarization and membrane fouling

The decline of permeate flux is mainly attributed to the phenomena, namely, concentration polarization and membrane fouling [5, 6]. Reversible decline of flux may be due to both of these phenomena separately or when they act in concert. Irreversible flux decline is generally due to the membrane fouling. Concentration polarization is a phenomena in which solute concentration in the feed side tend to build up on the membrane surface due to accumulation of the retained solute particles by the membrane [7]. This may lead to several consequences which in turn become responsible for the reduction of permeate flux; e.g., (i) increased solute concentration on the membrane surface leads to an increase in osmotic pressure of the solution, thereby, reducing the effective driving force for the process; (ii) formation of a cake or gel type layer on the membrane surface which offers an extra resistance to the flow; (iii) increase in solution viscosity, change in solute diffusivity and solution density adjacent to the membrane surface also affect the passage of permeate flux adversely; (iv) membrane pores and pore mouth may be partially or completely blocked by the adsorption of solute particles and therefore, the permeability of the membrane may get reduced to a large extent. The last consequence in this list leads to membrane fouling. Hence, membrane fouling may not be a separate phenomenon, but is a direct consequence of concentration polarization. In any membrane process, one or more of these effects of concentration polarization can occur simultaneously.

Concentration polarization and membrane fouling are the most important factors in membrane processes because they restrict the efficacy of the process. Therefore, quantification and control of these factors which dictates the system performance are the critical issues to the process design and development engineers.

1.3 Control of concentration polarization

It can be noted here that concentration polarization cannot be avoided altogether in any membrane processes; only it can be controlled or its effects can be minimized through some techniques. The most conventional way to reduce concentration polarization is through stirring of the feed solution or to allow the feed to flow tangentially over the membrane surface (cross flow filtration) [8]. Thus the growth of the concentration boundary layer can be restricted. Several module designs are based on the alteration of hydrodynamics in the feed channel for the control of concentration polarization; namely, introduction of turbulent promoters like spacers, inserts etc. [9, 10], pulsatile flow [11, 12], pressure pulsation [13], ultrasonic perturbation [14], dean vortices, etc. [15, 16]. Surface modification of the membrane by chemical treatment (like surfactant treatment, etc.) [17] can also reduce concentration polarization by lowering the tendency of the surface to adhere to the solute particles. External field (e.g. electric field) can also disturb the solute accumulation on the membrane surface through electrophoresis and electroosmosis [18].

1.4 Prediction of permeate flux

A theoretical prediction of permeate flux and permeate concentration for various operating conditions is essential for the design of UF system. General prediction procedure involves solving of differential mass balance equation in the polarized layer (concentration boundary layer), along with the solution of Navier-Stokes equations for the velocity flow field, coupled with a suitable phenomenological equation for transport through the porous membrane. The detailed solution for all such coupled

partial differential equations are quite formidable. They involve numerical schemes (e.g. finite difference) which are quite restrictive for the practical industrial use. Therefore, an objective of the present work was also to obtain a simpler but accurate solution technique for boundary layer problems. Further, boundary layer treatment and/or classical filtration theory with appropriate approximations are common in the literature of UF [19, 20]. Presence of membrane fouling (reversible or irreversible) further complicates the theoretical approach for the prediction of flux [21–23]. In essence, simultaneous prediction of flux and rejection from a concrete theoretical basis is still scarce in the literature of membrane separation. Most of the theories are approximate or semi-empirical. Chapter 2 of this thesis, therefore, deals a critical review of the relevant literature.

1.5 Mass transfer coefficient

Design of UF unit (stirred or cross flow) is mostly based on stagnant film theory for the prediction of mass transfer coefficient [24]. The available Sherwood number relations are generally in the form of correlations which are derived for the flow through impermeable conduits from heat and mass transfer analogies [25]. These correlations lack in several influencing aspects of the process, e.g. effect of suction, effect of variation of physical properties, effect of osmotic pressure build up near the wall, incomplete solute retention, etc. [26, 27]. Moreover, stagnant film theory assumes mass transfer across a fully developed concentration boundary layer whereas most of the cross flow systems operate under developing boundary layer. This necessitates to relook into the development of such Sherwood number relations incorporating above effects with appropriate theoretical basis.

1.6 Applications of membrane technologies

While developing theoretical understanding for the prediction of flux and retention characteristics of membrane, it was thought appropriate to match the experimental results not only with the standard solutes but also with industrial effluents. Several experiments were also conducted with the industrial effluent for the testing of the various developed models. During the course of experiments, some encouraging results were obtained. Promptly detailed experiments were conducted to treat the effluent with membranes with the sole objective being technological development. Therefore, the present work also undertook the applications of the membrane processes as one of its important objectives. Applications of membrane technology, its analysis and interpretation of experimental data would be of immense help to design and process development.

To summarize, the objectives of this thesis can broadly be categorized as, (i) to develop theoretical and semi-empirical models for prediction of permeate flux and solute retention during UF process in different modules with standard solutes and industrial effluent; (ii) to develop empirical and theoretical relations for the estimation of mass transfer coefficient in different flow regimes for different flow configurations, incorporating the effects of suction and to analyze their use in RO and UF; (iii) to develop a membrane based technology for the recovery of water and inorganic solutes from black liquor (paper plant effluent). The hierarchy of the present work can be presented pictorially in Fig. (1.1).

1.7 Organization of the thesis

Keeping in mind the broad objectives of the work, the present thesis is organized as follows. Apart from this introductory chapter, a critical review of flux decline theories with the emphasis on recently published work is presented in chapter 2.

Chapter 3 is divided into four sections. These sections deal with several aspects

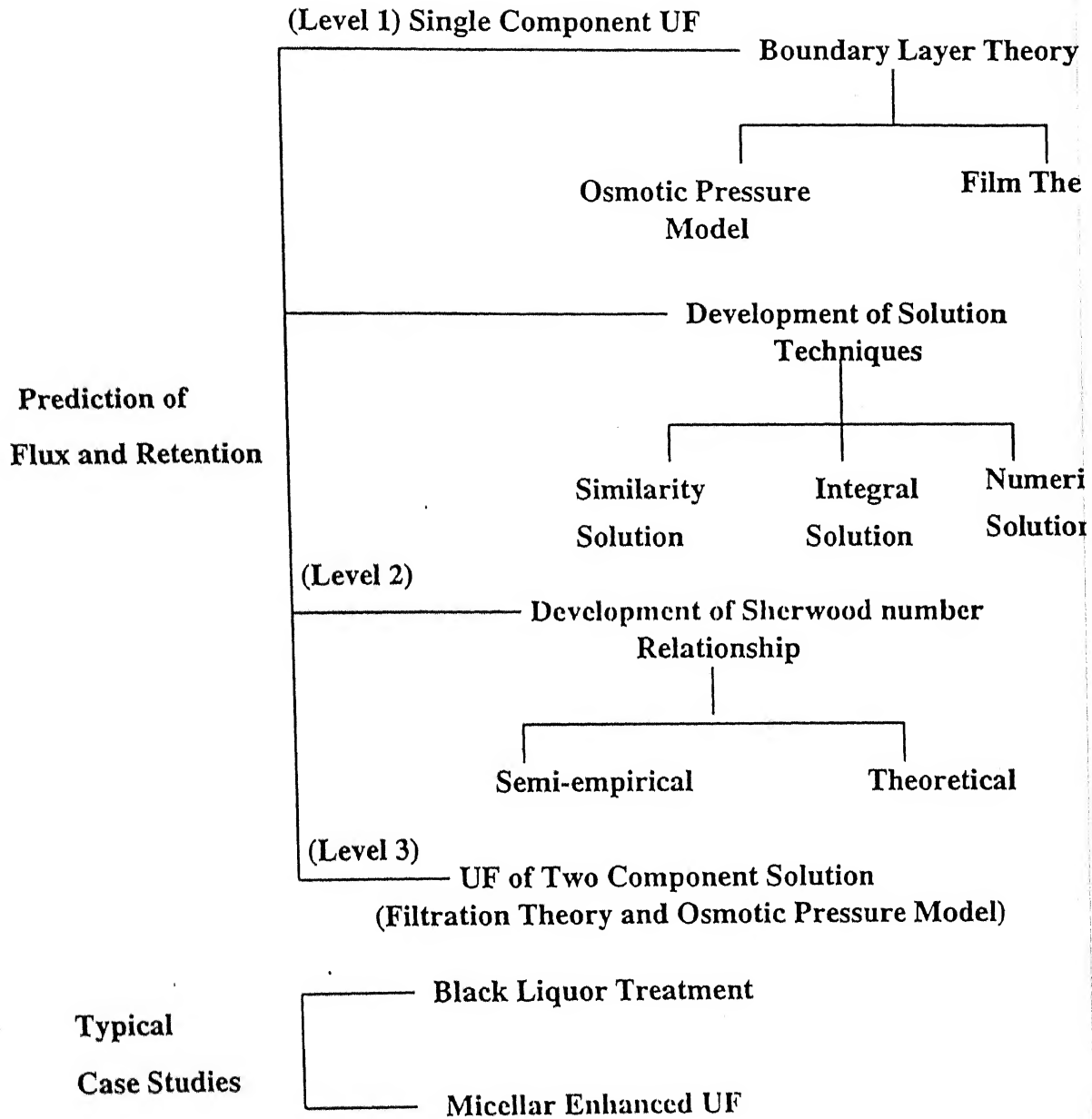


Figure 1.1: Hierarchy of the present work

of flux decline in UF. Each section is exclusive by itself. First section is devoted to model development for cross flow UF of standard solutes as well as of black liquor; second section aims at the development of semi-empirical model to quantify the polarization in a stirred UF cell; third section is devoted to development of a model to predict both flux and rejection of a two component solution in a stirred UF cell, and the fourth section covers the development of several simplified boundary layer solutions in various flow configurations for prediction of flux and rejection using similarity and integral transforms and also, their comparisons.

Two sections are created for chapter 4. Development of Sherwood number relations for determination of mass transfer coefficient in laminar flow regime for different flow modules incorporating the effects of suction and their applications in context of prediction of flux and retention are described in the first section of this chapter, whereas, second section essentially contains establishment of different Sherwood number relations for different modules, including the effects of suction through semi-empirical routes.

The first section of Chapter 5 describes, a novel membrane based technology developed for the recovery of inorganic chemicals along with water from black liquor. Further, an attempt has been made in second part of this chapter, in the direction of removal of phenol from an aqueous stream through micellar enhanced ultrafiltration. Each section of chapter 3, 4, 5 contains its own introduction, brief literature review, development of theory (if necessary), experimental section (if necessary), results and discussions and conclusions. Therefore, each section of these chapters is a complete unit by itself. Finally, general conclusions drawn from this study are summarized in chapter 6.

Chapter 2

Literature review

2.1 Introduction

The field of pressure driven membrane separation processes has come out to be a matured discipline after extensive research during past thirty five years [28]. Performance of separation without phase change, less energy consumption, operability at the ambient temperature, without any need of additives are typical characteristics which has given an edge to such processes over conventional techniques. RO, UF, MF are increasingly integrated in the downstream of several biological and chemical processes [12, 3, 29] for the treatment of process streams. Among these membrane based separation processes, UF is the most versatile due to its suitability for filtering solutes having wide range of sizes. Research on UF and other processes have been mainly focused on three directions, namely, (i) development of membranes; (ii) modifications on hydrodynamics and flow configurations to improve flux; (iii) pre-treatment of process streams to enhance the performance of separation. All these aspects are broadly aimed at a common objective i.e., to control and improve flux decline, which is an inherent limitation of the process. Flux decline is the most important phenomena which restricts the widespread applicability of membrane processes. During UF of skimmed milk in a dead end cell (without agitation), flux drops to 5% of its initial value within 25 seconds [24, 30, 31]; even during stirred UF of bovine serum albumin (BSA) solution, flux drops to 6% of its initial value within

half an hour [32]. The extent of decline in flux can be understood from the above observations.

For filtration of pure water through the polymeric membranes, permeate flux is governed by Darcy's law [3]. When a macromolecular solution is subjected to membrane filtration, permeability of the membrane decreases over time, causing a decline in flux and finally, a steady state is attained. Most of the membrane permeability can be regained after cleaning of the membrane and a part of it is lost permanently [4]. Consequently, flux decline can be classified as reversible and irreversible. Understanding of flux decline phenomena and its causes, consequences and remedies are therefore of utmost interest for module design and evaluation of system performance. These aspects are looked into detail in the subsequent sections.

2.2 Decline in flux and attainment of limiting flux

In a UF process, permeate flux drops sharply during initial period of filtration and then gradually attains a steady state value, known as limiting flux. Extent of this decline and its long term limiting value are the major consideration factors from the view point of any industrial process. This leads to a theoretical development for understanding the principles of flux decline and quantification of limiting flux.

Limiting flux in UF is generally a function of operating conditions, namely, (a) feed concentration, (b) operating pressure, and (c) shear rate at the membrane surface which is a manifestation of stirring or cross flow velocity. Increase in transmembrane pressure, increases permeate flux due to enhancement of driving force [1]. Increase in flux is almost linear at lower pressure; however, at higher pressure, flux becomes almost invariant with pressure [24]. Therefore, limiting flux can be categorized under two major classes, namely, (a) pressure controlled domain and (b) mass transfer controlled domain. In the latter, flux is independent of the pressure and flux can be enhanced by improving the mass transfer in the module i.e., by increasing the

turbulence or lowering the feed concentration [1–4]. Therefore, the flux decline and limiting flux are the performance index of the membrane processes.

2.3 Causes of flux decline

Flux decline during UF is broadly attributed to two related phenomena, concentration polarization and membrane fouling [1–4]. During filtration, solute particles migrate towards the membrane under the driving force and tend to accumulate over the membrane-solution interface due to a balance between convective drag towards and through the membrane (leading to permeate flux) and backward diffusion from the membrane surface to the bulk of the solution. Concentration polarization can manifest itself into several outcomes which are summarized in Fig. (2.1). It is obvious from the figure that general outcome of concentration polarization is reduction of permeate flux. In a process, any one or more of these manifestations can occur concurrently. It must be noted here that the majority of flux decline due to concentration polarization can be recovered after membrane cleaning and therefore, it is at times called as reversible fouling [1, 2]. However, the last manifestation (Fig. 2.1) (i.e. the pore blocking, etc.) may not be a reversible phenomena. Membrane pores may permanently get blocked partially or completely by solute adsorption. This is termed as irreversible fouling [33]. Even an extensive cleaning schedule is unable to regain the lost permeability due to irreversible fouling. Therefore, it can be stated that the membrane fouling is a consequence of concentration polarization.

2.4 Mass transfer analysis in membrane modules

Quantification of concentration polarization and membrane fouling warrants mass transfer analysis to evaluate the system performance. Typical approaches for mass transfer analysis are based on the simulation of a single phase fluid flow in the module and its analysis to obtain the velocity fields; coupling them with solute mass

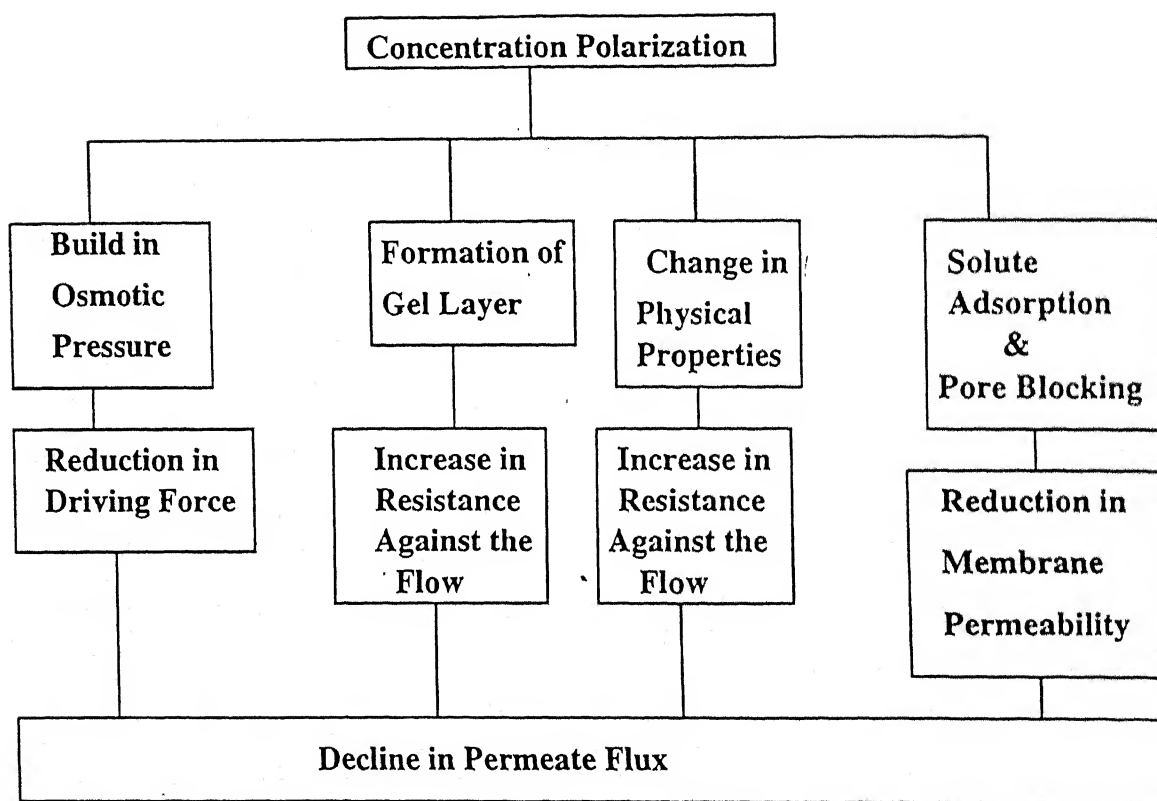


Figure 2.1: Possible outcomes of concentration polarization

balance equation (convective-diffusion equation) in order to solve for the concentration distribution which in turn provides the system efficiency. Steps of mass transfer analyses are followed in the order as shown in Fig. (2.2). Over the years, several methods of solution techniques have emerged to analyze the mass transfer in the membrane modules [34–36]. To obtain the velocity fields, continuity and momentum balance equations are either solved numerically or analytically. Several models are available in this regard [37, 38]. Numerical schemes mainly evolved around finite difference [39]. Berman first gave an analytical solution for velocity fields using perturbation techniques [37] for flow through a two dimensional porous slit. The same was also available for a circular tube [38]. The following assumptions were made to simplify the problem, namely, (i) steady state operation; (ii) laminar, fully developed flow; (iii) uniform permeate flux along the channel; (iv) no external forces and, (v) with constant physical properties. The velocity fields, thus obtained are inserted into the solute mass balance equation. The resultant equation was either solved numerically (finite difference) [39] or analytically by similarity solution techniques [19, 20, 40], Laplace transform [41, 42], series solution [43], integral methods [9, 44, 45], etc. These solution techniques and their limitations are critically reviewed in the subsequent sections. Another approach of mass transfer analysis is to use a mass transfer coefficient for a fully developed stagnant concentration boundary layer under steady state operation [24], instead of solving the detailed solution procedure as outlined in Fig. (2.2). It must be clear by now that the improvement of system performance depends upon the reduction of concentration polarization and membrane fouling. This can be achieved either by improvement of mass transfer in the module or by cleaning the membrane.

2.5 Reduction of concentration polarization

Typical methods to reduce concentration polarization are described in Fig. (2.3). Each of these is briefly discussed as follows.

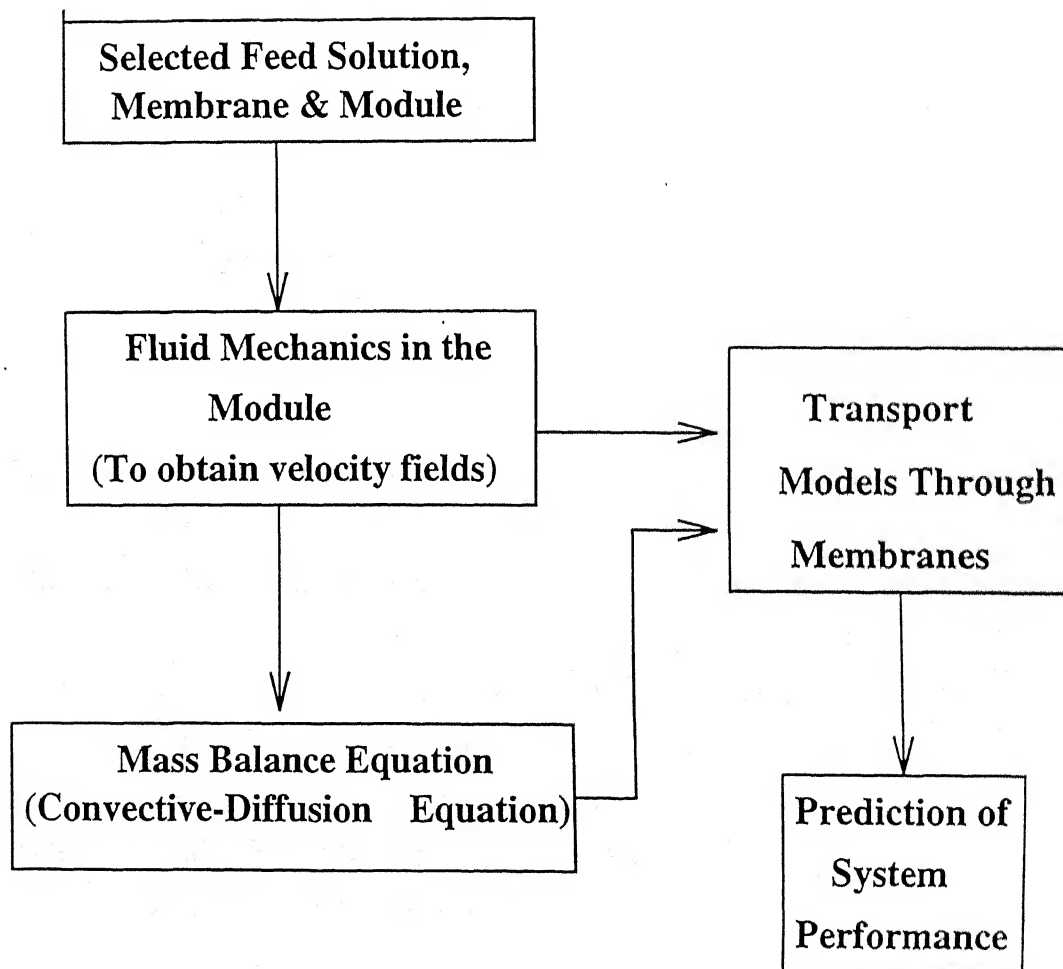


Figure 2.2: Steps of mass transfer analysis

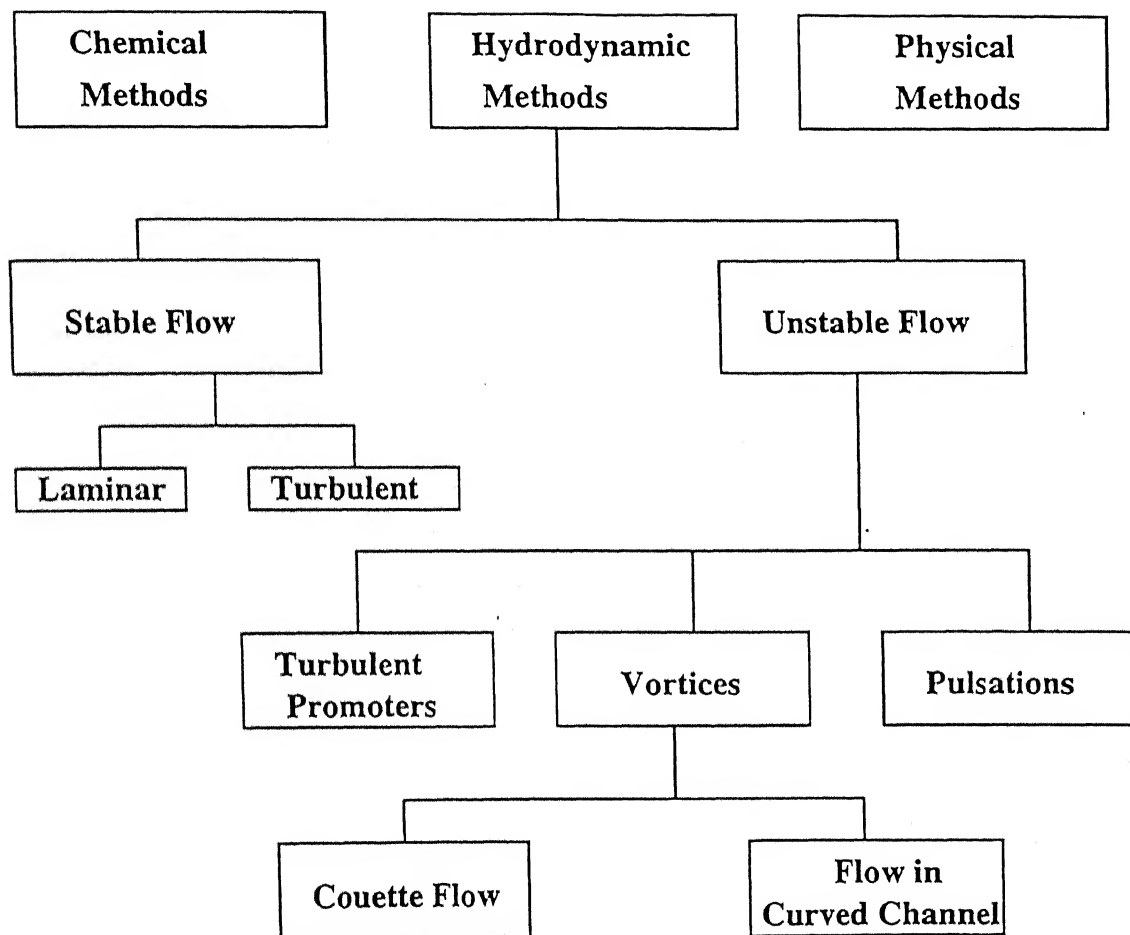


Figure 2.3: Methods for controlling concentration polarization

2.5.1 Chemical methods

Fouling of membrane can be minimized if the interaction between membrane and solutes can be controlled. Development of both hydrophilic (cellulose acetate) and hydrophobic (teflon, polypropylene, etc.) membranes is a major step in this area. Changes in membrane material was illustrated to be effective to control the surface charge which resulted in reduced biological fouling [46]. The use of conducting polymeric materials in the manufacture of the membranes and electrochemical control of the transport through the membrane are being investigated by several researchers [47–49]. Another route to control membrane fouling is to pre-treat the membrane with a suitable chemical such that the attraction between membrane materials and solute particles can be reduced and their mutual repulsion increases. Direct chemical treatments such as heterogeneous chemical modification [50], adsorption of hydrophilic polymers, surface modification by ionic and non-ionic surfactants [51–59], irradiation methods [60] and low temperature plasma activation [61] have been suggested.

2.5.2 Hydrodynamic methods

By chemical treatment of membrane surface, the interaction between membrane-solute system can be made favourable to minimize fouling. But, once there is a gel or cake layer formation on the membrane, only alternative left is to alter the hydrodynamics such that mass transfer is improved. Hydrodynamics in a conduit can be altered either by steady state technique or by imposing instabilities to the flow. In the steady state technique, high cross flow velocity or stirring can be imposed [24, 62]. Reynolds number may be chosen high enough so that the flow falls in turbulent regime. With this turbulence, the growth of the deposited layer becomes restricted [24]. Turbulent eddies near the wall tend to depolarize the concentration build-up [24, 62]. But, high turbulence may create large axial pressure drop which in turn decreases transmembrane pressure drop and increases the pumping overhead [62].

Unsteady flows and induction of instabilities

Induction of instabilities in the flow results in augmentation in mass transfer was first observed by Thomas in 1973 [10]. Insertion of rods at different positions in the channel resulted higher mass transfer. Hydrodynamic instabilities can be caused (as shown in Fig. 2.3) by (a) turbulent promoters, (b) secondary and (c) pulsatile flows.

Turbulent promoters

Main objective of turbulence promoters are to create instabilities close to membrane - solution interface where the solute build up is maximum [10]. Placing of protuberances [10], well defined spacers [63], baffles [12, 64], etc. are some of the examples of turbulent promoters. Analysis of spacer filled flow and design criteria of spacers are also available [65]. Another approach is to replace the flat membrane by a corrugated one [66]. Here, the fluid flows into each corrugation and forms vortices and induces instabilities. Introduction of fluidized particles [67] or intermittent jets [68] in the flow chamber, screw threaded flow promoters [69, 70], static mixers [71], gas sparging [72], natural convection instabilities [73], etc. are examples of recently studied instability inducing techniques. Permeate flux was found to be enhanced several times in magnitude.

Pulsatile flow

Superimposition of pulsed flow over bulk axial flow makes the velocity profile bimodal [15], where both the peaks appear near the wall. This is called 'Richardson's annual effect' [74]. Due to this, the solute build up near the wall gets disturbed and back diffusion increases, which finally resulted in enhanced flux. Use of pulsatile flow in RO of sucrose solution [75] and UF and MF of whey protein [76], whole blood flow [76], and, protein solutions [77-80] are reported. The entire mass transfer boundary value problem for oscillatory Newtonian laminar flow was solved by Illias and Govind [11] and the results were compared with the experimental data of Kennedy et al. [75]. In addition to flow pulsation, transmembrane pressure pulsations were also employed to improve flux [81]. Combination of pulsatile flow with

baffles were also investigated [77, 78] and were found to improve flux significantly.

Secondary flow

Taylor vortices are useful to depolarize the membrane lining in the annulus of a rotating cylindrical membrane device. This was studied separately by Lopez-Leiva [82] and Leibherr [83]. Excellent fluid mixing, high wall shear rate and weakly decoupled cross flow with transmembrane flux are the major advantages in rotating membranes [84]. Several investigators observed that the permeation rate and solute retention can be improved significantly using this technique compared to the traditional cross flow filtration [85, 86]. Several companies have recently commercialized the rotating disk membranes [87]. High energy consumption to rotate the system, difficulties in maintenance and replacement of the membrane, problem of scaling, etc. are major limitations of such rotating devices.

To overcome these limitations, Dean vortices are prescribed in place of Taylor vortices by Winzeler [88], Belfort and his coworkers [89–93]. Dean vortices are produced by forcing the fluids in a curved channel at a modified Reynolds number (Dean number). These vortices result the flow to transit from stable laminar to unstable laminar regime [94, 95] and cause to depolarize the solute build-up. Experiments were conducted to treat well defined colloids, baker's yeast broth and dairy whey [89, 96] where it was observed that the filtration performance increased significantly using Dean vortices.

2.5.3 Physical methods

External fields (electric, magnetic, etc.) are often utilized to reduce the effect of concentration polarization. The approach can be developed and implemented separately from that of the membrane module design. This way, intentional introduction of turbulent promoters are not necessary.

Use of electric field is the most widely explored area in the application of external field to improve the membrane performance. Electric field enhanced technologies

utilize a phenomenon, called electrokinetics. Electrophoresis (movement of charged particles in the relatively stationary medium) and electroosmosis (movement of fluid through the porous media) are the outcome of electrokinetics which govern the reduction of concentration polarization. Several reports on the use of electric field and its optimization related to membrane fouling are available in the literature [97–103]. Use of ultrasonic field to dislodge the particles from the membrane surface and pores was also reported [14].

2.6 Theories of concentration polarization and flux decline

Among the membrane separation processes, UF is the most versatile in terms of range of particle sizes to be filtered. RO is a process where separation of a homogeneous solution is carried out; whereas, in MF, colloidal suspensions or slurries are filtered. Therefore, boundary layer treatment is extensively used in RO for prediction of flux. On the other hand, engineers take recourse to classical filtration theory to predict permeate flux decline in MF. Both the theoretical routes are applied widely to quantify the permeate flux and its quality in UF (which is supposed to be an intermediate operation between RO and MF). Apart from these two theories, another semi-empirical route is often utilized. In this case, all the resistances to the solvent flow are assumed to be in series and the theory is termed as resistance in series model. Such models are phenomenological in nature and the flux data are generally correlated in terms of different resistances [6].

2.6.1 Boundary layer theory

It is assumed that during filtration, a thin concentration boundary layer develops all along the channel length. Within the boundary layer, the convective solute mass flux towards the membrane in the feed side and away from the membrane in the permeate side is balanced by the diffusion of solutes from the membrane surface to the bulk

of the solution at the steady state. Therefore, equations of continuity and motion are solved simultaneously with the pertinent initial and boundary conditions to get the velocity profiles in the boundary layer. Using this velocity profiles, solute mass balance equation is solved to get the solute distribution on the membrane surface. Finally, the boundary layer solution is coupled with an appropriate model for transport through the membrane and thus the permeate flux is obtained. The boundary layer treatment is quite complicated and no complete analytical solutions to these problems exist. Therefore, simplification of boundary layer problem using suitable approximations was a common approach in late sixties and early seventies. This led to analytical expressions for velocity profiles. For solution of convective diffusion mass balance equation in the boundary layer, constant membrane surface concentration [19, 40] or constant wall flux [41, 104] were often assumed to simplify the solution schemes. Some of the solution techniques utilized to solve these problems are perturbation and series solutions [37, 43], integral methods [9, 44, 45], similarity approach [19, 20, 40], etc. Among these approximate solution techniques, integral and similarity solutions are quite accurate and widely used. In the integral method, a suitable concentration profile within the boundary layer is assumed. Solution of the mass balance equation after inserting this profile results the surface concentration; a knowledge of surface concentration provides the estimate of permeate flux via a membrane transport model. Integral solution results of Leung and Probstein [44], Probstein et al. [4], Srinivasan et al. [45] showed very good agreements with the experimental results. Integral method subsequently was successfully used for different channel configurations and solute systems [105, 106].

In the similarity method, self-similar concentration profile is assumed. In this case, mass balance equation is solved using similarity technique in terms of similarity parameter and the solution provides the surface concentration and consequently, permeate flux. This method also provides a close agreement between experimental and predicted results [19, 20, 40].

However, the approximations in the above methods often cause deviations from

the practical situation in the filtration process where both permeate velocity and surface concentration are functions of axial position (in CFUF) or operation time (in unstirred batch cell). Therefore, detailed numerical schemes are often adopted to solve the boundary layer problem using finite difference [39, 107–112], orthogonal collocation [113], etc. However, with the increasing access to the computation facilities, numerical schemes are gaining prominence.

Concentration polarization near the membrane surface results the following three features in the boundary layer, namely, (i) increase in osmotic pressure, (ii) formation of gel layer, and (iii) change in solution viscosity and solute diffusivity in the boundary layer. To incorporate these effects in the boundary layer theory, two separate branches have evolved: (a) osmotic pressure model and (b) gel layer model. Both of these models have received widespread attention in flux decline analyses.

2.6.1.1 Osmotic pressure model

Concentration polarization results in the build up of solutes near the membrane surface which in turn increases the solution osmotic pressure; thus the effective driving force for solvent transport decreases. Goldsmith [114] incorporated osmotic pressure in the modeling of UF process for the first time. Osmotic pressure, a colligative property is related to the solute concentration linearly for a dilute solution using van Hoff equation. For a concentrated solution, this dependence is non-linear and it can be expressed in terms of concentration by a virial type of expression. For macromolecules, the second and third virial coefficients become important and osmotic pressure of the solution cannot be neglected. Osmotic pressure of polymeric dextran and polyethylene glycol have been reported by Goldsmith [114]. A correlation form of osmotic pressure with concentration based on Flory's equation was proposed. Correlations of osmotic pressure of different solutes with concentration are available [115–118]. The chemical environment (ionic strength and pH) also plays an important role for the osmotic pressure of proteins like, BSA, ovalbumin,

immunoglobulin, etc., [116].

Osmotic pressure difference between membrane - solution interface in the upstream and permeate side provides the barrier to the driving force. The lowering in flux due to osmotic pressure build up was first obtained for RO system by Kedem and Katchalsky [119] from non-equilibrium thermodynamics. However, inadequacy to describe the flux decline by classical filtration theory resulted in the introduction of osmotic pressure model to explain the flux decline behaviour for macromolecular UF.

Osmotic pressure model is adapted in the boundary layer theory in two ways. In the first approach, solute mass transport equation is solved by detailed solution of the flow field in the boundary layer to obtain the concentration distribution; consequently, osmotic pressure model is utilized to obtain the permeate flux [116, 120].

In the second approach, the velocity field is not obtained through the solution of continuity and momentum balance equations. A stagnant mass transfer boundary layer (film theory) is assumed to form over the membrane surface. The flow characteristics are lumped in the mass transfer coefficient. Permeate flux can then be obtained from the solute mass balance equation at the membrane surface, using the obtained mass transfer coefficient. This expression of flux is solved along with that obtained through the phenomenological equation (for transport through the membrane pores). Surface concentration and permeate flux can thus be obtained, iteratively [2]. This is known as the film theory - osmotic pressure model.

Importance of osmotic pressure model is emphasized by several recent studies [26, 115, 121]. Clifton [109] used osmotic pressure model for hollow fiber UF; predictions agreed closely with the experimental data. Jonsson [122] used osmotic pressure model for prediction of flux in CFUF for both dextran and whey protein, both in laminar and turbulent flow regimes. Bhattacharjee and Bhattacharya used osmotic pressure model for low molecular weight solutes in unstirred UF [123]. Ganguly and Bhattacharya used this model in radial CFUF [113].

However, this model cannot be used indiscriminately to all UF processes. There are several drawbacks of this model. The most important is that the model cannot account for any other cause of flux decline apart from osmotic pressure build-up. Experimental determination of osmotic pressure for various solutes are scant in the literature and the determination procedures are prone to error. For filtration of colloids, osmotic pressure is often negligible but still the flux decline occurs. Formulation of other flux decline models are therefore getting attempted regularly.

2.6.1.2 Gel layer model

In gel layer model, it is assumed that during filtration of macromolecules, a porous gel like layer is formed on the surface. Deposition of this layer is basically due to phase separation of the solute at the solution-membrane interface because of high concentration. Therefore, gel concentration is assumed to be constant throughout this layer. Decline in flux is ascribed to the hydraulic resistance offered by this layer [124]. Hence, total resistance to the flow may be looked into as gel layer resistance in addition to the membrane resistance. With the course of time of operation, gel layer further increases in thickness and the resistance to the flow intensifies; consequently, flux declines to the steady state value. Steady state is attained by the balance between convective solute transport towards membrane and back diffusion away from the membrane.

The gel layer model is first put forward by Michaels [125]. Later on, it was developed by Blatt et al. [24] and Porter [126]. It was assumed that steady state permeate flux is invariant with pressure after the formation of gel. Therefore, gel layer model is often utilized to quantify the pressure independent limiting flux. Beyond threshold pressure, flux may increase momentarily and then quickly dies down and attains the steady state value [127–129]. Gel layer is often assumed to be a filter cake and it may be characterized by filtration theories [124].

Extensive studies are available to characterize the gel layer UF [130–135]. Gel con-

centration is assumed to be independent of operating conditions. It was supposed to be a sole characteristic of the solute and the solution. However, this hypothesis is severely contended and reports are available where gel concentration is found to be dependent on feed concentration and cross flow velocity [130, 132]. When the whole membrane is polarized, membrane fouling plays a very minor role to limit the flux; diffusion through the gel layer dictates the decline in flux. Hence, in macromolecular UF, pressure independent flux is assigned to the gel polarization.

It is very common in literature that gel layer model was used to characterize the flux decline behaviour, whereas actual gel may not have formed [124, 136]. This necessitated the gel concentration to be an adjustable parameter. Determination of gel characteristics like specific cake resistance, cake compressibility, etc. are carried out using filtration theory. UF flux decline data in unstirred conditions are also utilized for this purpose. Therefore, estimation of these parameters become erroneous and even misleading when there is no actual gel formation (for most of the macromolecules). Cake filtration theory is based on the particles of well defined shape whereas gel layer is extensively used for macromolecular (straight or branched chained) UF. Solution properties like viscosity, diffusivity, etc. are altered significantly in the concentrated gel layer. Availability of property variations with concentration (especially for diffusivity) is limited in the literature. Therefore, values of diffusivity, used in the gel layer model, is generally difficult to establish. Some researchers prefer diffusivity at gel concentration [9] whereas, others prefer a mean diffusivity over the concentration boundary layer [19, 137]. Therefore, very often, gel layer model becomes a fitting model and it is unable to provide insight to the predictive nature of a self-sufficient model. However, it may be concluded that the boundary layer theories are versatile enough to accommodate the variations of properties with concentration in the polarized layer.

2.6.1.3 Mass transfer coefficient and variations of physical properties in the boundary layer

Both in film theory and gel layer model, a knowledge of mass transfer coefficient is required for calculation of permeate flux. Mass transfer coefficient in membrane processes are generally obtained by heat-mass transfer analogies in an impervious conduit. Several correlations are available depending on flow regimes in different geometries [26, 27]. In both the reviews [26, 27], it has been identified that mass transfer coefficients for membrane processes need to be modified to incorporate various factors appearing in the process. Of which, most important factors are surface roughness, effects of suction, changes of physical properties, etc. Major problem is that there exists no universal correlations for all the solutes in a specific flow regime and configuration. Researchers proposed separate correlations for different solutes empirically from the flux decline data itself [1, 138, 139]. Recently, mass transfer coefficients for non-Newtonian fluids are also reported [140–142].

In the polarized layer, increase in solute concentration results in several changes of transport properties near the solution - membrane interface [26, 27, 143, 144]. Solute diffusivity and solution viscosity are the main transport properties which get affected significantly. Incorporation of changes in properties in the boundary layer analysis can be carried out in two ways; first of all, complete boundary layer problem is solved numerically using the property variations as function of concentrations. In the second approach, property variations are directly incorporated in mass transfer coefficient and Sherwood number relationships are modified accordingly [26, 27, 145–147]. Using the modified mass transfer coefficient, film theory or gel layer model may be solved to calculate the permeate flux.

It may however, be noted in many cases, that boundary layer models are not able to provide quantitative estimation of flux decline even after incorporation of property variations. Therefore, an alternate approach may be considered to analyze the flux decline of suspensions or particulate UF. This approach highlights the hydrodynam-

ics of the solvent in light of viscous resistances offered by the solute particles of finite shapes and sizes.

2.6.2 Filtration theory

Drawbacks of boundary layer theories compel the researchers to explore theoretical developments to account flux decline behaviour of macromolecules under the framework of classical filtration theory. It is assumed that during unsteady state flux decline, a cake or gel type layer is deposited on the membrane which grows with time offering more resistance to the solvent flux. The characteristics of this layer is evaluated by filtration theory. Nakao et al. [133] used the unsteady state gel layer model to define the flux decline; they used Kozney-Karman equation (which is applicable to flow through packed bed) to characterize the gel layer. The concentration of this layer was considered to be constant and equal to the gel concentration. However, it may be noted that Kozney-Karman equation is valid for particle bed in a continuous fluids, with particle of defined shape and size. Macromolecules for UF are generally polymeric in nature and they have a chained structure. Therefore, determination of gel layer characteristics using Kozney-Karman equation may be inadequate. Nevertheless, classical filtration theory is used widely for colloidal suspensions in MF. Trettin and Doshi [105], provided a theoretical contribution regarding suitability of application of modified filtration theory for UF. They tried to unify the mass transfer limited UF and filtration theory. They proposed a criteria whether UF is entirely mass transfer controlled or it can be described by only filtration theory. Their model was general enough to account the situation when both of these mechanisms are competitive.

Chudacek and Fane [124], studied stirred UF of colloids (syton) and proteins (dextran, BSA) and used filtration theory to analyze their data. They also pointed out the problem of classical filtration theory for straight chained polymers. It was observed that specific cake resistance is a function of pressure and concentration. Comparing the results of BSA and syton, it was concluded that increase in particle size provided

the cake structure more porous and consequently, flux will be more for larger particles. Operating pressure and feed concentration affect the cake layer [105, 124]. Increase in pressure results into compaction of specific cake resistance and therefore, resistance to the flow increases. It has been observed [105] that cake resistance is directly proportional to the feed concentration. This observation is in contrast to the classical filtration theory. Trettin and Doshi [105] explained this anomaly in terms of solution environment (pH, ionic strength, etc.) at low concentration; at higher concentration this effect debilitates leading to formation of more compact layer. In stirred UF using completely rejecting membranes, flux decline is rapid and concentration profile establishes quite early. But, for less retentive membranes, flux decline is quite gradual [148]. This is attributed to increase in cake layer thickness as well as solute adsorption in the membrane pores [149, 150].

Trettin and Doshi [19] tried to unify the osmotic pressure and gel layer model for UF of BSA solution considering a constant surface concentration. They observed that below a particular pressure (689 kPa) UF is osmotic pressure controlled and above it the process is gel layer controlled. Further, filtration theory can be utilized to analyze the flux decline. Reinhanian et al. [151] further highlighted hydraulic control approach (filtration theory) in their unstirred experiments. Recently, van Oers et al. [152] used filtration theory for flux decline of CFUF of silica particles. In UF of proteins, governing mechanism for flux decline is quite uncertain and both boundary layer and filtration theory are applied. For UF of BSA solution osmotic pressure model was shown to be adequate by adjusting the diffusivity [117]. Whereas, filtration theory was observed to quantify the flux decline successfully for the same BSA solution [124]. This problem of applicability of filtration theory arises due to lack of experimental evidences of formation of gel layer on the membrane surface. Recently, Song and Elimelech [153] proposed a model based on minimum energy principles for CFUF/CFMF of colloidal suspensions and proposed critical filtration number as a criteria for cake formation.

Thus, the filtration theory is found to be more suitable to MF, although it has been

widely used for UF. Filtration theory excludes to incorporate the solution osmotic pressure which may be significant for macromolecules. Apart from this, for solutes known not to form gel, cake properties cannot be found out using Kozney-Karman equation directly. These properties have to be determined from the experimental flux decline data itself. This renders the filtration theory as a fitting model instead of a predictive one.

2.6.3 Resistance in series model

It must be clear by now that the models for flux decline are not general enough to accommodate all the causes for flux decline. Especially, for a complex industrial effluent, properties of which are difficult to estimate, the models for flux decline become highly inadequate. Therefore, a more pragmatic approach was adopted to model the flux decline, in terms of accounting all the resistances in series. This resistance in series models correlates the experimental flux decline data with all the resistances. These resistances comprise of osmotic pressure resistance, gel layer resistance, resistance due to solute adsorption, etc., in addition to membrane hydraulic resistance. However, all the resistances may not appear simultaneously in a UF process.

Some of the pioneering works involving boundary layer resistances were carried out by Wijman's et al. [154], Nakao et al. [155], van den Berg and Smolders [156], etc. Their model takes care of resistances arise out of concentrated boundary layer and gel layer along with the hydraulic resistance of the membrane. van den Berg and Smolders [156] used boundary layer resistance model for treating the dead end UF. Their method includes film theory for the concentration profile near the membrane surface in conjunction with the boundary layer resistance model equations. They observed good agreement with experimental data. However, wherever, solute adsorption becomes dominant, resistances due to adsorption and irreversible fouling were also taken into account. Nabateni et al. [121] used a resistance in series model to analyze the flux decline of ovalbumin data in CFUF. Resistances due to osmotic

pressure build up and solute adsorption were also taken into consideration. Several works have been reported using this model for UF and MF [157–159]. Therefore, resistance in series models have been developed as a simplest tool to correlate the flux decline data with the phenomenology.

2.6.4 Effects of solute-solute and solute-membrane interactions

Solute-solute and solute-membrane interactions play a vital role in flux decline during UF and MF. Solute-solute interactions are mainly due to the chemical environment of the solution. Studies on filtration of protein mixtures reveal that the flux decline behaviour is entirely different from that of a single component system. Complex fluids like milk, fruit juice, industrial effluent, etc. consist of macromolecules of various sizes and properties. Presence of large molecules can alter the retention of smaller ones [160, 161]. Change in ionic strength or pH of the solution can alter the flux and retention of the same feed solution [162]. It has been observed that presence of oppositely charged macromolecules can reduce the resistance offered by the concentration boundary layer quite significantly. Whereas, for particles of same charges, resistance is altered marginally [156]. Tsapiuk et al. [163] emphasized this aspect of solute-solute interaction in their study of fractionation of lignosulfonates. Presence of microsolute (salts) at higher concentrations, altered the fractionation, whereas, fractionation is dictated by the membrane itself at lower salt concentrations.

Membrane-solute interactions also play an active role in governing the flux decline. It has been observed that for cationic dispersions, flux decline is more rapid compared to anionic dispersions through a polysulfone or polyacrylic membrane. Surface charges of both the solutes and membrane affect the interaction mechanisms. Therefore, coulombic forces and hydrophobic interactions are important for a UF system. Besides, membrane permeability, retention of solutes also gets affected by solute-membrane interactions. This effects arise out of attractive or repulsive interactions between solute particles and membrane pore wall. Several models are available for flow through membrane pores under the influence of membrane-solute

interactions [164–170]. Steric effects, attractive or repulsive interactions on solute retention are taken into account in these models. Understanding of membrane-solute interactions would help in development of new membranes which will be less prone to membrane fouling and adsorption [171]. Solute-membrane interactions may foul the membrane in two ways, namely, physiochemical solute adsorption on the pore wall and clogging the pores by solute aggregates [172]. These mechanisms can occur either separately or simultaneously. Many works in this area have been reviewed earlier [173–179].

In a recent work, it has been identified that the role of solute-solute interactions are manifested in variation of diffusivity and osmotic pressure, which govern the transport of the solution across the polarized layer and through the membrane [180]. The solute-membrane interactions further affect the transport of solute and solvent through the membrane pores. The interactions between solute-solute interactions may be quantified in terms of interaction potentials. The interaction potentials between two solute molecules in aqueous solution comprise of three components, the apolar Lifshitz-van der Waals, polar acid-base and electrostatic. Addition of these potentials gives the extended DLVO potential for the solute-solute interactions in a polar solvent. Estimates of the osmotic pressure and diffusivity may be obtained using these potentials which in turn may be used in the boundary layer theories for prediction of flux.

2.6.5 Flux paradox for colloidal suspensions and possible explanations

Film theory in terms of gel-polarization model is often used to calculate the steady state flux in CFUF or CFMF. These predictions are based on the mass transfer coefficient in the boundary layer. Brownian diffusivity obtained from Stokes-Einstein relation, is generally used for the estimation of mass transfer coefficients from their correlations. Based on this diffusivity, flux values predicted are one or more order in magnitude less than the experimental results [24, 126]. Green and Belfort [181]

termed this phenomena as flux paradox for colloidal suspensions. Several alternative mechanisms are proposed and they are broadly based on mechanisms of shear induced diffusivity, inertial lift and surface transport.

In the shear induced diffusion, solute particles experience random motion in the boundary layer and mutual interactions among them is more under the influence of high shear. Zydney and Colton [182] proposed in their model that Brownian diffusivity should be replaced by the shear induced diffusivity which is larger in magnitude (more than two orders). Shear induced diffusivity was first measured by Eckstein et al. [183] and was found to be proportional to the solute size. Davis and Sherwood [40] performed exact similarity solution of convective-diffusion equation for the solute mass balance using shear induced diffusion which is the dominant mechanism in back transport of the solutes. Their analysis included concentration dependency of viscosity and diffusivity which were obtained from Leighton and Acrivos [184, 185]. An alternative explanation was provided by Belfort and coworkers [181, 186–190]. According to them, inertial lift is responsible for augmented flux of colloidal suspensions. Inertial lift basically results out of nonlinear interactions between solute particles. If Reynolds number based on particle size are not small, then inertial term in Navier-Stokes equation cannot be neglected; inertial lift will then increase the lateral migration of particles away from the membrane and consequently, deposition on the surface becomes less.

Surface transport mechanisms suggest that the deposited particles on the surface experience a drag longitudinally due to shear forces. The rejected particles form a sort of flowing cake layer on the membrane surface [191, 192]. Both continuum and single particle models have been used to explain this mechanism. In the continuum approach, convective Navier-Stokes equations are solved in the cake layer [193] and in single particle models, force balance is performed on a single particle [194–198].

However, none of these mechanisms could provide satisfactory answers to flux paradox and incorporation of them in macroscale observations are quite difficult. Therefore, all the models discussed so far have their own limitations. For filtra-

tion of different solutes, different mechanisms are provided to explain flux decline phenomena.

2.6.6 Typical applications: Treatment of black liquor (BL) and micellar enhanced UF

Process streams from pulp and paper industries contain large volumes of water and valuable inorganic chemicals. Conventional regeneration process [199] recovers inorganic chemicals while destroying the organics, present in the BL, causing environmental pollution. Further, huge amount of scarce water is lost during the process. Membrane processes may be an attractive alternative in pulp and paper industry compared to conventional recovery process. Applications of membrane processes in pulp and paper industries have been reviewed extensively in this context [200–203]. Usage of membrane processes were identified broadly in the following applications: (i) concentration and recovery of water from process streams; (ii) recovery of valuable products which includes fractionation and purification of lignosulfonates from spent sulfite liquor and that of lignin from kraft black liquor. Potential impact of membrane based technology is usually three fold; namely, (i) it is less energy intensive; (ii) causes much less environmental pollution and, (iii) both inorganic and organic chemicals can be recovered [204].

Concentration of sulfite liquor and bleach plant effluent were carried out extensively by Wiley and his coworkers [205–208] using RO. They observed that the permeate stream was of high purity, having low BOD and COD. Membrane rejection of both organic and inorganic components were as high as 90%. A combination of RO and freeze concentration was also attempted [209]. In this case, RO was utilized to remove 90% of water from a stream containing 5 g/L of total dissolved solids. Retentate was further concentrated by freeze concentration to about 200 g/L. Attempts have also been made by Bhattacharya and his coworkers to treat BL, in context of separation, concentration and recovery of inorganic chemicals, using different membrane modules [216–220]. RO and UF were used to treat paper mill white wa-

ter [203]. A membrane rejection of over 99% was achieved. Removal of coloured chlorinated lignin from effluent of alkali extraction step was also reported [202]. Ten fold concentration of dilute pulp wash water from a high yield chemi-mechanical pulping process was observed [210]. High values of solids rejection were achieved. However, a decrease in flux rate due to fouling by colloidal organics was observed. Much of these as well as other treatments of BL using membrane technology were extensively reviewed earlier [200–203].

UF can play an important role in fractionation and purification of lignosulfonates (from spent sulfite liquor) and that of lignin (from kraft BL). The purpose of UF is two fold: (i) separation of lignin compounds from low molecular weight organic and inorganic compounds and, (ii) fractionation of high molecular weight lignin compounds. Typical spent sulfite liquor contains approximately 60% lignin, 30% reducing sugar and 10% inorganic materials. Using UF, it is possible to separate the spent liquor into purified fractions of lignosulfonates and sugars [203, 211]. Purity of lignosulfonates to a tune of 80% was reported with simple UF and upto 95% was obtained using a combination of diafiltration and UF [202, 212]. Lignin in kraft BL occurs in the form of alkali lignin [221, 222]. Fractionation and recovery of lignin was studied by several researchers [163, 222–224]. With the development of high temperature and alkali resistant membranes, UF is used extensively for this purpose. Woerner and McCarthy [204] suggested that to produce purified high molecular weight lignin, UF should be operated at low pressure and high alkalinity. Purity of 85–90% of lignin was reported using a combination of ultrafiltration and diafiltration [213]. Lin and Detroit fractionated kraft lignin and obtained products with a wide a range of molecular weights [214]. UF was observed to reduce viscosity of kraft BL by removing high molecular weight lignin; BL then can be concentrated further before putting into the furnace. The recovery scheme may then become attractive from both economic and operational viewpoint [215]. A recent work highlighted determination of lignin molecular weight distribution in BL using UF membranes [225]. This method provides valuable insight to fractionation of BL

interactions [164–170]. Steric effects, attractive or repulsive interactions on solute retention are taken into account in these models. Understanding of membrane-solute interactions would help in development of new membranes which will be less prone to membrane fouling and adsorption [171]. Solute-membrane interactions may foul the membrane in two ways, namely, physiochemical solute adsorption on the pore wall and clogging the pores by solute aggregates [172]. These mechanisms can occur either separately or simultaneously. Many works in this area have been reviewed earlier [173–179].

In a recent work, it has been identified that the role of solute-solute interactions are manifested in variation of diffusivity and osmotic pressure, which govern the transport of the solution across the polarized layer and through the membrane [180]. The solute-membrane interactions further affect the transport of solute and solvent through the membrane pores. The interactions between solute-solute interactions may be quantified in terms of interaction potentials. The interaction potentials between two solute molecules in aqueous solution comprise of three components, the apolar Lifshitz-van der Waals, polar acid-base and electrostatic. Addition of these potentials gives the extended DLVO potential for the solute-solute interactions in a polar solvent. Estimates of the osmotic pressure and diffusivity may be obtained using these potentials which in turn may be used in the boundary layer theories for prediction of flux.

2.6.5 Flux paradox for colloidal suspensions and possible explanations

Film theory in terms of gel-polarization model is often used to calculate the steady state flux in CFUF or CFMF. These predictions are based on the mass transfer coefficient in the boundary layer. Brownian diffusivity obtained from Stokes-Einstein relation, is generally used for the estimation of mass transfer coefficients from their correlations. Based on this diffusivity, flux values predicted are one or more order in magnitude less than the experimental results [24, 126]. Green and Belfort [181]

termed this phenomena as flux paradox for colloidal suspensions. Several alternative mechanisms are proposed and they are broadly based on mechanisms of shear induced diffusivity, inertial lift and surface transport.

In the shear induced diffusion, solute particles experience random motion in the boundary layer and mutual interactions among them is more under the influence of high shear. Zydney and Colton [182] proposed in their model that Brownian diffusivity should be replaced by the shear induced diffusivity which is larger in magnitude (more than two orders). Shear induced diffusivity was first measured by Eckstein et al. [183] and was found to be proportional to the solute size. Davis and Sherwood [40] performed exact similarity solution of convective-diffusion equation for the solute mass balance using shear induced diffusion which is the dominant mechanism in back transport of the solutes. Their analysis included concentration dependency of viscosity and diffusivity which were obtained from Leighton and Acrivos [184, 185]. An alternative explanation was provided by Belfort and coworkers [181, 186–190]. According to them, inertial lift is responsible for augmented flux of colloidal suspensions. Inertial lift basically results out of nonlinear interactions between solute particles. If Reynolds number based on particle size are not small, then inertial term in Navier-Stokes equation cannot be neglected; inertial lift will then increase the lateral migration of particles away from the membrane and consequently, deposition on the surface becomes less.

Surface transport mechanisms suggest that the deposited particles on the surface experience a drag longitudinally due to shear forces. The rejected particles form a sort of flowing cake layer on the membrane surface [191, 192]. Both continuum and single particle models have been used to explain this mechanism. In the continuum approach, convective Navier-Stokes equations are solved in the cake layer [193] and in single particle models, force balance is performed on a single particle [194–198].

However, none of these mechanisms could provide satisfactory answers to flux paradox and incorporation of them in macroscale observations are quite difficult. Therefore, all the models discussed so far have their own limitations. For filtra-

tion of different solutes, different mechanisms are provided to explain flux decline phenomena.

2.6.6 Typical applications: Treatment of black liquor (BL) and micellar enhanced UF

Process streams from pulp and paper industries contain large volumes of water and valuable inorganic chemicals. Conventional regeneration process [199] recovers inorganic chemicals while destroying the organics, present in the BL, causing environmental pollution. Further, huge amount of scarce water is lost during the process. Membrane processes may be an attractive alternative in pulp and paper industry compared to conventional recovery process. Applications of membrane processes in pulp and paper industries have been reviewed extensively in this context [200–203]. Usage of membrane processes were identified broadly in the following applications: (i) concentration and recovery of water from process streams; (ii) recovery of valuable products which includes fractionation and purification of lignosulfonates from spent sulfite liquor and that of lignin from kraft black liquor. Potential impact of membrane based technology is usually three fold; namely, (i) it is less energy intensive; (ii) causes much less environmental pollution and, (iii) both inorganic and organic chemicals can be recovered [204].

Concentration of sulfite liquor and bleach plant effluent were carried out extensively by Wiley and his coworkers [205–208] using RO. They observed that the permeate stream was of high purity, having low BOD and COD. Membrane rejection of both organic and inorganic components were as high as 90%. A combination of RO and freeze concentration was also attempted [209]. In this case, RO was utilized to remove 90% of water from a stream containing 5 g/L of total dissolved solids. Retentate was further concentrated by freeze concentration to about 200 g/L. Attempts have also been made by Bhattacharya and his coworkers to treat BL, in context of separation, concentration and recovery of inorganic chemicals, using different membrane modules [216–220]. RO and UF were used to treat paper mill white wa-

ter [203]. A membrane rejection of over 99% was achieved. Removal of coloured chlorinated lignin from effluent of alkali extraction step was also reported [202]. Ten fold concentration of dilute pulp wash water from a high yield chemi-mechanical pulping process was observed [210]. High values of solids rejection were achieved. However, a decrease in flux rate due to fouling by colloidal organics was observed. Much of these as well as other treatments of BL using membrane technology were extensively reviewed earlier [200–203].

UF can play an important role in fractionation and purification of lignosulfonates (from spent sulfite liquor) and that of lignin (from kraft BL). The purpose of UF is two fold: (i) separation of lignin compounds from low molecular weight organic and inorganic compounds and, (ii) fractionation of high molecular weight lignin compounds. Typical spent sulfite liquor contains approximately 60% lignin, 30% reducing sugar and 10% inorganic materials. Using UF, it is possible to separate the spent liquor into purified fractions of lignosulfonates and sugars [203, 211]. Purity of lignosulfonates to a tune of 80% was reported with simple UF and upto 95% was obtained using a combination of diafiltration and UF [202, 212]. Lignin in kraft BL occurs in the form of alkali lignin [221, 222]. Fractionation and recovery of lignin was studied by several researchers [163, 222–224]. With the development of high temperature and alkali resistant membranes, UF is used extensively for this purpose. Woerner and McCarthy [204] suggested that to produce purified high molecular weight lignin, UF should be operated at low pressure and high alkalinity. Purity of 85–90% of lignin was reported using a combination of ultrafiltration and diafiltration [213]. Lin and Detroit fractionated kraft lignin and obtained products with a wide a range of molecular weights [214]. UF was observed to reduce viscosity of kraft BL by removing high molecular weight lignin; BL then can be concentrated further before putting into the furnace. The recovery scheme may then become attractive from both economic and operational viewpoint [215]. A recent work highlighted determination of lignin molecular weight distribution in BL using UF membranes [225]. This method provides valuable insight to fractionation of BL

using UF processes. Electrodialysis (ED) is a well-studied field to recover sodium compounds from BL [226, 227]. However, It has been observed that recovery is not satisfactory whereas, energy cost is very high for ED process.

Surfactant based separation processes are a new generation of industrial separation techniques which are emerging rapidly. Micellar enhanced UF (MEUF) is an effective method to remove dissolved organics as well as inorganics from aqueous streams, either separately or simultaneously. Beyond a certain surfactant concentration, known as critical micelle concentration, surfactants form aggregates (micelles) in the bulk of the solution. In aqueous solution, the outer part of the micelles is hydrophilic and inner core is hydrophobic. Ionic species having charges opposite to that of the micelles are bound to the micelles through electrostatic attraction. Any organic solute present in the solution will be solubilized in the hydrophobic core of the micelles. If now the resultant solution is filtered by a UF membrane having pores less than the sizes of the micelles, permeate will then be almost pure water. Scamehorn and his coworkers attempted pioneering works in the field of MEUF [228–232]. They established that cationic surfactants are best in general for removal of organic solutes from aqueous streams [228, 229]. In these studies, 4-t-butyl phenol was used as organic solute and cetyl pyridinium chloride (CPC) was used as surfactants. Effects of concentration polarization on the performance of MEUF was also studied [228]. Using a 10K membrane, solute retention as high as 99.6% was achieved. Solubilization of cresols by CPC micelles and removal of micelles by UF was also studied in detail [231]. In this case also, a retention of more than 97% was reported. Gibbs et al. [230], studied MEUF of n-alcohols by CPC micelles. They observed that alcohol rejection varied from 71% to 98.8% for different operating conditions. Rejection increases with increase in hydrocarbon chain length of the alcohol and decrease in alcohol/surfactant ratio. Excellent fluxes through the membrane were reported. Removal of ionic pollutants and their mixtures using MEUF was also available [228, 232]. In this case also high solute rejections were observed.

Chapter 3

Prediction of flux and retention

It is clear from the earlier chapters that the decline of flux during UF, as a consequence of concentration polarization, is the most vital issue in designing the UF systems. This chapter deals with some analyses of the various consequences of concentration polarization on flux decline. Attempts have been made to develop predictive models both theoretical and semi-empirical. Efforts have been made to cover as broad horizon as possible, including different module configurations and several feed solutions.

3.1 Flux prediction for black liquor in a cross flow ultra-filtration

First section of this chapter deals with experimental (parametric) study of flux decline and retention characteristics of BL in CFUF system. A theoretical model is also developed for this purpose. Standard solutes are used for the testing of the model.

3.1.1 Introduction

Recovery of inorganic chemicals from black liquor is an integral part of kraft pulping process. Black liquor (BL) of 15% total dissolved solids (tds) is concentrated and then incinerated and causticized to recover sodium hydroxide, the required chemical for alkaline pulping, in conventional kraft recovery process. A large volume of

water is thus also evaporated during concentration. With rising energy cost, capital investment and stricter environmental regulations, more economical alternatives are necessary for the treatment of BL. Ultrafiltration (UF) is one such viable unit operation which offers promise to this problem. The process may be used not only to recover water, but also to recover valuable chemicals from black liquor. Further, the process being non-destructive, will be attractive with regard to pollution.

Several attempts were made to concentrate the weak BL [205, 206] by reverse osmosis (RO) with high rejection values. These attempts were not observed to be attractive because of the cost and fouling of the membranes. It was thought that UF being less energy intensive compared to RO as well as membrane being more open may be of more use for treating BL. However, in any pressure driven membrane processes, flux declines with time which makes it less attractive for industries to accept. Several efforts have been made to treat BL and study its limiting flux phenomena in stirred ultrafiltration [137, 216–219], unstirred ultrafiltration [123, 204] and diafiltration [204].

In ultrafiltration, the flux decline is due to concentration polarization [125]. Several theories have been put forward to understand, quantify and control this phenomena of concentration polarization [11, 24, 145, 150, 233]. Black liquor, a polydispersed solution of solutes of wide molecular weight range, is susceptible to severe polarization in batch cells. One way to reduce concentration polarization is to allow the feed solution to flow tangentially over the membrane surface, known as cross flow ultrafiltration (CFUF). This causes reduction in growth of the boundary layer near the surface and increase in back diffusion from the surface to the bulk of the solution. Hence, permeate flux can be increased significantly.

Prediction of flux and membrane surface concentration (and so, real rejection and extent of concentration polarization) is of utmost importance for the process engineers in UF processes. An attempt has been made in the present work to predict flux under cross flow ultrafiltration of kraft BL. Earlier, CFUF in laminar flow regime for high molecular weight solutes in a channel was studied in detail [19, 44] and

an integral solution to predict flux was proposed. The similarity solution for cross flow microfiltration, where a lumped variable out of the independent variables was used to simplify the governing mass balance equation, was also proposed [40]. A similarity model for gel layer controlled UF was proposed [20] where the solutes were supposed to form a gel and constant gel concentration was determined from an independent set of experiments. From the earlier studies [113, 123, 137], it was observed that BL does not exhibit distinct gel layer formation in the range of moderate operating conditions of ultrafiltration. Further, UF of low molecular weight solutes is generally considered and analyzed through osmotic pressure controlled phenomena [19, 123, 152]. Studies [113, 123, 137] have also revealed that osmotic pressure of BL is appreciable and more so, when it is in degraded form [219]. In view of this, an attempt has been made to modify the model proposed by Shen et al. [20] for the osmotic pressure controlled UF to predict flux and real rejection.

Since BL is a mixture of the solutes of different molecular weights, the treatment of it was studied in three different schemes to observe rejection behaviour and flux. Two different cut-off membranes were selected; one with low rejection (LRUF) and the other with high rejection (HRUF). Apart from their direct use with BL, a combination (LRUF followed by HRUF) was also attempted. The present work also incorporated the effect of permeate concentration in comparison to the earlier model [20] of 100% rejection analysis. Thus, the developed model may be utilized to predict the permeate flux for both LRUF and HRUF.

The efficacy of the model was supported by the use of standard macromolecules (PEG-6000 and dextran-18,600) with LRUF membrane. Choice of these solutes were made to obtain moderate rejection for PEG and complete rejection for dextran. Taking the whole range on rejection behaviour from the low rejection of BL to the total rejection of dextran, may prove the wide applicability of the analysis of the model. An effort was also made to predict concentration build up on the surface, concentration profile across the channel length and development of the concentration boundary layer. Finally, it should be mentioned that the purpose of this paper

presentation is not to address the technological aspects of BL treatment, rather the emphasis is on to predict flux and rejection behaviour of BL ultrafiltration.

3.1.2 Theory

An attempt is now being made to modify [20] and develop a model to predict permeate flux averaged over its length of flow from the basic approach of solving the governing solute mass balance equation along with its boundary conditions. Fig. (3.1) shows the schematic of a cross flow system.

Assumptions made in this model are, i) flow is steady; this is reasonable due to the fact that steady permeate flux is obtained within a short period of time from beginning of the operation, ii) diffusion in x-direction is negligible compared to convection in x-direction, iii) flow is laminar and fully developed, iv) since permeate velocity is very small compared to the bulk velocity, the parabolic velocity profile is assumed to be unperturbed, v) neglecting the variation of surface concentration (c_m) in the x-direction at $y=0$, c_m is assumed to be constant, vi) physical properties are constant.

With the above assumptions, solute mass balance gives,

$$u \frac{\partial c}{\partial x} + v \frac{\partial c}{\partial y} = D \frac{\partial^2 c}{\partial y^2} \quad (3.1)$$

where the axial velocity profile may be taken [234], as:

$$u = \frac{3}{2} u_0 \left[1 - \left(\frac{y-h}{h} \right)^2 \right] \quad (3.2)$$

Within the thin concentration boundary layer, y is much smaller than the channel half height h and so, Eq. (3.2) can be approximated as (neglecting y^2/h^2),

$$u = \frac{3u_0 y}{h} \quad (3.3)$$

Assuming no permanent (irreversible) adsorption of the solutes on the membrane surface which may be possible under cross flow and with the choice of non-

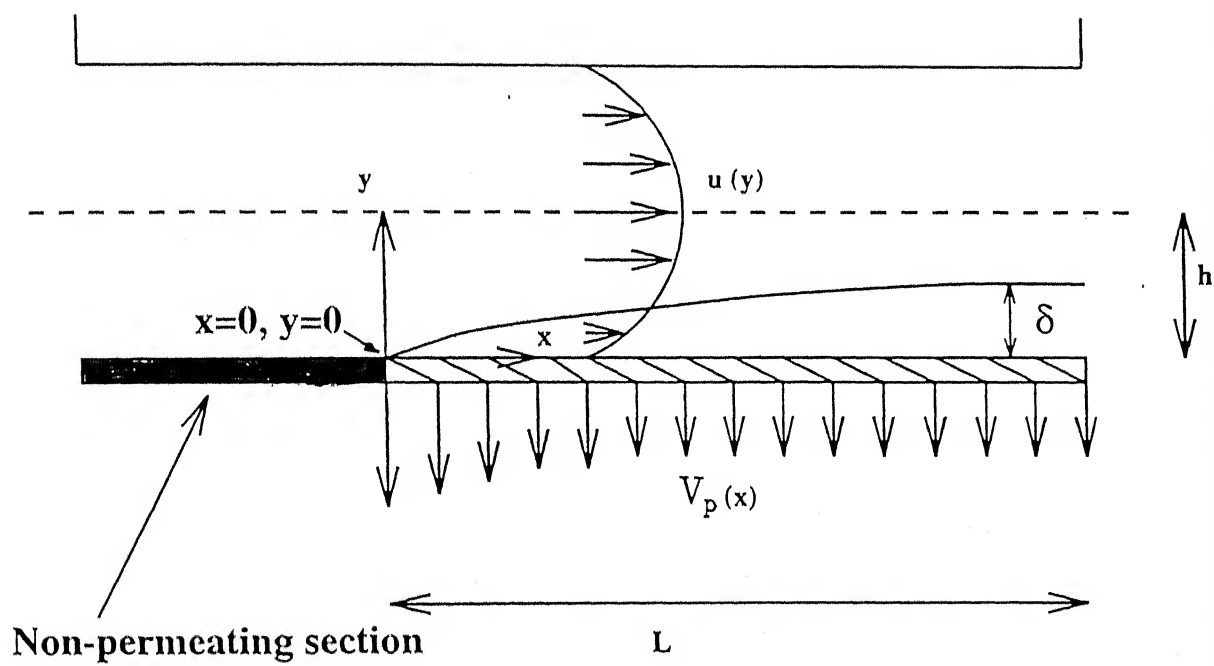


Figure 3.1: Schematic diagram of a cross flow unit

adsorbing membranes. This was verified from the measurement of water permeability before and after each of the experimental runs,

$$v = -v_p \quad (3.4)$$

The boundary conditions of the differential Eq. (3.1) are as follows

$$c = c_m \text{ at } y = 0 \quad (3.5)$$

At the membrane surface, the concentration is more than the bulk; back diffusion occurs from the surface to the bulk. This is opposite to the convective movement of the solutes towards the membrane surface. At steady state, the combinations of these two opposing fluxes are equal to the convective flux of the permeating solute. This gives rise to the following boundary condition,

$$v_p c + D \frac{\partial c}{\partial y} = v_p c_p \text{ at } y = 0 \quad (3.6)$$

Finally, in the bulk, solute concentration is constant beyond the concentration boundary layer, the thickness of which is negligible compared to the channel height. Hence, a common way [20, 235] to represent a boundary condition is,

$$c = c_0 \text{ at } y = \infty \quad (3.7)$$

A similarity solution of the above differential Eq. (3.1), with boundary conditions, is obtained by defining a dimensionless variable (lumped parameter),

$$\eta = y \left[\frac{u_0}{hx D} \right]^{\frac{1}{3}} \quad (3.8)$$

and dimensionless concentration as

$$c^*(\eta) = \frac{c}{c_0} \quad (3.9)$$

In terms of η and c^* , Eq. (3.1) becomes an ordinary differential equation of second order as follows,

$$\frac{d^2 c^*}{d\eta^2} = - \left(\eta^2 + \left[\frac{hx}{u_0 D^2} \right]^{\frac{1}{3}} v_p \right) \frac{dc^*}{d\eta} \quad (3.10)$$

For constant physical properties and channel geometry [234], we have, $v_p x^{\frac{1}{3}} = \text{constant}$. Thus, a non-dimensional form of the same can be defined as,

$$v_p \left[\frac{hx}{u_0 D^2} \right]^{\frac{1}{3}} = A_1 \quad (3.11)$$

Therefore, Eq. (3.10) becomes,

$$\frac{d^2 c^*}{d\eta^2} = -(\eta^2 + A_1) \frac{dc^*}{d\eta} \quad (3.12)$$

The transformed boundary conditions are,

$$c^* = 1 \quad \text{at} \quad \eta = \infty \quad (3.13)$$

$$\frac{dc^*}{d\eta} + A_1 c^* = A_1 c_p^* \quad \text{at} \quad \eta = 0 \quad (3.14)$$

The solution of Eq. (3.12) with the boundary conditions, Eqs. (3.13) and (3.14), is given as,

$$c^*(\eta) = K_1 \int_0^\eta \exp \left[-\frac{\eta^3}{3} - A_1 \eta \right] d\eta + K_2 \quad (3.15)$$

where,

$$K_1 = A_1 \frac{1 - c_p^*}{A_1 I_1 - 1} \quad (3.16)$$

$$K_2 = \frac{A_1 I c_p^* - 1}{A_1 I_1 - 1} \quad (3.17)$$

$$I_1 = \int_0^\infty \exp \left[-\frac{\eta^3}{3} - A_1 \eta \right] d\eta \quad (3.18)$$

Further, total average flux over the length of the membrane is obtained by using Eq. (3.11) as,

$$\begin{aligned} V_p &= \frac{1}{L} \int_0^L v_p dx \\ &= 1.5 \left[\frac{u_0 D^2}{hL} \right]^{\frac{1}{3}} A_1 \end{aligned} \quad (3.19)$$

Flux is predicted with the help of above analysis in conjunction with phenomenological equation,

$$V_p = L_p (\Delta P - \Delta \pi) \quad (3.20)$$

where,

$$\Delta\pi = \pi_m - \pi_p \quad (3.21)$$

With a guess value of A_1 , V_p and c_m can be predicted by trial and error from Eqs. (3.19) and (3.20) and the concentration profile can be obtained using Eq. (3.15). For a membrane with 100% rejection, c_p^* must be put to zero in the above equations. One may note that in this analysis, experimental c_p values are used for the prediction of flux. Further, all the physical properties are evaluated at the bulk concentrations.

3.1.3 Experimental

3.1.3.1 Materials

Asymmetric cellulose acetate membrane was used for ultrafiltration as low rejecting membrane (LRUF). It was obtained from *Permionics (India)*. The molecular weight cut off (MWCO) was approximately 1000 as specified by the manufacturer. For high rejection, a thin film composite (TFC) membrane was used which was supplied by *Hydranautics India Ltd (HRUF)*. The MWCO of this membrane was approximately 500 as specified by the manufacturer. The membranes were anisotropic, hydrophilic and of flat rectangular sheet type with an operating pH range of 2–12. The water permeability and general rejection behaviour of these membranes with respect to standard non-ionic solutes are presented in the appendix (Fig. A1). The membrane was supported on a porous sheet. The solutes for UF were : (i) polyethylene glycol (average molecular weight 6000), obtained from *Loba Chemie Indo-Austranal Co. India*, (ii) dextran (average molecular weight 18,600), obtained from *Sigma Chemicals, USA* and Black liquor was procured from *Central Pulp Mills, Surat*. BL was diluted with distilled water for different concentrations.

3.1.3.2 Apparatus

A cross sectional diagram of the rectangular cell, used in this study, is shown in Fig. (3.2). It was cast in gun metal and to avoid corrosion, nickel plating was done. The cell was of 0.4 m in length and 0.06 m in width. A neoprene rubber gasket of width 0.01 was placed inside the cell. The channel height was determined by the thickness of the gasket. Incidentally, two gaskets of different thicknesses had to be used because of the availability. Runs for LRUF were carried out with 1.5 mm thickness whereas 5.4 mm thickness was used for HRUF runs. Since, the objective was to keep the cross flow velocity for HRUF runs as constant, it was not felt to be a big hindrance for the work in changing the gasket thickness. In order to allow the feed to be fully developed in the channel, the maximum entrance length was determined to be 0.05 m depending upon the maximum Reynolds number [235] possible to attain with the set up. Hence, this much entrance length was kept blank with a plastic sheet. Effective filtration area was $0.33 \text{ m} \times 0.04 \text{ m}$ for low rejecting and $0.25 \text{ m} \times 0.04 \text{ m}$ for high rejecting membranes (the filtration areas for the membranes are different due to the availability of different sizes of the original membrane sheets). The cross flow cell was connected to a reciprocating pump of capacity 5 liter/min.

3.1.3.3 Analysis

The black liquor analysis is given in Table 3.1. The major inorganic contents were calculated by pH metric triple titration method [236]. The molecular weight of black liquor was obtained from the studies of Bhattacharjee and Bhattacharya [123]. Total dissolved solids in black liquor was determined by evaporating the sample in an oven at $105 \pm 3^\circ\text{C}$. The concentrations of non-ionic organic solutes were determined by the refractive index calibration. A Bausch and Lomb refractometer was used for this purpose. The physical properties of the solutes used in UF are listed in the appendix B.

Table 3.1: Analysis of black liquor

Total dissolved solids	15%
Organics (dry basis)	68%
Inorganics (dry basis)	32%
Na ₂ S	1.11 g/l
NaOH	0.174 g/l
Na ₂ CO ₃	3.50 g/l

3.1.3.4 Experimental design

Experiments were designed to observe the variation of operating conditions (pressure difference, cross flow velocity and feed concentration) on the steady state flux and rejection. The range of independent variables were: pressure (275, 415 and 550 kPa), recirculation flow rate (2.22×10^{-5} , 2.80×10^{-5} , 3.33×10^{-5} m³/s) and feed concentration of BL (10, 30, 50 and 70 kg/m³) and that for PEG and dextran (10, 30 and 50 kg/m³). One parameter was varied and the other two were held constant to get an exact picture of dependence. All possible combinations were taken into account. Therefore, a total number of experiments for PEG and dextran were 54 (27 each). For black liquor, total 36 runs were carried out with all possible combinations of the operating conditions. To study the rejection behaviour of BL, three schemes were chosen. In scheme A and B, BL was subjected directly to LRUF and HRUF, respectively. In scheme C, the permeate of LRUF was taken as feed to HRUF. The operating conditions for HRUF runs were: pressure 1722 kPa and recirculation flow

rate $2.22 \times 10^{-5} \text{ m}^3/\text{s}$.

3.1.3.5 Procedure

First, membranes were compacted at 690 kPa (for LRUF) and at 1895 kPa (for HRUF) which are higher than the highest operating pressures at $2.22 \times 10^{-5} \text{ m}^3/\text{s}$ for six hours with distilled water. At the same flow rate, water flux was measured at different pressures to determine the membrane permeability. The schematic diagram of the experimental set up is shown in Fig. (3.3). Feed tank was filled with 2.5 – 3.0 liter feed solution and the pump was made operative. Instantaneous pressure difference was reached (within 10 seconds). Cumulative volume of permeate was measured as a function of time at a fixed operating conditions. This was continued till steady state flux value was reached. All the experiments were carried out between 26°C and 31°C . Hence, all properties were corrected at 30°C . Typically, steady state was reached within 6–8 minutes with low rejecting membranes. Therefore, LRUF runs were of half an hour duration. However, runs with high rejecting membrane were of one hour duration. In scheme C (LRUF followed by HRUF), for the treatment of BL, LRUF runs were of very long duration ranging from 12 to 16 hours to collect sufficient (~ 3 liter) volume of the permeate, maintaining the feed concentration constant. This was done approximately by adding freshly prepared feed solution, equal to the measured concentration and volume of the permeate solution to the feed tank after every 15 minutes. After each run, feed tank and the set up including the membrane was washed with recirculating distilled water at the lowest pressure and highest flow rates for nearly 30 minutes. After washing, water run was taken afresh to measure the membrane permeability and to check for its adsorption. Once original permeability was regained the next run was taken. Apart from major results discussed in the following section, some typical results for BL are also produced in the form of Tables 3.2, 3.3, and 3.4.

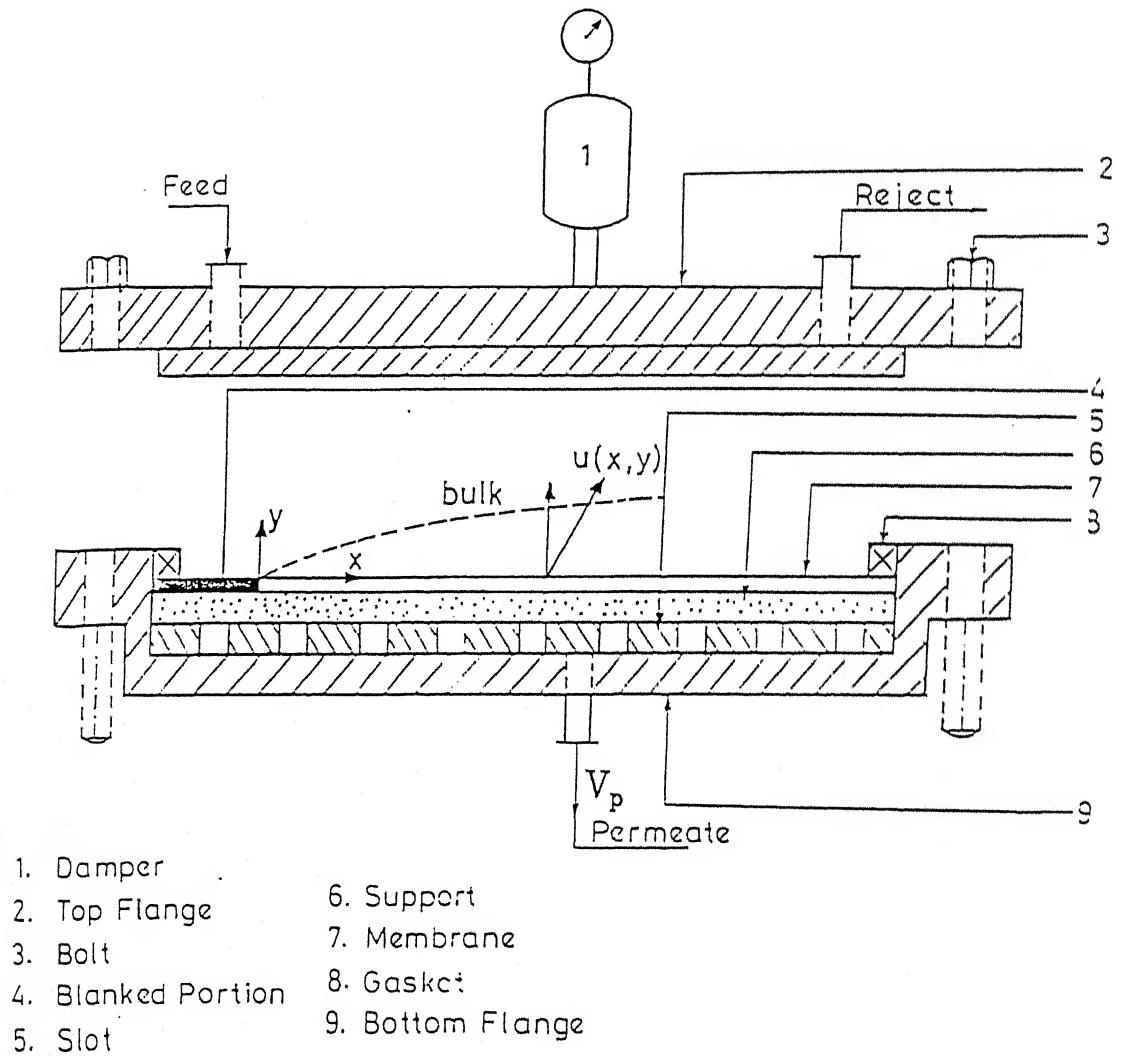
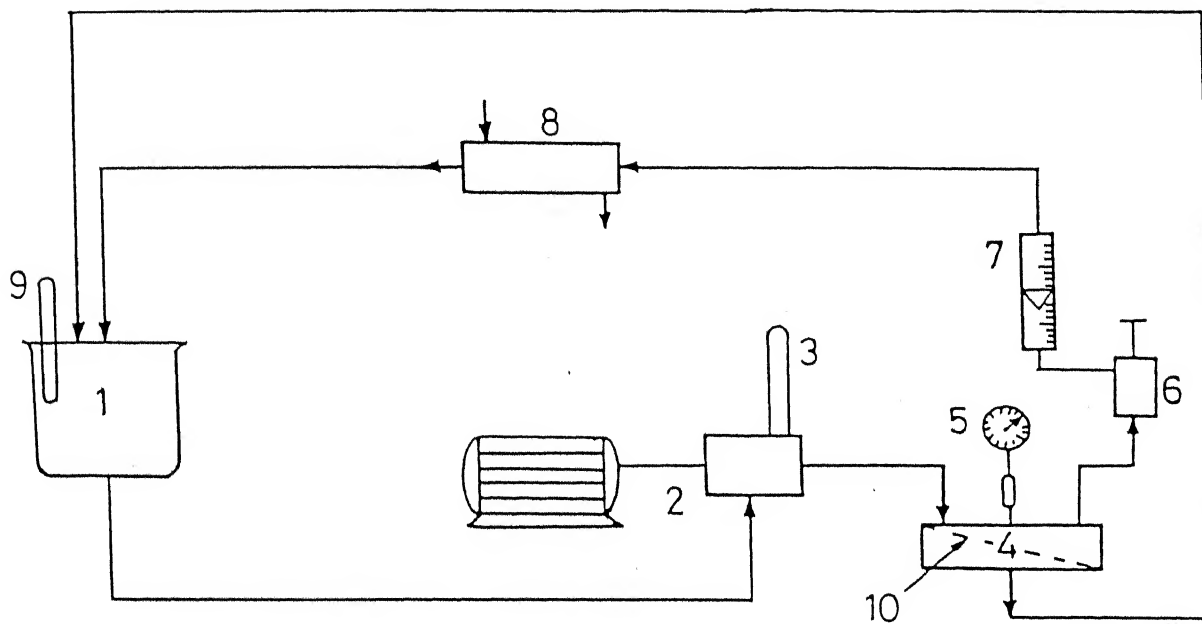


Figure 3.2: Cross section view of the cross flow cell



- | | |
|-------------------|----------------------------|
| 1. Feed tank | 6. Back pressure regulator |
| 2. Pump | 7. Rotameter |
| 3. Damper | 8. Heat exchanger |
| 4. UF Cell | 9. Thermometer |
| 5. Pressure gauge | 10. Membrane |

Figure 3.3: Line diagram of the experimental set up

Table 3.2: Results for scheme A (Direct LRUF of BL)

c_0	ΔP	$Q(\times 10^5)$	c_p	R_0	$v_p^{exp}(\times 10^6)$	Feed pH	Permeate pH
kg/m ³	kPa	m ³ /s	kg/m ³	%	m ³ /m ² .s		
30	275	2.22	22.8	24	3.60	11.20	11.55
50			36.0	18	2.93	11.49	11.83
70			50.4	18	1.97	11.60	11.95

Table 3.3: Results for scheme B (Direct HRUF runs)

c_0	ΔP	$Q(\times 10^5)$	c_p	R_0	$v_p^{exp}(\times 10^6)$	Feed pH	Permeate pH
kg/m ³	kPa	m ³ /s	kg/m ³	%	m ³ /m ² .s		
30	1722	2.22	2.4	92	3.66	11.20	11.50
50			6.0	88	2.75	11.49	11.75
70			10.5	85	2.23	11.60	11.92

Table 3.4: Results for scheme C (LRUF followed by HRUF)

c_0	ΔP	$Q(\times 10^5)$	c_p	R_0	$v_p^{exp}(\times 10^6)$	Feed pH	Permeate pH
kg/m ³	kPa	m ³ /s	kg/m ³	%	m ³ /m ² .s		
22.8	1722	2.22	1.14	95	4.22	11.55	9.80
36.0			2.52	93	3.10	11.83	10.43
50.4			4.54	91	2.58	11.95	11.05

3.1.4 Results and Discussions

3.1.4.1 Selection of feed solution concentration

Depending on the type of alkaline pulping, capacity of the industry and raw materials used, paper mills produce black liquor of different composition and concentration. The concentration of effluent from brown stock washers in bigger mills is around 15% and that for smaller mills is 1–8% (total dissolved solids content).

The selection for concentration of black liquor to be treated by asymmetric membranes is important. At higher concentrations, osmotic pressure of BL increases [219], therefore, permeate flux decreases to a large extent. Hence, at higher concentrations, low flux values poses difficulties for comparative studies in the laboratory scale. Further, viscosity of BL also increases at higher concentration and handling of concentrated liquor by the ordinary pumps becomes difficult.

BL is composed of large number of macromolecular solutes of different molecular weights. During the ultrafiltration operation, solutes of lower molecular weight clog the pores; therefore, reuse of the membrane becomes difficult. For all these reasons, concentrations of BL chosen as 10, 30, 50 and 70 kg/m³. This range of concentration covers small scale paper industry effluents as well as half of the bigger paper mills. For comparative studies, PEG and dextran concentrations are chosen as 10, 30 and 50 kg/m³.

3.1.4.2 Effect of operating conditions on flux and rejection

The effect of operating pressure on the permeate flux for different solute concentrations is shown in Fig. (3.4) and (3.5) along with pure water flux. From the figures it can be observed that permeate flux increases with pressure but at higher pressure increment is gradual. At higher pressure, rise in concentration polarization results in an increase in membrane surface concentration which in turn increases osmotic pressure of the solution at the membrane surface. Therefore, net driving force to

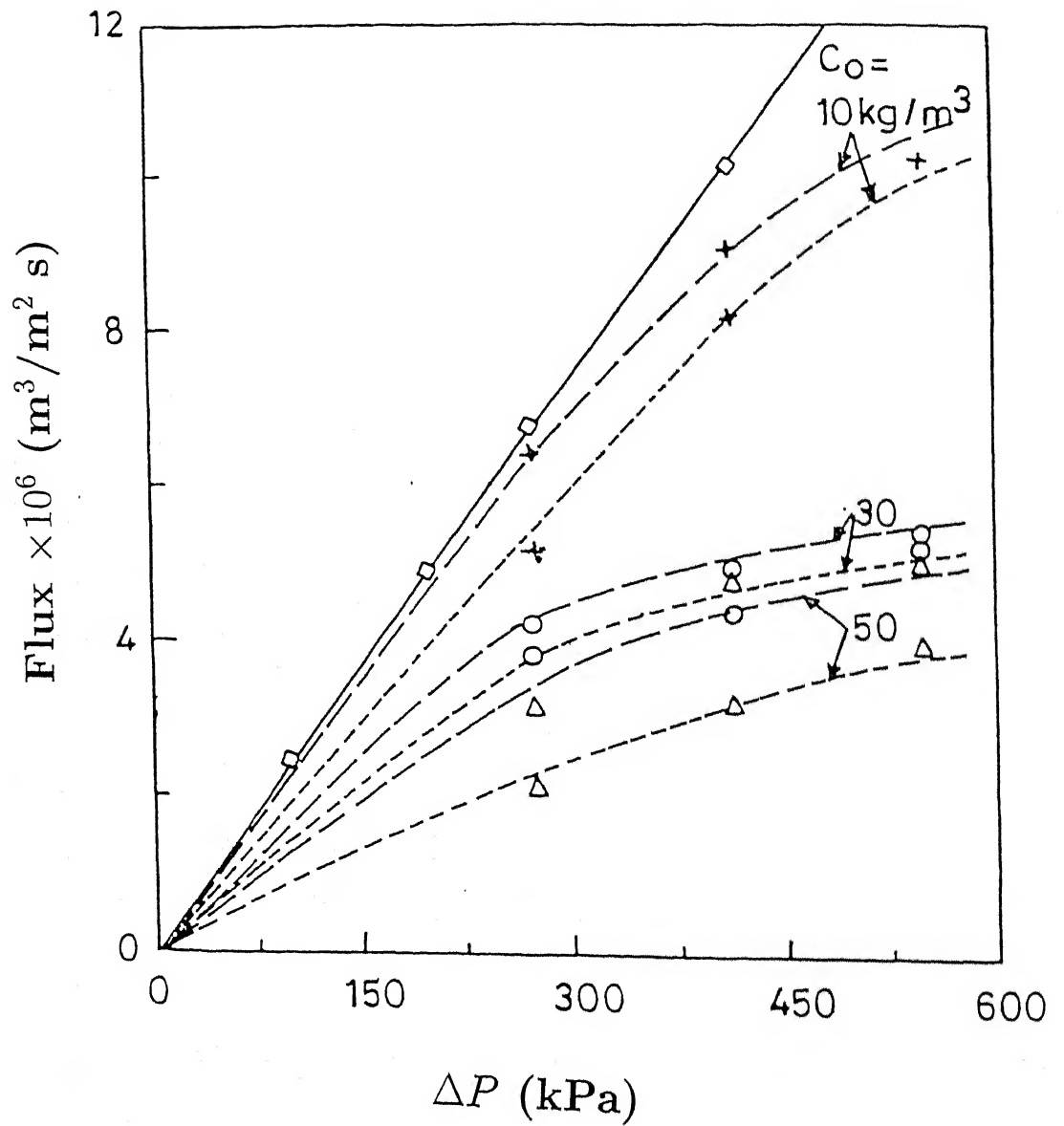


Figure 3.4: Effect of pressure on experimental flux for PEG and dextran at $Q = 2.80 \times 10^{-5} \text{ m}^3/\text{s}$. Solid line is for water flux, long dashed lines are for dextran and small dashed lines are for PEG.

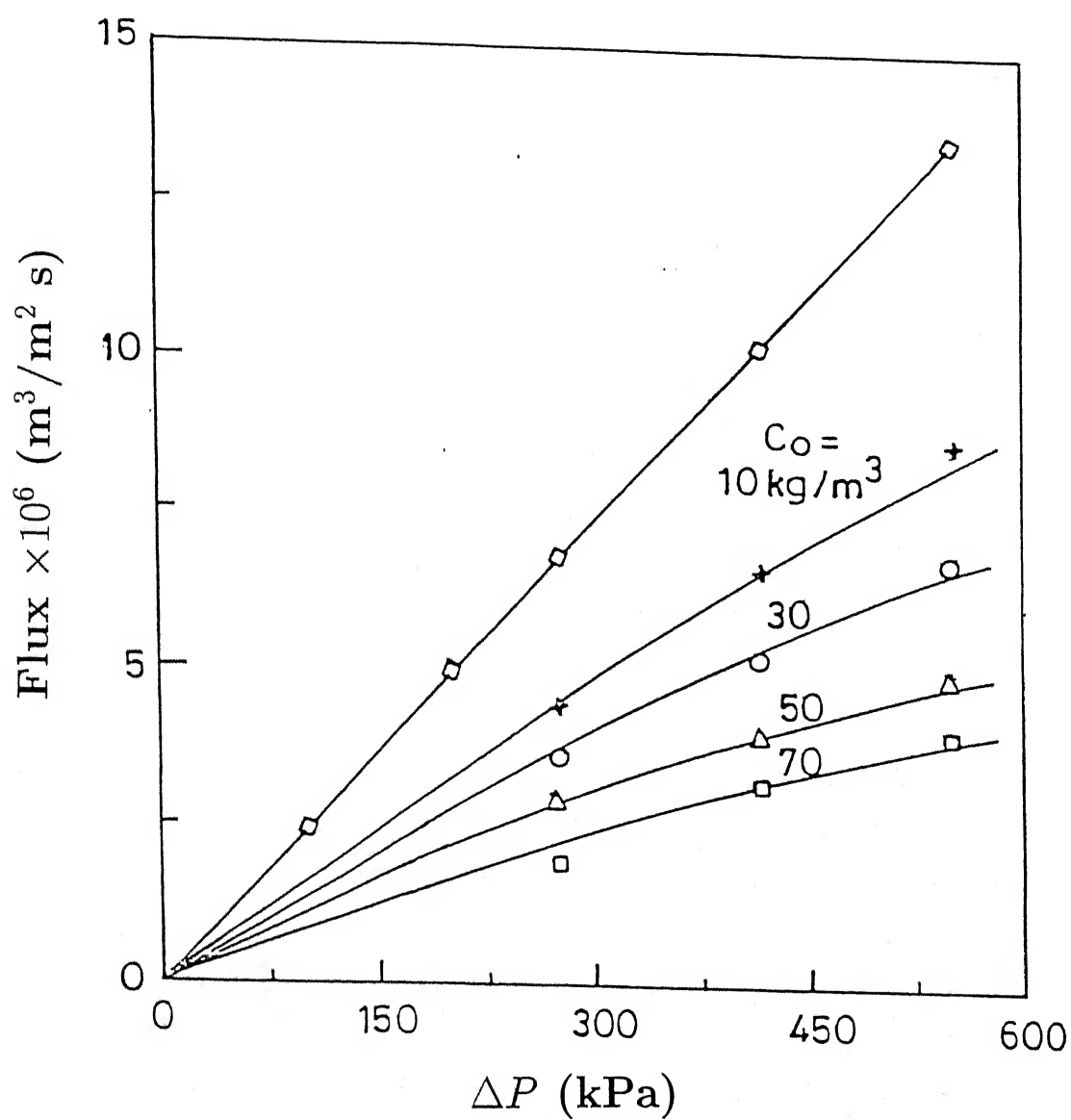


Figure 3.5: Effect of pressure on experimental flux for BL at $Q = 2.22 \times 10^{-5} \text{ m}^3/\text{s}$. Curve with diamonds is for water flux.

CENTRAL LIBRARY
I I T. KANPUR

Acc. No. A 123605

the transport of solutes decreases and flux decreases. Since, osmotic pressure varies with concentration non-linearly, the increase in flux at higher pressure is gradual. This trend of permeate flux with pressure was also reported by Tsapiuk et al. [237] for PEG and Van Oers et al. [152] for dextran. From Fig. (3.4) and (3.5), it is also evident that flux decreases at higher feed concentrations at a fixed operating pressure. At higher feed concentration membrane surface concentration increases and so, osmotic pressure of the solution also increases and thereby, permeate flux decreases.

Fig. (3.6), shows the variation of the observed rejection with pressure. Dextran solutions of all concentrations and PEG with lowest concentration i.e. 10 kg/m^3 were completely retained by the membrane. However, with increase in concentration of PEG, the rejection decreases. This is obvious because of the increase of concentration polarization with increase in feed concentration. Further, even with increase in pressure as depicted in Fig. (3.6), the rejection of PEG decreases. This may be again attributed to the fact that increase in pressure increases convective motion of solutes towards the membrane, causing severe concentration polarization. Concentration polarization results in increasing local solute concentration on the membrane surface which promotes the solute flux through the membrane [238]. Therefore, R_0 decreases as polarization increases. Similar rejection behaviour was also observed for PEG by Tsapiuk et al. [237], for protein bovine serum albumin by Opong et al. [239], and for γ -albumin by Pradanos et al. [240]. Also, at higher pressure, flexible PEG molecules deform and pass through the membrane [114, 217, 237]. For BL, observed rejection increases with pressure and reaches an asymptotic value; however, it decreases with increase in feed concentration. BL is a complex mixture of inorganics (NaOH , Na_2S , Na_2CO_3 , etc.) and organics (alkali lignins, etc.), present in both bound and free form. Even organics have a wide molecular weight distribution. As pressure increases, concentration polarization allows more solute to permeate but higher molecular weight organics retained by the membrane increases viscosity of the solution near the membrane surface. This viscous layer is responsible for pre-sieving of the organic

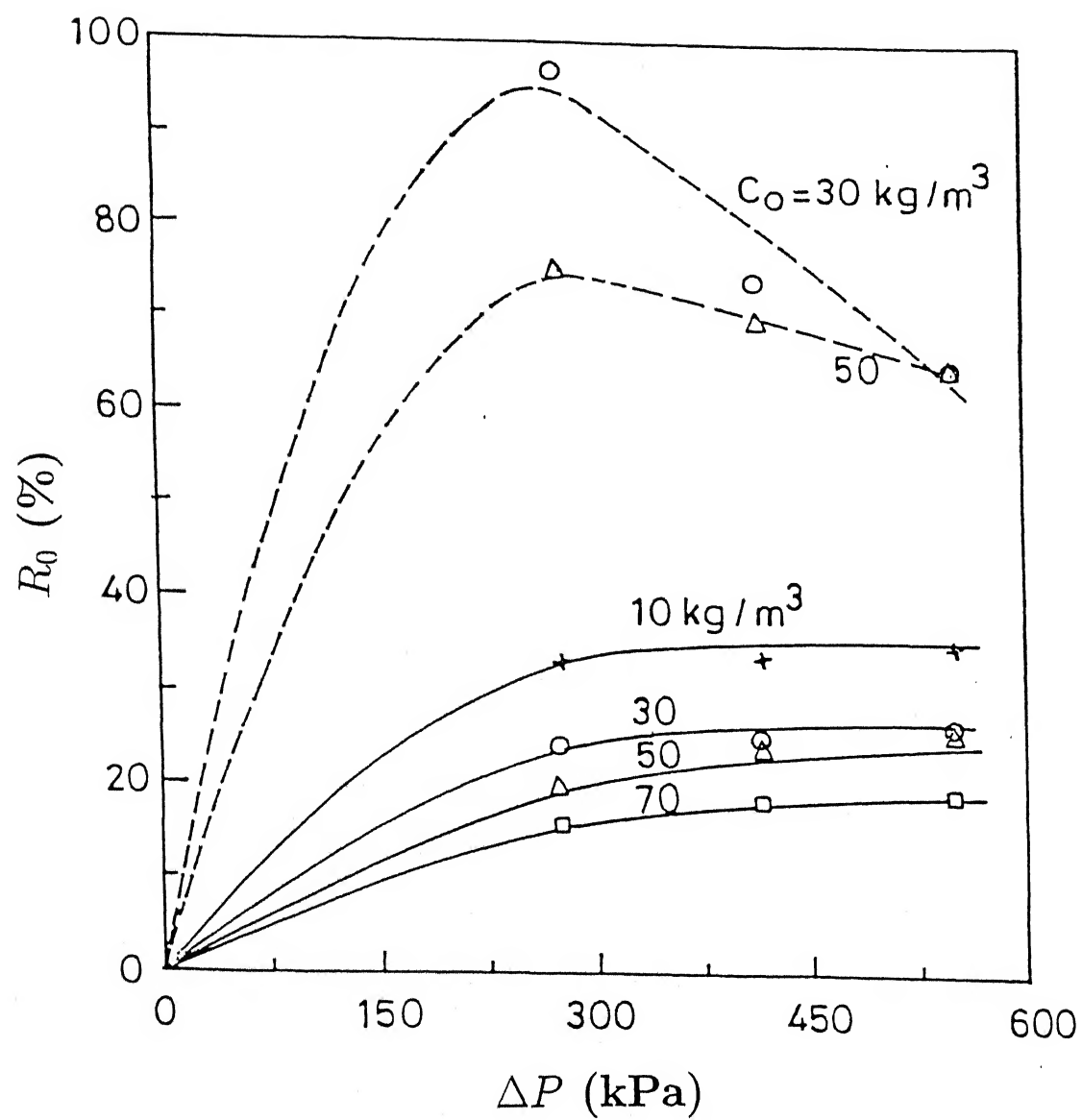


Figure 3.6: Effect of pressure on observed rejection for BL at $Q = 2.22 \times 10^{-5} \text{ m}^3/\text{s}$. Solid curves are for BL and dashed curves are for PEG.

solutes. However, free inorganics pass through the membrane.

Probably, due to the combined effects of these factors lead to almost constant rejection of BL at higher pressure.

3.1.4.3 Flux and membrane surface concentration

In general, for UF, permeate flux and surface concentration are interrelated. If c_m increases, osmotic pressure at the surface increases, therefore, flux declines. Hence, an estimate of c_m provides an insight in flux decline behaviour, extent of concentration polarization and other informations.

3.1.4.4 Algorithm used for V_p and c_m prediction

- i) A value of A_1 was assumed.
- ii) V_p was computed from Eq. (3.19).
- iii) c_m was computed from the phenomenological equation i.e. Eq. (3.20).
- iv) c_m was computed from Eq. (3.15).
- v) If the difference between c_m values calculated from step (iii) and (iv) were less than 0.001, the program was terminated and corresponding V_p and c_m values were recorded. If not, another value of A_1 was guessed in step (i) and the process was iterated till the prescribed convergence was achieved.

3.1.4.5 Growth of concentration boundary layer

Near the membrane surface, solute concentration is more than that in the bulk. Within the channel, along the length, c reaches c_0 at different normal locations, thereby giving rise to a concentration boundary layer. Improvement of flux depends on reduction of this layer. The developed model equations provide the concentration boundary layer at particular operating conditions as shown in Fig. (3.7). This illustrates the trajectory for different solutes to attain the bulk concentration. The concentration boundary layer decreases for PEG, BL and dextran (in that order).

This may be explained due to their back diffusion phenomena. Since diffusivity is inversely proportional to the molecular weight and molecular weight of the solutes in the increasing order are PEG (6000), BL (7000) and dextran (18,600), PEG diffuses faster than dextran to attain the bulk concentration. It can be observed from the figure that for PEG and BL, the boundary layer growth is around 5% of the half channel height. For dextran it is around 3%. Hence, the boundary layer is very thin compared to the channel height which justifies the theoretical consideration in the present model. However, boundary layer reaches an asymptotic value at the end of about 80% channel length. Obviously, such growth of concentration boundary layer can further be minimized by increasing cross flow velocity as shown in Fig. (3.8). Increase in cross flow velocity increases back diffusion, therefore reduces the growth of boundary layer. As Q increases by 33% (from 2.22×10^{-5} to $3.33 \times 10^{-5} \text{ m}^3/\text{s}$), steady state boundary layer thickness reduces by 8% for PEG and 12% for BL.

3.1.4.6 Concentration profile

Concentration profile for BL in the channel at different longitudinal positions is shown in Fig. (3.9). At a fixed axial position, concentration drops almost linearly from the membrane surface concentration to the bulk concentration. As the solute travels downstream of the channel, the drop of concentration to the bulk value is delayed i.e. at a longer distance along the channel, membrane surface concentration achieves the bulk value at a higher normal distance. This is obvious because physically, along the length, as distance increases more solutes deposit on the surface which increases boundary layer thickness and so, attainment of the bulk concentration is prolonged. In conjunction of Fig. (3.7) it can be observed that rate of attainment of bulk concentration is slowed down along the downstream of the channel which signifies that boundary layer thickness tends to reach an asymptotic value.

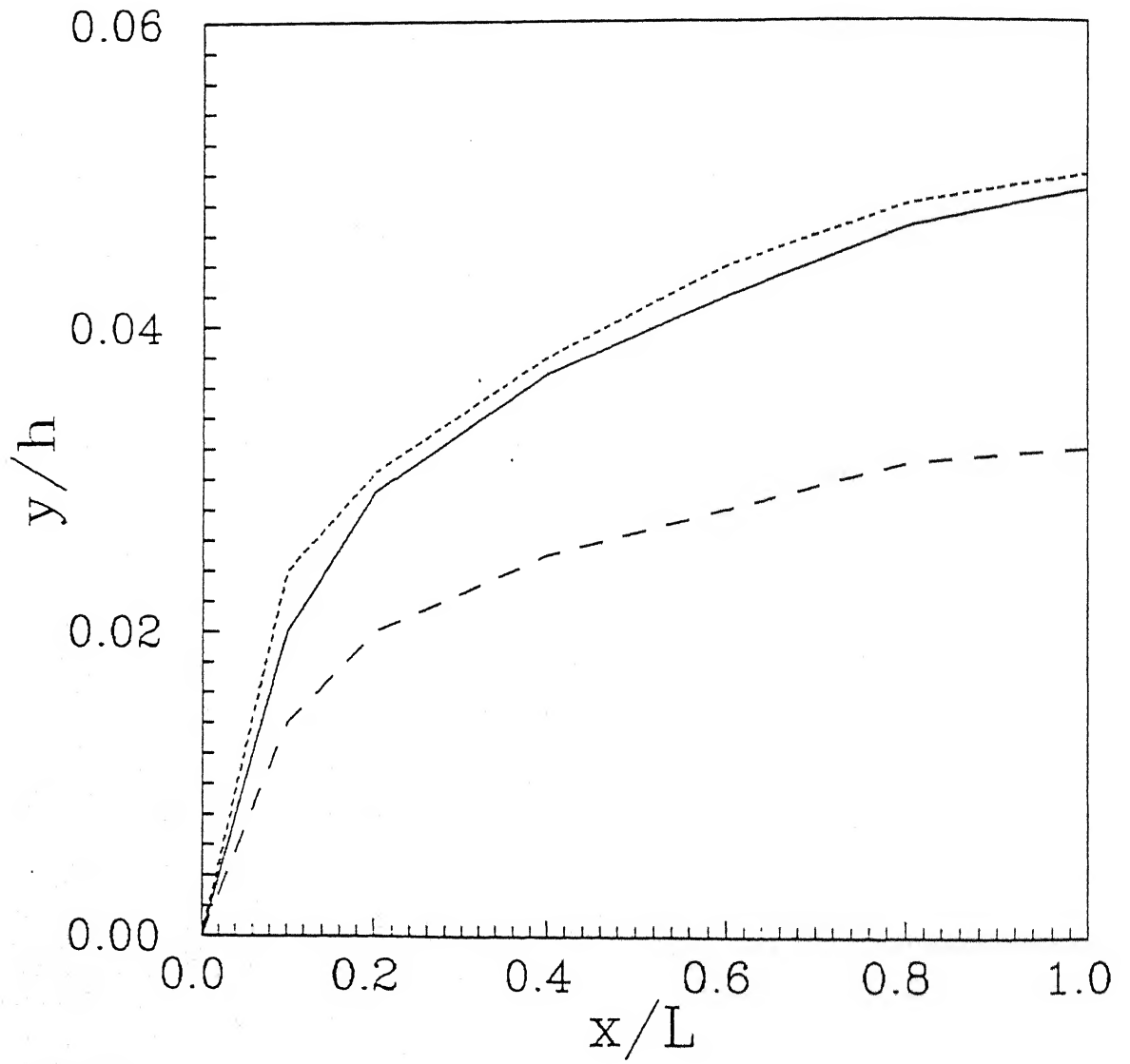


Figure 3.7: Development of concentration boundary layer at $\Delta P = 415$ kPa, $c_0 = 50$ kg/m³ and $Q = 2.22 \times 10^{-5}$ m³/s. Solid line is for black liquor, dashed line is for dextran and dotted line is for PEG.

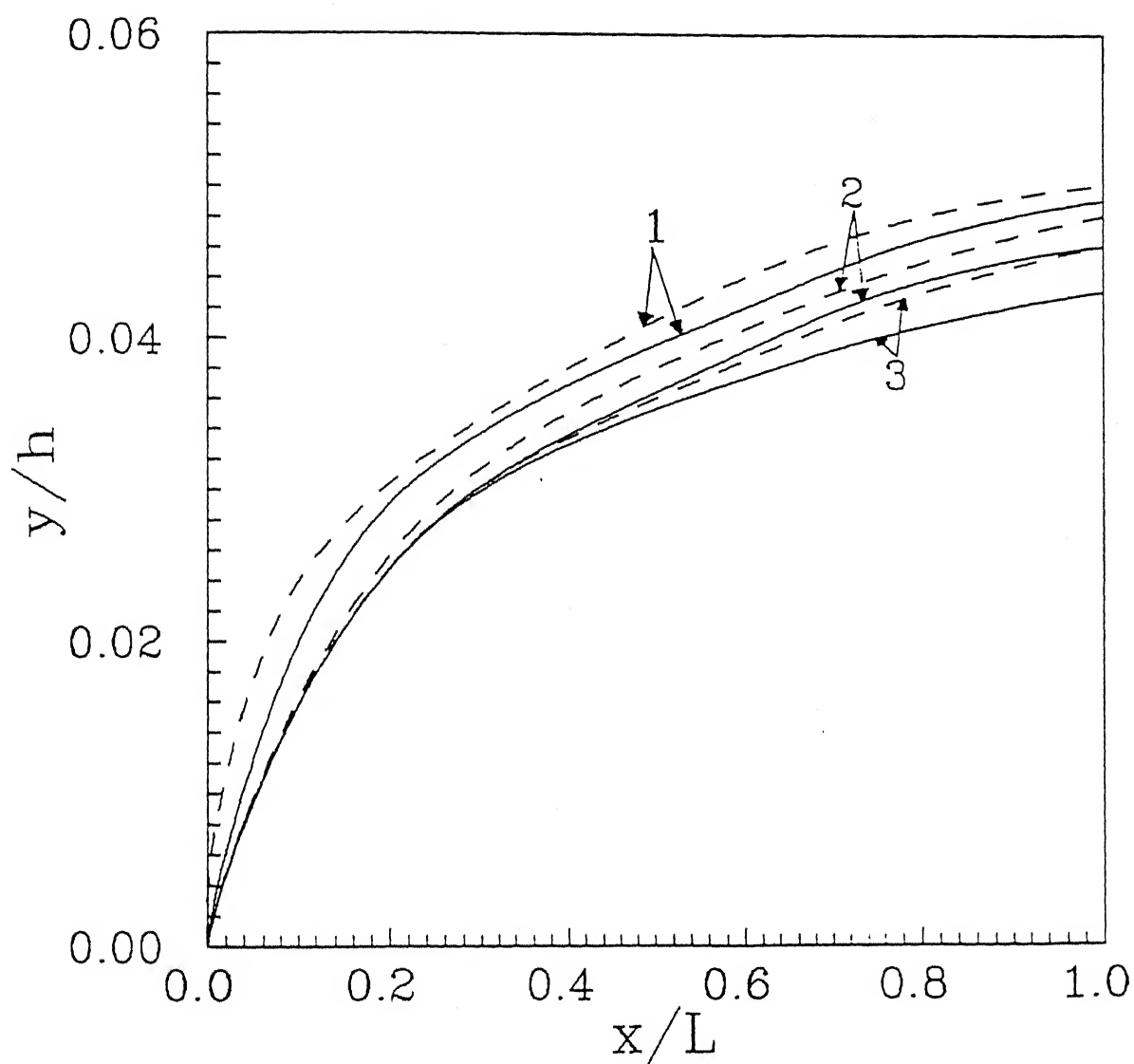


Figure 3.8: Effect of cross flow on concentration boundary layer at $\Delta P = 415$ kPa, $c_0 = 50$ kg/m³. 1: $Q = 2.22 \times 10^{-5}$; 2: $Q = 2.80 \times 10^{-5}$; 3: $Q = 3.33 \times 10^{-5}$ m³/s. Solid lines are for BL and dashed lines are for PEG.

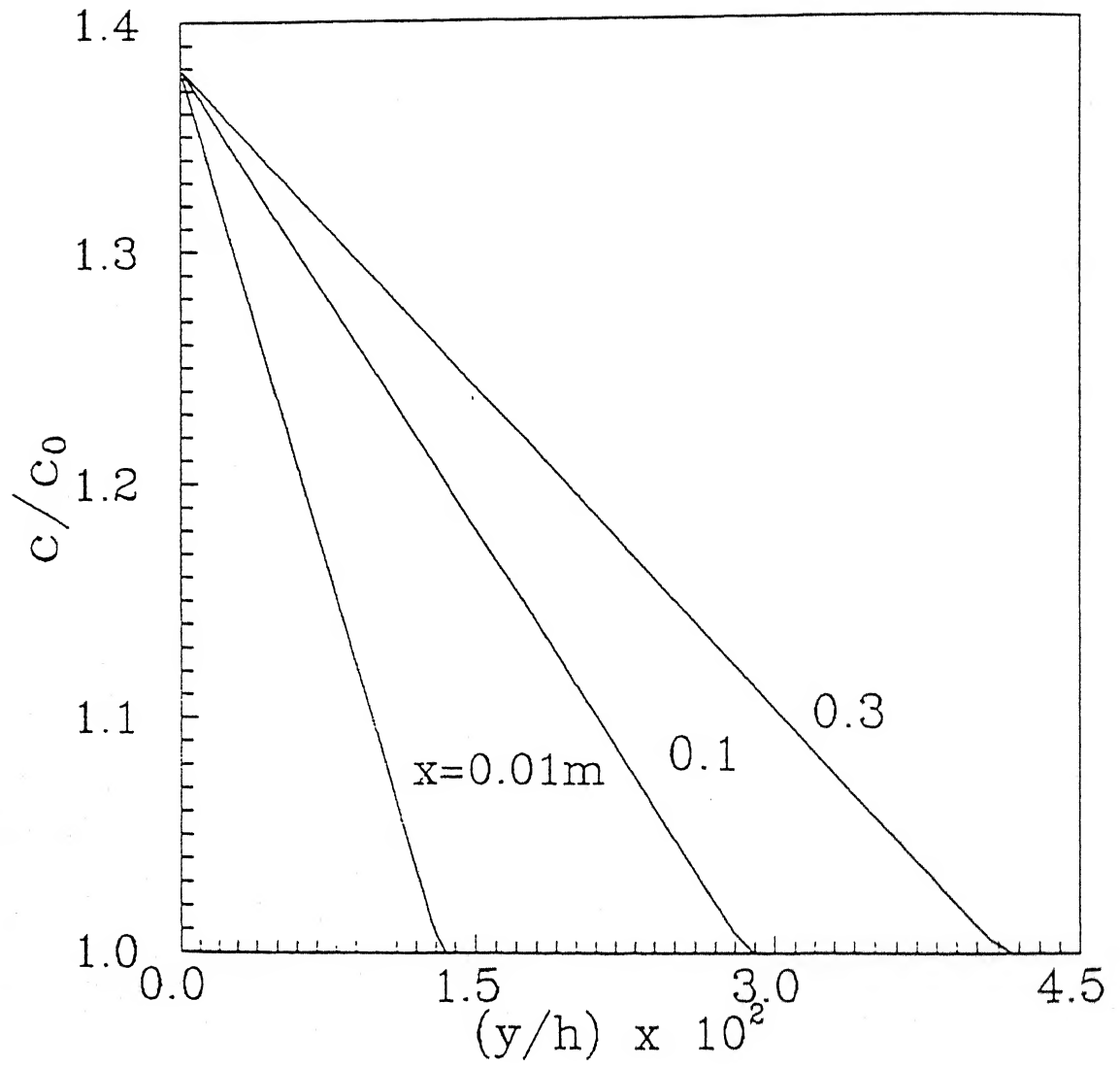


Figure 3.9: Concentration profile for black liquor at $\Delta P = 415$ kPa, $c_0 = 50$ kg/m³ and $Q = 3.33 \times 10^{-5}$ m³/s.

3.1.4.7 Flux and rejection

Permeate flux for a set of known operating conditions can be predicted from Eq. (3.19) along with Eq. (3.15) and (3.20) by trial and error. Comparison between predicted and experimental flux is presented in Fig. (3.10) at all conditions in the low rejecting membrane. This shows an excellent agreement between the predicted and experimental results.

The iterative solution for calculating V_p , also provides the membrane surface concentration c_m . From this, for every operating conditions, R_r can be calculated. Fig. (3.11) describes the variation of real rejection with operating pressure (keeping other parameters constant) for BL and PEG at different concentrations. Since PEG at 10 kg/m³ and dextran for all concentrations exhibit 100% observed rejection, R_r for them is also 100%. Compared with Fig. (3.6), R_r is always greater than R_0 for identical operating conditions. In Fig. (3.11), the trends obtained for PEG and BL are in contrast. As pressure increases rejection of PEG decreases. This may be explained [114, 218] by the deformation of PEG molecules at the pore mouth at high pressure leading to the increase in permeate concentration. This is more prominent at higher concentrations. For BL, R_r increases with pressure and reaches an asymptotic value. If we consider, finely porous membrane model to characterize the rejection behaviour of the solute, R_r is given by [238],

$$R_r = \sigma_f \frac{1 - \exp(-Pe)}{1 - \sigma_f \exp(-Pe)} \quad (3.22)$$

Here, Pe signifies the ratio of the convective to the diffusive solute transport mechanisms. As pressure increases, forced convection through the membrane increases. So at high pressures, convective mode of transport becomes dominant and R_r approaches a maximum asymptotic value of σ_f . Similar type of behaviour is observed with BSA [239] and γ -albumin [240]. But, as feed concentration increases R_r decreases for a fixed operating pressure. At a fixed pressure, membrane surface concentration increases as feed concentration increases, therefore, concentration gradient across the membrane becomes higher and solute transport by the diffusive

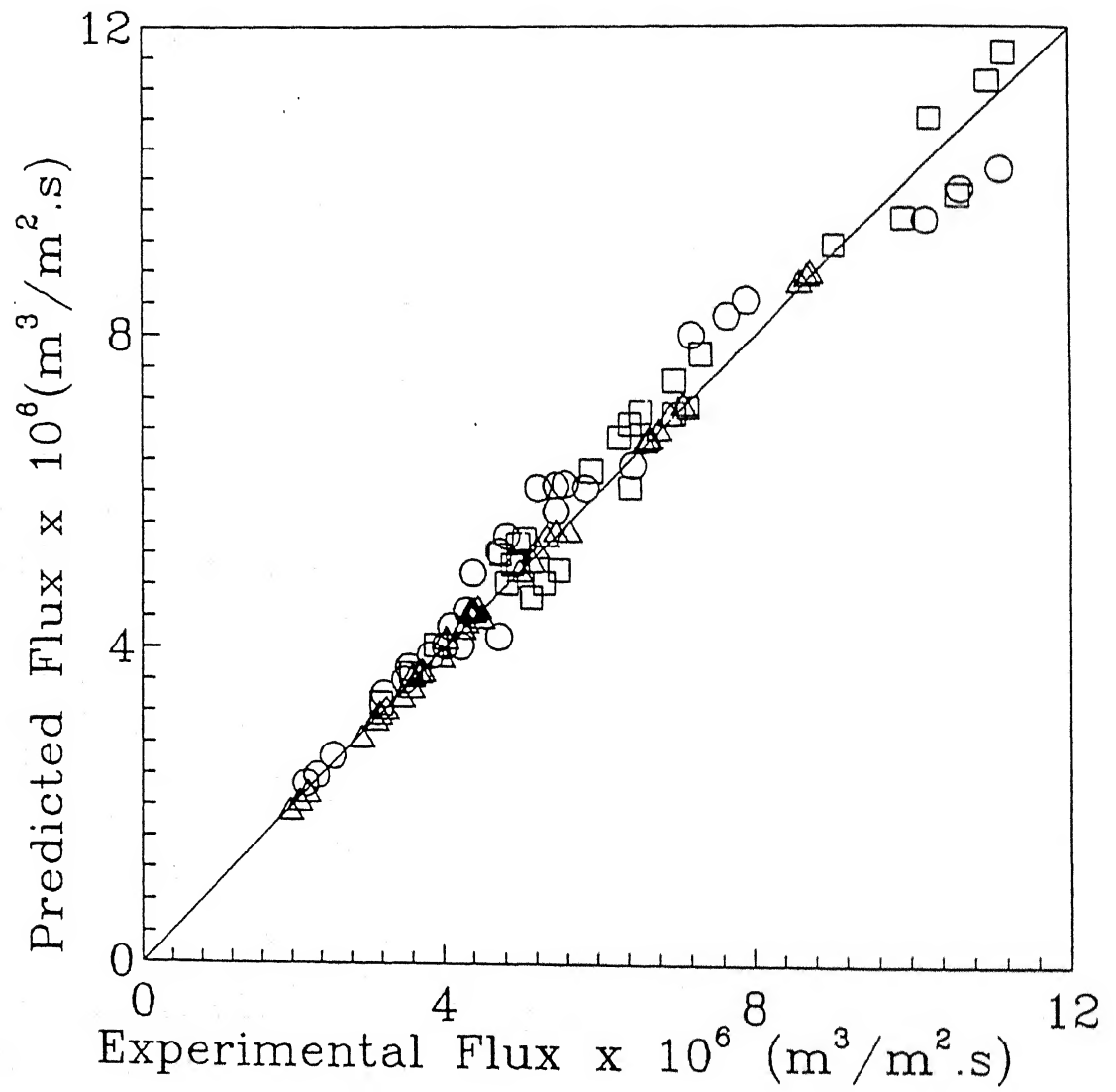


Figure 3.10: Comparison of predicted and experimental flux for LRUF under all operating conditions. Δ - BL; \circ - PEG; $+$ - Dextran.

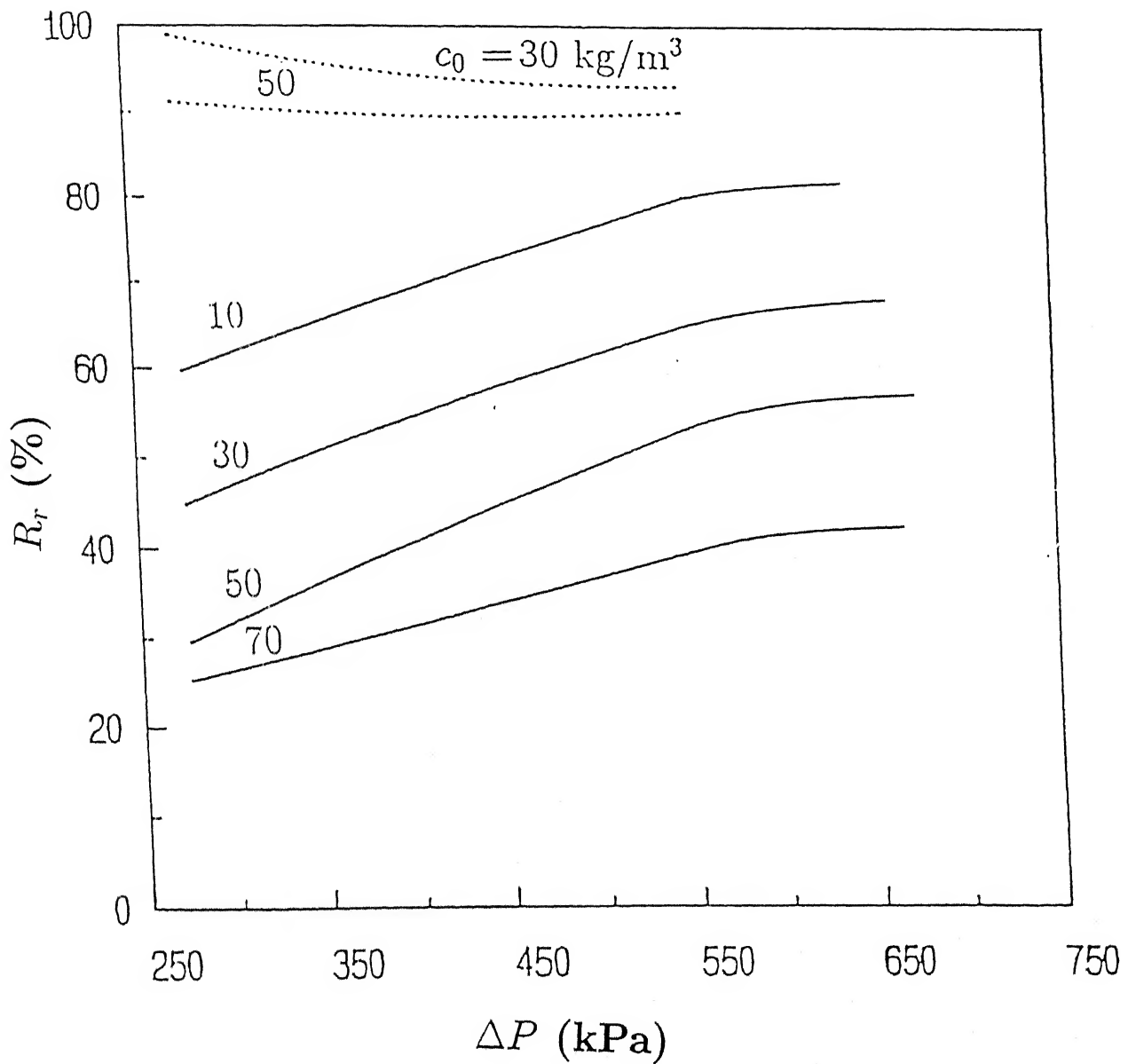


Figure 3.11: Variation of real rejection (theoretical) with pressure for LRUF at $Q = 3.33 \times 10^{-5} \text{ m}^3/\text{s}$. Solid lines are for BL and dotted lines are for PEG.

mechanism prevails [166, 217]. So, R_r decreases with increase in feed concentration at a fixed operating pressure. This may be more obvious from the study of Opong et al. [239] with the retention characteristics of BSA. It is concluded that there is a possibility of the concentration dependence of the parameters associated with the convective and diffusive mechanisms of the solute transport through the membrane pores.

3.1.4.8 Membrane surface concentration

The calculation procedure for c_m can be obtained as mentioned previously. Fig. (3.12) shows the variation of membrane surface concentration of BL and other solutes with bulk concentration at different flow rates and at constant pressure. As bulk concentration is increased for a particular flow rate, surface concentration also increases. But at a particular bulk concentration, cross flow velocity reduces the surface concentration. This is because at higher flow rates back diffusion of the solutes from the surface to the bulk is enhanced. For example, for BL at c_0 30 kg/m³, c_m reduces from 53.6 kg/m³ to 52.0 kg/m³ as flow rate increases from 2.22×10^{-5} m³/s to 2.80×10^{-5} m³/s and c_m further reduces to 50.7 kg/m³ as flow rate is increased to 3.33×10^{-5} m³/s. The effect would have been more pronounced with wide range of cross flow velocities. c_m values are highest for dextran, followed by PEG and BL. Since dextran is completely rejected by the membrane, its c_m is the highest. PEG (R_0 varies from 65% to 100%) which is moderately rejected has R_0 value higher than that of BL (R_0 varies from 18% to 40%). For all the cases, the increase of c_m is more gradual at high feed concentration.

3.1.4.9 High rejecting membrane ultrafiltration of BL

The rejection of BL can be improved by subjecting it to a high rejection ultrafiltration (HRUF). This has been verified by using two schemes, namely, scheme B and scheme C. In scheme B, BL is directly subjected to HRUF and in scheme C, permeate from LRUF is subjected to HRUF. Some typical results are tabulated in Tables 3.1, 3.2 and

3.3. From the tables, it can be observed that both the flux and rejection have been improved in scheme C compared to those in scheme B.

The model developed in the present work is tried to predict the flux decline behaviour of BL with operating conditions for high rejecting membrane. The results are shown in Fig. (3.13). This figure reveals two trends: a) the model overpredicts the steady state flux, b) flux in scheme C is more than that in scheme B. The increase in flux is on an average 15%. From the first observation, it may be concluded that apart from the resistance due to the osmotic pressure, there exists another resistance in HRUF of BL. This may be deposition of a polarized layer on the surface which adds to the resistance. In scheme C, although higher molecular weight alkali lignins are separated out by LRUF, the model still overpredicts flux. This shows that even in scheme C, a polarized layer is formed on the membrane surface. From the second observation, it is clear that polarized resistance in scheme C is less compared to that in scheme B. Fig. (3.14) shows the variation of real rejection with feed concentration. Rejection decreases as feed concentration increases which may be explained by hindered diffusion of the solutes through the membrane pores at high polarization as discussed earlier [166, 239].

It may be noted that the model overpredicts the permeate flux in comparison to the experimental values for HRUF runs. This may be attributed to the inherent difficulties to estimate the physical properties of BL solutions in scheme C. Difficulties in measurements of the permeate concentration by gravimetric analysis may be another possible limitation. Apart from this, there exists a possibility that BL forms a polarized layer on the membrane surface for HRUF runs (with small pores) which increases the resistance to the solute transport; the present model does not incorporate such additional resistances. Further, the membrane being hydrophilic, BL has a less tendency to foul the membrane (irreversible adsorption, etc.) [137]. This was verified by observing negligible change in the membrane permeability.

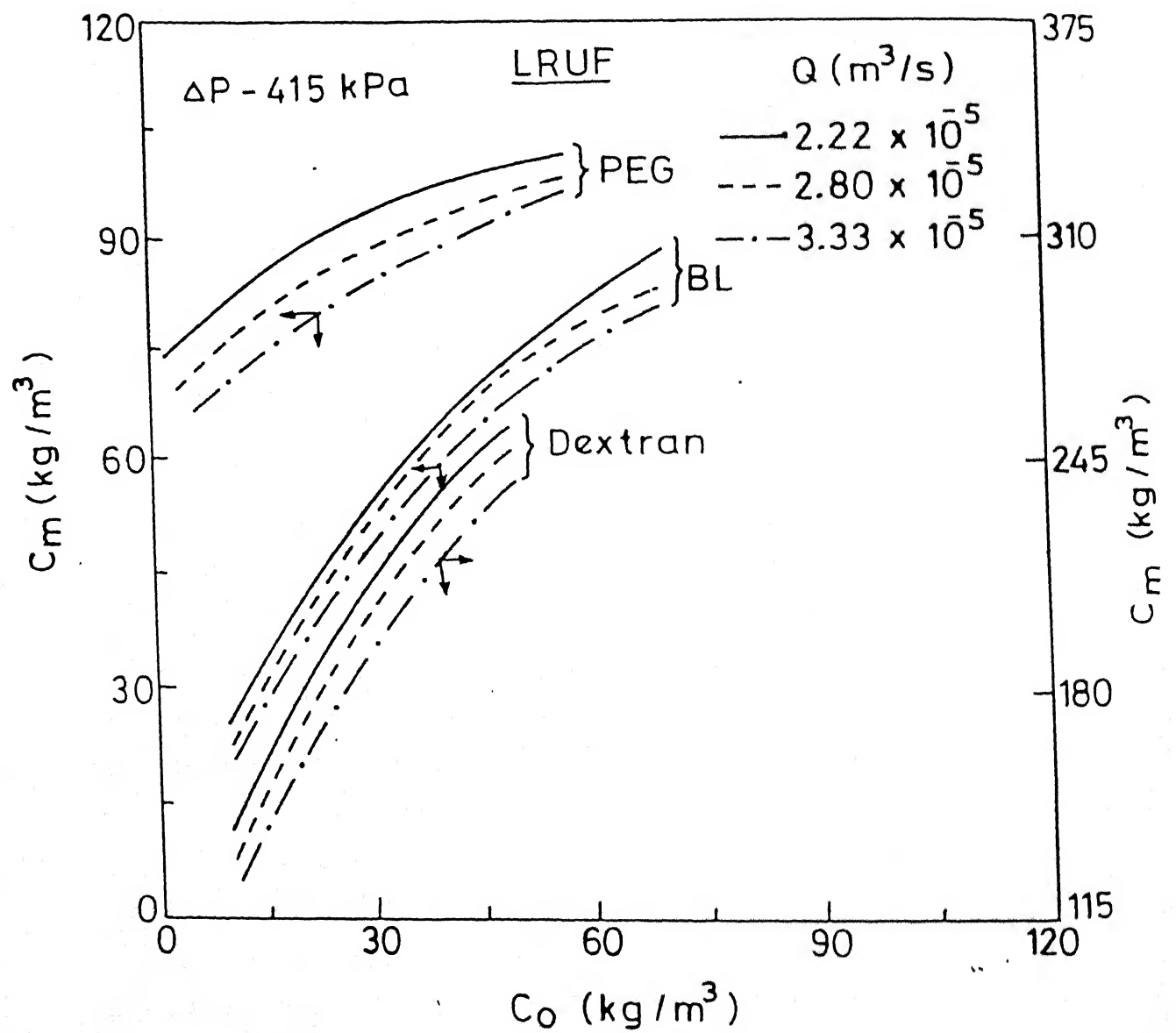


Figure 3.12: Variation of c_m with c_o for LRUF

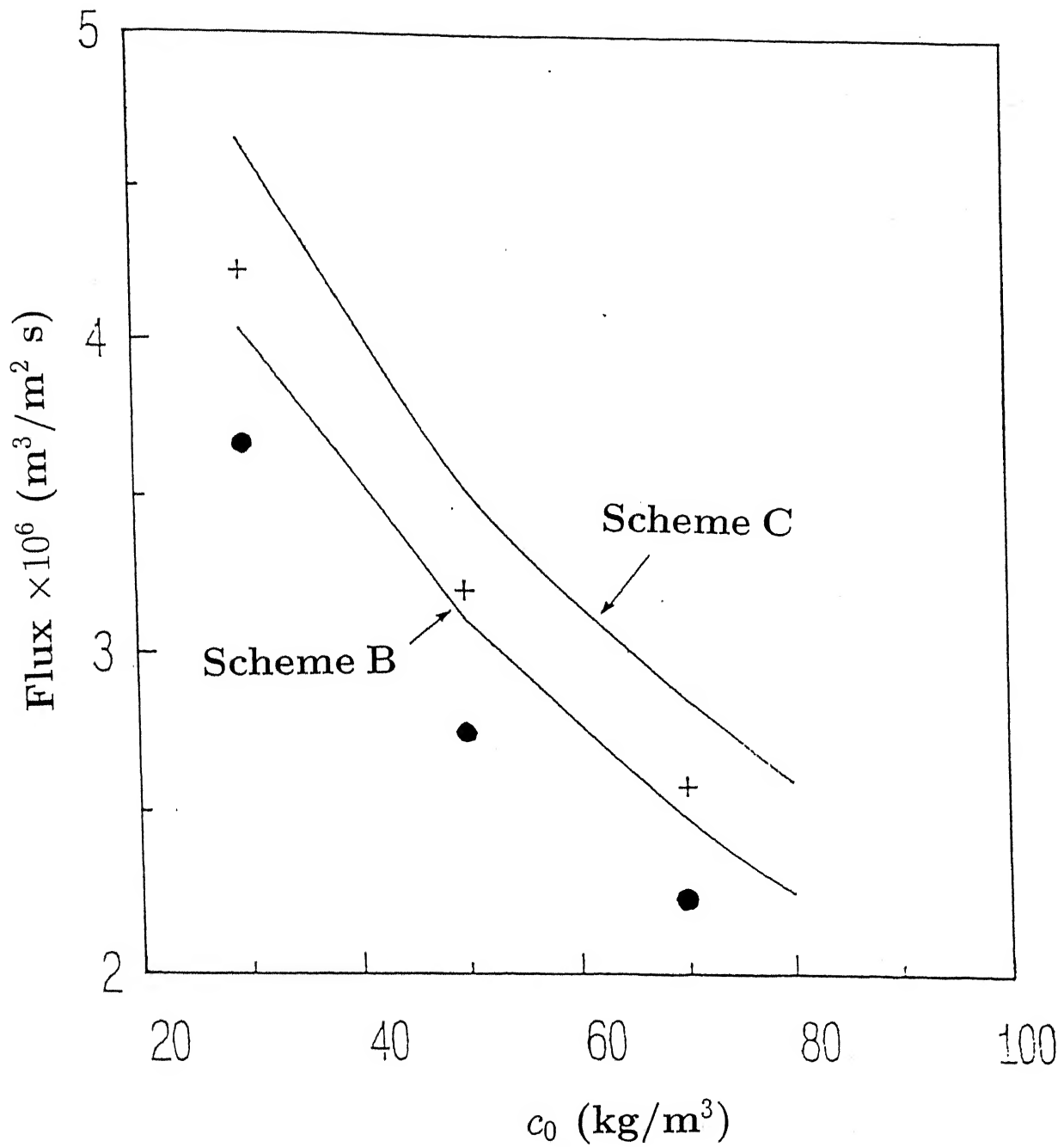


Figure 3.13: Flux versus concentration for HRUF at $\Delta P = 1722$ kPa and $Q = 2.22 \times 10^{-5} \text{ m}^3/\text{s}$. • - scheme B; + - scheme C. Solid lines are for theoretical predictions

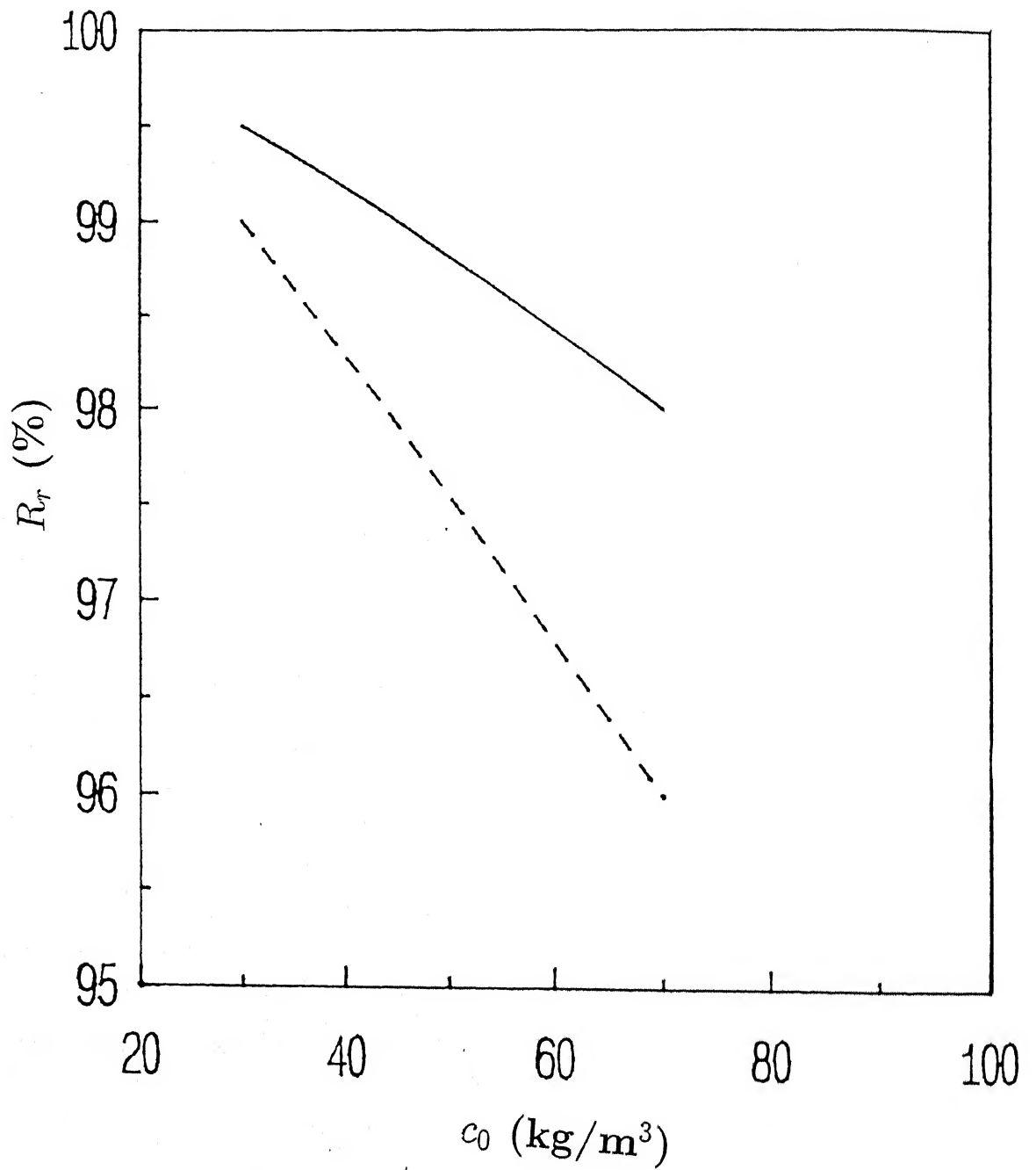


Figure 3.14: Real rejection (predicted) versus concentration for HRUF at $\Delta P = 1722$ kPa and $Q = 2.22 \times 10^{-5} \text{ m}^3/\text{s}$. Solid line is for scheme C and dashed line is for scheme B.

3.1.5 Conclusions

From the experiments, it is clear that UF of BL, PEG and dextran are osmotic pressure controlled within the range of operating pressure which is generally encountered in UF. Increase in cross flow velocity decreases c_m , thereby, increases flux. Development of concentration boundary layer near the membrane surface results flux decline during UF. Characteristics of UF of BL can be explained by the similarity solution model. Predicted flux for BL and other solutes agrees well with the experiments. Treatment of BL by HRUF via LRUF gave better flux and rejection than direct HRUF. Flux and real rejection can be predicted using the same model.

3.2 Short and long term flux decline analysis in ultrafiltration

In this section, short and long term flux decline of BL is quantified in a stirred cell through a semi-empirical route by including the resistance of polarized layer. A correlation of mass transfer coefficient, incorporating changes in properties, due to concentration polarization, is also proposed and utilized in this context.

3.2.1 Introduction

The decline in flux may be categorized into two time domains; namely, (a) short term and (b) long term flux decline [241]. In short term flux decline, the decline of flux is osmotic pressure limited and membrane surface concentration increases due to build up of osmotic pressure of the solution. This build up of the concentration boundary layer is very fast, within a few seconds [123, 241]. it reaches a steady state value. In short term decline domain, rapid decline in flux can be quantified by the combination of film theory and osmotic pressure model [121], if the solution properties (osmotic pressure, density, viscosity, etc.) are known a priori as a function of concentration. At the end of this domain, onset of a polarized layer on the membrane surface starts [241]. During the long term decline, the membrane surface concentration remains the same but the thickness of the polarized layer grows gradually and reaches a steady state value depending on the external hydrodynamical conditions (e.g. Reynolds number imposed by the stirring, cross flow velocity in cross flow filtration, etc.) [137, 241].

In earlier attempts [218, 220] the flux decline were attributed to the formation of the polarized layer resistance which was obtained as a function of time for different sets of operating conditions, quantitatively. Attempts [220] were also made to analyze this polarized layer resistance through formation of a secondary gel layer. It was understood that through the gel layer model, the flux decline may be attributed to the formation of the secondary layer, thickness of which grows with time, thus giving

extra resistance against the permeate flow. In many studies, formation of gel layer was assumed even without the formation of a real gel [122, 180]. Therefore, strictly speaking, the secondary layer may not be a gel layer unless the characteristics of the solutes tend to form gel.

The present work has been undertaken to analyze the overall flux decline behaviour of polyethylene glycol (PEG-4000) and polyvinyl pyrrolidone (PVP-10000) in a stirred cell, both in short and long term. The short term decline is modeled through the combination of film theory and osmotic pressure model by taking into account the variations of solution properties (e.g. density, viscosity, etc.) with concentration. A simple semi-empirical model for long term flux decline is also attempted. It can be noted here that for practical purposes, the long term flux decline is the main interest for the process engineers and such semi – empirical approach will be extremely useful for design purposes. Further, the analysis is extended to UF flux decline using BL.

3.2.2 Theory

In this section, the pertinent theoretical developments for both short and long term flux decline have been discussed separately.

3.2.2.1 Short term flux decline

The initial flux decline in UF is osmotic pressure controlled. The permeate flux can be represented by the phenomenological equation, Eq. (3.20).

The unsteady state solute mass balance near the membrane surface for constant diffusivity can be written as,

$$\frac{\partial c}{\partial t} - v_p \frac{\partial c}{\partial y} = D \frac{\partial^2 c}{\partial y^2} \quad (3.23)$$

where, y is normal distance away from the membrane. The initial condition to Eq. (3.23) is

$$c = c_0 \text{ at } t = 0 \quad (3.24)$$

The boundary condition at $y = 0$ can be obtained from the mass balance at the membrane surface as

$$v_p(c - c_p) + D \frac{\partial c}{\partial y} = 0 \quad (3.25)$$

and at $y = \delta$

$$c = c_0 \quad (3.26)$$

The steady state solution of Eq. (3.23) can be written in the form of well known film theory as,

$$v_p = k \ln \left(\frac{c_m - c_p}{c_0 - c_p} \right) \quad (3.27)$$

The mass transfer coefficient k can be evaluated from the correlations given by Colton [24] for stirred cell,

$$Sh = \frac{kr}{D} = 0.285(Re)^{0.55}(Sc)^{0.33} \text{ for } Re < 32000 \quad (3.28)$$

or,

$$Sh = \frac{kr}{D} = 0.0443(Re)^{0.75}(Sc)^{0.33} \text{ for } Re > 32000 \quad (3.29)$$

In these mass transfer correlations, properties (density, viscosity, etc.) are evaluated at the bulk concentrations. But, in a realistic situation, properties may vary significantly with concentration near the membrane surface [27, 144, 147] which in turn alters the mass transfer coefficient to a perceptible level. Therefore, properties are to be evaluated at the membrane surface concentration [27]. If the variations of the physical properties with concentration are known a priori, Eqs. (3.20) and (3.27) can be solved by successive substitution [137] to obtain c_m and v_p . The algorithm for successive substitution is presented in Fig. (3.15).

This method enables to recast the Sherwood correlations for property variations as,

$$Sh = a(Re)^{n_1}(Sc)^{n_2} \left(\frac{Sc}{Sc_m} \right)^{\beta_1} \quad (3.30)$$

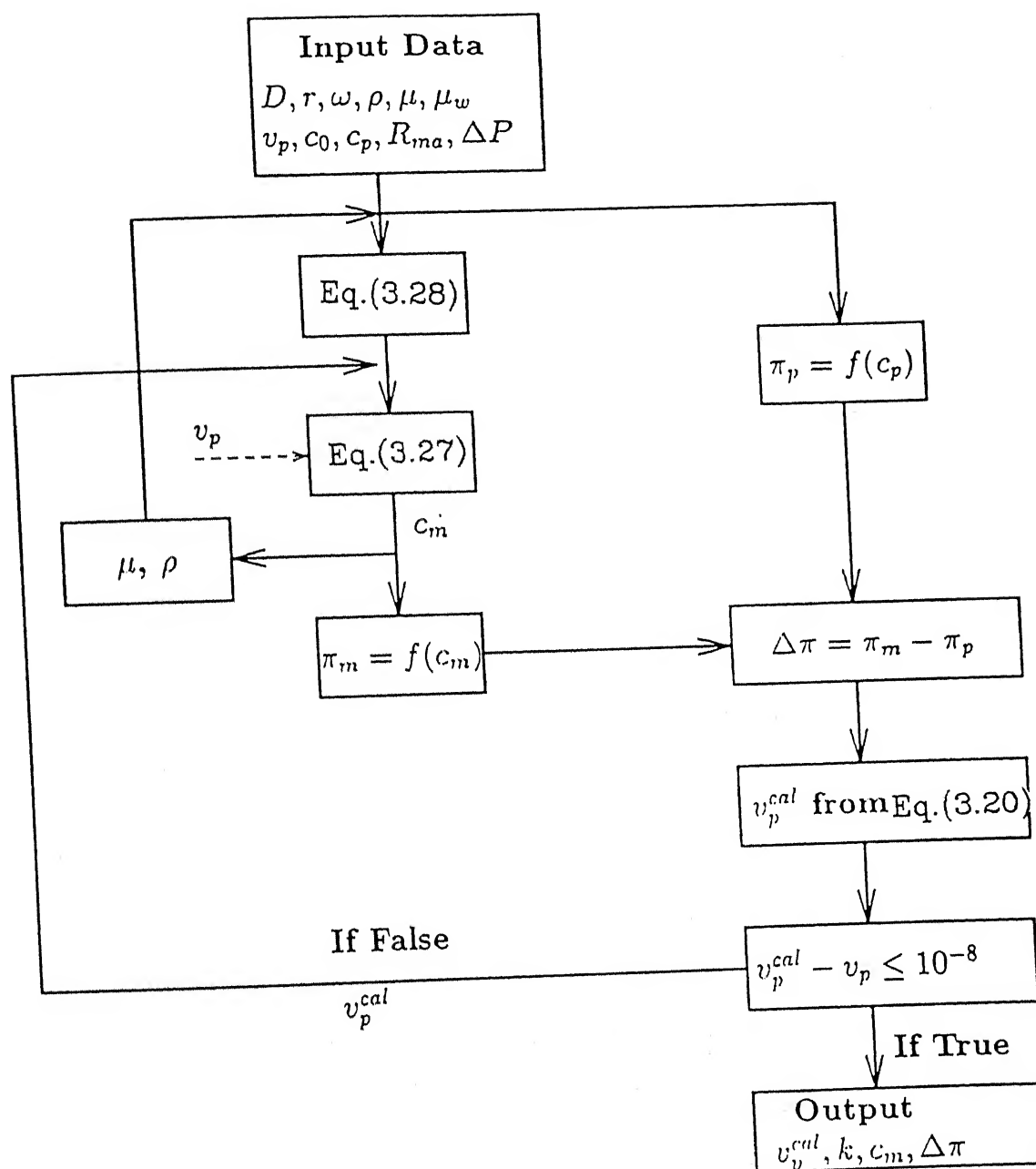


Figure 3.15: Block diagram for algorithm of successive substitution

The transient behaviour of short term flux decline can be obtained by numerical solution of Eq. (3.23) subject to the pertinent initial (Eq. 3.24) and boundary conditions (Eqs. 3.25 and 3.26). The δ is obtained from the steady state analysis ($\delta = D/k$), which is determined by the cell geometry and hydrodynamics only.

3.2.2.2 Long term flux decline

Previous studies [123, 241] show that short term flux decline is extremely rapid, within a few seconds from starting of the operation in most of the cases. Therefore, gradual growth of the polarized layer dictates the long term flux decline behaviour. It may be noted here that this domain of flux decline is of major interest for the industrial applications. The flux equation can be written for long term domain as,

$$v_p = \frac{\Delta P - \Delta \pi}{\mu_w(R_{ma} + R_p(t))} \quad (3.31)$$

Since the osmotic pressure limited flux decline is very fast, the limiting flux of the osmotic controlled flux decline can be assumed as the initial flux for an actual UF operation which is generally of several hours of duration. Therefore, Eq. (3.31) can be recast as,

$$v_p = \frac{v_p^0}{1 + R_p^*(t)} \quad (3.32)$$

where, $R_p^* = R_p/R_{ma}$ and $v_p^0 = (\Delta P - \Delta \pi)/(\mu_w R_{ma})$.

For an unstirred batch UF, polarized layer grows continuously due to the absence of any external hydrodynamic restrictions. But, in a stirred cell, the rate of growth of the polarized layer resistance is limited by the imposition of external stirring. Therefore, in a stirred cell, R_p increases with time but in a diminishing rate and finally reaches an asymptote leading to a steady state flux after a longer period of operation [220]. Consequently, the rate of growth of R_p can be expressed as,

$$\frac{dR_p^*}{dt} \propto (R_{ps}^* - R_p^*)$$

or,

$$\frac{dR_p^*}{dt} = k_0(R_{ps}^* - R_p^*) \quad (3.33)$$

Solution of Eq.(3.33) can be expressed as,

$$R_p^* = R_{ps}^*(1 - \exp(-k_0 t)) \quad (3.34)$$

Putting the expression of R_p^* in Eq.(3.32), we obtain,

$$v_p(t) = \frac{v_p^0}{1 + R_{ps}^*(1 - \exp(-k_0 t))} \quad (3.35)$$

In the present study, some general trends (in the forms of simple correlations) of the parameters R_{ps}^* and k_0 with operating conditions are investigated for different solutes. Once, these parameters are known for different operating conditions, the long term flux decline can be modeled in combination with theory of short (estimation of v_p^0) term flux decline.

3.2.3 Experimental

3.2.3.1 Materials

Polyethylene glycol (PEG-4000), in the molecular weight range 3500 to 4500 was obtained from, Fluka, Germany. Poly vinyl pyrrolidone (PVP) of average molecular weight 10,000 was obtained from Sigma Chemicals, USA. Black liquor was obtained from Central Paper Mill, Surat, based on the kraft process. The average molecular weight of BL was taken as 7000 [123]. Cellulose acetate membrane, obtained from Permionics (India) Ltd. was used in the experiments. The membrane was characterized in our laboratory and was found to be approximately 1K diffused molecular weight cut-off (MWCO). The retention curve of the membrane for different molecular weight solutes is presented in the appendix (Fig. A1). The membranes were hydrophilic, resistant to temperatures up to 90°C and have low adsorption characteristics. They were usable in the pH range of 2 to 12. The hydraulic resistance of the membrane was found to be $6.75 \times 10^{13} \text{ m}^{-1}$.

3.2.3.2 Apparatus

A stirred ultrafiltration cell, modified to operate in a continuous mode was designed and fabricated with the following specifications: material, SS-316; useful volume 450 ml; residual volume nil; filter diameter, 76 mm; effective filtration area, 26.4 cm²; maximum testing pressure 3.5 Mpa; stirring facility, mechanical, using a variable speed motor.

3.2.3.3 Analysis

The concentration of PEG and PVP in different streams were measured through the refractive index calibration curve. A Bosch and Lomb refractometer was used for this purpose. The concentration of black liquor was determined gravimetrically by drying the samples in the oven at 105 ± 2 °C. All the solutions were prepared using distilled water.

Viscosities and densities were determined by Ostwald viscometer and specific gravity bottle, respectively, for various PEG, PVP and BL concentrations. The correlations developed for viscosities and densities with concentration for different solutes are presented in the appendix B. The osmotic pressure relationship with concentration for different solutes are also presented in the appendix.

3.2.3.4 Experimental set up

Experiments were conducted using a batch cell ultrafilter. Since experiments were carried out to study the effect of various factors on flux decline phenomenon, it was necessary to carry out the experiments on a continuous mode. This was done by recycling the permeate back into the cell, thereby maintaining a constant bulk concentration. A metering pump was used to maintain pressure in the cell. It was also used to pressurize the system initially, thus eliminating the need of compressor.

Two dampers were used to smoothen the fluctuations in pressure. The schematic diagram of the set up is shown in Fig. (3.16).

3.2.3.5 Design of experiments

The independent operating parameters in the experiments were applied pressure, feed concentration and stirrer speed. During the experiments, two variables were held constant while the third one was varied to get an exact picture of the dependence.

Concentrations were varied as 50, 70 and 90 kg/m³ for PVP. For PEG and BL a fixed concentration of 90 kg/m³ was selected. Pressure was varied as 550, 690 and 830 kPa while the stirrer speeds were 325, 425 and 525 rpm.

3.2.3.6 Experimental procedure

Initially, the membrane was compacted at a pressure of 1000 kPa for five hours and hydraulic resistance R_m was measured. The cell was dismantled and the membrane was washed with distilled water.

For an actual run, the membrane was placed back and the cell was assembled. The stirrer speed for the required rpm was adjusted by the voltage supply through a variac. Rotational speed of the stirrer was measured using a tachometer. The feed solution was pumped into the cell by a metering pump. Once the desired pressure was attained, the piston movement regulated to maintain the pressure. To calculate the flux, 5 cc of the permeate was collected in a measuring cylinder and time taken for this collection was noted. This procedure was repeated for specific time intervals and therefore, fluxes at different times were calculated. Experiments were terminated when two consecutive flux readings were found to be identical.

After each run, the whole cell was rinsed with distilled water. Further, the membrane was rinsed with distilled water for at least two hours to remove any deposition. The

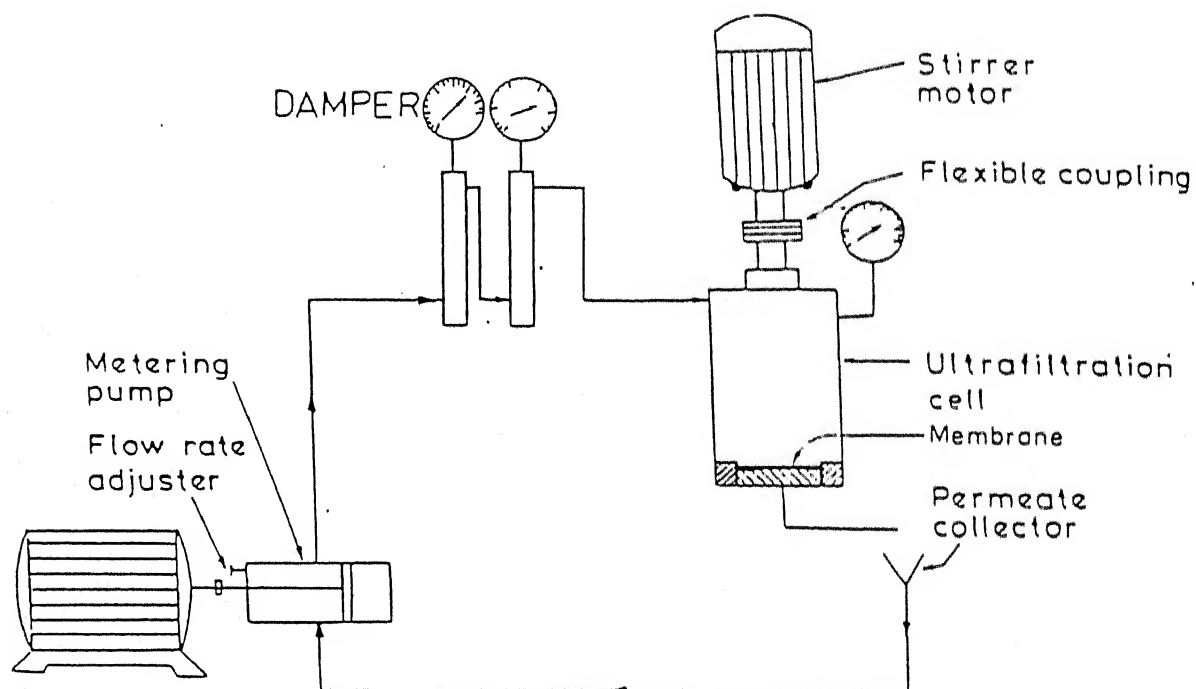


Figure 3.16: Line diagram of the experimental set up

water flux was then measured to check any adsorption resistance which act in series with membrane hydraulic resistance for the next run. This procedure was repeated for each set of operating conditions. All the runs were taken at room temperature (28 to 30 °C). All the data are available [242].

3.2.4 Results and Discussion

In this section, the results for both short and long term flux decline are presented. Before that, the irreversible fouling of the membrane over successive runs is discussed.

It is interestingly observed during experiments that the membrane resistance over successive runs increased. This implies that over different runs, there was irreversible fouling of the membrane and consequently there was permanent loss of membrane permeability. A representative plot of percent increase in R_{ma} for different solutes for the feed bulk concentration of 90 kg/m³ is presented in Fig. (3.17). From the figure, it can be observed that virtually there is no alteration of membrane resistance for PEG; but, there is a significant increase in resistance for PVP and BL. Between PVP and BL, BL shows a steep increase in resistance. This behaviour indicates that the irreversible membrane fouling which is caused by solute adsorption, pore blocking, etc. (as discussed earlier) inside the membrane pores, is almost absent for PEG. Therefore, PEG does not foul the membrane under study permanently. While, black liquor, being a complex mixture of solutes of various molecular weights tend to foul the membrane the most compared to PVP in terms of irreversible fouling.

3.2.4.1 Short term fouling

Limiting flux for osmotic pressure controlled UF

In the concentration boundary layer adjacent to the membrane surface, the membrane surface concentration increases. The properties like density, viscosity, etc.

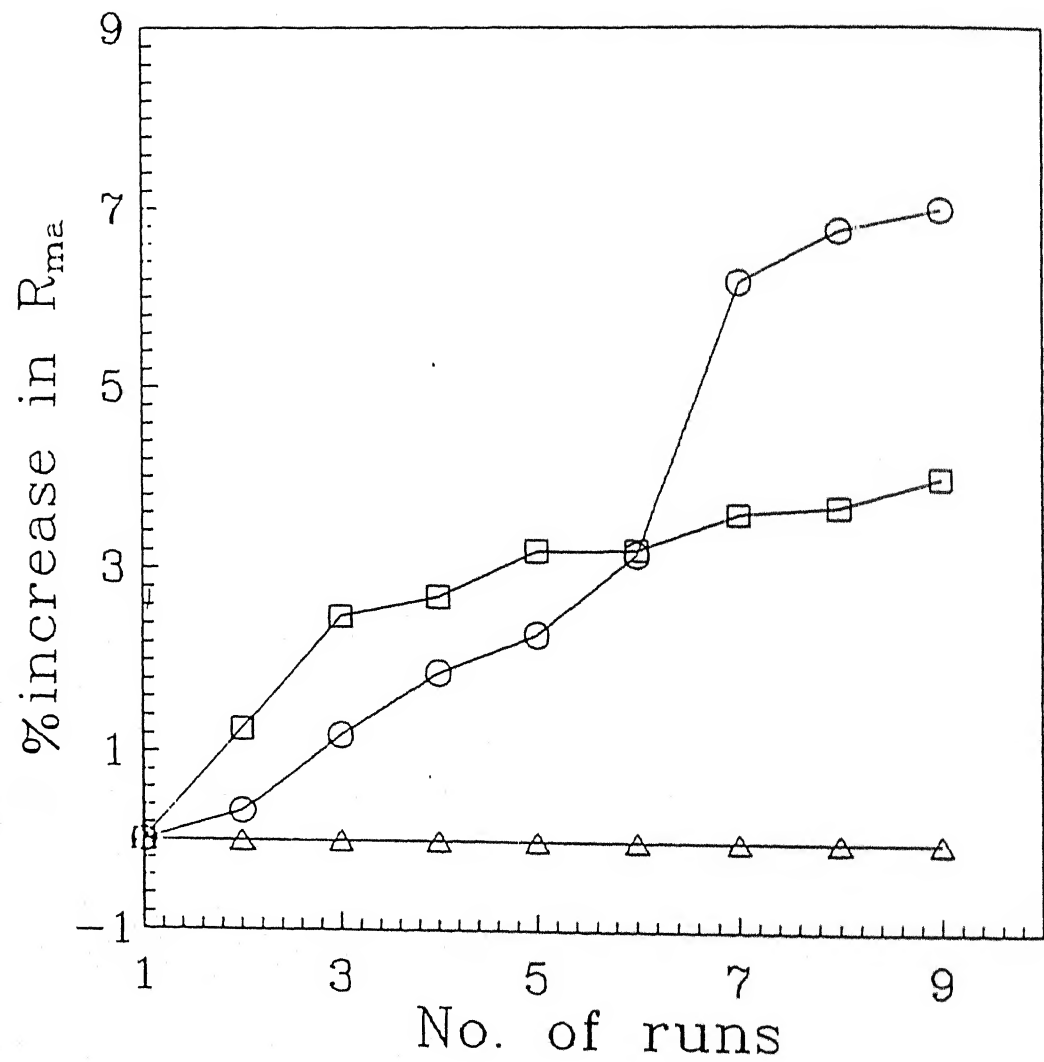


Figure 3.17: Variation of membrane resistance over successive runs. $c_0 = 90 \text{ kg/m}^3$;
○ (BL); △ (PEG); □ (PVP)

are strong function of solute concentration for all the solutes studied here. The change in properties affect the hydrodynamic conditions prevailed in the concentration boundary layer significantly as studied by [144, 147]. Therefore, estimation of limiting flux due to osmotic pressure controlled UF is required to incorporate the variations of properties in the film model. This necessitates the development of a Sherwood correlation for determining the mass transfer coefficient including the effects of variations of physical properties. A general algorithm, namely, successive substitution (as shown in Fig. (3.15)) is adopted to estimate c_m and v_p through iterative solution of Eq. (3.20) and Eq. (3.27). This also leads to determination of wall Sherwood number (Sh_m), where, properties like ρ and μ are evaluated at the membrane surface concentration. It was observed in the calculations that for all the operating conditions and for all the solutes studied in this work, the Reynold number lies in the range of 4000 to 26000. Therefore, it can be concluded that the hydrodynamic conditions prevailed in this study are mostly in the laminar zone and the Sherwood number correlation given by Eq. (3.28) is relevant to this study. The effect of the variation of properties is included in the ratio Sc/Sc_m as suggested in the earlier studies [27]. The plot of Sh_m/Sh with Sc/Sc_m for all the solutes and for all the runs is shown in Fig. (3.18). This plot shows that the value of slope of the curve (value of β in Eq. (3.30)) is 0.22. Therefore, Sherwood number correlation can be modified for a stirred cell in the laminar zone ($Re < 32000$) including the effects of variations of properties as,

$$Sh = \frac{kr}{D} = 0.285(Re)^{0.55}(Sc)^{0.33}(Sc/Sc_m)^{0.22} \quad (3.36)$$

Earlier studies [27] considered the value of the exponent β as 0.11 for cross flow filtration and it was derived from the Nusselt number correlations through heat and mass transfer analogies. For laminar flow in a channel, the property variation was incorporated in the Sherwood number correlations as $(\mu_0/\mu_m)^{0.27}$ by [147].

Transient solution of the osmotic pressure controlled UF

The transient mass balance equation (Eq. 3.23) along with the pertinent initial and

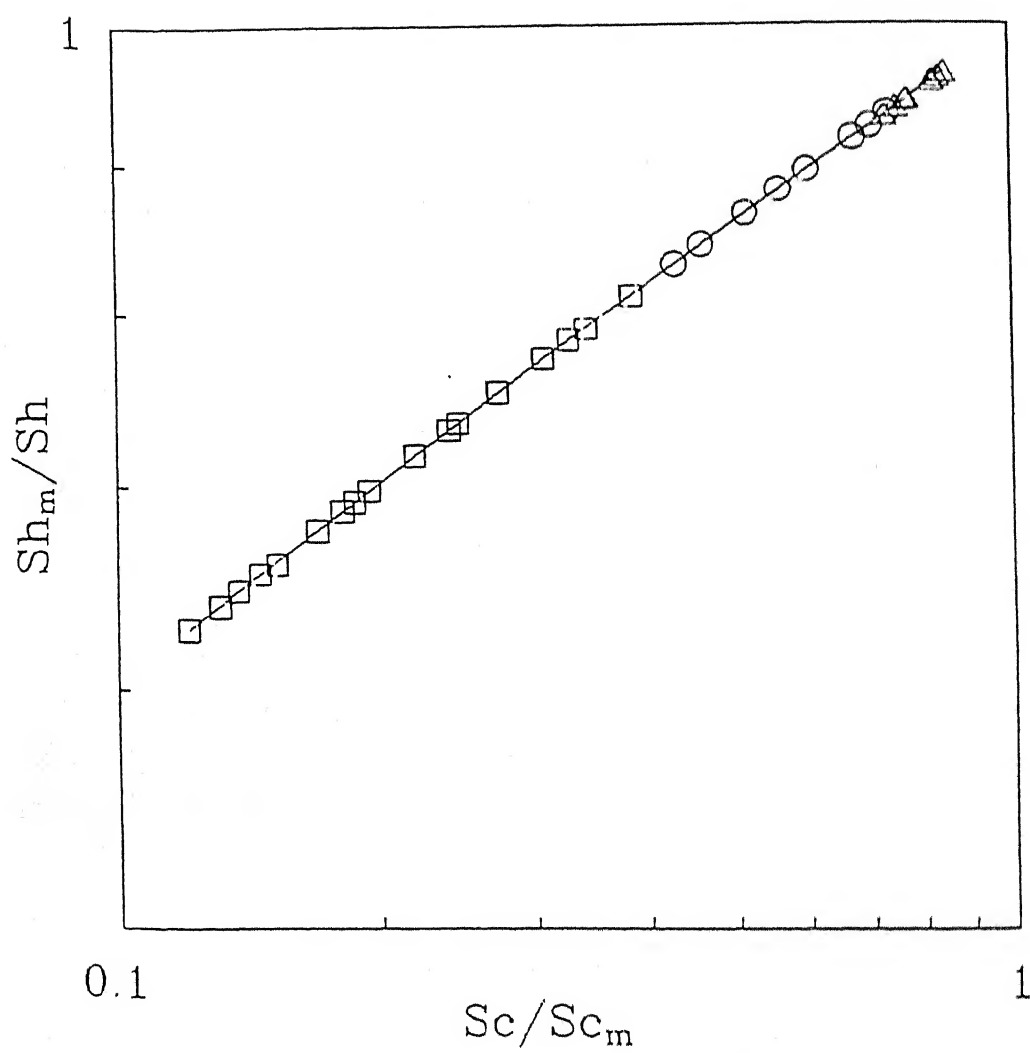


Figure 3.18: Variation of Sh_m/Sh with Sc/Sc_m for all the solutes under all the operating conditions. \circ (BL); \triangle (PEG); \square (PVP).

boundary conditions were solved numerically using a finite difference scheme [243]. The discretization of the two independent variables (y, t) was done using a form of Chebyshev polynomial which gradually increases step sizes as distance from the origin ($y, t \rightarrow 0$) increases. This technique gives more accurate results compared to a uniform mesh spacing. The finite differencing over the N mesh points resulted in a set of N coupled ODEs in time. These ODEs were then solved simultaneously using a backward difference method. Computations were done using 75 mesh points, for which results were insensitive to number of grid points.

The solution of this simulations show that the steady state (osmotic pressure limited steady state) profile for c_m is reached within few seconds. Durations required to reach the concentration profile to the osmotic pressure limited value for different solutes under some representative operating conditions are given in Table 3.5. From the table, it is obvious that the film layer occurs almost instantaneously in most of the cases. The table also shows that time required to reach steady state concentration is less for a less severe conditions (high stirring). It can also be observed that for identical conditions BL takes maximum and PEG takes minimum time. This may be due to the strongest (among the three solutes studied) dependence of properties of BL with concentration which leads to delaying of concentration to reach the steady state. Fig. (3.19) shows that the development of the concentration profile within the film layer for all the solutes under the same operating conditions for different periods. Initially, a flat profile ($c_m/c_0 = 1.0$ for all y) prevails throughout the region; gradually this develops to a steady state concentration profile.

The steady state concentration profile with for different stirrer speed for all the solute is shown in Fig. (3.20). From this figure, it is clear that concentration at any position y decreases with increase in stirrer speed. This is expected because at higher stirring, back diffusion increases which subsequently lowers the membrane surface concentration within the film. It can also be observed from the figure that at any position at the same stirring, concentration of PEG, BL and PVP increases in that order. As the molecular weight of the solute increases (MWs 4000, 7000, 10000) their

Table 3.5: Durations required for c_m to reach osmotic pressure limited value for different solutes at $\Delta P = 550$ kPa and $c_0 = 90$ kg/m³

Solute	stirrer speed (rpm)	time (s)
PVP	325	1.32
	525	1.01
PEG	325	1.02
	525	0.78
BL	325	2.26
	525	1.32

diffusivity decreases; therefore, for higher molecular weight solutes back diffusion will be less and its concentration at any position within the film layer will be more than that of a solute of lower molecular weight.

3.2.4.2 Long term fouling

In the long term flux decline, the flux profile over time was fitted by a non - linear regression analysis to the Eq. (3.35) to obtain the parameters R_{ps}^* and k_0 for different solutes and for all operating conditions. It was found that for all three solutes, R_{ps}^* varied with the operating conditions with similar trends. The operating conditions were categorized in three non-dimensional groups, namely, Re , $\Delta\pi/\Delta P$ and $(c_m - c_p)/(c_0 - c_p)$. R_{ps}^* was correlated with these groups and the results are given below:

PEG:

$$R_{ps}^* = 9.846 \times 10^5 (Re)^{-1.59} \left(\frac{c_m - c_p}{c_0 - c_p} \times \frac{\Delta\pi}{\Delta P} \right)^{0.06} \quad (3.37)$$

BL:

$$R_{ps}^* = 1.130 \times 10^2 (Re)^{-0.80} \left(\frac{c_m - c_p}{c_0 - c_p} \times \frac{\Delta\pi}{\Delta P} \right)^{0.88} \quad (3.38)$$

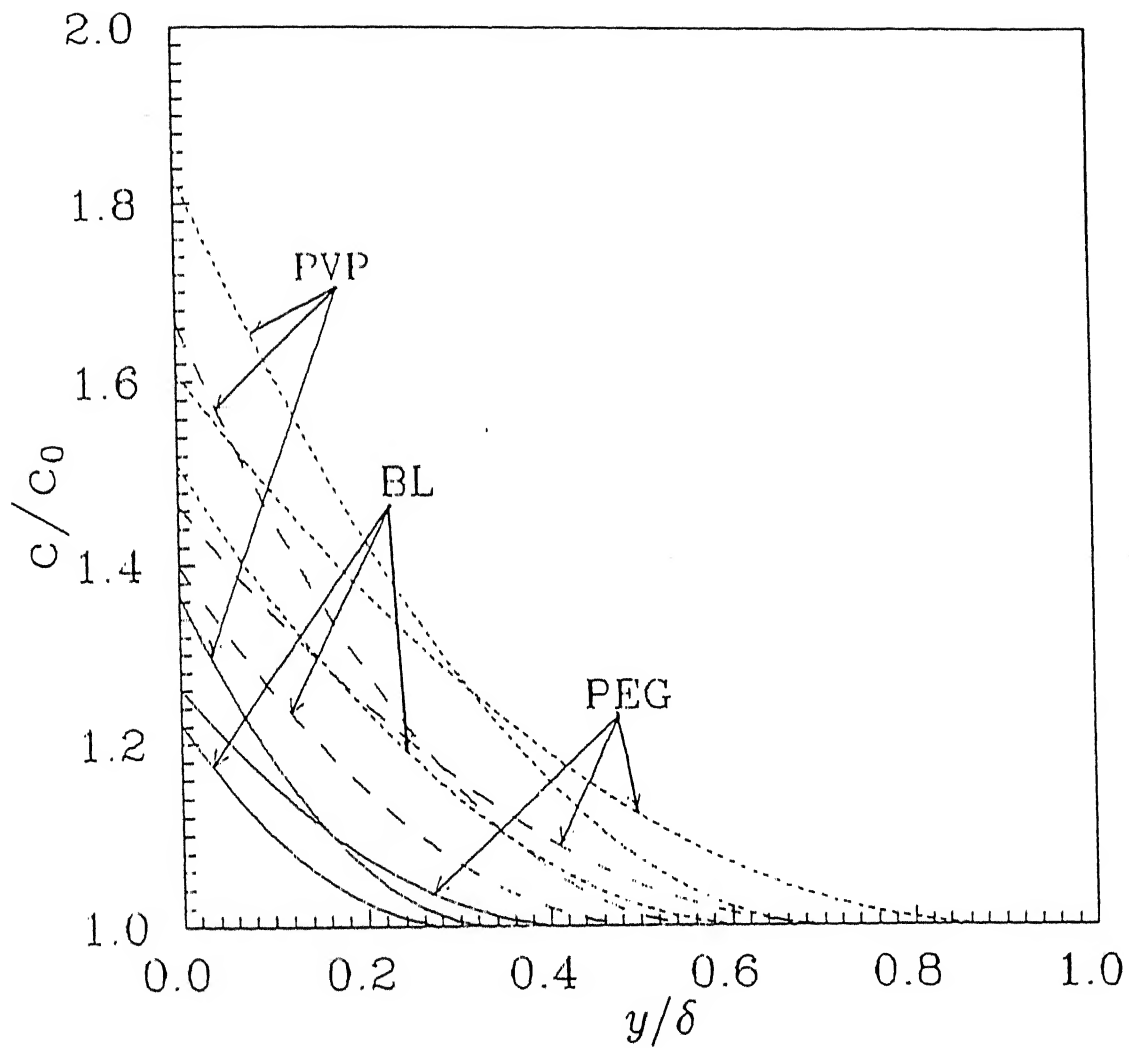


Figure 3.19: Concentration profiles across the boundary layer for different solutes at different points of time at $\Delta P = 830$ kPa, $c_0 = 90$ kg/m³ and 545 rpm. Solid lines are for $t = 0.1$ sec; long dashed lines are for $t = 0.3$ sec and short dashed lines are for $t = 0.5$ sec.

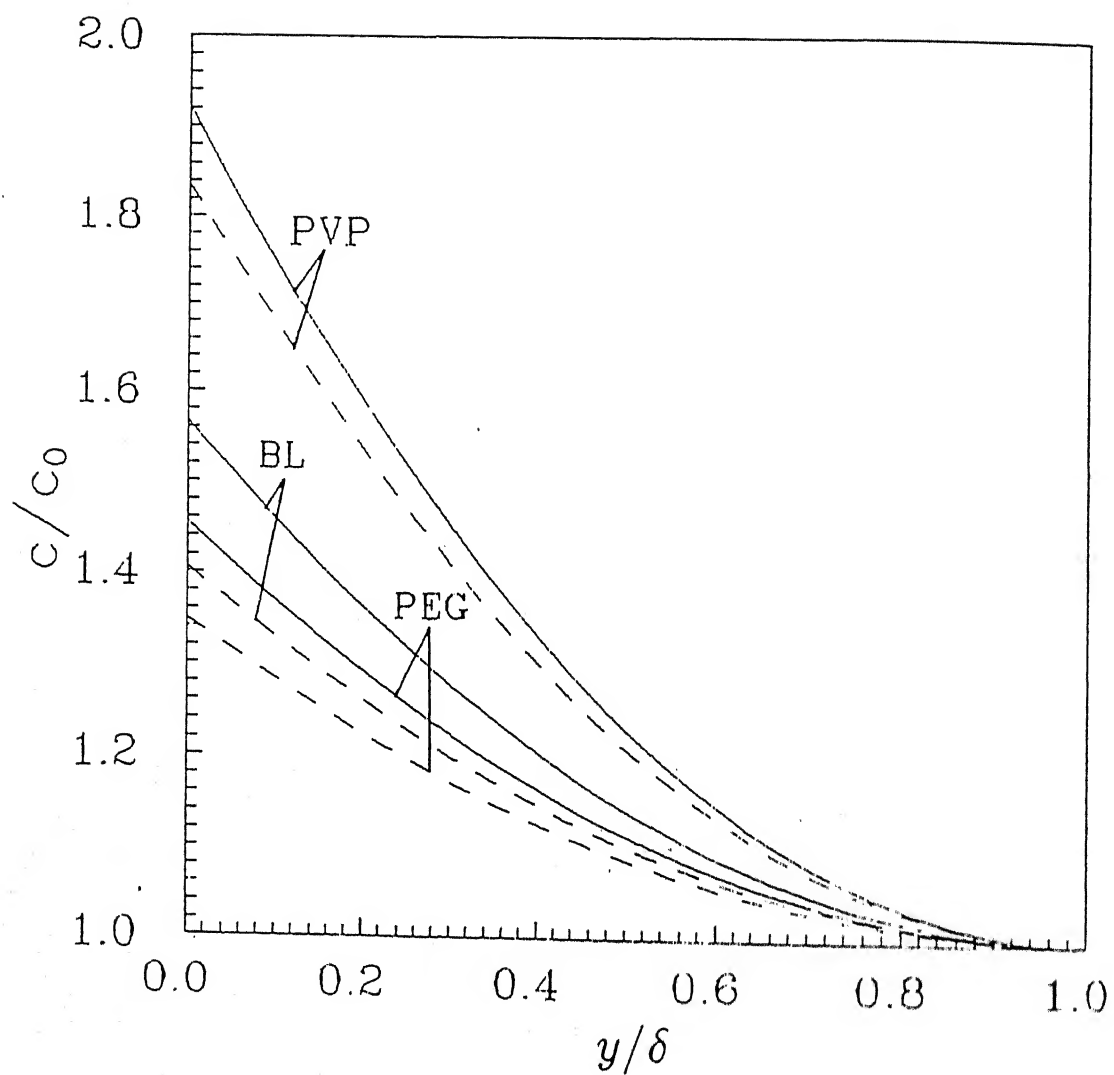


Figure 3.20: Concentration profiles for different solutes under different stirrer speeds at the end of short term flux decline. $\Delta P = 830$ kPa; $c_0 = 90$ kg/m³. Solid lines are for $\omega = 325$ rpm and dashed lines are for $\omega = 525$ rpm.

PVP:

$$R_{ps}^* = 2.0 \times 10^4 (Re)^{-1.73} \left(\frac{c_m - c_p}{c_0 - c_p} \times \frac{\Delta\pi}{\Delta P} \right)^{0.58} \quad (3.39)$$

It can be observed that R_{ps}^* is inversely proportional to Reynolds number and directly proportional to the group $\left(\frac{c_m - c_p}{c_0 - c_p} \times \frac{\Delta\pi}{\Delta P} \right)$. This is because as Reynolds number increases the polarization becomes less severe which consequently reduces the polarized layer resistance. On the other hand, as the second dimensionless group increases the polarization becomes more severe and polarized layer resistance increases. The variations of R_{ps}^* with Reynolds number and the group $\left(\frac{c_m - c_p}{c_0 - c_p} \times \frac{\Delta\pi}{\Delta P} \right)$ are shown in Figs. (3.21) and (3.22) respectively. The figures show the same trend with the dimensionless group as discussed earlier.

The regression analysis over the flux profiles for all the runs also provide the variation of the parameter k_0 for different solutes over different experimental operating conditions. Interestingly, it was observed that for all the experimental runs, the value of k_0 varies over a very narrow range for a particular solute. For example, the variation of k_0 is from 0.27 to 0.32 for PEG, 0.085 to 0.091 for BL and 0.15 to 0.22 for PVP. Therefore, an average value of k_0 for different solutes may be assumed and can be used for prediction purposes within a certain range of accuracy. The value of k_0 determines the curvature of growth of R_{ps}^* with time. Physically, it signifies, whether the growth of the polarized layer is steeper (for larger k_0) or more gradual (for smaller k_0). Therefore, it can be concluded that for PEG, the growth of polarized layer is the steepest and for BL it is the most gradual. For PVP and PEG, this can be explained by the fact that PVP having higher MW than PEG, back diffusion of the solutes is less for PVP and hence, polarized layer grows up more gradually. BL, being a polydispersed mixture, some of its higher molecular weight components virtually have very low diffusivity and they tend to increase the polarized layer more slowly thereby, delaying the approach to the steady state.

Having determined the parameters R_{ps}^* and k_0 , the long term flux decline can be predicted in conjunction of osmotic pressure limited flux (Short term decline), for different operating conditions. Some representative predictions of flux decline are

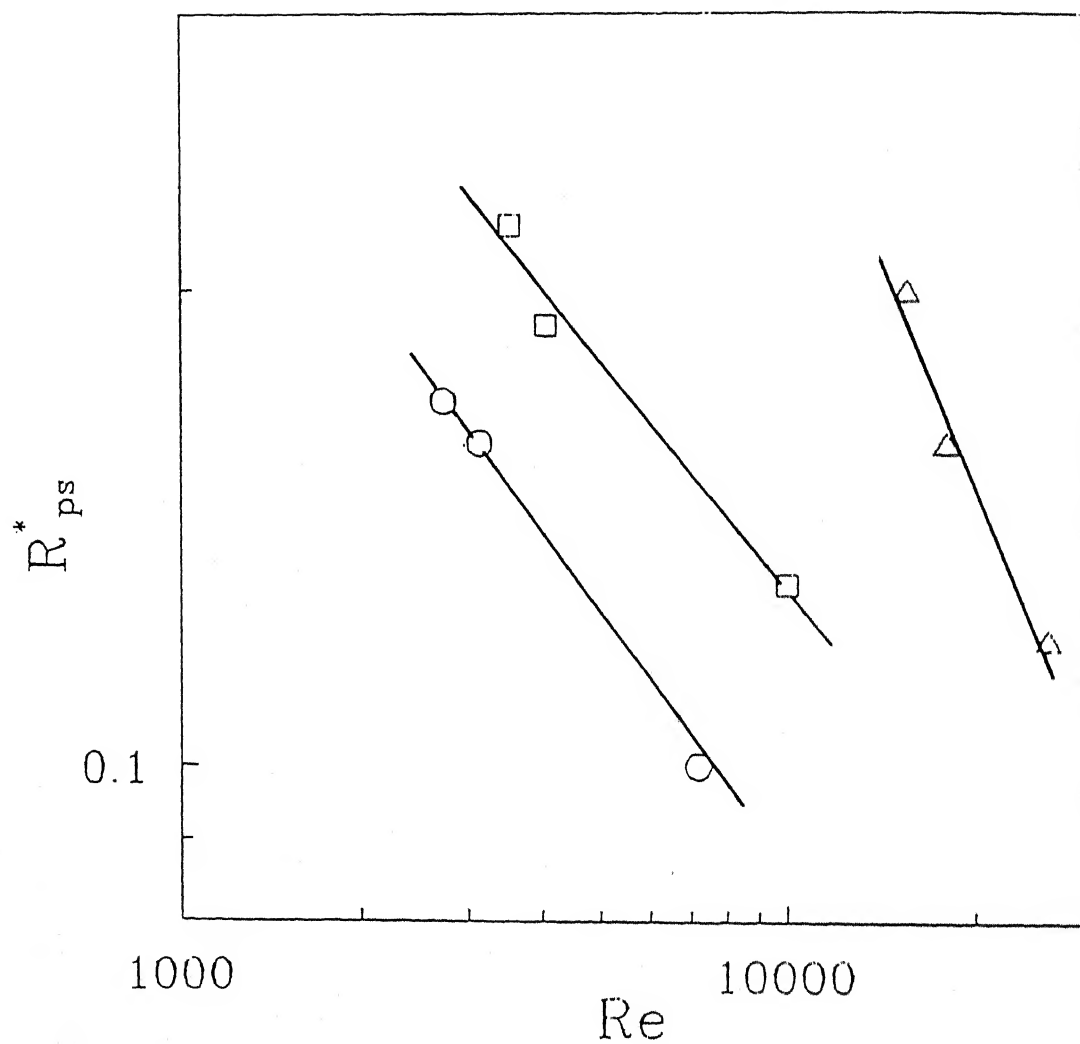


Figure 3.21: Variation of the dimensionless steady state polarized layer resistance with Reynolds number at $\Delta P = 690$ kPa and $c_0 = 90$ kg/m³. \circ (BL); \triangle (PEG); \square (PVP).

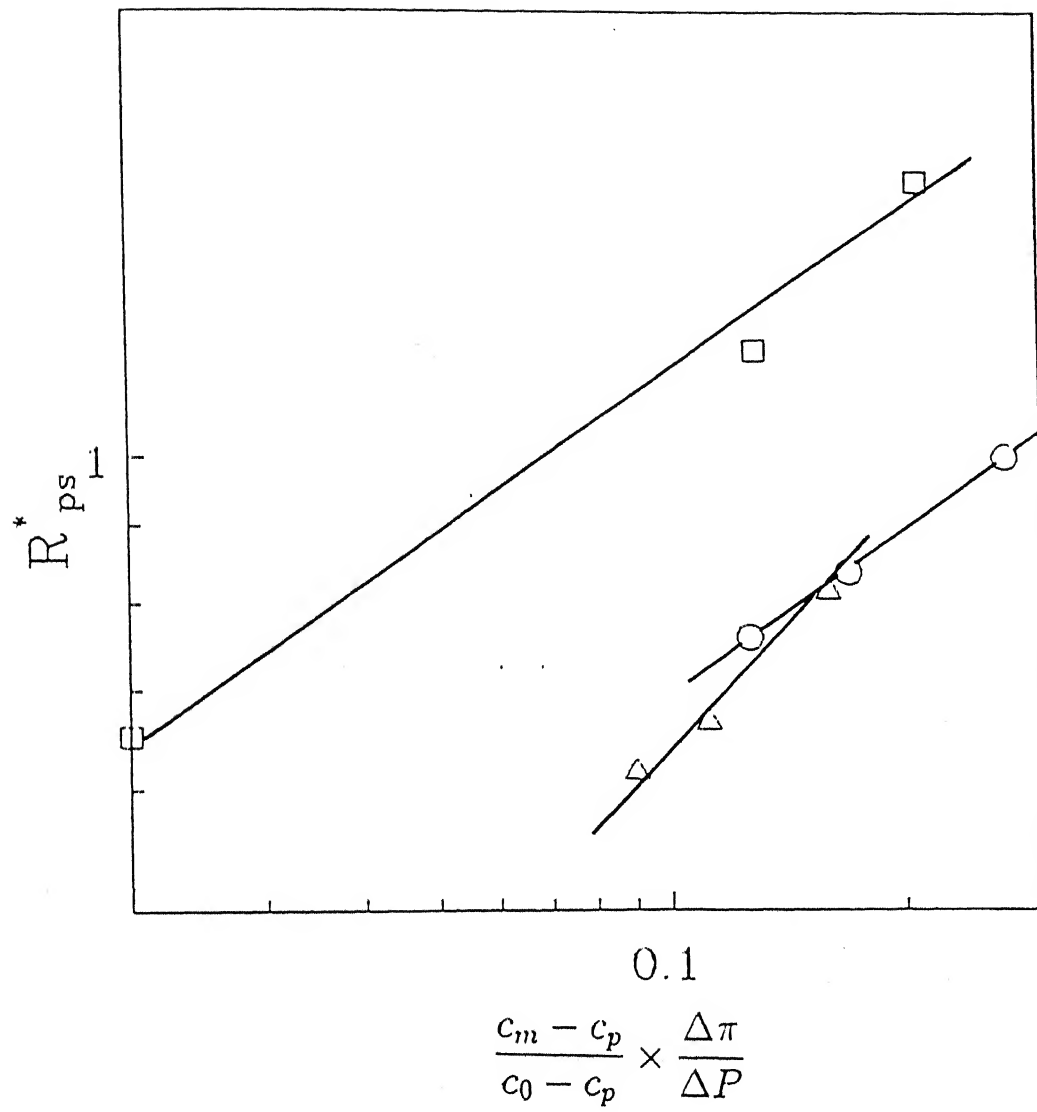


Figure 3.22: Variation of the dimensionless steady state polarized layer resistance with the group $\left(\frac{c_m - c_p}{c_0 - c_p} \times \frac{\Delta\pi}{\Delta P}\right)$ at $\omega = 325$ rpm and $c_0 = 90$ kg/m³. \circ (BL); \triangle (PEG); \square (PVP).

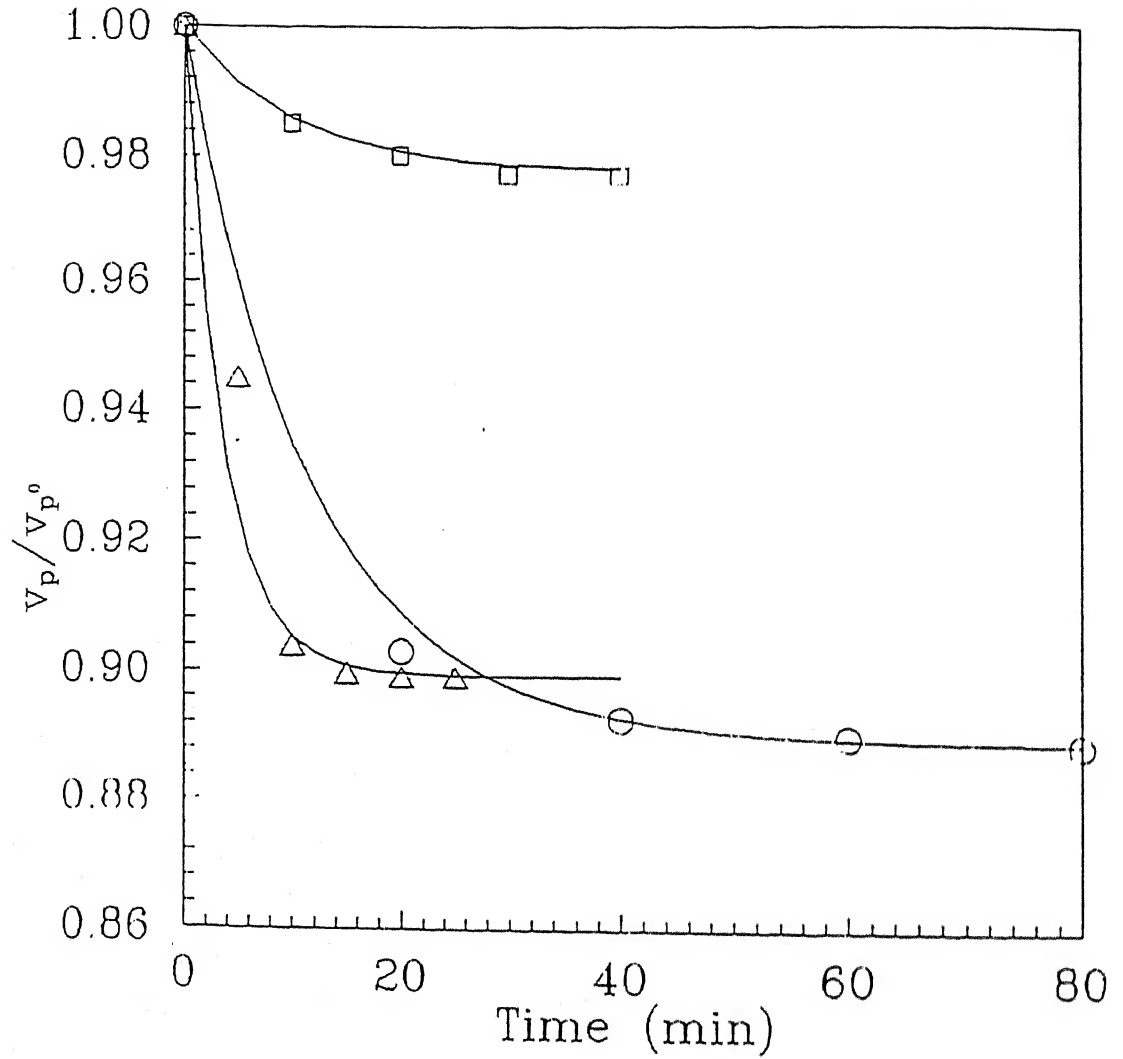


Figure 3.23: Long term flux decline profiles for different solutes at $\Delta P = 550$ kPa; $c_0 = 90$ kg/m³ and $\omega = 425$ rpm. The solid lines are for predicted profiles and symbols are for the experimental data. \circ (BL); \triangle (PEG); \square (PVP).

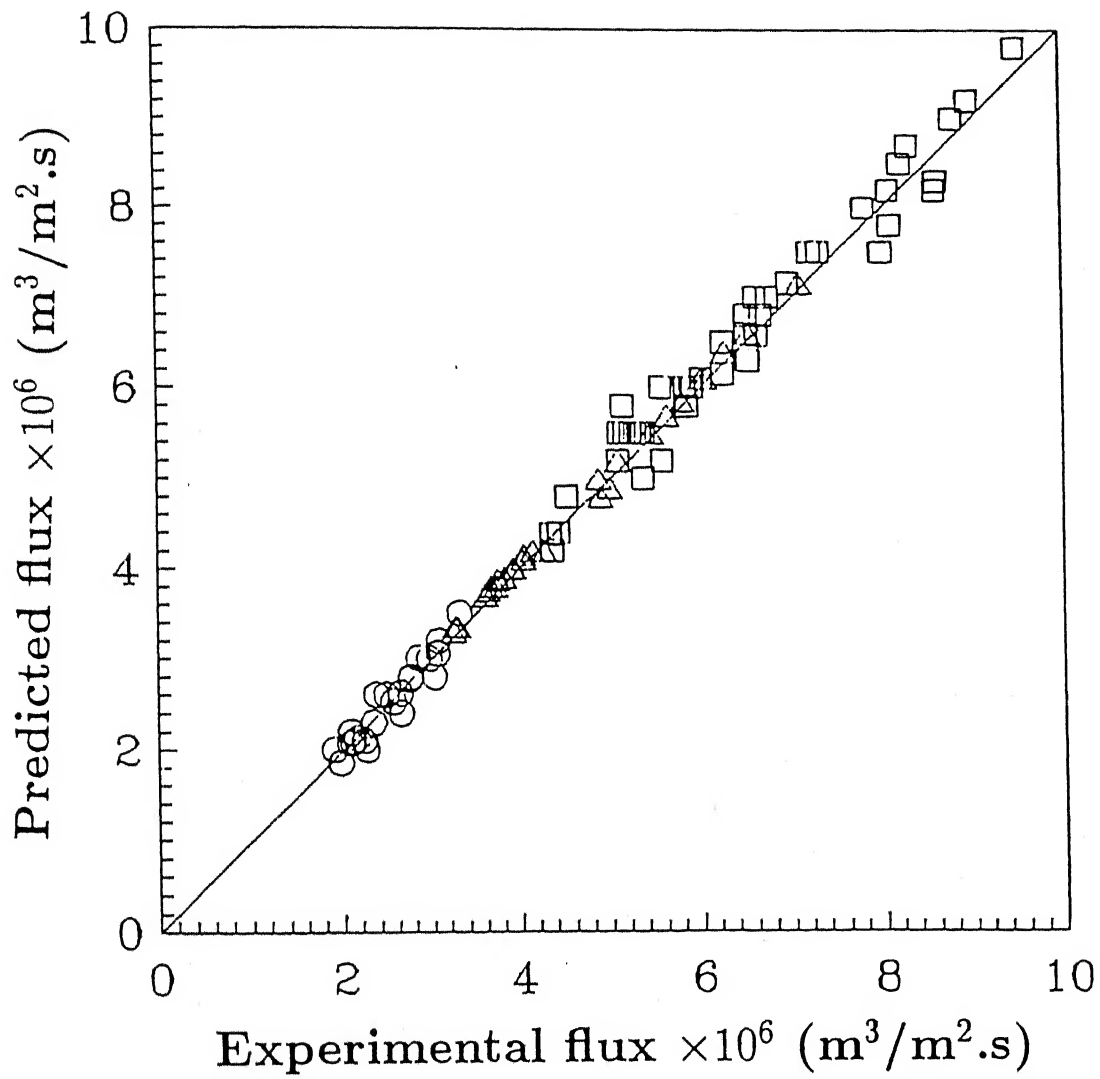


Figure 3.24: Comparison of the predicted and experimental fluxes for all the solutes under all the operating conditions at different points of time.

plotted in Fig. (3.23) for three solutes under the same operating conditions. From the figure, it shows excellent agreement of the correlated and experimental flux profiles. Fig. (3.24) shows predicted and experimental fluxes for all the solutes under all the operating conditions at different times. It can be observed from the figure that the model in this study predicts the flux data quite accurately over all the operating conditions selected in this study.

3.2.5 Conclusions

Initial flux decline in ultrafiltration is osmotic pressure controlled. This decline is very rapid and may be complete within a few seconds. The film theory in conjunction with the phenomenological equation can be used iteratively including the variation of the physical properties (like density, viscosity, etc.) to predict the osmotic pressure limiting flux. The regular Sherwood number correlations can be modified by introducing a correction factor $(Sc/Sc_m)^{0.22}$ to account the variation of properties for the laminar flow in stirred ultrafiltration.

The long term flux decline may be attributed to the gradual growth of a polarized layer over the membrane surface which is limited by the hydrodynamics (stirring in this case). Flux decline in this domain may be modeled using a two parameter model. The parameter R_{ps}^* is found to be a function of operating conditions for all the solutes. The other parameter k_0 is found to be a constant for a particular solute. The value of k_0 is the largest for PEG; it indicates the rate of growth of polarized layer resistance is the fastest for PEG among the three solutes. Whereas, k_0 is the smallest for BL. This indicates that the rate of growth of polarized layer resistance is the most gradual for BL.

3.3 Modeling of Ultrafiltration Process for a Two Component Aqueous Solution of Low and High (Gel-Forming) Molecular Weight Solutes

In the continuing study of various consequences of concentration polarization on flux decline and changes in retention characteristics, it was thought to attempt multicomponent mixture feed solution as well, for UF processing. Filtration of a mixture of low molecular weight and gel forming (high molecular weight) solutes is often encountered in industrial applications. Therefore, to formulate a mathematical model for simultaneous prediction of permeate flux and observed rejection, the system of multicomponent mixture was considered to be constituted by two separate entities of solutes.

3.3.1 Introduction

Formation of gel layer on the membrane surface during filtration of macromolecular solution is a major problem with ultrafiltration (UF) and microfiltration (MF). Deposition of gel layer and its subsequent growth with time lead to very low solvent flux. Further, in some process industries, a practical feed solution may comprise several components (gel forming, high molecular weight non-permeating and low molecular weight permeating solutes). In most of such cases, formation of gel layer is unavoidable and due to this, transport of the desired permeating solutes gets affected. For example, in sugar industry where UF is becoming a viable alternative for clarification of post-limed thin cane juice [244–246], there are two such classes of solutes to be ultrafiltered. Among the non-permeating class of solutes, limed juice contains high molecular weight solutes like proteins, wax, etc. and low molecular weight (LMW) solutes, mainly sucrose [247] fall in the class of permeating solutes. Objective of UF of the limed juice is to retain high molecular weight solutes (which tend to form gel on the membrane surface) and to allow sucrose pass through to the permeate as much as possible. This objective has prompted us to undertake the

study of two component (one high MW gel forming, non-permeating, say, PVA, and the other permeating LMW, say sucrose, solutes) UF process model development to predict the flux decline and sucrose retention characteristics. Instead of taking actual limed juice which is a complex mixture of several components, a synthetic mixture of PVA and sucrose was, therefore, taken for their known properties and easily estimable characteristics. Further, a predictive mathematical model is formulated to depict the transient flux decline and rejection behaviour; the model is tested and the results are compared with the experimental observations. However, testing of the model with actual limed cane juice solution is a subject of future work. It may be noted that the present work is a continuation of the research efforts undertaken in our laboratory to develop such predictive models for typical feed solutions and industrial effluents [113, 137, 216–220].

Filtration of a single component gel forming material is well studied in the literature of UF [24]. The salient feature of gel-layer UF is that the steady state flux is independent of pressure and can be altered by alteration of the hydrodynamic conditions [24, 248]. The simple stagnant film theory enables to predict the steady state permeate flux quite accurately. However, the transient flux decline due to growth of gel layer is also studied [124, 152, 249] in detail. In contrast, UF of a solution of two components, one is permeable and the other is not, is very scant in literature. Baker and Strathmann [129] reported the experimental observations of UF of a mixture of bovine serum albumin (BSA) and γ -globulin through high flux membranes. Nakao and Kimura [132] investigated the retention of vitamin B₁₂ in presence of ovalbumin gel layer and correlated their data using transport mechanism based on phenomenology [119]. However, the semi-empirical model does not provide any significant insight to the transient characteristics of flux decline or rejection behaviour of the solutes and also, is unable for prediction purposes in terms of scaling-up of the process. Recently, UF of a mixture of two proteins, ovalbumin and γ -globulin (both are known to form gel) is carried out [250]. In this work, an important observation was made that the steady state flux of the mixture agrees

with the smaller flux in the corresponding single protein system. Starov [251] presented a mathematical model for UF of macromolecular solutions containing LMW contaminants. But, the model was based on *unknown* interaction potential between gel layer and LMW solute. Therefore, it has been a necessity to develop a predictive model for two component UF.

At this stage, it may be necessary to point out that there have been some difference in opinion regarding gel characteristics. Gel may not mean deposition of a distinct solid-like phase, but a highly viscous solution of a 'pseudo' gel-layer like, owing to the increasing concentration of macromolecular solutes adjacent to the membrane surface [155, 249, 252]. Further, physical observation of the membrane after an experiment also led us to believe that there is no such deposition of solutes but a highly viscous layer. Thus, it is unclear as to what exactly a gel layer signifies. Absence of a gel layer deposition on membrane in case of bovine serum albumin (at pH 4.5) is also reported earlier [116]. These observations confirm that in the case of PVA, a true gel phase may not have formed on the membrane as in the case of BSA [249].

The present work deals with UF of aqueous solution of PVA and sucrose in the same proportion as sucrose and high molecular weight solutes occur in thin limed juice in sugar industry. Various parameters in the model are estimated independently from separate sets of experiments and as such, there is no adjustable parameters. Permeate flux declines over time and attains the constant value which is equal to the steady state value of only PVA solution under the same operating conditions. Observed rejection of sucrose increases rapidly over time and reaches a constant value. Rejection of sucrose is more for a tight membrane (low MWCO) and less for a high MWCO membrane.

3.3.2 Theory

Formation of gel layer on the membrane surface in UF of a mixture of gel forming and LMW solutes is described in Fig. (3.25). The coordinate system adopted in the development of theory is also presented in the same figure. In this figure, y is the solvent flow direction, v_p is the volumetric permeate flux, L_g is the gel layer thickness, and δ is the thickness of concentration boundary layer. Subscripts 1 and 2, in the text, refer to the gel forming and LMW solutes, respectively.

A material balance for the gel forming component in the concentration boundary layer results the following equation,

$$\text{for } 0 < y < \delta,$$

$$j_1 = \text{mass flux} = \rho_g \frac{dL_g}{dt} = v_p c_1 - D_1 \frac{dc_1}{dy} \quad (3.40)$$

where, ρ_g is density of gel forming layer.

The pertinent boundary conditions are,

$$c_1 = c_{1b} \quad \text{at } y = 0 \quad (3.41)$$

$$c_1 = c_{1g} \quad \text{at } y = \delta \quad (3.42)$$

Solution of Eq. (3.40) subject to the boundary conditions given by Eqs. (3.41) and (3.42) is,

$$\rho_g \frac{dL_g}{dt} = v_p \frac{c_{1g} - c_{1b} \exp(v_p/k_1)}{1 - \exp(v_p/k_1)} \quad (3.43)$$

where, $k_1 (= D_1/\delta)$ is the mass transfer coefficient for the gel forming solute.

A mass balance for LMW solute in the concentration boundary layer gives,

$$j_2 = v_p c_{2p} = v_p c_2 - D_2 \frac{dc_2}{dy} \quad (3.44)$$

In the bulk, the boundary condition is,

$$c_2 = c_{2b} \quad \text{at } y = 0 \quad (3.45)$$

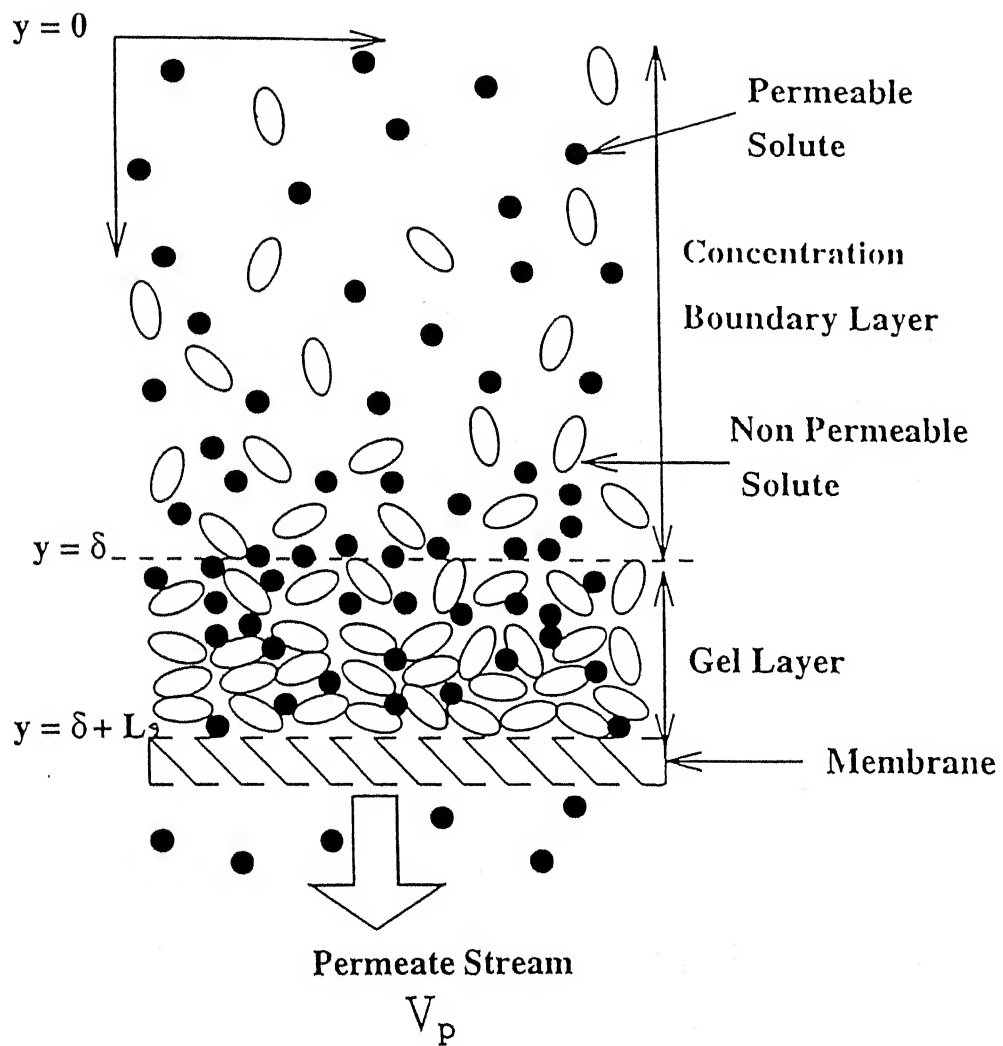


Figure 3.25: Schematic of gel polarized UF of two components

Solution of Eq. (3.44), subject to the boundary condition, Eq. (3.45) is,

$$\frac{c_2(y) - c_{2p}}{c_{2b} - c_{2p}} = \exp\left(\frac{v_p y}{D_2}\right) \quad (3.46)$$

A mass balance of LMW solute in the gel layer gives,

$$\text{for } \delta < y < \delta + L_g,$$

$$j_2 = v_p c_{2p} = v_p c_2 - \epsilon_g D_2 \frac{dc_2}{dy} \quad (3.47)$$

where, ϵ_g is gel porosity. The boundary conditions for Eq. (3.47) at the membrane surface is,

$$c_2 = c_{2m} \text{ at } y = \delta + L_g \quad (3.48)$$

LMW solute gets adsorbed in the gel layer. Its concentration at the boundary layer and gel layer interface remains at equilibrium and is dictated by the partition coefficient between the boundary and gel layer. Therefore, a linear relationship may be described as,

$$c_2(\delta^-) = \gamma_g c_2(\delta^+) \quad (3.49)$$

where, γ_g is the partition coefficient for LMW solute at the boundary layer and gel layer interface.

Solution of Eq. (3.47) with boundary condition, Eq. (3.49), is,

$$c_2(y) - c_{2p} = \exp\left(\frac{v_p(y - \delta)}{\epsilon_g D_2}\right) \frac{c_{2p}(1 - \gamma_g) + (c_{2b} - c_{2p})\exp(v_p/k_2)}{\gamma_g} \quad (3.50)$$

where, $k_2 (= D_2/\delta)$ is the mass transfer coefficient for LMW solute. Using the boundary condition Eq. (3.48) we get,

$$c_{2m} - c_{2p} = \exp\left(\frac{v_p L_g}{\epsilon_g D_2}\right) \frac{c_{2p}(1 - \gamma_g) + (c_{2b} - c_{2p})\exp(v_p/k_2)}{\gamma_g} \quad (3.51)$$

Now, for a membrane - solute pair, assuming the actual rejection coefficient (R_{r2}) to be constant [239], we therefore, have,

$$R_{r2} = 1 - \frac{c_{2p}}{c_{2m}} \quad (3.52)$$

Putting Eq. (3.52) in Eq. (3.51) and eliminating c_{2p} we obtain, after rearrangement,

$$c_{2m} = \frac{c_{2b} \exp \left[v_p \left(\frac{1}{k_2} + \frac{L_g}{\epsilon_g D_2} \right) \right]}{\gamma_g R_{r2} + (1 - R_{r2})(\gamma_g - 1) \exp \left(\frac{v_p L_g}{\epsilon_g D_2} \right) + (1 - R_{r2}) \exp \left[v_p \left(\frac{1}{k_2} + \frac{L_g}{\epsilon_g D_2} \right) \right]} \quad (3.53)$$

Permeate flux can be expressed through the phenomenological equation:

$$v_p = \frac{\Delta P - \Delta \pi}{\mu(R_m + R_g)} \quad (3.54)$$

where, R_g is the gel layer resistance. The gel layer, characteristics of which has been discussed earlier, has been dealt in several ways for mathematical purpose. If it is assumed as a deposit of porous cake, one may then use filtration theory. Therefore, gel layer resistance and its other characteristics may be described under the framework of conventional filtration cake theory [124, 152]. Thus, R_g can be expressed as,

$$R_g = \alpha(1 - \epsilon_g)\rho_g L_g \quad (3.55)$$

The specific cake resistance (assuming gel characteristics to be same as of a cake) α , is obtained from the Kozney-Karman equation [124] in terms of particle properties,

$$\alpha = 180 \frac{(1 - \epsilon_g)}{\epsilon_g^3 d_p^2 \rho_g} \quad (3.56)$$

where, ϵ_g is the porosity, ρ_g is the density of the gel forming solutes and d_p is its equivalent spherical diameter.

Osmotic pressure due to gel-forming component is assumed to be negligible compared to that of the LMW solute [1]. Therefore, overall osmotic pressure difference may be expressed as,

$$\Delta \pi = \pi(c_{2m}) - \pi(c_{2p}) \quad (3.57)$$

The solution of Eq. (3.43) along with Eqs. (3.53) and (3.54) provides the permeate flux, v_p , and permeate concentration and consequently, observed rejection of LMW solute

($R_{02} = 1 - (c_{2p}/c_{2b})$) as a function of time. The experimental techniques adopted

to determine different parameters of the model and the results are described in the subsequent sections. The relevant physical properties of the of the solutes are presented in the appendix B.

3.3.3 Experimental

3.3.3.1 Materials

Spectra Por cellulose ester disc membranes (76 mm diameter) of molecular weight cut off (MWCO) 1K and 10K, obtained from Spectrum Medical Industries Inc., USA were used for the UF experiments.

Polyvinyl alcohol (PVA, average MW 52,000) were obtained from Robert Johnson, India and sucrose was procured from BDH Chemicals, England. All the chemicals were of analytical grade and of high purity.

3.3.3.2 Choice of feed concentration of the mixed feed

Since the motivation behind this work was to develop a workable model for UF of thin limed cane juice, the composition of the feed solution was chosen close to a value which normally occurs in limed cane juice. The ratio of the permeable to non-permeable materials in limed juice was roughly 85:15 (on a dry basis) [253]. Therefore, the feed solution was prepared containing 40 kg/m³ of sucrose and 10 kg/m³ of PVA. All the feed solutions were prepared by dissolving the solute in distilled water.

3.3.3.3 Apparatus

The concentration of the permeate streams were measured by a refractometer (Bosch and Lomb). The refractive index of the solutions were measured and compared

against the calibrated curves. The viscosity of the feed solutions were measured using an Ostwald viscometer. The stirrer speeds of the UF cell were measured using a stroboscope. The permeate flux was measured volumetrically by measuring cumulative volume permeated against time.

The experiments were performed in a continuous UF cell, fitted with a stirrer. The effective filtration area is about 35 cm². The membrane was placed on a polymeric support at the base of the cell; the permeate was collected from the bottom.

3.3.3.4 Procedure

UF of the mixed feed

The membranes were compacted by subjecting them to 850 kPa pressure, higher than the maximum operating pressure, for 3 hours with distilled water. The operating pressures were chosen as 482, 620 and 792 kPa; whereas, the stirrer speed was varied as 400, 525 and 600 rpm. The feed tank was filled up by 1.5 liter of the feed solution and was subjected to UF for half an hour. It was observed that both the flux and rejection became steady within 4 to 5 minutes, which is a typical well known observation for stirred UF [124]. Both the retentate and permeate streams were recycled to the feed tank to maintain the constant feed concentration. Permeate flux and concentration were measured with time. Water run using distilled water was taken before actual UF experiments to measure the hydraulic resistance of the membrane. After completion of an experiment, membrane was rinsed thoroughly with distilled water and again water run was taken in order to check the membrane resistance. These measurements revealed that there was no permanent membrane fouling due to solute adsorption. The membrane hydraulic resistances were measured as 5.85×10^{13} for 1K and $2.60 \times 10^{13} \text{ m}^{-1}$ for 10K membrane. Fresh solutions were used for all experimental runs. All the experiments were conducted at room temperature, $30 \pm 2^\circ\text{C}$.

Determination of PVA gel concentration

To determine gel concentration, PVA solution was subjected to continuous stirred UF, at 655 kPa and stirrer speeds 600 and 525 rpms with 1K membrane. Feed concentrations used were 10, 45 and 100 kg/m³.

Determination of viscosity effect on mass transfer coefficient of PVA solution

To determine the viscosity effect on mass transfer coefficient, experiments were conducted in stirred, continuous UF with PVA solution with 1K membrane. The feed concentration and operating pressure were chosen as 10 kg/m³ and 655 kPa, respectively. Stirrer speeds were varied from 150 to 600 rpm.

Determination of specific gel resistance

To determine the specific resistance of PVA gel, unstirred batch UF experiments were conducted using 10 kg/m³ PVA solution at 482, 620 and 723 kPa pressure with 1K membrane.

Determination of real rejection of sucrose

A 10 kg/m³ of sucrose solution was subjected to continuous, stirred UF. The steady state permeate flux and concentration were measured. Extremely high (1600 rpm) stirrer speed and low pressure, 275 kPa were used as the operating conditions in order to eliminate the effect of concentration polarization as suggested in the literature [237]. The value of real rejection was also tested against higher pressures 482 kPa and 724 kPa.

Average partition coefficient of sucrose in gel layer

A gross experiment was designed and conducted to measure the average partition coefficient of sucrose in PVA gel layer. First, 25 ml of 50 kg/m³ of PVA solution was ultrafiltered at 482 kPa in the batch cell, using a 20K membrane. The UF was carried out till the permeate stopped coming after around 12 hours. The difference in volume (feed and permeate volume) was the volume of water entrapped in the gel layer. After that, 50 ml of 40 kg/m³, sucrose solution was put on the PVA gel and

kept for one hour. Then, again UF was started and 10 ml of permeate was collected. The concentration of sucrose in the retentate and permeate were measured. The difference in weight must be the amount of sucrose adsorbed in the gel layer. The ratio of retentate to sucrose concentration in gel layer provides the average partition coefficient.

3.3.4 Results and discussions

This section has been designed into two parts. First part deals with the experimental determination of various parameters required in the developed model (as outlined in the previous section) and the second part deals with the solution of the model and its comparison with the experimental observations of the mixed feed UF.

3.3.4.1 Experimental estimation of various parameters

Estimation of gel concentration of PVA

Continuous stirred UF with PVA solution at different concentrations were conducted to determine the gel concentration of PVA as described earlier. The steady state permeate flux with feed concentration at different stirrer speeds has been plotted in Fig. (3.26) in a semi-log scale. From the figure, it can be observed that both the curves converge close to a concentration 350 kg/m^3 on extrapolation. The measured gel concentration of PVA is in agreement with the literature data [249].

Estimation of viscosity effect on mass transfer coefficient for PVA

A 10 kg/m^3 PVA solution has a viscosity 2.18 cp (whereas, that for the mixed feed is 2.20 cp) and density is almost same as that of pure water. With this viscosity, Reynolds number in stirred cell ($\omega r^2 \rho / \mu$) for all the operating range of stirrer speeds from 150 to 600 rpm, is less than 32,000; i.e. hydrodynamic flow condition is in the laminar range. For laminar flow, mass transfer coefficient may be calculated from the correlation [24],

$$k_1 = 0.285(D_1/r)(Re)^{0.55}(Sc)^{0.33}f \quad (3.58)$$

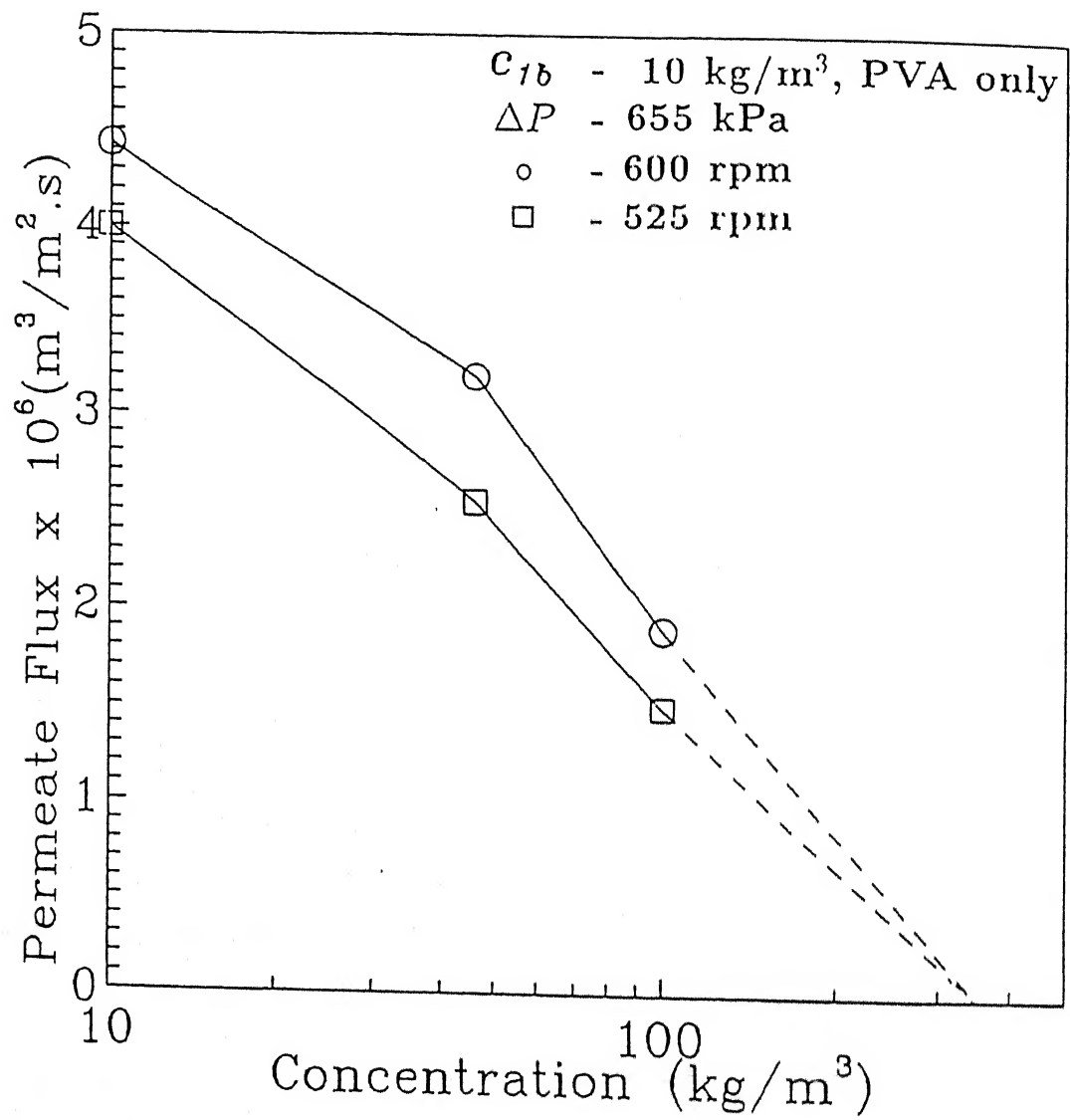


Figure 3.26: Steady state flux versus concentration of PVA solution

where, f is the viscosity correction factor given by $(\mu_b/\mu_g)^{0.14}$ [27]. In order to estimate f , the steady state flux was measured at different stirrer speeds (as described earlier). The flux versus stirrer speed is shown in Fig. (3.27). Using gel-polarization model, steady state flux was calculated from the following equation,

$$v_p = k_1 \ln \frac{c_g}{c_b} \quad (3.59)$$

where, k_1 is estimated from Eq. (3.58). From the experimental values of steady state flux, c_g , Re , Sc , etc., f was estimated for different stirrer speeds. It was observed that f has value ranging from 0.42 to 0.46. Therefore, an average value of 0.44 was taken and used for the computations. However, for sucrose, feed concentration itself is 40 kg/m³ and the membranes are not highly retentive one (10K membrane does not retain sucrose at all) and hence, build up of sucrose concentration in the boundary layer is not significant; therefore, viscosity correction for mass transfer coefficient in case of sucrose was not felt necessary.

Determination of specific gel resistance

Using the approach of filtration theory [124], specific resistance of gel layer was obtained by fitting the experimental data of unstirred UF to the following expression,

$$\frac{1}{v_p^2} = \frac{1}{J_w^2} + \alpha \phi t \quad (3.60)$$

where, $\phi = 2c_b\mu_w/\Delta P$ is constant for a given pressure. The slope of $1/v_p^2$ versus t plot, gives the value of specific cake resistance. For different pressures (in the range of actual operating pressures of the mixed feed UF), these plots are shown in Fig. (3.28). Variation of α values obtained from the slopes of the curves in Fig. (3.28), with pressure are shown in the inset of Fig. (3.28). The experimental data were correlated with pressure by a simple relation,

$$\alpha = \alpha_0(\Delta P)^{0.38} \quad (3.61)$$

where, $\alpha_0 = 2.223 \times 10^{14}$ m/kg and ΔP is in Pa.

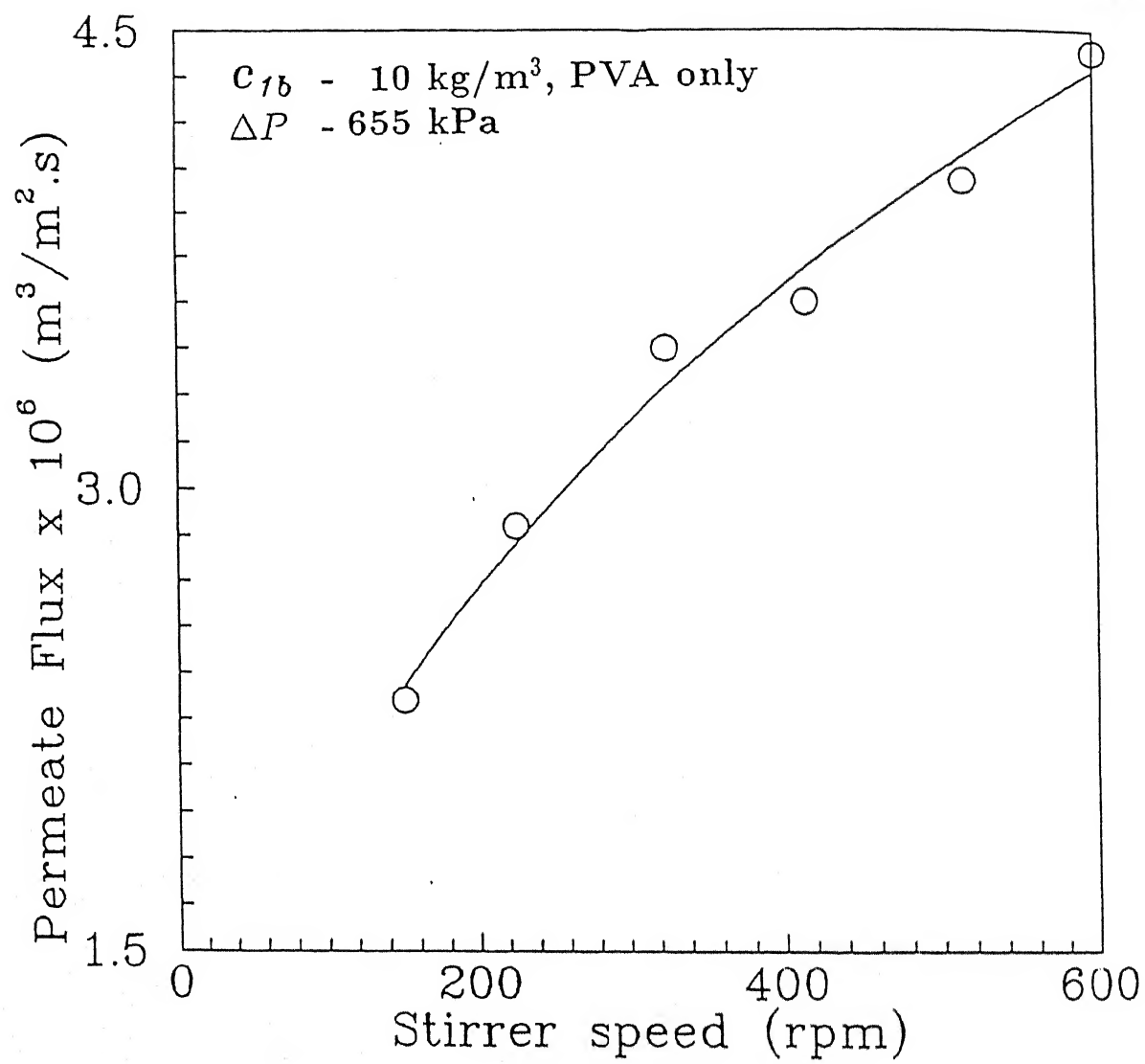


Figure 3.27: Steady state flux versus stirrer speed of PVA solution

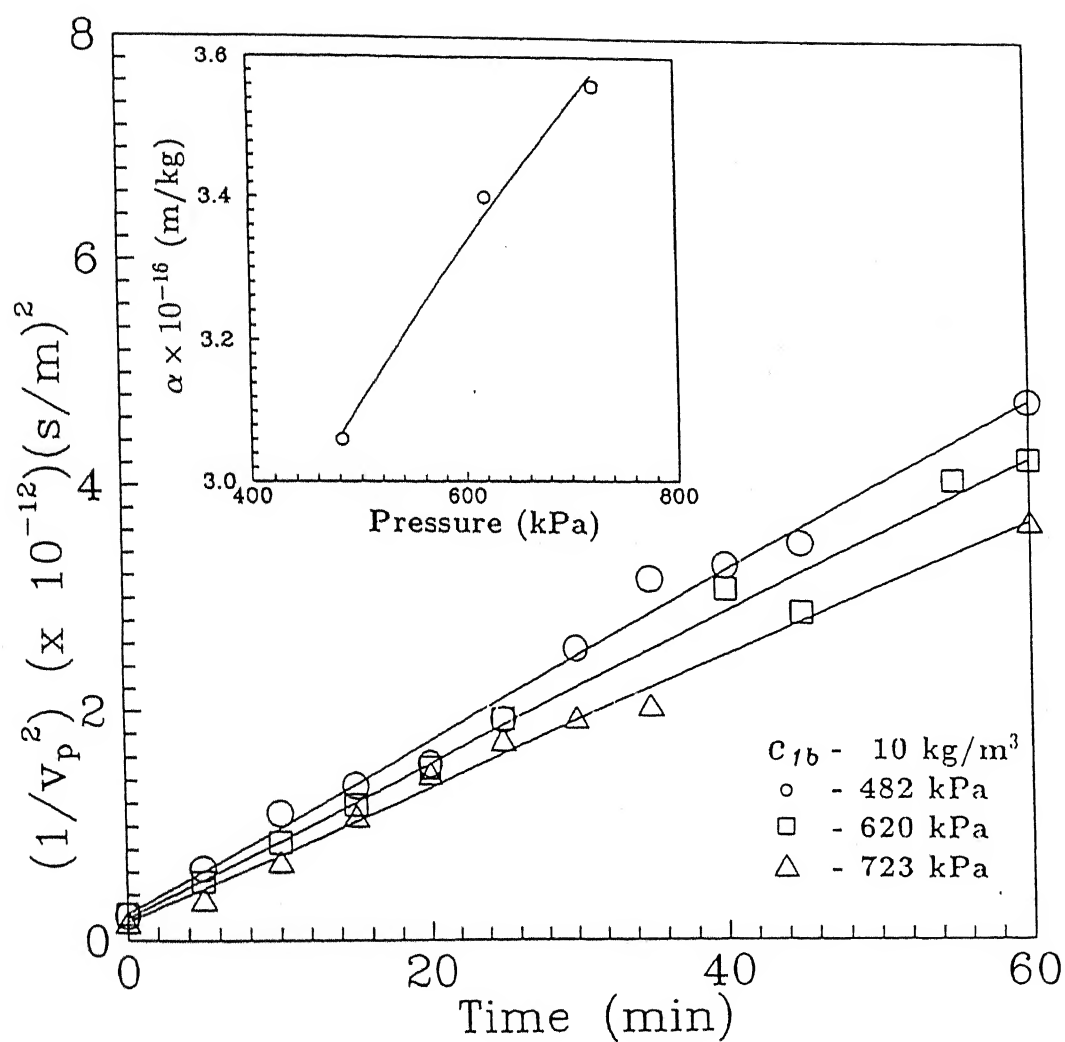


Figure 3.28: $1/v_p^2$ versus time plot for PVA in unstirred UF. Specific cake resistance versus pressure (inset)

Determination of gel porosity (ϵ_g) and equivalent spherical diameter (d_p) of the gel forming particles

It may be noted here, that PVA, being a branched chain polymeric material does not have particulate conformation. Therefore, in the 'pseudo' gel layer, it forms a fine microporous structure with high specific resistance (Table 3.6). Such high values of specific resistances of polymeric dextran and PVA solution are also available in literature [124, 249]. Specific cake resistance, α is expressed as given by Eq. (3.61). Gel porosity can be related to d_p [124, 249] as,

$$\epsilon_g = 1.0 - 10^3 \frac{\pi}{6} c_g \frac{N_A d_p^3}{M_w} \quad (3.62)$$

where, N_A is Avogadro number, M_w is molecular weight of the solute and c_g is the gel concentration. From Eq. (3.62), α can be expressed as a function of only unknown d_p (density of PVA is taken as 1270 kg/m³ [254]). For a given operating pressure, α can be calculated from Eq. (3.61) and therefore, Eq. (3.56) can be solved along with Eq. (3.62) by Newton-Raphson technique to obtain d_p (as well as ϵ_g). The evaluated parameters for different pressures are presented in Table 3.6). It may be pointed out here, that PVA does not form a packed bed of spherical particles with diameter given in Table 3.6, but rather that the gel layer has the resistance of such a packed bed.

Real rejection of sucrose

The membrane of 1K MWCO rejects sucrose to some extent, whereas, 10K membrane does not retain it at all. For determination of R_{r2} in case of 1K membrane, experiments in stirred continuous UF are conducted and R_{r2} was found to be 0.73. For 10K membrane, it was 0.0.

Partition coefficient of sucrose in PVA gel

The experimental procedure to determine the average partition coefficient ($\overline{\gamma_g}$) has been outlined in the previous section. The obtained value $\overline{\gamma_g}$ can be expressed according to the following relation,

$$\overline{\gamma_g} = \frac{\overline{c_b}}{\overline{c_{gel}}} \quad (3.63)$$

Table 3.6: Gel porosity and equivalent spherical solute diameter for different pressures

$\Delta P(kPa)$	$\alpha (m/kg)$	$d_p(nm)$	ϵ_g
482	3.06×10^{16}	6.56	0.40
620	3.40×10^{16}	6.60	0.39
724	3.56×10^{16}	6.62	0.38

where, \bar{c}_b is the average concentration within the boundary layer from the bulk to the gel surface and \bar{c}_{gel} is the average concentration of sucrose in the gel layer. Experimentally obtained value of $\bar{\gamma}_g$ was 2.28. Now, γ_g in the model is the value at the gel layer and boundary layer interface. Having determined other parameters in the model, value of γ_g is established through the following technique.

Average value of solute concentration in the boundary layer is obtained as,

$$\bar{c}_b = \frac{1}{\delta} \int_0^{\delta} c_2(y) dy \quad (3.64)$$

where, $c_2(y)$ can be obtained from Eq. (3.46). Average value of solute concentration in the gel layer can be obtained as,

$$\bar{c}_{gel} = \frac{1}{L_g} \int_{\delta}^{\delta+L_g} c_2(y) dy \quad (3.65)$$

where, $c_2(y)$ can be obtained from Eq. (3.50). Now, assuming different values of γ_g , the model equations are solved for filtration through a 10K membrane (since, 10K and higher MWCO membranes do not retain sucrose at all, the rejection characteristics of sucrose does not depend on the membrane permeability for such membranes and is solely governed by the gel layer) and using the steady state values of $v_p, c_{2p}, \delta,$

etc., integrals in Eqs. (3.64) and (3.65) are evaluated and finally, Eq. (3.63) gives a theoretical estimate of $\overline{\gamma}_g$. Using the above technique, the value of γ_g is obtained as 2.42 which results in $\overline{\gamma}_g = 2.28$. Subsequently, this value of γ_g has been utilized in the model for the prediction of flux and rejection.

Having determined all the relevant parameters of the model, the model can now be solved without any adjustable parameter and further can be used for the prediction purposes. In the subsequent section, the results of the model and its comparison with the experimental observations are presented.

3.3.4.2 Analysis of model predictions and comparison with the experimental observations for UF of mixed feed

In order to solve the proposed model, Eq. (3.43) is solved using fourth order Runge-Kutta technique along with the algebraic Eqs. (3.53) and (3.54). Time steps for numerical integration are taken extremely close initially and gradually relaxed later on. A Newton-Raphson iteration is employed to solve the last two algebraic equations for a particular time step.

The steady state concentration profile of both PVA and sucrose is shown in Fig. (3.29), for a typical operating conditions. The concentration of PVA increases from its bulk to gel concentration in the boundary layer and then remains constant; whereas, the profile of sucrose concentration suggests that its concentration increases from the bulk value both in boundary as well as in the gel layer. It may be noted that in the boundary-gel layer interface, sucrose concentration distribution is dictated by its partition coefficient, while its permeate concentration is governed by the membrane characteristics. The enlarged view of sucrose concentration profile is presented in the inset of Fig. (3.29). These profiles are marginally linear.

Fig. (3.30) describes the effect of stirrer speed on concentration boundary layer and gel layer thicknesses at steady state. As stirring increases, back diffusion of the solute particles towards the bulk increases and therefore, boundary layer thickness

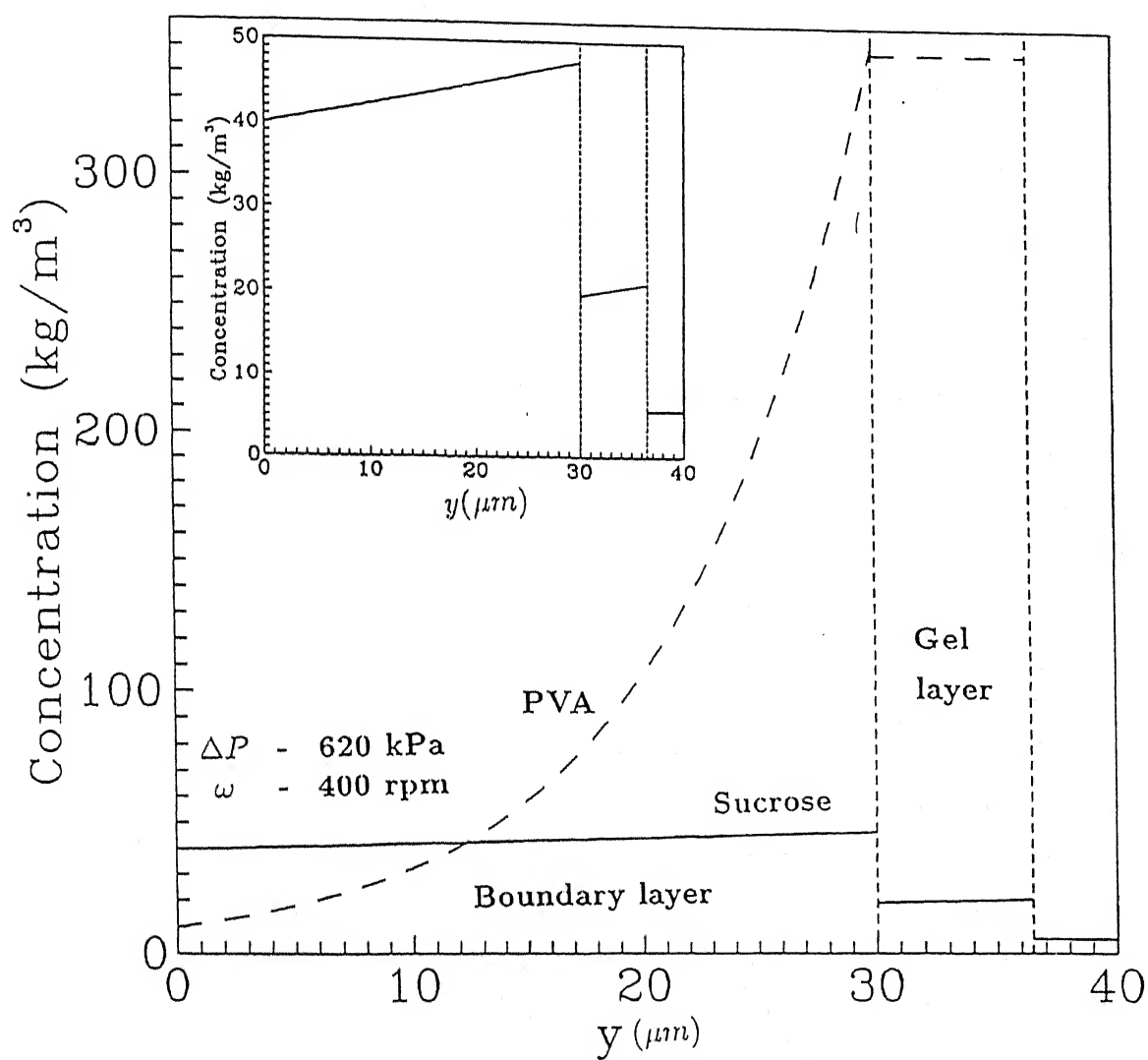


Figure 3.29: Concentration profiles of PVA and sucrose with distance for a typical operating condition. Concentration profile of sucrose (inset)

diminishes. Also, increase in stirrer speed limits the growth of the gel layer as higher stirrer speed promotes more turbulence in the feed side. The figure also describes the effect of pressure on the gel layer thickness. The specific cake resistance of gel layer increases with pressure as it causes compaction of the layer which facilitates further growth of the layer (Table 3.6). Therefore, at high pressure, gel layer thickness is found to be more. However, even at higher pressure, gel layer thins down with increase in stirrer speed.

Magnitude of different resistances against the solvent flux provides a better understanding towards the flow controlling mechanism. Apart from the membrane hydraulic and gel layer resistances, osmotic pressure resistance also plays an important role at least for a lower MWCO (e.g., 1K membrane in this study) membranes which retain LMW solutes partially. For a more open membrane (e.g., 10K membrane), osmotic pressure resistance becomes insignificant and gel layer controls the solvent flux. Osmotic pressure resistance (R_{osm}) is calculated from the following relationship,

$$v_p = \frac{\Delta P - \Delta \pi}{\mu(R_m + R_g)} = \frac{\Delta P}{\mu(R_m + R_g + R_{osm})} \quad (3.66)$$

Contributions of different resistances for typical operating conditions at steady state are tabulated in Table 3.7. From this table, it is apparent that R_{osm} is merely 11 to 15% of the total resistance (R_T) for 1K membrane at different operating conditions. For higher pressure and lower stirrer speed, both gel layer and membrane hydraulic resistance become competitive. For a 10K membrane which does not retain sucrose at all (for experiments carried out in absence of PVA), osmotic pressure resistance is zero (when both components are present) for all the operating conditions. Gel layer resistance is found to be dominant. In this case also, it can be observed that R_g increases with increase in pressure and decrease in stirrer speed.

The model predictions for permeate flux for 1K membrane for different operating pressures and stirrer speeds are shown in Figs. (3.31a) and (3.31b). The experimentally obtained flux values are also shown in these figures. It can be observed

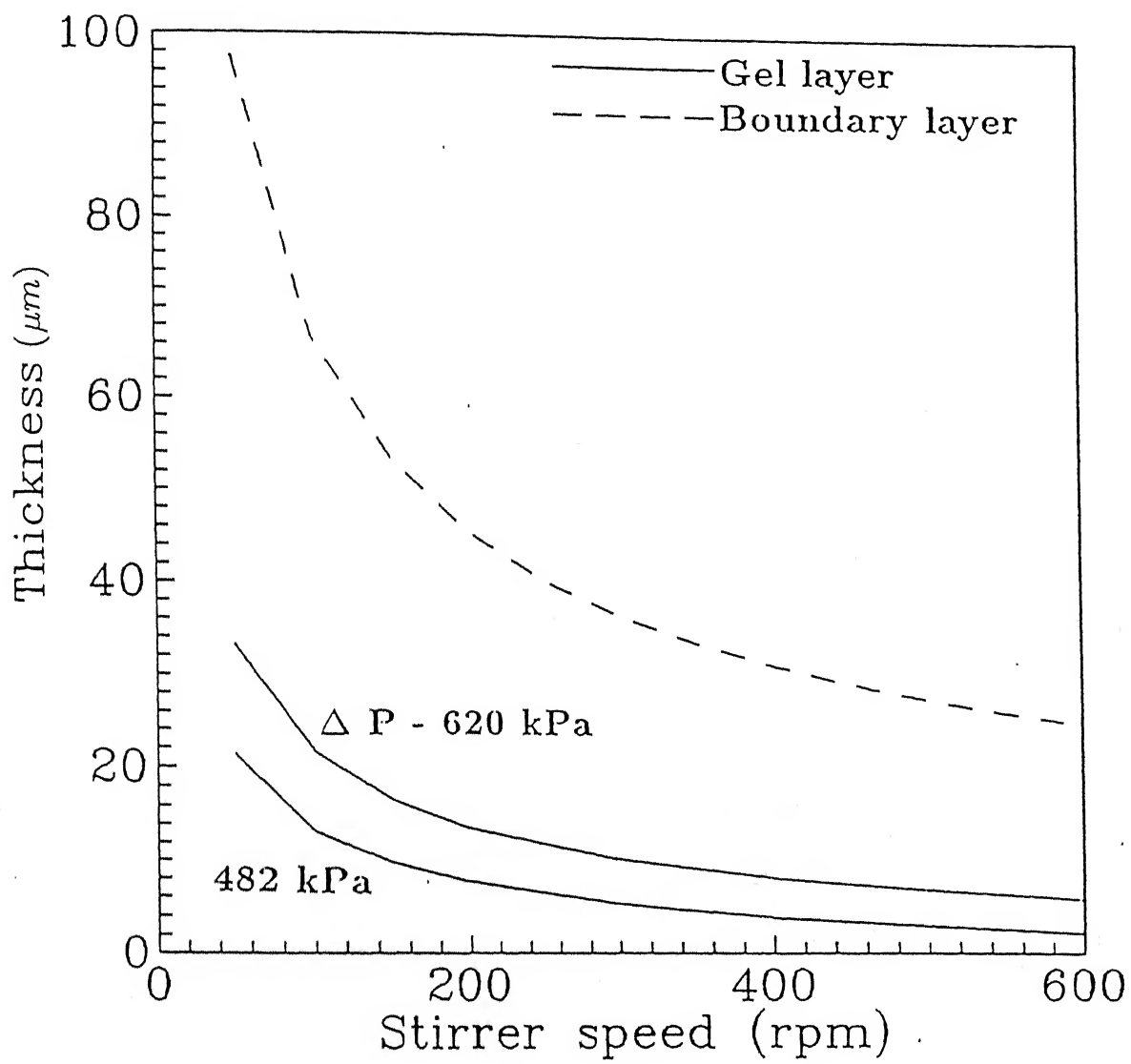


Figure 3.30: Variation of gel and boundary layer thicknesses with stirrer speed

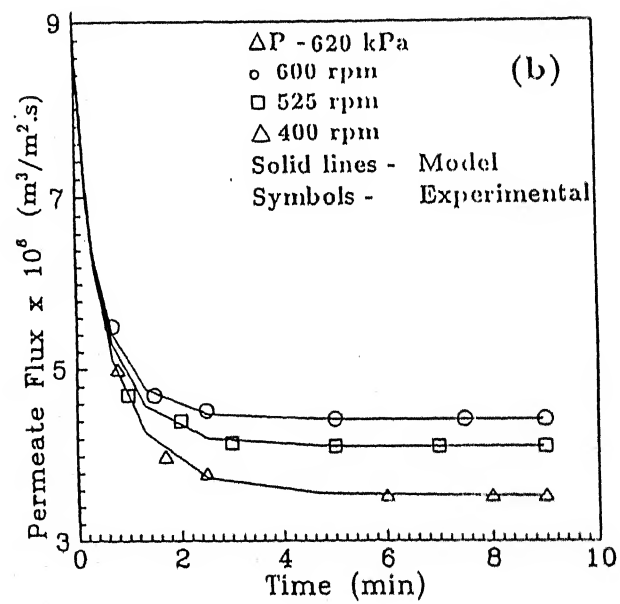
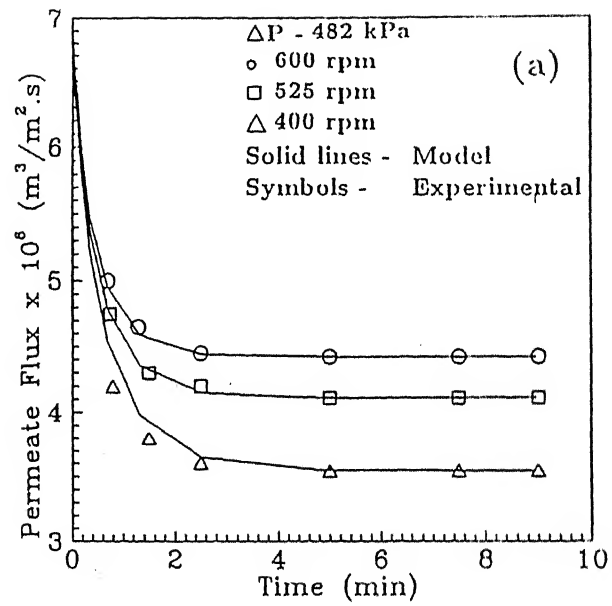


Figure 3.31: Permeate flux of the mixed feed UF with time, for 1K membrane. (a) $\Delta P = 482 \text{ kPa}$; (b) $\Delta P = 620 \text{ kPa}$

Table 3.7: Comparison of various resistances for typical operating conditions

Membrane	ΔP (kPa)	ω (rpm)	R_g/R_T (%)	R_{osm}/R_T (%)	R_m/R_T (%)
1K	482	600	31.53	14.85	53.62
		400	42.07	14.98	42.95
	620	600	46.43	11.84	41.73
		400	54.59	12.04	33.37
10K	482	600	76.15	0.0	23.85
		400	80.91	0.0	19.09
	620	600	81.47	0.0	18.53
		400	85.16	0.0	14.84

that the flux declines as gel layer grows over time and reaches a steady value as dictated by Eq. (3.43). The steady state values were observed exactly the same as the flux for single component PVA solution (in absence of sucrose) under the same operating conditions. Experimental data for such runs (single component) are not reported for the purpose of convenience. It can also be observed that typical time required to reach the steady state flux is about 5 minutes for both the pressures. Hydrodynamics play an important role to the flux decline behaviour; flux decline is steeper for higher stirrer speed and more gradual for lower stirrer speeds. This is because higher stirrer speed does not allow the gel layer to grow rapidly unlike lower stirrer speed. A close look at Fig. (3.31b) also reveals that at higher operating pressure, initial flux is higher compared to that of the initial flux at lower pressure (Fig. 3.31a) due to increased driving force but eventually flattens at the same steady state value. This also demonstrates that steady state flux in the gel layer controlled UF is pressure independent. The experimental flux values are in good agreement of the predicted values.

Model predictions and experimental observed rejection of sucrose are presented

(for 1K membrane and different operating conditions) in Figs. (3.32a) and (3.32b). Both the figures show that observed rejection increases with time and attains a steady value. The time required to attain steady value is about 3 minutes for higher stirrer speeds and about 4 minute for lower stirrer speed. Higher stirrer speed increases observed rejection. At higher stirrer speed growth of gel layer is less and therefore, the extent of adsorption of sucrose by the gel layer is minimal; moreover, concentration polarization in the boundary layer is also reduced at higher stirrer speeds; therefore, observed rejection increases with stirrer speed. The same trend can be observed for both the operating pressures. The experimental observations match closely to the model predicted values. Initial deviations are because of errors incurred in the measurement; whereas, the steady values match quite well with the model predictions.

The model predictions and experimental observations for permeate flux and observed rejection for 10K membrane are presented in Figs. (3.33) to (3.34). In Figs. (3.33a) and (3.33b), the flux starts initially from a very high value but declines rapidly and within 5 minutes reaches steady state. Therefore, the decline of flux is solely governed by the gel layer and hydrodynamics, irrespective of the membranes chosen. More open membrane only results an augmentation of initial flux. The rejection characteristics also show an interesting trend (Figs. 3.34a and 3.34b). Observed rejection increases and attains a steady state value shortly. The nature of rejection behaviour reveals two important features; firstly, unlike 1K membrane, steady state observed rejections are identical for all the hydrodynamic conditions; secondly, 10K membrane which allows sucrose to pass through completely in absence of PVA, rejects around 52% in presence of gel layer. Hence, the observation suggests that only gel layer (not the membrane) governs the sucrose rejection. Whereas, for 1K membrane which partially retains sucrose ($R_{r,2}=0.73$), the membrane surface concentration gets affected by the concentration polarization (for different hydrodynamic conditions) and therefore, observed rejections are different for different stirrer speeds. The later observation makes it clear that the PVA gel acts as a dynamic membrane which

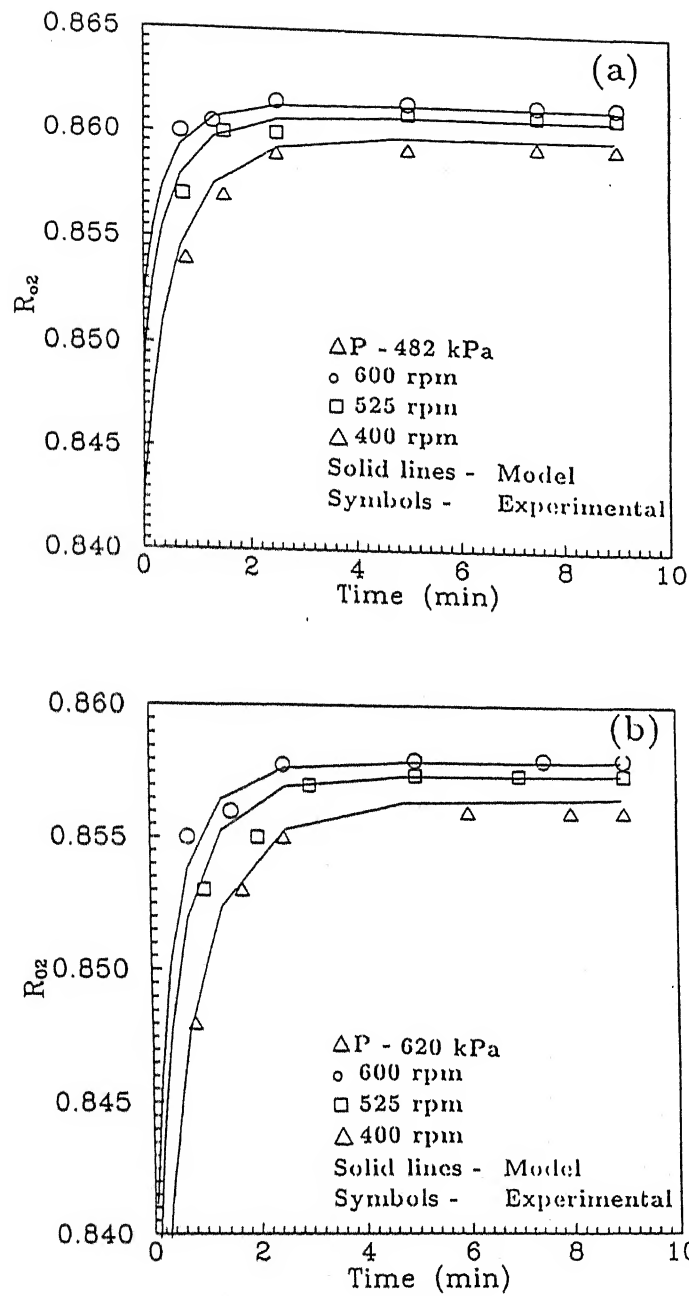


Figure 3.32: Observed rejection of sucrose with time, for 1K membrane. (a) $\Delta P = 482$ kPa; (b) $\Delta P = 620$ kPa

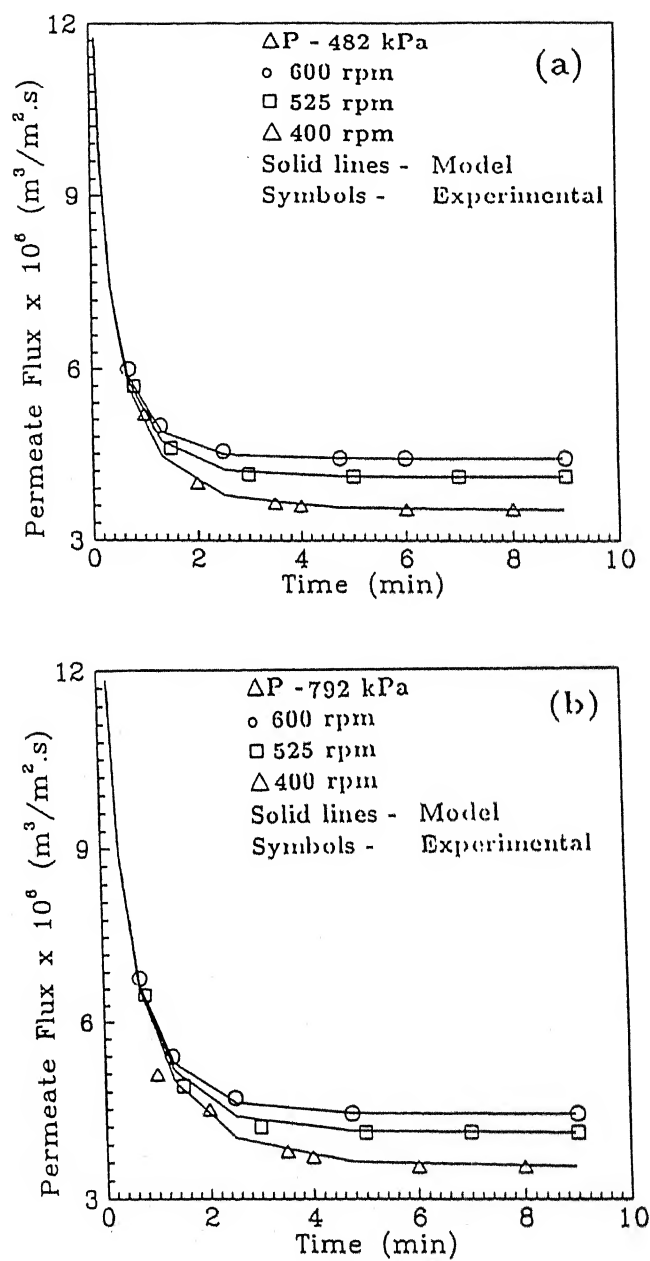


Figure 3.33: Permeate flux of the mixed feed UF with time, for 10K membrane. (a) $\Delta P = 482$ kPa; (b) $\Delta P = 792$ kPa

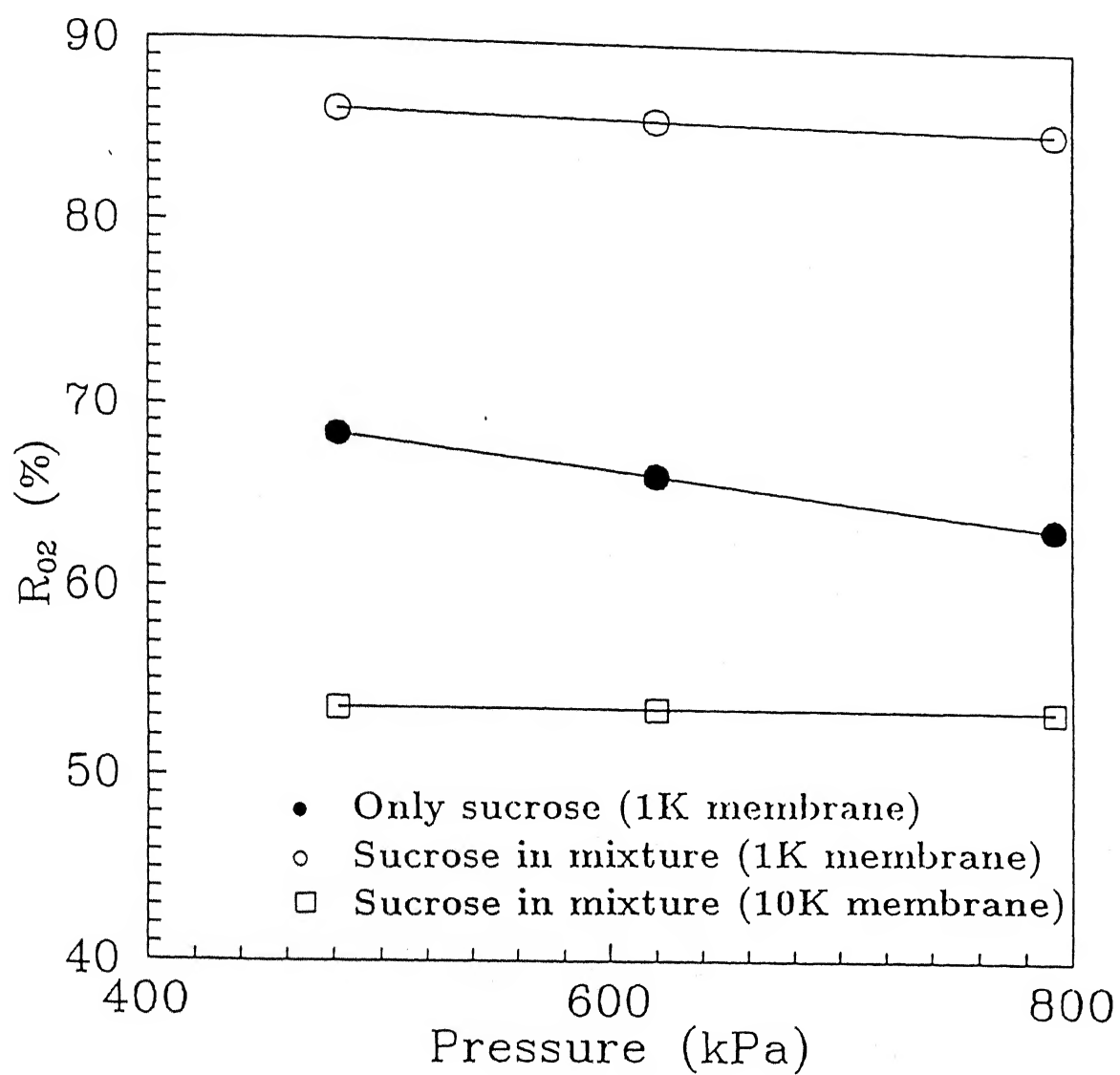


Figure 3.35: Observed rejection of sucrose versus pressure

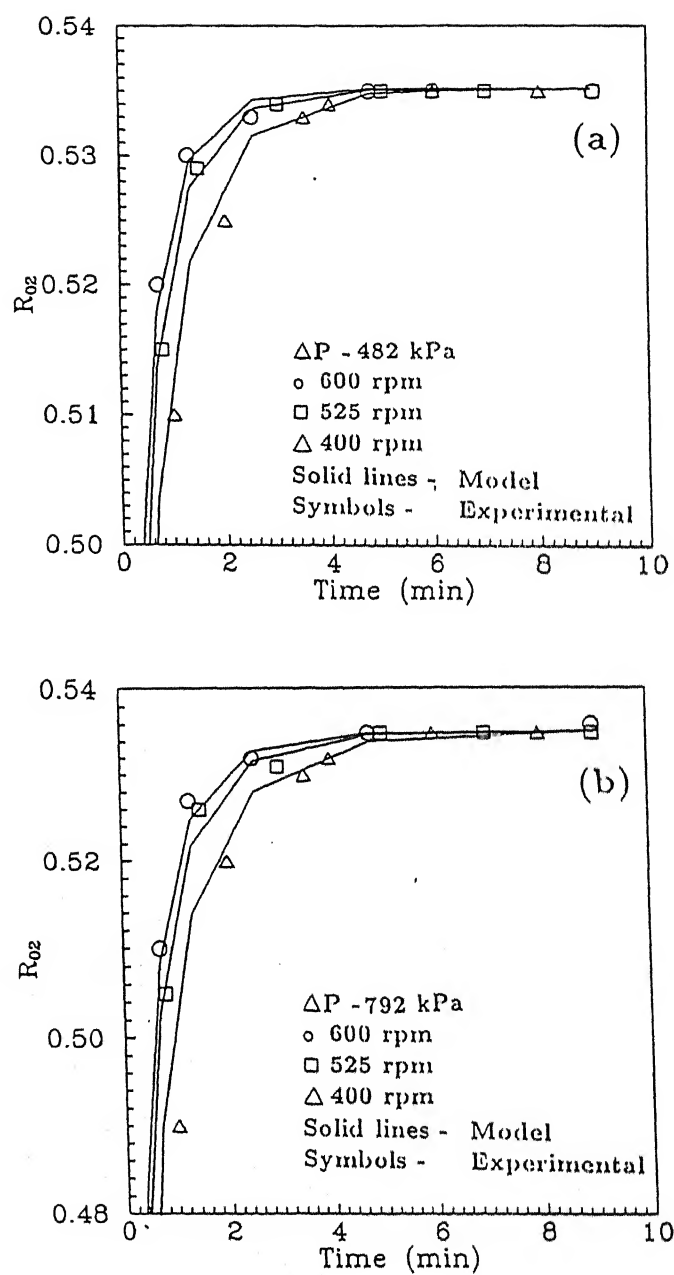


Figure 3.34: Observed rejection of sucrose with time, for 10K membrane. (a) $\Delta P = 482$ kPa; (b) $\Delta P = 792$ kPa

rejects the sucrose molecules. In the figures, it can be observed that the experimental observations agree quite well with the model predictions.

The steady state observed rejection of sucrose for all the operating pressures and for different membranes are presented in Fig. (3.35). For 1K membrane observed rejection of sucrose (in absence of PVA) are shown by open circles. The data show a downward trend with pressure because of concentration polarization; the same trend of sucrose rejection under high polarization is also observed earlier [237]. The observed rejection for the mixed feed in 1K membrane increases to about 86% from about 68%. 10K membrane which does not retain sucrose at all (in absence of PVA), rejects it to 53% in presence of PVA gel. These observations establish that the gel layer acts as an additional membrane.

In summary, the study carried out in this work, can be looked in wider spectrum which encompasses the possible suggested applications in various process industries e.g. sugar industries, effluent treatments of different industries like tanneries paint, etc. The model developed in this work can be utilized for other components also and the relevant parameters can be estimated in the similar manner. Finally, the model can be used for predictions and scaling up.

3.3.5 Conclusions

The present work provides a study on different aspects of UF of a mixed feed, namely sucrose and PVA, on a wide range of operating conditions. Experimental observations indicate that flux declines as gel layer of PVA grows with time and the steady state flux value is same as that of the PVA solution alone (in absence of sucrose). Steady state flux depends on the hydrodynamic conditions but is independent of pressure. The rejection is mostly governed by the gel layer for a higher MWCO membrane. Gel layer further rejects the solute in addition of membrane, if it is partially retentive to the solute. For 1K membrane, rejection of sucrose is 86% whereas true rejection by the membrane is 73% (in absence of PVA). In case of 10K

membrane, rejection is 52%, whereas, the membrane itself does not retain sucrose. The mathematical model developed in this work, predicts the flux and rejection quite satisfactorily. The various parameters used in this model can be evaluated from independent sets of experiments.

3.4 Generalized Integral and Similarity Solutions of The Concentration Profiles for Osmotic Pressure Controlled Ultrafiltration

In the previous sections, we have seen the modeling of polarization phenomena in CFUF and stirred UF as well as stirred UF of a two component (one component is gel forming) solution. The developed models were also applied to treatment of BL, an industrial effluent. In this section, a series of approximate boundary layer solutions for this phenomena are presented, in case of osmotic pressure controlled UF in cross flow as well as in unstirred conditions. Similarity and integral transforms are employed under various approximations as solution techniques. A generalized and detailed integral method for solving the governing convective-diffusion equation (incorporating the variation of diffusivity in the boundary layer) is also formulated which predicts permeate flux as accurate as that obtained using detailed numerical methods. Being extremely simple, one can circumvent the computational intensiveness of detailed numerical solution using this method. Therefore, the major objectives of this section can be categorized as, (i) formulations of similarity and integral solutions of the boundary layer equations in the polarized layer under various approximations; (ii) formulation of a generalized integral solution, incorporating the variable diffusivity in the polarized layer as an accurate and faster solution scheme; (iii) prediction of permeate flux using different techniques; (iv) comparison among various schemes in terms of accuracies and validity and applicabilities of these techniques based on different approximations.

3.4.1 Introduction

Flux decline during a pressure driven membrane separation process like ultrafiltration (UF) occurs due to concentration polarization, *i.e.*, the build-up of solute concentration near the membrane surface [24]. Modeling of the polarization phenomenon, leading to the prediction of flux, is a pre-requisite for the design of plants

using these processes. Several studies have modeled the flux decline in membrane processes due to concentration polarization [9, 19, 20, 44, 45, 105, 115]. These models of coupled mass transport and the fluid flow in UF vary widely in their complexity, details and the solution methodology. These models are based on certain simplifications which are applicable only to particular systems and operating conditions, thus making extrapolations difficult. On the other hand, detailed models [39, 108, 123] are computation intensive and are mathematically more complex.

Film theory is the simplest theory on which the development of the earliest models of flux decline were based [26]. Subsequently, the boundary layer theories incorporating greater details of fluid flow have been used more frequently in modeling flux decline [9, 44, 45, 106, 145]. Several simplifications of the boundary layer models also exist, *e.g.*, similarity solutions [19, 40], integral solutions [9, 44, 45], perturbation and series solutions [43]. These simplified models differ on assumptions regarding the flow behaviour (velocity profiles), nature of the polarized layer (concentration profiles, membrane surface concentration, gel layer or osmotic pressure control, *etc.*) and mathematical simplifications (like expansions using truncated series, *etc.*). For instance, assumptions of constant permeate flux [41, 104] or constant membrane surface concentration [19, 39] do not describe the exact physical situations where both of these vary with time (unstirred batch ultrafiltration) or axial distance (cross flow ultrafiltration). Such approximations are therefore restrictive and cannot be employed under different experimental conditions encountered during UF.

The modeling of the concentration polarization involves the modeling of the coupled convective – diffusion encountered in a boundary layer. The solution methodologies using the boundary layer approximations involve the solution of the coupled velocity and concentration fields in a concentrated boundary layer near the membrane surface. Solution of the governing differential equations requires the incorporation of an appropriate model for the transport of the permeate through the membrane as a boundary condition. Based on this membrane transport model, the UF process is generally classified as osmotic pressure or gel layer controlled. In osmotic pressure

governed UF, the membrane surface concentration changes during the UF operation. This concentration build-up, as well as the consequent changes in the permeate flux, are governed by the solution osmotic pressure. In addition, variations of solute diffusivity with concentration can alter the diffusive transport in the boundary layer, which affects the permeate flux. A model for flux decline should therefore be capable of incorporating all these effects in order to be considered sufficiently general.

Models for prediction of the gel layer controlled UF flux using simplified boundary layer theory are available [20, 44, 105, 106]. In this case, the membrane surface concentration is assumed to be constant. However, there is no simple treatment for osmotic pressure controlled UF [114], where, the osmotic pressure dependence on solute concentration is usually nonlinear, and the membrane surface concentration varies with time or axial length of a channel. Moreover, the variation of diffusivity is often an important factor [23, 44]. Analytical solutions for such cases may be ruled out. In such cases, the prediction of osmotic pressure controlled flux are possible only by detailed numerical simulations [39, 108, 123]. There is however, no consistent and computationally efficient simplification of the general model available, which is accurate under a wide range of operating conditions.

In addition to modeling permeate flux, which is only one aspect of a UF operation, the observed solute rejection and its variation with operating conditions, time, and channel length is also required for designing a UF process. Flux and rejection are coupled parameters, and existing models have not been used to predict both of them simultaneously. While a class of studies focused on the prediction of the flux alone [19, 20, 39, 44, 104, 106], the prediction of the rejection [41, 112] is also important.

Based on the above observations, it seems pertinent to assess the applicability of various existing simplified boundary layer solutions in different UF processes, under a wide range of operating conditions and flow configurations. In addition to assessing the limitations of these simplified models, their modifications for the case under consideration (osmotic pressure governed UF) have also been suggested. In this context, a new generalized solution scheme of the governing transport equations is

developed in the present study. This scheme, based on an integral approach, can be used for the coupled prediction of the permeate flux and solute rejection for osmotic pressure governed UF, and can additionally incorporate the variations of solute diffusivity with concentration. Variation of solution viscosity with solute concentration is also considered in several studies [144, 147]. However, in the present context, the viscosity variations are not taken into account in the development of the models. It may be stated here, that the enhancement in the viscosity near the membrane surface does not alter the velocity profiles in cross flow UF to any significant extent [108, 112]. Detailed parametric studies using these models have been performed to determine the role of operating conditions, variations of diffusivity and osmotic pressure, and flow geometries on the predictions of flux and solute rejection. Considering the detailed numerical approaches to yield the most accurate results, the simplified model predictions of flux are compared to the numerical results. Comparisons have also been made with experimental observations of flux for UF of Dextran (T20) in a cross flow system and PEG and Dextran in an unstirred batch cell under different operating conditions. The main objective of the study is to compare and contrast the generalized integral model, developed subsequently in the theoretical section, with existing detailed numerical solutions and other simplified solution schemes.

3.4.2 Theory

The permeate flux during an osmotic pressure governed UF process is given by

$$v_p = L_p \Delta P \left(1 - \frac{\Delta \pi}{\Delta P} \right) \quad (3.67)$$

When the osmotic pressure difference, $\Delta \pi$ is known, Eq.(3.67) can be used to obtain the permeate flux. However, $\Delta \pi (= \pi_m - \pi_p)$ can be determined if the concentrations at the membrane surface and the permeate are known. Permeate concentration is usually zero for highly rejecting membranes in UF or can be determined if R_r , the intrinsic solute rejection of the membrane is known *a priori*. The intrinsic rejection relates the permeate concentration with the membrane surface concentration, while

the observed rejection, R_o is defined to relate the permeate concentration to the feed concentration, c_0 . The problem of predicting permeate flux is coupled with the estimation of the membrane surface concentration. These terms are defined as

$$R_r = 1 - \frac{c_p}{c_m} \quad \text{and} \quad R_o = 1 - \frac{c_p}{c_0} \quad (3.68)$$

The membrane surface concentration and the concentration profiles near the membrane surface can be known by considering the diffusive and convective transport of the solute in the boundary layer during polarization process. The transient diffusion problem associated with UF in different membrane configurations is expressed in a general form by the following mass balance equation

$$\frac{\partial c}{\partial t} + \mathbf{V} \cdot \nabla c = \nabla [D \nabla \cdot c] \quad (3.69)$$

where \mathbf{V} is the velocity vector, with its x and y components denoted by u and v , respectively.

Eq.(3.69) is the mass balance for transfer of a solute species across a porous barrier without reaction and adsorption.

The incorporation of the cell geometry and the hydrodynamic parameters makes Eq.(3.69) applicable to specific UF systems. The appropriate initial and boundary conditions associated with Eq.(3.69) are

$$c(x, y, 0) = c_0(\text{constant}) \quad (3.70)$$

$$c(x, \infty, t) = c_0 \quad (3.71)$$

and the mass balance at the membrane surface,

$$v(c_m - c_p) = D \left[\frac{\partial c}{\partial y} \right]_{y=0} \quad (3.72)$$

The velocity components u and v are in general obtained from the continuity equation, $\nabla \cdot \mathbf{V} = 0$, together with the Navier-Stokes equations describing the fluid flow.

However, as is shown below, further simplifications are possible for the membrane modules / configurations used in this study.

Unstirred Batch Cell:

Neglecting end effects, and assuming 1-D flow normal to the membrane surface ($u = 0$), Eq.(3.69) can be written,

$$\frac{\partial c}{\partial t} + v \frac{\partial c}{\partial y} = \frac{\partial}{\partial y} \left\{ D \frac{\partial c}{\partial y} \right\} \quad (3.73)$$

The initial and boundary conditions for the unstirred cell are given by Eqs.(3.70) to (3.72).

Cross Flow System:

The general steady-state mass balance equation within the mass transfer boundary layer ($0 \leq y \leq \delta$) for this system can be expressed as

$$u \frac{\partial c}{\partial x} + v \frac{\partial c}{\partial y} = \frac{\partial}{\partial y} \left\{ D \frac{\partial c}{\partial y} \right\} \quad (3.74)$$

It is known that the time invariant (steady state) profile in a cross flow system is attained rather fast because of the forced convection. Hence, the analysis of the steady state operation is more relevant for this system.

For relatively small values of v_p typically encountered in UF ($v_p \ll u_0$; $Re_y < 0.5$), variation of u_0 is small along the channel length [243] and hence, within thin concentration boundary layer, the profiles of u and v can be approximated [39, 108, 112] as,

$$\begin{aligned} u &= \frac{3u_0}{h}y \\ v &= -v_p \end{aligned} \quad (3.75)$$

Further, if viscosity increases with concentration Re_y is lowered. This renders the expressions for u and v in Eq. (3.75) more appropriate [180].

The boundary conditions for Eq.(3.74) are given by Eq.(3.72) and,

$$c(x, y, 0) = c(0, y, t) = c(x, \delta, t) = c_0 \quad (3.76)$$

Since analytical solutions are not possible for nonlinear concentration dependence of $\Delta\pi$ and D , the above set of equations are solved numerically. In this context, we explore approximate simplified solution techniques, based on the integral and similarity methods. Further, all these simplified solutions reduce the computational efforts, while resulting in good approximations of the flux and polarization behaviour.

3.4.2.1 Integral Solutions

1. Generalized Integral Method (GIM)

In the integral approach, a concentration profile for the system under consideration is assumed. The concentration profiles in the polarized layer change with time in a batch cell, while the steady-state profiles vary with the axial distance in case of a cross flow system. Based on the observed qualitative behaviour of concentration profiles from numerical simulations [123, 243], a versatile power law dependence of the form

$$c = c_0 + (c_m - c_0) \left(1 - \frac{y}{\delta}\right)^n \quad (3.77)$$

is assumed.

In Eq.(3.77), the quantities c_m , δ and n are in general, functions of time in case of a batch cell, while they are functions of the axial distance in a cross flow system. The profiles become flat as t or $x \rightarrow 0$. This assumed profile incorporates the time (or axial distance) dependence of the membrane surface concentration and also accounts for the growth of the boundary layer, δ with time (in the batch cell) or axial distance (in a cross flow system). Clearly, it satisfies all the boundary / initial conditions for both the systems. Earlier, the power law profile, Eq.(3.77), has been used with constant values of c_m and n in case of gel-layer controlled UF [19, 106], with constant

c_m and adjustable n to fit the experimental observation of flux [2], as well as with a truncated power series expansion for constant n [9].

In what follows, c_m , δ and n are obtained for the unstirred batch cell and the cross flow systems.

Formulation for the unstirred batch cell

The concentration profile given by Eq. (3.77) represents the development of the concentration boundary layer in an unstirred batch cell with time. The parameters governing the shape of the profile, namely, c_m , δ and n are function of time, while c is a function of both time and distance y from the membrane surface. To obtain the integral formulation for the batch cell system, the time and space derivatives ($\partial c/\partial t$, $\partial c/\partial y$ and $\partial^2 c/\partial y^2$) of the concentration profile are first substituted in the governing differential solute mass balance Eq. (3.73). Considering the concentration dependence of the solute diffusivity, ($D = D(c)$), the resulting equation needs to be integrated over time to obtain the time dependence of concentration, boundary layer thickness, and n .

The boundary condition at the membrane surface is given by

$$v(c_m - c_p) = D(c_m) \left. \frac{\partial c}{\partial y} \right|_{y=0} \quad (3.78)$$

which, after substitution of the derivative of $\partial c/\partial y$ yields

$$v = -\frac{(c_m - c_0)D(c_m)(n/\delta)}{(c_m - c_p)} = -L_p \Delta P \left(1 - \frac{\Delta \Pi}{\Delta P}\right) \quad (3.79)$$

where, c_p is related to c_m through Eq. (3.68).

Rearrangement of Eq. (3.79) and subsequent differentiation with respect to time gives:

$$\frac{dc_m}{dt} = \frac{(c_m - c_0)}{F_1} D(c_m) \frac{n}{\delta} \frac{d\delta}{dt} - \frac{(c_m - c_0)}{F_1} D(c_m) \frac{dn}{dt} \quad (3.80)$$

where,

$$F_1 = \{D(c_m) + (c_m - c_0)D'(c_m)\} n - R_r L_p \Delta P \delta \left\{1 - \frac{\Delta \pi}{\Delta P} - \frac{(c_m)}{\Delta P} \frac{d\Delta \Pi}{dc_m}\right\} \quad (3.81)$$

and D' is the derivative of $D(c)$ with respect to time.

Next, we perform the integration of Eq. (3.73) over the boundary layer thickness, δ by substituting the concentration profile and its derivatives. The resulting expression is

$$\begin{aligned} \frac{\delta}{(n+1)} \frac{dc_m}{dt} + \frac{(c_m - c_0)}{(n+1)} \frac{d\delta}{dt} - \frac{(c_m - c_0)\delta}{(n+1)^2} \frac{dn}{dt} + \frac{nD(c_m)}{\delta} \frac{(c_m - c_0)^2}{(c_m - c_p)} \\ = \frac{(c_m - c_0)n(n-1)}{\delta^2} I_1 + (c_m - c_0)^2 \frac{n^2}{\delta^2} I_2 \end{aligned} \quad (3.82)$$

where,

$$I_1 = \int_0^\delta D(c) \left(1 - \frac{y}{\delta}\right)^{(n-2)} dy \quad (3.83)$$

and,

$$I_2 = \int_0^\delta D'(c) \left(1 - \frac{y}{\delta}\right)^{2(n-1)} dy \quad (3.84)$$

It should be noted here that there are three unknowns in the model, namely, c_m , δ and n , for which we have so far obtained two equations, *i.e.*, Eq.(3.80) and (3.82). To obtain a third equation, we apply the moment technique to Eq. (3.73) [106]. Using the first moments, Eq.(3.73) can be written as

$$\begin{aligned} \frac{\delta}{(c_m - c_0)} \frac{dc_m}{dt} + 2 \frac{d\delta}{dt} - \frac{(2n+3)\delta}{(n+1)(n+2)} \frac{dn}{dt} + \frac{(c_m - c_0)n(n+2)}{(c_m - c_p)\delta} D(c_m) \\ = (c_m - c_0) \frac{n^2}{\delta^3} (n+1)(n+2) I_3 + \frac{n(n+1)(n+2)(n-1)}{\delta^3} I_4 \end{aligned} \quad (3.85)$$

where,

$$I_3 = \int_0^\delta y D'(c) \left(1 - \frac{y}{\delta}\right)^{2(n-1)} dy \quad (3.86)$$

and,

$$I_4 = \int_0^\delta y D(c) \left(1 - \frac{y}{\delta}\right)^{(n-2)} dy \quad (3.87)$$

Substitution of Eq. (3.80) in Eqs. (3.82) and (3.85) results in two coupled ordinary differential equations for δ and n after some mathematical rearrangements:

$$\frac{d\delta}{dt} = \frac{E_3 E_5 - E_2 E_6}{E_1 E_5 - E_2 E_4} \quad (3.88)$$

and,

$$\frac{dn}{dt} = \frac{E_3 E_4 - E_1 E_6}{E_1 E_5 - E_2 E_4} \quad (3.89)$$

where, E_1 to E_6 are defined as

$$\begin{aligned} E_1 &= 1 + \frac{nD(c_m)}{F_1} \\ E_2 &= \frac{D(c_m)\delta}{F_1} + \frac{\delta}{(n+1)} \\ E_3 &= -\left(\frac{c_m - c_0}{c_m - c_p}\right) D(c_m) \frac{n(n+1)}{\delta} + \frac{(n-1)n(n+1)I_1}{\delta^2} + (c_m - c_0) \frac{n^2}{\delta^2} (n+1)I_2 \\ E_4 &= 2 + \frac{nD(c_m)}{F_1} \\ E_5 &= \frac{D(c_m)\delta}{F_1} + \frac{\delta(2n+3)}{(n+1)(n+2)} \\ E_6 &= -\left(\frac{c_m - c_0}{c_m - c_p}\right) \frac{n(n+2)D(c_m)}{\delta} + \frac{n^2(n+1)(n+2)(c_m - c_0)I_3}{\delta^3} + \frac{(n-1)n(n+1)(n+2)I_4}{\delta^3} \end{aligned} \quad (3.90)$$

Simultaneous solution of Eqs.(3.79), (3.88) and (3.89) provides the concentration profiles and consequently, the permeate flux decline.

If diffusivity is constant, or, if a linear variation of the diffusivity with solute concentration may be assumed [255, 256], then the analytical evaluations of the integrals I_1 to I_4 become straightforward. Analytical integrations, though increasingly tedious, are also possible for variations of D expressed as higher order polynomials in c . However, it may be noted that for a complex variation of diffusivity with concentration, the integrals I_1 to I_4 should be evaluated numerically.

Considering a linear dependence of the diffusivity on the solute concentration,

$$D = D_\infty(1 + Kc) = g(y) \quad (3.91)$$

where, the relation between c and y is provided by Eq. (3.77), we obtain:

$$I_1 = D_\infty(c_0K + 1)\frac{\delta}{(n-1)} + D_\infty K(c_m - c_0)\frac{\delta}{(2n-1)} \quad (3.92)$$

$$I_2 = D_\infty K\frac{\delta}{(2n-1)} \quad (3.93)$$

$$I_3 = D_\infty K\frac{\delta^2}{2n(2n-1)} \quad (3.94)$$

and,

$$I_4 = D_\infty(1 + Kc_0)\frac{\delta^2}{n(n-1)} + D_\infty K(c_m - c_0)\frac{\delta^2}{2n(2n-1)} \quad (3.95)$$

Cross flow system

In case of cross flow system, the steady state solution is required, and in this case the parameters, c_m , δ and n , governing the concentration profile are functions of the axial distance from the channel entrance, instead of time. c in this case is a function of x and y .

The governing solute mass balance equation for variable diffusivity in a cross flow system becomes,

$$u\frac{\partial c}{\partial x} + v\frac{\partial c}{\partial y} = D'(c)\left(\frac{\partial c}{\partial y}\right)^2 + D(c)\frac{\partial^2 c}{\partial y^2} \quad (3.96)$$

The differential equation for c_m remains identical to Eq.(3.80) except that time derivatives (dc_m/dt , $d\delta/dt$, dn/dt) are replaced by the spatial derivatives (dc_m/dx , $d\delta/dx$, dn/dx). By inserting the concentration profile and its derivatives in Eq.(3.96), and then integrating it over boundary layer thickness (as in the case of unstirred batch cell), the following equation is obtained,

$$\begin{aligned} k'\delta^3\frac{dc_m}{dx} + 2k'(c_m - c_0)\delta^2\frac{d\delta}{dx} - k'(c_m - c_0)\frac{(2n+3)}{(n+1)(n+2)}\delta^3\frac{dn}{dx} \\ = -\frac{(c_m - c_0)^2}{(c_m - c_p)}n(n+1)(n+2)D(c_m) + (c_m - c_0)^2\frac{n^2}{\delta}(n+1)(n+2)I_2 \\ + (c_m - c_0)\frac{n}{\delta}(n-1)(n+1)(n+2)I_1 \end{aligned} \quad (3.97)$$

where, I_1 and I_2 are given by the Eqs.(3.83) and (3.84) and $k' = 3u_0/h$.

Similarly, the first moment of Eq.(3.96), analogous to Eq.(3.85) for the unstirred batch cell, yields the following equation,

$$\begin{aligned}
 2k'\delta^3 \frac{dc_m}{dx} &+ 6k'(c_m - c_0)\delta^2 \frac{d\delta}{dx} - k'(c_m - c_0)\delta^3 \frac{6n^2 + 24n + 22}{(n+1)(n+2)(n+3)} \frac{dn}{dx} \\
 &= - \frac{(c_m - c_0)^2}{c_m - c_p} D(c_m)n(n+2)(n+3) + (c_m - c_0) \frac{n(n-1)(n+1)(n+2)(n+3)}{\delta^2} I_4 \\
 &\quad + (c_m - c_0)^2 \frac{n^2(n+1)(n+2)(n+3)}{\delta^2} I_3
 \end{aligned} \tag{3.98}$$

where, I_3 and I_4 are given by the Eqs.(3.86) and (3.87).

Expression for dc_m/dx is given by the right hand side of Eq.(3.80) with $d\delta/dt$ and dn/dt replaced by $d\delta/dx$ and dn/dx , respectively. Substitution of dc_m/dx in Eqs. (3.97) and (3.98), and subsequent simplification gives equations for $d\delta/dx$ and dn/dx which can be written in the form of Eqs.(3.88) and (3.89), respectively, where, coefficients E_1 to E_6 are redefined as

$$\begin{aligned}
 E_1 &= \frac{k'\delta^2 D(c_m)n}{F_1} + 2k'\delta^2 \\
 E_2 &= \frac{k'\delta^3 D(c_m)}{F_1} + k'\delta^3 \frac{2n+3}{(n+1)(n+2)} \\
 E_3 &= - \left(\frac{c_m - c_0}{c_m - c_p} \right) n(n+1)(n+2)D(c_m) + \frac{(n-1)n(n+1)(n+2)I_1}{\delta} \\
 &\quad + \frac{(c_m - c_0)n^2(n+1)(n+2)I_2}{\delta} \\
 E_4 &= 2 \frac{k'\delta^2 D(c_m)n}{F_1} + 6k'\delta^2 \\
 E_5 &= \frac{2k'\delta^3 D(c_m)}{F_1} + k'\delta^3 \frac{6n^2 + 24n + 22}{(n+1)(n+2)(n+3)} \\
 E_6 &= - \left(\frac{c_m - c_0}{c_m - c_p} \right) D(c_m)n(n+2)(n+3) + \frac{(n-1)n(n+1)(n+2)(n+3)I_4}{\delta^2} \\
 &\quad + \frac{(c_m - c_0)n^2(n+1)(n+2)(n+3)I_3}{\delta^2}
 \end{aligned} \tag{3.99}$$

For a linear variation of D with c , the integrals I_1 , I_2 , I_3 and I_4 take the same form as in the case of unstirred cell. Finally, Eqs.(3.79), (3.88) and (3.89) are to be solved

simultaneously. Eqs.(3.88) and (3.89) are ordinary differential equations for which initial conditions have to be supplied in order to obtain a solution. Eq.(3.77) suggests that as $t \rightarrow 0$ or $x \rightarrow 0$, $c_m \rightarrow c_0$ and $\delta \rightarrow 0$. These values of c_m and δ , however, make the permeate flux indeterminate at t or $x \rightarrow 0$ according to Eq.(3.72), since the assumed variation of c (Eq.(3.77)) is not strictly valid at $t = 0$. To overcome this initialization problem, we obtain an asymptotic solution for n and δ as t or $x \rightarrow 0$.

Initial conditions for cross flow and unstirred batch cell

In case of cross flow UF, as $x \rightarrow 0$, D becomes constant ($D(c_0)$). Substituting Eq.(3.80) in Eqs.(3.97) and (3.98) respectively, we get,

$$\begin{aligned} k'\delta^2 \left(\frac{D(c_0)n}{F_1} + 2 \right) \frac{d\delta}{dx} - k'\delta^3 \left(\frac{D(c_0)}{F_1} + \frac{(2n+3)}{(n+1)(n+2)} \right) \frac{dn}{dx} \\ = D(c_0)n(n+1)(n+2) \frac{(c_0 - c_p)}{(c_m - c_p)} \end{aligned} \quad (3.100)$$

and

$$\begin{aligned} k'\delta^2 \left(\frac{2D(c_0)n}{F_1} + 6 \right) \frac{d\delta}{dx} - k'\delta^3 \left(\frac{2D(c_0)}{F_1} + \frac{(6n^2 + 24n + 22)}{(n+1)(n+2)(n+3)} \right) \frac{dn}{dx} \\ = D(c_0)(n+2)(n+3) \frac{c_m + nc_0 - (n+1)c_p}{(c_m - c_p)} \end{aligned} \quad (3.101)$$

As $x \rightarrow 0$, $\delta \rightarrow 0$, $c_m \rightarrow c_0$; also $F_1 \rightarrow D(c_0)n$. Neglecting terms containing δ^3 from Eqs.(3.100) and (3.101), we get, $n(x \rightarrow 0) = 9/5$ and

$$\delta(x \rightarrow 0) = \left(\frac{2394 D(c_0)x}{125 k'} \right)^{1/3} \quad (3.102)$$

In case of a batch cell, assuming δ to be small for small t , Eqs.(3.82) and (3.85), written in the modified form after substitution of Eq.(3.80), can be similarly simplified by neglecting higher order terms from the resulting equations. This procedure gives $n(t \rightarrow 0) = 4$ and

$$\delta(t \rightarrow 0) = \sqrt{20D(c_0)t} \quad (3.103)$$

For the integration to start, an arbitrarily small "initial" value of t or x is chosen, and corresponding δ computed from Eq.(3.103) is used as the "initial" value of δ . The

dependence of δ on x or t , as given by Eqs.(3.102) and (3.103) for cross flow and unstirred batch cell respectively, are similar to those obtained earlier [9, 45].

The solution provides the time or axial distance dependence of c_m , δ and n . Based on these, the evolution of the concentration profile with time or axial distance can be obtained from Eq.(3.77). Further, the determination of the membrane surface concentration as a function of time or axial distance leads to the prediction of the transient permeate flux through Eq.(3.72). For constant diffusivity, the GIM becomes even simpler. In the subsequent development of more simplified solution schemes, D is taken as constant.

2. Quasi steady integral method (QSIM)

The equations obtained in GIM can be further simplified by assuming the variation of c_m and n to be small compared to the variation in δ after a short time. Therefore, in such a quasi steady state case, the equations (3.80), (3.82) or (3.97) and (3.98) can be further simplified by dropping the dc_m/dt , dn/dt or dc_m/dx and dn/dx terms. This results in the following explicit relations for the unstirred batch cell,

$$n = -\frac{1}{4} + \sqrt{\left[\frac{1}{16} + \frac{1}{2} \left(\frac{c_m - c_p}{c_0 - c_p} \right) \right]} \quad (3.104)$$

and,

$$\delta \frac{d\delta}{dt} = \frac{n(n+1)D(c_0 - c_p)}{c_m - c_p} \quad (3.105)$$

The initial conditions for Eq.(3.105) are obtained by simplifying Eqs.(3.82) and (3.85) in the limit $t \rightarrow 0$. These quantities are $n = 1/2$ and $\delta = \sqrt{1.5Dt}$. Eqs.(3.104) and (3.105) are solved alongwith Eq.(3.79) to give the variation of n , δ and c_m with time.

For the cross flow system, the analogous expressions are

$$n = \frac{1}{4} \left[\frac{c_m - c_p}{c_0 - c_p} + \sqrt{\left\{ \left(\frac{c_m - c_p}{c_0 - c_p} \right)^2 + 24 \frac{c_m - c_p}{c_0 - c_p} \right\}} \right] \quad (3.106)$$

and,

$$2k'\delta^2 \frac{d\delta}{dx} = \frac{n(n+1)(n+2)D(c_0 - c_p)}{c_m - c_p} \quad (3.107)$$

The initial conditions for Eq.(3.107) are $n = 3/2$ and $\delta = (19.7Dx/k')^{1/3}$. Eqs.(3.106) and (3.107) together with Eq.(3.79) provides the variation of c_m , δ and n with the axial distance.

From the above equations it is clear that c_m adapts to the changes in the boundary layer thickness, δ . The QSIM is simpler form of the GIM; in that it requires the solution of only one ODE, coupled with two non-linear algebraic equations, Eq. (3.104 or 3.106) and Eq.(3.79).

3. Integral method for constant membrane surface concentration (IMCC)

If a constant value of c_m is provided, like in case of gel layer governed UF, where the gel concentration $c_m = c_g$ (constant) is known independently, an extremely simple solution of the integral equation is possible [106]. For a constant preset c_m , Eq.(3.82) and (3.85) can be simplified to the form of equations used earlier [106] for a batch cell. Simplification of Eqs.(3.97) and (3.98) lead to the corresponding expressions for the cross flow system [19, 20]. The value of c_m used in this method for osmotic pressure governed UF should ideally be the osmotic pressure limiting concentration, c_{wa} , which is obtained from Eq.(3.67) by substituting $v_p = 0$ at a given operating pressure [106]. Thus, c_{wa} is the concentration at which the osmotic pressure of the solution equals the applied pressure. This method will give the limiting flux (at $t \rightarrow \infty$ in a batch cell or for an infinitely long cross flow channel).

3.4.2.2 Similarity Methods

1. Quasi steady similarity method (QSSM1)

The transport equations (3.73) and (3.74), also admit a similarity solution, $c = c(\eta)$ where $\eta = y/\delta$, if the membrane surface concentration is assumed to be constant [19, 20]. This approximation works best when a gel layer forms on the membrane surface ($c_m = \text{constant}$) and UF becomes gel-layer controlled. However, the similarity solution of Trettin and Doshi [19] may be further modified for osmotic pressure controlled UF considered here, whenever the variation of c_m is slow. The modified

similarity solution in such cases may be termed as quasi steady state similarity method.

In quasi steady state similarity formalism, we assume that membrane surface concentration remains constant between a small interval of time t and $t + \Delta t$ (for batch cell) or between x and $x + \Delta x$ (for cross flow system). The overall profile can then be obtained by integrating these elements using similarity transformation which essentially considers different c_m values to be constant over each of these elements. Flux can be evaluated by trial and error using constitutive relationship Eq.(3.67). Thus, in the limit $\Delta t \rightarrow 0$ or $\Delta x \rightarrow 0$, a continuous profile for c_m or v_p is obtained.

For cross flow system, the similarity variable chosen as given by Eq. (3.8). This is of the same form as $\eta = y/\delta$ where, dependence of δ on x is similar as obtained earlier in the case of GIM in the limit $x \rightarrow 0$. Eq.(3.74) can be expressed as a second order ODE in terms of η and $c^*(c/c_0)$, given by Eq. (3.12). The local permeate flux v_p can be expressed given by, Eq. (3.11). The transformed boundary conditions are exactly in the same form as Eqs. (3.13) and (3.14). Eq.(3.12) along with boundary conditions (3.13) and (3.14) can be solved and membrane surface concentration can be expressed [19, 20] as,

$$\frac{c_m - c_0}{c_m - c_p} = v_p \int_0^\infty \exp \left[- \left(\eta^3/3 + A_1 \eta \right) \right] d\eta \quad (3.108)$$

v_p can be related to the constitutive relation Eq.(3.67). Eq.(3.108) can be solved along with Eq.(3.67) by trial and error to give profiles of c_m and v_p . Average flux can be obtained by integrating Eq.(3.11) over L expressed by Eq. (3.19).

For a batch cell, the similarity variable is chosen [19] as,

$$\eta = \frac{y}{\sqrt{4Dt}} \quad (3.109)$$

and the transformed equation becomes,

$$\frac{d^2 c^*}{d\eta^2} = -(2\eta + A_{12}) \frac{dc^*}{d\eta} \quad (3.110)$$

where,

$$A_{12} = v_p \sqrt{4t/D} \quad (3.111)$$

The transformed boundary conditions remain as in the case of cross flow. The solution of the above equation in a batch cell is derived in the analogous manner as before. The corresponding integral in this case, can be evaluated analytically and the solution can be expressed as [106],

$$\frac{c_m - c_0}{c_m - c_p} = \frac{\sqrt{\pi}}{2} A_{12} \exp(A_{12}^2/2) \operatorname{erfc}(A_{12}/2) \quad (3.112)$$

Eq.(3.112) along with Eq.(3.67) can be solved by trial and error to obtain the flux profile with time.

2. Simplified quasi steady similarity method (QSSM2)

Another variant of the QSSM1 may also be very successful in providing the average permeate flux in a cross flow cell. In this method, the membrane element over which c_m is assumed to be constant (as discussed in the context of QSSM1) is equivalent to the channel length. The average c_m and v_p are given by Eqs.(3.108) and (3.19), respectively. Therefore, Eqs.(3.108) and (3.19) in conjunction with the constitutive relation given by Eq.(3.67) should be solved by trial and error to predict average c_m and v_p . As shown later, this method is very fast, as well as accurate for prediction of average permeate flux despite its simplicity. However, it cannot be used for prediction of variation of flux with distance in a cross flow cell.

3. Similarity solution for constant membrane surface concentration (SMCC)

In this case, c_m is assumed to be constant and its value is assigned to c_{wa} for osmotic pressure controlled [19] or c_g for gel layer controlled UF [20]. Therefore, Eq.(3.108) or Eq.(3.112) can be directly solved for V_p . The average flux for cross flow system can be obtained from Eq.(3.19) and flux profile with time can be obtained from Eq.(3.111) for batch cell.

In the theoretical developments presented above, we have considered gradual simplifications of two classes of boundary layer solutions, namely, the integral and the

similarity solutions. Some of the general features of these solution schemes are now discussed.

None of the simplified solutions can provide the initial flux ($t \rightarrow 0$) accurately. The schemes become accurate after longer times (or axial distances) as further simplifications are made. In the integral solutions, the accuracy of the solutions at small times or axial distances is maximum using the GIM (although it fails to give a solution at t or $x = 0$), while the IMCC should be strictly valid only in the t or $x \rightarrow \infty$ limit. Comparing all the simplified solution schemes, it also becomes evident that the GIM is the most general among all the solutions and is comparable to the numerical solution schemes in its generality. The method is further capable of simultaneously predicting the flux and rejection, and can incorporate the effects of concentration dependent diffusivity variations. The differences between QSIM and IMCC, and likewise, between QSSMs and SMCC, are very subtle. In case of QSIM and QSSMs, the membrane surface concentrations are considered constant locally. The solutions are done iteratively, with the c_m being adjusted at each iteration to adapt to the variations of δ . IMCC and SMCC, on the other hand, require an independent preset value of c_m (a constant), which is the gel concentration in case of gel-layer governed UF [19].

3.4.3 Experimental

UF experiments were performed in an unstirred batch cell and a cross flow system. The permeate flux was measured under different operating conditions encompassing feasible ranges of pressure differentials, feed concentrations and cross flow velocities.

Materials

'Spectra Por' cellulose acetate disc membranes of 76 mm diameter, supplied by Spectrum Medical Industries Inc., were used in the batch cell experiments. The membranes were of molecular weight cut off (MWCO) 5K and 10K. A different cellulose acetate membrane, supplied by Permionics Ltd. (India), was used for the

cross flow experiments. This membrane had a diffused MWCO of about 1K. The membranes are hydrophilic, anisotropic and compatible with a pH range of 2 to 10. The solutes used were polyethylene glycols (MW 6000, obtained by Fluka, Germany) and Dextrans (T-20: MW 18,600 and T-40: MW 39000, both obtained from Sigma Chemicals, USA).

Apparatus

The batch cell and the cross flow module were both developed in our laboratory. The batch cell had a volume of 600 ml and effective filtration area $41 \times 10^{-4} m^2$. The cross flow system consisted of a rectangular channel with adjustments made for the entrance length effects, so that a fully developed cross flow was ensured in the effective area of the cell. The effective filtration area was $0.32 m \times 0.05 m$. The channel height was 0.0014 m. Both the modules could handle a pressure up to 1000 kPa. The maximum volumetric flow rate in the cross flow cell was 160 liter/hour. Pressurization in the batch cell was done by compressed nitrogen or air compressor. The cross flow cell was connected to a high pressure pump, feed tank (capacity 5 liters), pressure gauges and flow meters.

Analysis

The concentrations of the feed and permeate streams were measured by the refractive index calibration curves. A Bausch and Lomb refractometer was used for this purpose. The physical properties of the solutes like osmotic pressure, diffusivity, etc. used were obtained from the literature [154, 243]. The solutes, both PEG and Dextran have a distribution of molecular weight. According to the manufacturer, PEG had molecular weight range of 5000 to 7000 and average molecular weight of T-20 and T-40 are 18,600 and 39,000, respectively. However, this polydispersity over narrow range does not affect the properties like osmotic pressure, diffusivity, etc. to a significant extent [154, 243]. Therefore, solute properties in the solution were used based on the average molecular weight prescribed by the manufacturer.

Design of the experiments

Experiments were designed to observe the variation of operating conditions on the permeate flux and rejection. In the batch cell, experiments were carried out at 450, 600 and 750 kPa and at feed concentration of 10 kg/m³. Whereas, in the cross flow cell, the operating pressures were 275, 415 and 550 kPa, feed concentrations were 10, 30 and 50 kg/m³ and the cross flow rates were 80, 100 and 120 liter/hour. For cross flow cell, experiments were designed by varying one operating condition, keeping the other two constant in order to get an exact picture of the dependence. All possible combinations were taken into account.

Procedure

The experiments were designed for the study of osmotic pressure controlled flux decline. Due to possibilities of pore blocking and solute adsorption, the experiments cannot lead to the estimation of the osmotic pressure control unless the membranes are subjected to proper pretreatment. The pretreatment was done by compacting the membranes initially with distilled water at around 900 kPa for three hours. This was followed by UF with the feed solution for 1 hour at 750 kPa (690 kPa in the cross flow system), prior to the actual experimental run. This resulted in a constant R_m value of the membrane and effectively decoupled the effect of adsorption and fouling from osmotic pressure rise in the boundary layer. In the cross flow UF, permeate stream was recycled to the feed tank to maintain the feed concentration constant. After taking a run, the module and the membrane were dismantled and thoroughly washed with distilled water and water run was taken afresh to check the permeability of the membrane. The variation of R_m remained within 2% between two consecutive water flux measurement experiments, indicating that fouling or adsorption of the solutes were negligible in the experiments. The pure water permeabilities of the Spectra por membranes used in the batch cell experiments were found to be 2.4×10^{-11} m/Pa.s for the 5K MWCO, and 5.55×10^{-11} m/Pa.s for the 10 K MWCO membranes. The permeability of the Permionics membrane was 2.46×10^{-11} m/Pa.s.

3.4.4 Results and discussion

In this section we first perform the comparison of the GIM results with other simplified models for flux decline, like the QSIM, IMCC and different similarity solutions discussed in the ‘theory’ section, for both unstirred batch and cross flow systems. This part of the study assesses the extent of inaccuracies inherent in various simplified models due to the approximations used to obtain such solutions, and the consequent deviations of the results from those obtained using the more detailed formulations.

The second part of the section presents detailed parametric studies for variable diffusivity and incomplete intrinsic rejection in both unstirred batch and cross flow UF modules using detailed finite difference simulations (DS) and simplified generalized integral method (GIM). Here, apart from the presentation of the coupled predictions of flux decline and the observed rejections in different UF modules, comparisons have also been made between the GIM and the DS to highlight the exactly similar predictions of these quantities using the two methods.

Finally, we present some comparisons of the predicted fluxes using GIM with experimental observations.

Comparison of GIM with DS and simplified solution schemes:

The detailed simulation (DS) involved a finite difference solution of the governing equations. The discretization of the two independent variables ($\{x, t\}$ in the batch cell and $\{x, y\}$ in the cross flow module) was done using a form of Chebyshev polynomial which gradually increases step sizes as distance from the origin ($x, y, t \rightarrow 0$) increases. This technique gives more accurate results compared to a uniform mesh spacing. The finite differencing over the N mesh points resulted in a set of N coupled ODEs in time (for the batch cell) or axial distance (for cross flow cell). These ODEs were then solved simultaneously using a backward difference method. Computations were done using 75 mesh points, for which results were insensitive to number of grid points. The finite difference method used here, along with the advanced backward

difference solution scheme for the coupled ODEs lead to a much more reliable prediction of flux than the finite difference schemes used earlier [112] despite using a comparatively lower number of grid points.

In contrast to the solution of the full set of partial differential equations, the solution using GIM involved the numerical integration of only two initial value ODEs for δ and n , alongwith a non-linear algebraic equation for c_m . Comparisons of computation time using the improved finite difference method used for the detailed simulations in this study and the GIM reveal that the latter uses only 10 – 30 % of the CPU time required by the former. Consequently, the GIM would be much more efficient compared to the finite difference schemes with uniform grids [112], which generally require about 500 to 700 mesh points in solutions of UF problems. This implies a significant reduction in the computational effort in case of GIM without any loss of accuracy, which is especially important for the problem of parameter estimation from the flux data.

The other integral methods are even simpler compared to GIM. In QSIM, one initial value ODE for δ is solved alongwith a non-linear algebraic equation for n (Eqs.(3.104) and (3.105) for the batch cell and (3.106) and (3.107) for the cross flow system), while in case of IMCC, only one non-linear algebraic equation needs to be solved [19, 106]. Among the similarity methods, the QSSM1 requires the integration of a boundary value ODE (Eq.(3.12) or Eq.(3.110)) which can be performed semi-analytically as already discussed earlier. In QSSM2, which is used only for the cross flow system, the average flux and membrane surface concentration are obtained by iterative solution of Eqs.(3.67), (3.108) and (3.19). Finally, SMCC involves the iterative solution of a single algebraic equation, (3.108) or (3.112). Thus, all the other simplifications presented here are also computationally much more efficient compared to the DS.

The comparison of the different solution schemes were done by simulation of the UF of two polymeric solutions, namely, PEG and Dextran, in an unstirred batch cell and a cross flow rectangular channel system. In all the solution schemes, the osmotic pressure and diffusivity are primarily required. Theoretical estimates of osmotic

pressure of these solutes were obtained using Flory's equation [243, 257, 258]. For PEG, the constant value of the diffusivity, D_∞ , was taken as $1.51 \times 10^{-10} \text{ m}^2/\text{s}$ [113, 217]. For dextran, the corresponding value was taken as $6.75 \times 10^{-11} \text{ m}^2/\text{s}$ [255, 259, 260]. Comparisons of the different solution schemes in this part of the study were performed considering constant diffusivity and complete intrinsic solute rejection ($R_r = 1$).

For simulation in the unstirred batch cell, the operating pressure range was 200 – 750 kPa, and the feed concentration was 10 kg/m^3 . The operating conditions used for the simulations for cross flow system were, $\Delta P = 275 - 550 \text{ kPa}$, $c_o = 10 - 50 \text{ kg/m}^3$, and $u_0 = 0.3 - 0.45 \text{ m/s}$ (in laminar zone, $Re < 2000$). The dimensions of the UF modules used were as prescribed earlier in the experimental section. For the batch cell, the dimensions were taken from Bhattacharjee *et al.* [243].

In an earlier study [243], the experimental fluxes during unstirred batch cell and cross flow UF of PEG 6000 and Dextran (T-20) were found to agree remarkably well with the theoretical predictions obtained by solving the governing equations numerically. The numerical scheme used in the study was exactly similar to the one described here (DS). Thus, the DS results may safely be considered as reliable for prediction of osmotic pressure governed flux decline in unstirred batch cell as well as cross flow UF.

Comparison of the predicted flux using different schemes are presented next for the unstirred batch cell and the cross flow system, respectively.

Flux prediction for Unstirred Batch Cell:

In case of unstirred batch cell UF, the growth of the boundary layer is unconstrained. Thus, the flux continues to decrease with time. The transient non-dimensional flux, v_p/J_w at different operating pressures, as predicted by the different solution schemes, are plotted against time in Fig.(3.36). Each curve has been plotted in the figure using 4 solution schemes (DS, GIM, IMCC and QSSM1).

The predictions of all the simplified schemes (except QSIM, which is not shown

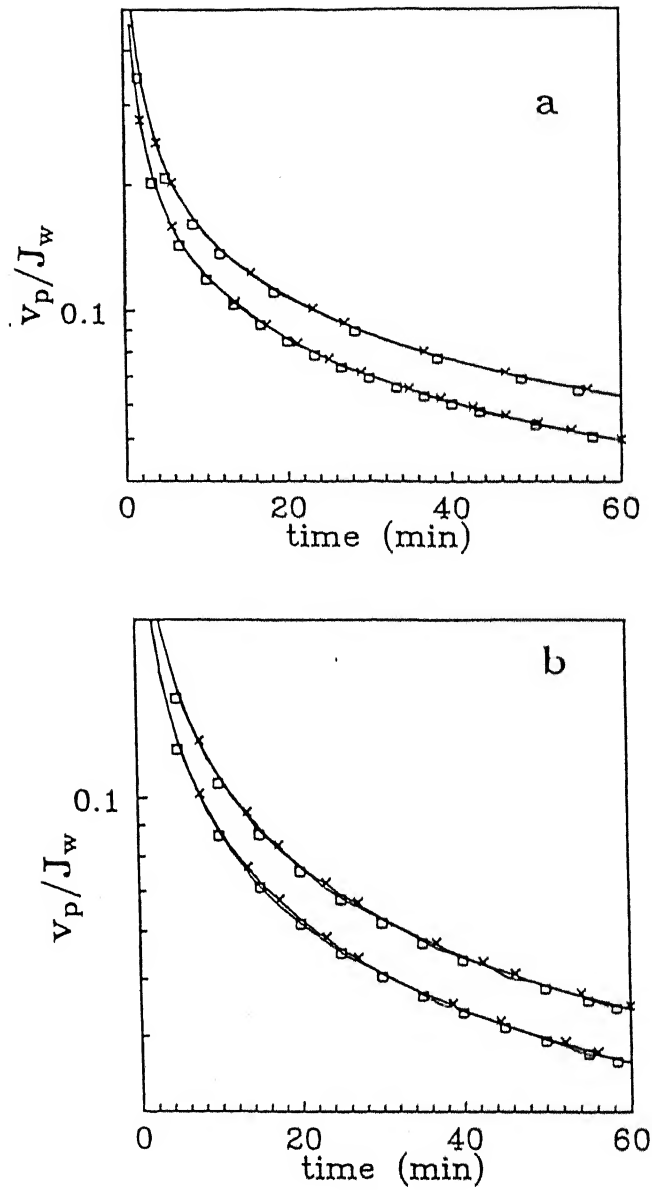


Figure 3.36: Comparison of the detailed numerical simulation results with different simplified solutions of the boundary layer – osmotic pressure model for unstirred batch cell UF of (a) Dextran (T-40); (b) PEG 6000. The detailed simulation (DS) and GIM results are represented by solid lines which virtually overlap. \square IMCC; \times QSSM1. $c_0 = 10$ kg/m³; $L_p = 2.4 \times 10^{-11}$ m/Pa.s. Upper curves in each figure represent $\Delta P = 450$ kPa while lower curves are drawn for $\Delta P = 600$ kPa.

in the figure) are remarkably close to the DS results. DS and GIM results (both solid lines) are indistinguishable in the scale of the figure. The results of GIM and IMCC virtually coincide with the DS predictions. QSSM tends to underpredict the flux. An inspection of the numerical results shows that the GIM, IMCC and QSSM1 differ from the DS predictions by 0.17, 0.35 and 1.26%, respectively, during UF using Dextran T-40 at 450 kPa. While GIM and QSSM1 underpredicts, IMCC overpredicts the flux. QSIM underpredicts flux by 10%. It is observed that even IMCC, which is considered suitable only for gel-layer governed UF, also gives an equally good prediction of the flux. This implies that the membrane surface concentration, c_m attains a constant value within a very short time in an unstirred batch cell during osmotic pressure controlled UF. Indeed, it is found that c_m attains a value close to the hypothetical osmotic pressure limiting concentration, c_{wa} , which is the concentration corresponding to the condition $\Delta P = \Delta \pi$ [19], within a few seconds. The variation of c_m is not significant after this initial period, and hence, it may be inferred that the constant membrane surface concentration assumption was valid, even in the case of osmotic pressure control.

The close agreement of the predictions by the different simplifications for the unstirred batch cell suggests that all of these may be equally useful for the prediction of osmotic pressure controlled flux for this system. However, when applied to a more commonly encountered flow configuration, *i.e.* cross flow system, the deviations between the various simplified solution schemes become more apparent.

Flux prediction for Cross Flow System:

In cross flow UF between parallel plates, feed is allowed to flow tangentially over the membrane surface. In the downstream of the channel, the growth of boundary layer becomes sluggish due to convective effects. The buildup of the membrane surface concentration is rapid near the entrance zone, and is more gradual at the downstream sections of the flow channel.

Fig. (3.37) shows the general trends of the variations of v_p with the axial distance in a cross flow cell as predicted by DS and other simplified solutions. The simulations

were done for the UF of Dextran T-20. The predictions from GIM merge with the profiles obtained using DS over the range of all operating conditions used in the simulations. The QSSM1 and QSIM, however, underpredict v_p , particularly at low feed concentrations and operating pressures.

From the dimensionless flux (v_p/J_w) profiles in Fig.(3.37), it is evident that all other simplified solutions deviate from the DS and GIM quite significantly, depending on operating conditions. Further, the deviations are more for smaller channel lengths and for lower concentrations and operating pressures. The flux profiles obtained from the IMCC are also plotted in the figure. Comparison of the predictions from different methods at a low operating pressure (275 kPa) shows that the GIM results in values coinciding with the DS, while the QSIM and QSSM1 underpredict the flux, the latter being closer to the DS results. The deviations of the last two simplified solutions from the DS predictions are 14.5 and 6.6%, respectively at channel length 1m. IMCC is, however, completely inadequate in predicting the flux decline under this condition. Although SMCC is not plotted in the same figure, it gives similar trends as IMCC. This will be shown subsequently when the predictions of average fluxes using different models are compared. As the operating pressure is increased, the deviations of the various simplified models from the DS decreases. Predictions from IMCC also improve with increase in operating pressure. However, unlike QSIM or QSSM1, it overpredicts the flux. Increasing the feed concentration at a given operating pressure results in the gradual worsening of the QSIM predictions, while QSSM and IMCC predictions improve. In all the cases, however, GIM always provides predictions as good as the DS.

The evolution of c_m/c_0 with the axial distance is shown in Fig. (3.38) for different combinations of operating conditions. While in a batch cell, c_m reaches the osmotic pressure limiting concentration, c_{wa} within a few seconds, a comparable residence time in cross flow is attained at large axial distance, $x \sim tu_0$. Thus, the approximation $c_m \sim c_{wa}$ is likely to hold only for very large axial distances in cross flow, which severely limits the applicability of SMCC and IMCC to channels smaller than a few

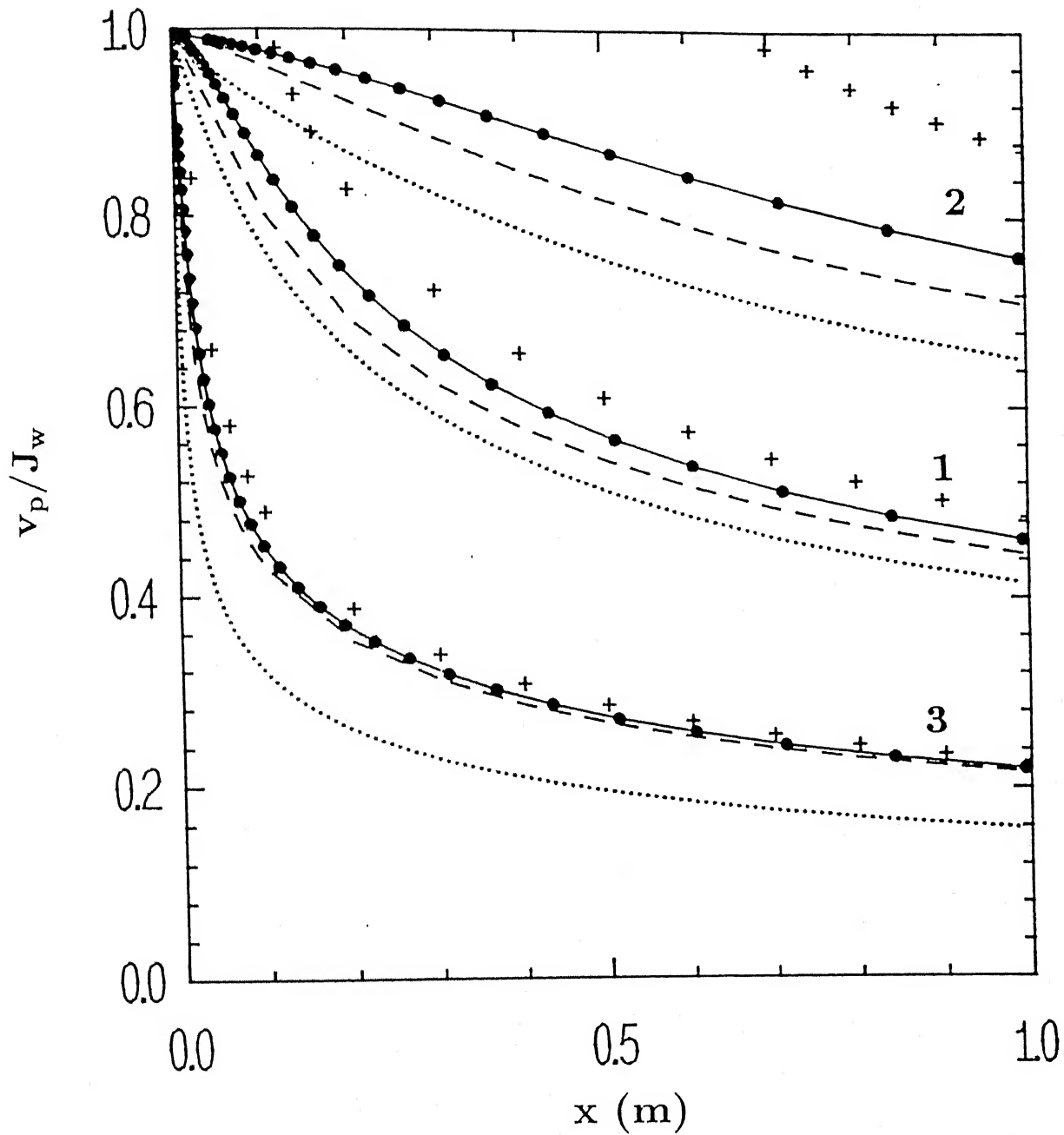


Figure 3.37: Variation of permeate flux with axial distance in a cross flow UF cell at a cross flow velocity $u_0 = 0.31$ m/s using DS and different simplified models proposed in the present work. $L_p = 2.46 \times 10^{-11}$ m/Pa.s 1: $c_0=10$ kg/m³, $\Delta P = 550$ kPa; 2: $c_0=10$ kg/m³, $\Delta P = 275$ kPa; 3: $c_0=50$ kg/m³, $\Delta P = 550$ kPa; Solid lines represent the solution obtained by GIM. ••• DS;QSSM1; --- QSIM. +++ IMCC.

meters.

The above observations regarding the flux decline behaviour and the predictions of different methods can be explained by considering the development of the concentration profiles (Fig. 3.38). At low pressures, the polarization is less severe and the buildup of the membrane surface concentration is slower. For instance, at 275 kPa, using a feed concentration of 10 kg/m^3 (c_0), the value of c_m attained at $x = 1\text{m}$ is 170.6 kg/m^3 while the value of c_{wa} is 296.4 kg/m^3 . Concentrations at lower values of x are much lower and vary considerably with x . Thus, the assumptions of quasi-steady state as well as constant membrane surface concentration are not accurate. Consequently, QSIM and QSSM1 do not predict the flux accurately. IMCC has an added drawback of completely neglecting the membrane resistance in its development. Therefore, the predictions using this method at low polarization, when the membrane resistance becomes comparable to the polarized layer resistance, are much higher. At higher pressures, the polarization is severe and the membrane surface concentration approaches c_{wa} rapidly. The resistance of the polarization layer governs the flux decline. Consequently, the simplified solutions become more accurate at higher pressures.

There are no restrictive assumptions regarding the behaviour of the membrane surface concentration in the GIM. This feature of GIM is reflected in the accurate predictions of this method, which virtually coincide with the DS predictions under all operating conditions.

Comparison of the membrane surface concentration and flux profiles in the cross flow module clearly shows that the GIM can be considered as good as the DS for prediction of fluxes under conditions of low as well as high polarization.

We next compare the average fluxes predicted by the different simplified models. The average flux for a given channel length, L was obtained by averaging the flux profile over L .

$$V_p = \frac{1}{L} \int_0^L v_p dx \quad (3.113)$$

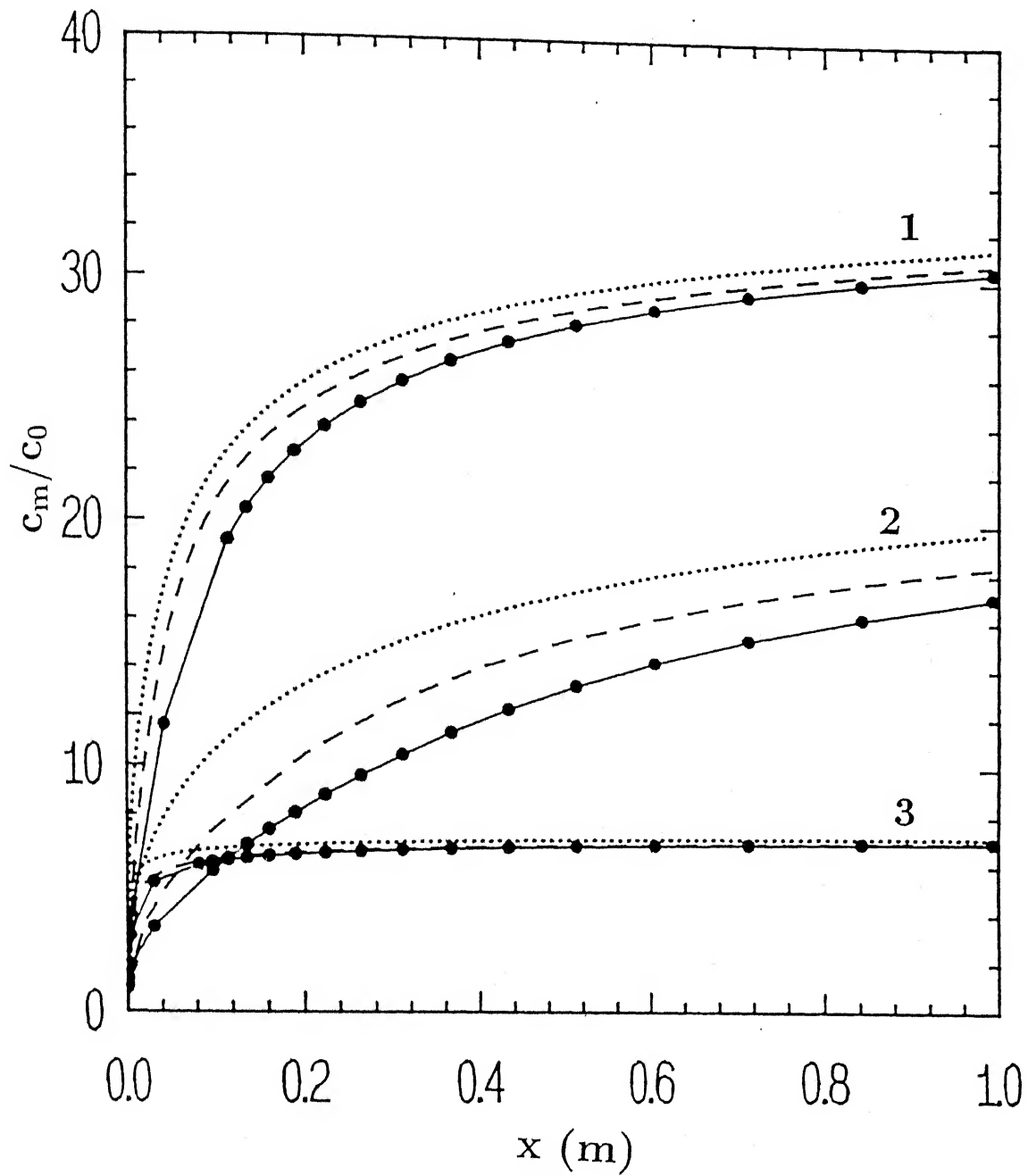


Figure 3.38: Concentration profiles of dextran (T-20) during laminar cross flow UF cell. Curves represented by 1, 2, 3 are generated using conditions specified in Fig. (3.37). Solid lines represent the solution obtained by GIM. ••• DS; -•-• QSSM1; --- QSIM;

In Fig. (3.39), the ratio of the fluxes predicted by various simplified models to the predictions of DS are plotted against channel length for different operating conditions. Comparisons are done for UF of Dextran T-20. The results of GIM coincide with those of the DS. QSSM1 gives much closer predictions of the average flux amongst all the other simplified solutions. The fluxes are underpredicted by about 5% for channel lengths less than 1m. At high pressures the predictions are even closer. QSIM gives almost a steady underprediction ranging between 5 – 12 % over all operating condition. The predictions seem to diverge slowly from the exact solution with increasing channel length. Both SMCC and IMCC overpredict the average flux significantly for smaller channel length and low pressure. The deviation becomes less for a very long channel. It can be seen that the predictions deviate by more than 50% for channel lengths of 1m at 275 kPa.

Another interesting result is also presented in Fig. (3.39) (shown by the triangles) which gives a very accurate prediction of average flux. This solution is obtained by the similarity method assuming constant membrane surface concentration and equating the resulting expression of the average flux, Eq.(3.19), with Eq.(3.67) (QSSM2). The solutions overpredict the average flux by only about 5%. This is an immense improvement over the SMCC solution. This method may be considered as a means of computing the flux at an average membrane surface concentration. Although this method does not provide the flux profile, it can still be useful, as the average permeate flux is usually the only measurable experimental data which can be compared to theoretical predictions.

To summarize, the proper choice of a concentration profile which is capable of accounting for the evolution of the polarized layer near the membrane surface, leads to a drastic simplification of the equations governing the flux decline behaviour during an UF process. The generalized integral method (GIM) presented in this work, although being much simple, is as accurate as the detailed simulation. This solution is clearly the most accurate simplified approach for prediction of the permeate flux during osmotic pressure controlled UF in which case, the membrane surface

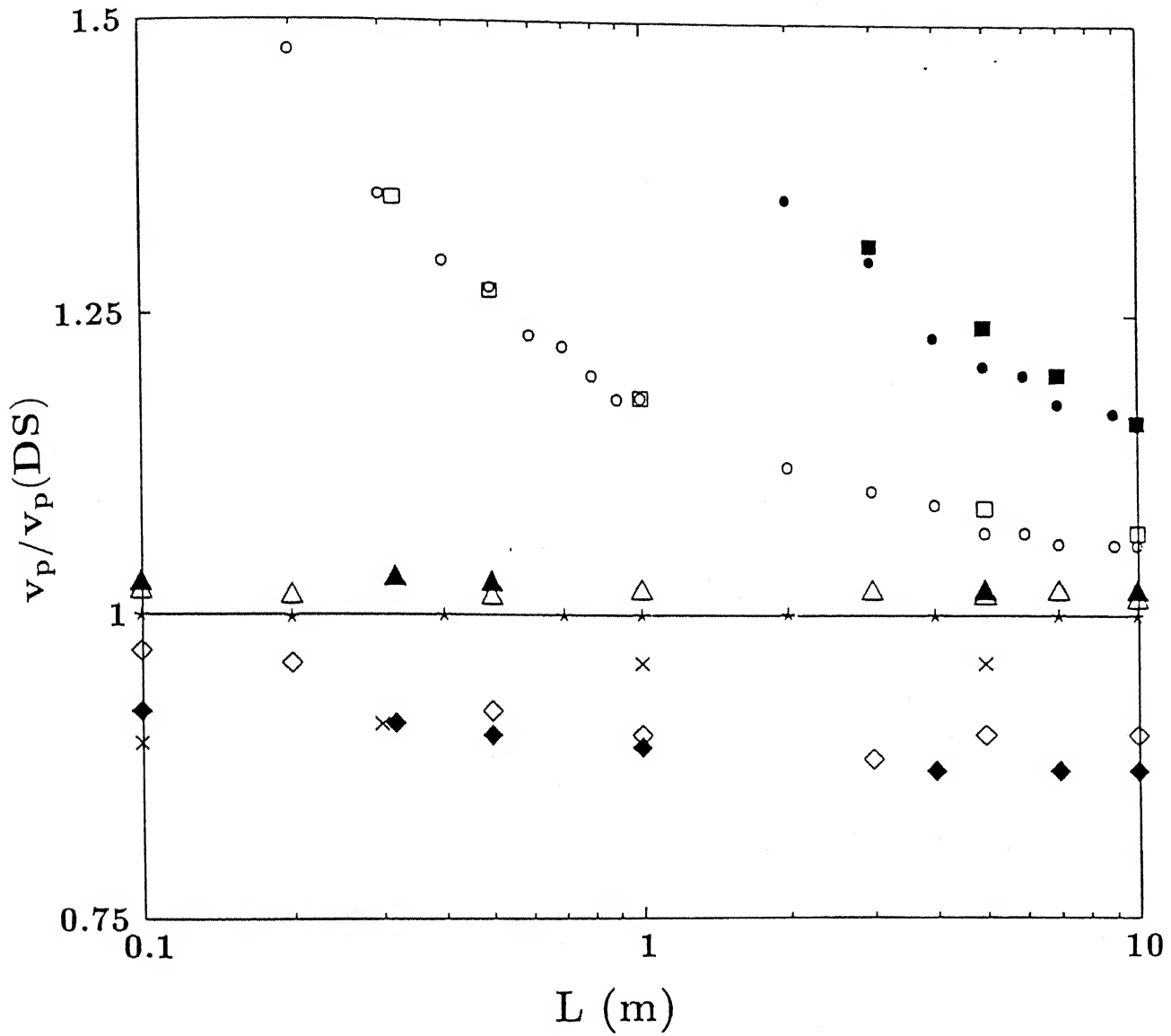


Figure 3.39: Comparison of average flux (Eq. (3.113)) of dextran (T-20) in a cross flow cell predicted by different simplified models with the predictions of DS. Filled symbols correspond to the operating conditions $\Delta P = 275$ kPa, $c_0 = 10$ kg/m³, $u_0 = 0.46$ m/s and open symbols correspond to $\Delta P = 550$ kPa, $c_0 = 10$ kg/m³, $u_0 = 0.31$ m/s. \circ IMCC; \square SMCC; \star GIM; \times QSSM1; \diamond QSIM; \triangle QSSM2.

concentration varies with time or axial distance. At low polarization, commonly encountered during cross flow UF at low pressures and high feed flow rates, the GIM is most suitable. At high polarization, other simplified methods like QSSMs, SMCC and IMCC also become competitive, especially for longer channel lengths. In unstirred batch cell, all the simplified models are almost equally good after a short transient period, because the membrane surface concentration attains a constant limiting value within a short time. In all cases, predictions of GIM match the detailed simulations. The GIM is a useful substitute for the detailed simulations, which are more computation intensive, while being more accurate than other simplified solution schemes.

It is, however, quite well known that the predictions of flux decline using a constant diffusivity in the boundary layer equations often deviate considerably from the experimental fluxes, particularly for proteins [20, 44, 116]. These deviations are attributed to variations of solute diffusivity with concentration. However, instead of incorporating the concentration dependence explicitly, an adjustable diffusivity was used in different models to match the experimental fluxes [106, 116]. Secondly, variations in the intrinsic membrane rejection, R_r , may also result in a change in the permeate flux as well as the observed rejection, R_o [112, 261]. Simultaneous prediction of flux and observed rejection is, therefore, a primary requisite for modeling an UF operation. A general model of UF should incorporate the concentration dependence of diffusivity as well as the effects of incomplete intrinsic rejection on both the flux decline and variations in the observed rejection. We next discuss the methodology, and the results of incorporating these features in the GIM by performing detailed parametric studies for the batch cell and the cross flow system.

Parametric studies for variable diffusivity and incomplete intrinsic rejection using GIM

Parametric studies for flux and observed rejection were carried out for both unstirred batch and cross flow systems using the DS and the GIM. Simulations were performed for different values of the intrinsic (real) rejection ($R_r \leq 1$) and variable

diffusivity. Remarkably, the maximum deviation between the results of GIM and the DS using finite differences never exceeded 0.17 % for all realistic values of parameters used; thus, the results displayed in subsequent figures are obtained from GIM, which are indistinguishable from detailed numerical simulations of governing partial differential equations.

The intrinsic rejection, R_r (Eq.(3.68)) is an intrinsic property of the membrane-solute system which does not generally depend on the operating conditions [112]. Therefore, as c_m is a function of time (t) in a batch cell or axial distance (x) in a cross flow system, c_p should also vary with t (in a batch cell) or x (in a cross flow cell), in order to maintain the intrinsic rejection (R_r) constant. Consequently, considering negligible variation of the feed bulk concentration, the observed rejection (R_o) varies with t or channel length.

The variation of diffusivity is studied considering a linear model for the variation of the property with concentration. As discussed earlier, such a variation renders the solution of the integral equations formulated here more facile. Moreover, the variation of diffusivity with solute concentration has been considered to be linear in several earlier studies [256, 262, 263] and seems to be quite adequate for several macromolecular systems upto sufficiently high solute concentrations. The variation of the diffusivity was incorporated in the model as a linear function of the solute concentration, c

$$D = D_{\infty}(1 + Kc) \quad (3.114)$$

where, c is in kg/m^3 . The extent of variation of the dimensionless quantity, D/D_{∞} depends on the parameter K . The parametric studies were carried out for different realistic values of K ranging between 0 (constant diffusivity) to $2 \times 10^{-3} \text{ m}^3/\text{kg}$, which closely follows the experimental trends for dextrans [154] and protein (BSA) solutions at high ionic strengths [256, 263].

Unstirred batch cell:

Parametric studies were performed for an unstirred batch cell to observe the influ-

ence of concentration dependence of the diffusion coefficient and the incomplete intrinsic rejection on the permeate flux and observed rejection. These studies were performed by selecting different values of K and R_r .

The variations in flux and observed rejection with time are shown in Fig. (3.40) for different combinations of R_r and K . The solid curves denote the dimensionless permeate flux, while the discontinuous curves and symbols (\square) denote the observed rejection. Curve 1, drawn for a fully rejecting membrane ($R_r = 1$) and a constant diffusivity shows the steepest decline in permeate flux. When the intrinsic rejection is 0.99, the decline is more gradual (curve 2). The flux is found to increase dramatically with further lowering of R_r (curve 5). The influence of diffusivity variations on the permeate flux becomes apparent from curves 2 and 3. The flux increases as K is increased from 0 (curve 2) to $2 \times 10^{-3} \text{ m}^3/\text{kg}$ (curve 3). It is indeed striking that a relatively small variation of the intrinsic rejection can result in such a drastic alteration in the flux decline behaviour (curves 1, 3, 4 and 5). The incomplete rejection tends to increase the permeate flux, while the observed rejection (discontinuous curves, 6 and 7) decreases. Even for a real rejection of 0.99, the observed rejection drops to about 0.5 within 5 – 10 minutes of UF. Thus, a slight imperfection in the membrane may result in a significant alteration of its actual performance. Although the flux is enhanced by reduction of the intrinsic rejection, the permeate concentration increases, which may partially or completely defeat the purpose of UF. Generally, it may be concluded from the trends shown in Fig. (3.40), that the observed rejection becomes negligibly small for $R_r \leq 0.98$ at longer times.

Cross flow UF:

Figs. (3.41) and (3.42) describe the effects of R_r and diffusivity on the build up of solute concentration on the membrane surface, c_m in a cross flow cell. As in the case of unstirred batch cell, the concentration build up is significantly restricted when R_r is lowered. For instance, lowering R_r from 1.0 to 0.9, results in a decrease of c_m/c_0 by almost three folds (from ~ 25 to ~ 10) for the operating conditions used in Fig. (3.41). Consequently, the permeate flux increases owing to a less severe buildup of

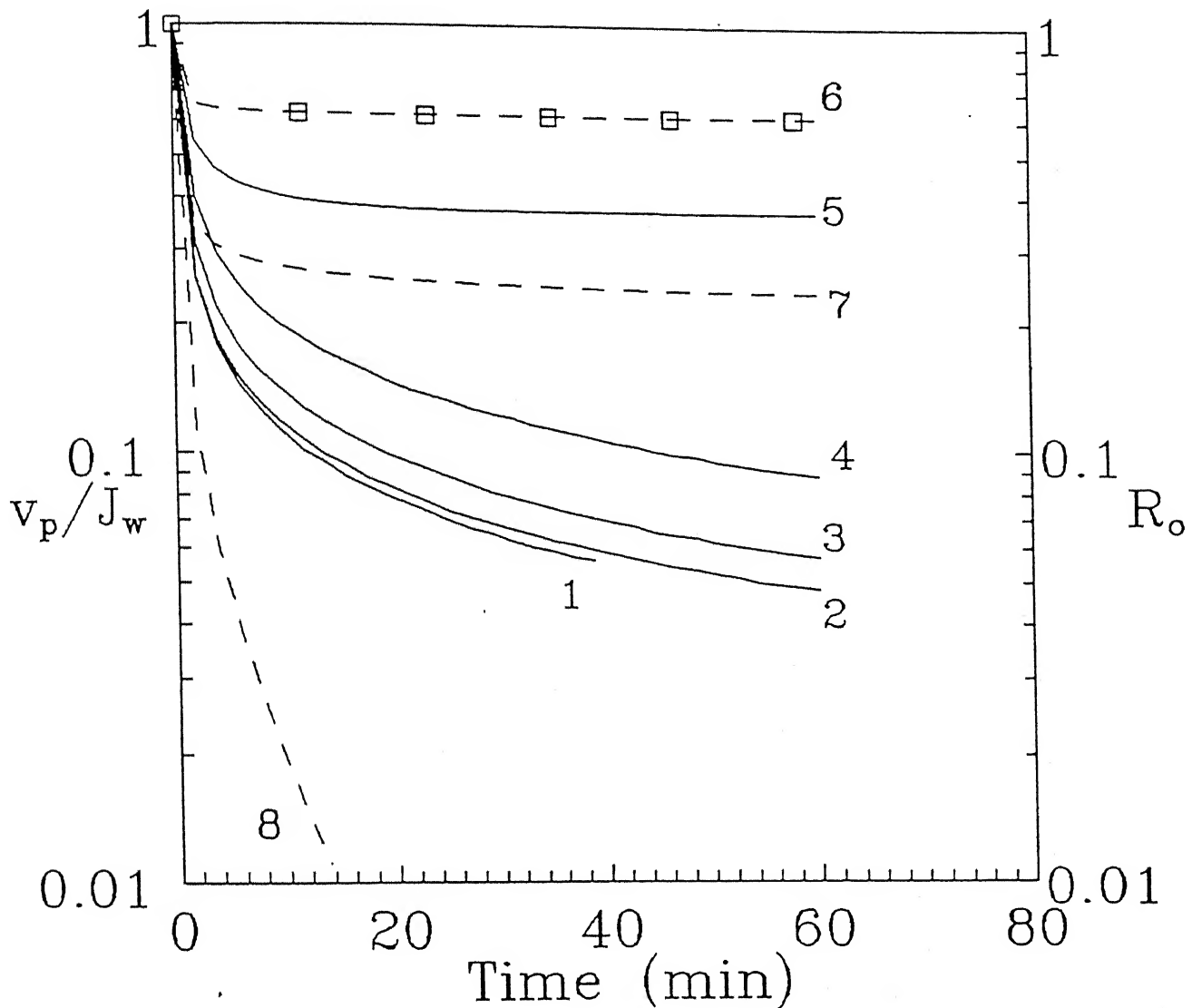


Figure 3.40: Variation of dimensionless permeate flux (solid lines) and observed rejection (discontinuous lines and symbol) with time in an unstirred batch cell. The variation of diffusivity, when considered is assumed to be linear, $D = D_{\infty}(1 + Kc)$, with K varying from 0 to $2 \times 10^{-3} \text{ m}^3/\text{kg}$. Osmotic pressure and other solution properties correspond to Dextran T-20. $c_0 = 10 \text{ kg/m}^3$; $\Delta P = 600 \text{ kPa}$. Curve 1: $R_r = 1.0, K = 2 \times 10^{-3} \text{ m}^3/\text{kg}$; 2: $R_r = 0.99, K = 0.0$; 3: $R_r = 0.99, K = 2 \times 10^{-3} \text{ m}^3/\text{kg}$; 4: $R_r = 0.98, K = 2 \times 10^{-3} \text{ m}^3/\text{kg}$; 5: $R_r = 0.97, K = 2 \times 10^{-3} \text{ m}^3/\text{kg}$; $K = 2.0 \times 10^{-3} \text{ m}^3/\text{kg}$ for curves 6 to 8. Curve 6: $R_r = 0.99$; 7: $R_r = 0.98$; 8: $R_r = 0.97$; symbols (\square): $K = 0.0, R_r = 0.99$

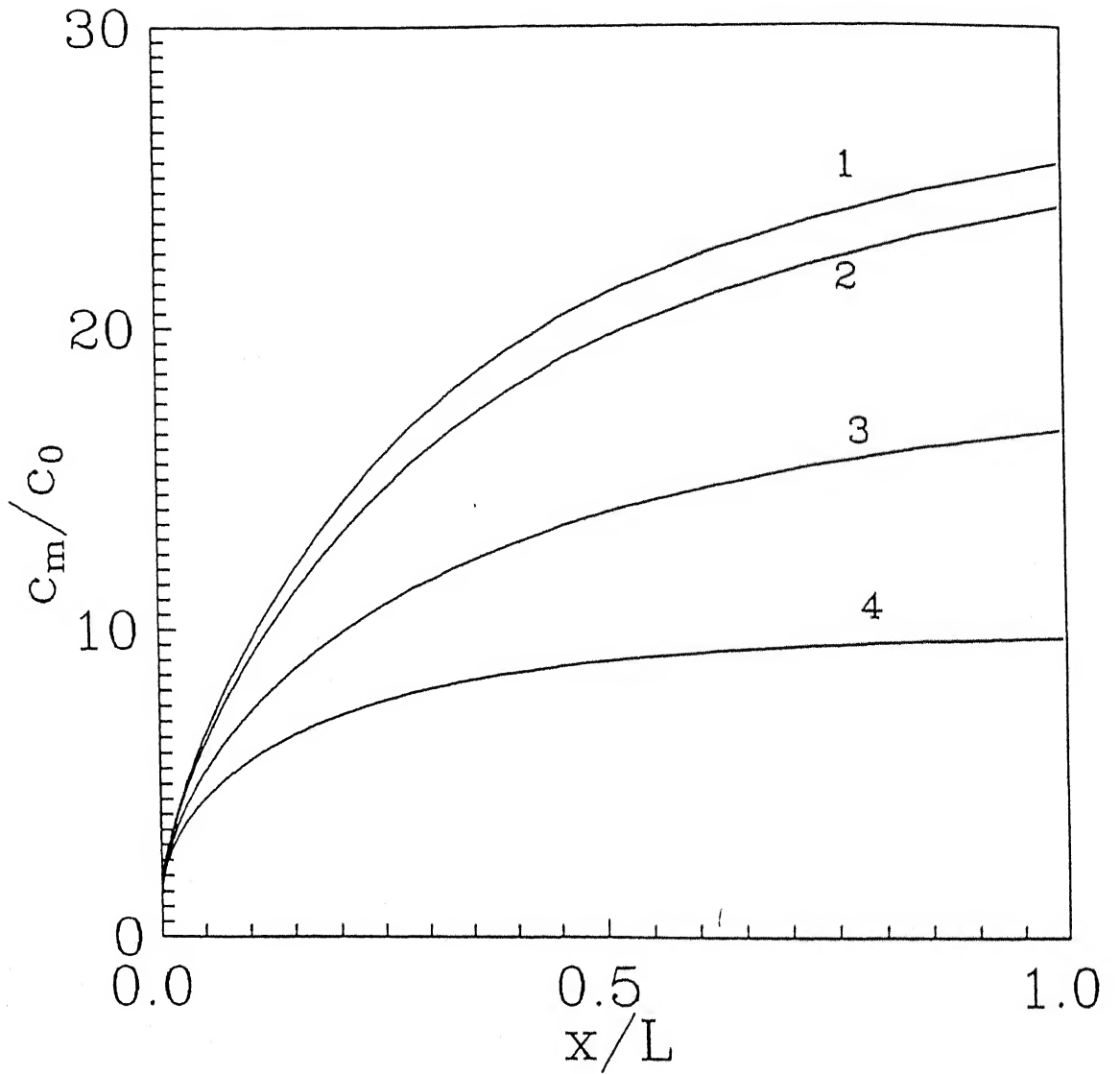


Figure 3.41: Variation of dimensionless membrane surface concentration with channel length in a cross flow ultrafiltration system for constant diffusivity. Simulations are performed using solution properties of Dextran T-20 with $L_p = 2.46 \times 10^{-11}$ m/Pa.s. $\Delta P = 550$ kPa; $Re = 1000$; $c_0 = 10$ kg/m³. Curve 1: $R_r = 1.0$; 2: $R_r = 0.99$; 3: $R_r = 0.95$; 4: $R_r = 0.90$;

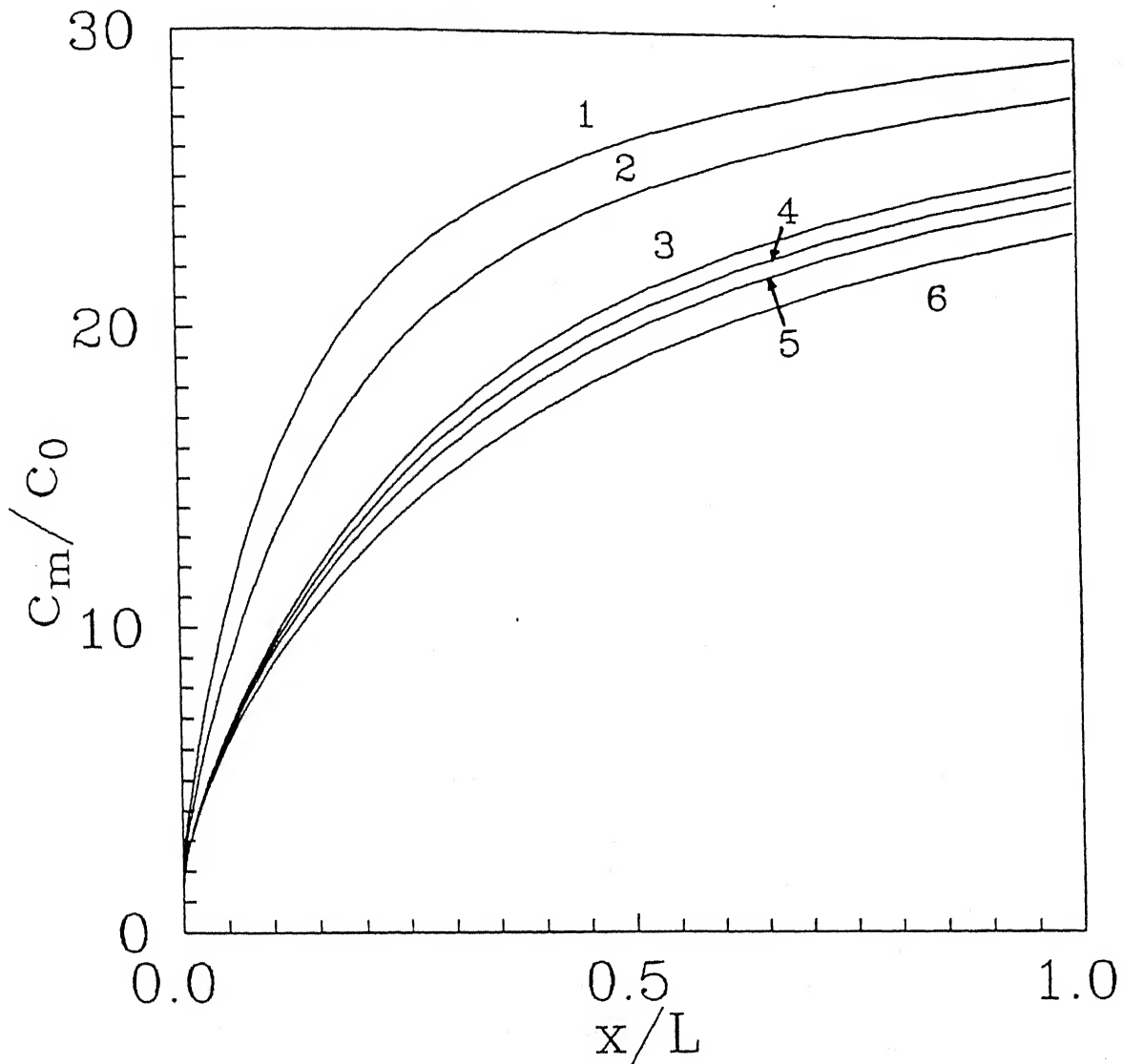


Figure 3.42: Variation of dimensionless membrane surface concentration with channel length in a cross flow system at constant R_r (1.0). Simulations are performed using solution properties of Dextran T-20. Operating conditions and membrane properties are same as Fig. (3.41). Variation of diffusivity is assumed to be linear. $K = 0$ for curves 1–3. Curve 1: $D_\infty = 6.75 \times 10^{-11} \text{m}^2/\text{s}$; 2: $D_\infty = 8 \times 10^{-11} \text{m}^2/\text{s}$; 3: $D_\infty = 10.34 \times 10^{-11} \text{m}^2/\text{s}$; K is varied for curves 4–6. Curve 4: $K = 0.5 \times 10^{-3} \text{m}^3/\text{kg}$; 5: $K = 1.0 \times 10^{-3} \text{m}^3/\text{kg}$; 6: $K = 2 \times 10^{-3} \text{m}^3/\text{kg}$;

the osmotic pressure difference across the membrane. In Fig. (3.42), the variation of the membrane surface concentration with variations in D_∞ and K is depicted. While the former causes a more drastic variation in the concentration profiles, the latter induces considerably lesser changes in c_m . For variation of D with concentration, the effects of altered D is felt only over a small portion of the concentrated boundary layer. Thus Fickian back - diffusion is larger over a smaller length of the boundary layer compared to that observed when D_∞ is varied.

The permeate flux gets affected quite severely for a slight variation of R_r . On the other hand, the effect of variation of diffusivity on flux is minor over the range of diffusivity variations studied here. The effect of R_r and D on flux is shown in Figs. (3.43) and (3.44). From Fig. (3.43), it can be shown that flux can be improved quite significantly by choosing a membrane - solute combination which has a slightly low R_r (0.9 - 0.95). This enhancement in flux, however, is achieved at the cost of very poor permeate quality. In contrast, it is evident from Fig. (3.44) that the enhancement in flux due to variations in diffusivity is not so marked. For instance, when K is $2.0 \times 10^{-3} \text{ kg/m}^3$, flux increases by only $\sim 2\%$ compared to that obtained using a constant diffusivity towards the end of the channel ($x/L \rightarrow 1$).

Fig. (3.45) shows the effects of R_r on observed rejection. R_o decreases along the channel length with decrease in R_r . If R_r is 0.85, R_o becomes almost zero in the downstream of the channel. This indicates that for a choice of a low rejecting membrane, permeate quality will be adversely affected although it is possible to obtain a higher flux. Therefore, choice of a proper membrane is a key design criteria to have a trade off between a desirable flux and quality of the permeate. The influence of D on the observed rejection were once again found to be quite small, as observed in case of unstirred batch cell (Fig. 3.40).

The cross flow velocity is also an important parameter which governs the quality of the permeate. Fig. (3.46) shows the variation of R_o with channel length obtained for different values of the Reynolds number (Re). It is observed that as Re increases, R_o also increases. At low Re , the concentration build-up is more severe, resulting in

a lowering of the observed rejections. From the figure, it can be seen that four fold decrease in Re causes to decrease R_o from 0.35 to 0.1. Therefore, cross flow velocity can be an optimizing parameter to obtain a desired balance between the permeate flux and observed rejection.

In case of osmotic pressure governed UF, the resistance due to the osmotic pressure, R_{osm} may be defined [6, 123],

$$v_p = \frac{\Delta P}{\mu(R_m + R_{osm})} \quad (3.115)$$

Treatment of the flux decline using this approach will be analogous to the use of the concept of gel layer resistances practiced in several hydrodynamic approaches [124]. It should, however, be noted that this resistance (R_{osm}), unlike the gel layer resistance used in earlier studies, is directly obtained from the concentration dependence of osmotic pressure, and is not an empirical adjustable parameter.

The variation of the dimensionless osmotic pressure resistance (R_{osm}/R_m) with R_r and diffusivity is shown in Fig. (3.47) illustrating the drastic variation of R_{osm} with R_r (discontinuous curves) as well as with the diffusivity, D_∞ (solid lines). For incomplete intrinsic rejections, $R_r < 1$, the permeate concentration increases, which reduces $\Delta\pi$. Consequently, osmotic resistance buildup is also arrested. R_{osm} also decreases with an increase in K because of enhancement of back diffusion of the solutes. But this effect is not very significant as shown in Fig. (3.47).

The parametric study reveals that for high intrinsic rejections, $R_r \geq 0.95$, a small difference in R_r may lead to a significant alteration in the observed rejection along the channel length (Fig. 3.43). This may be utilized for fractionation of multicomponent macromolecular solutions with its different solute components showing slightly different intrinsic rejection by a particular membrane in a cross flow system. For such a system, permeate 'cuts' at different locations in the axial direction will have different compositions; the permeate will be enriched with the solute having a lower intrinsic rejection near the channel entrance.

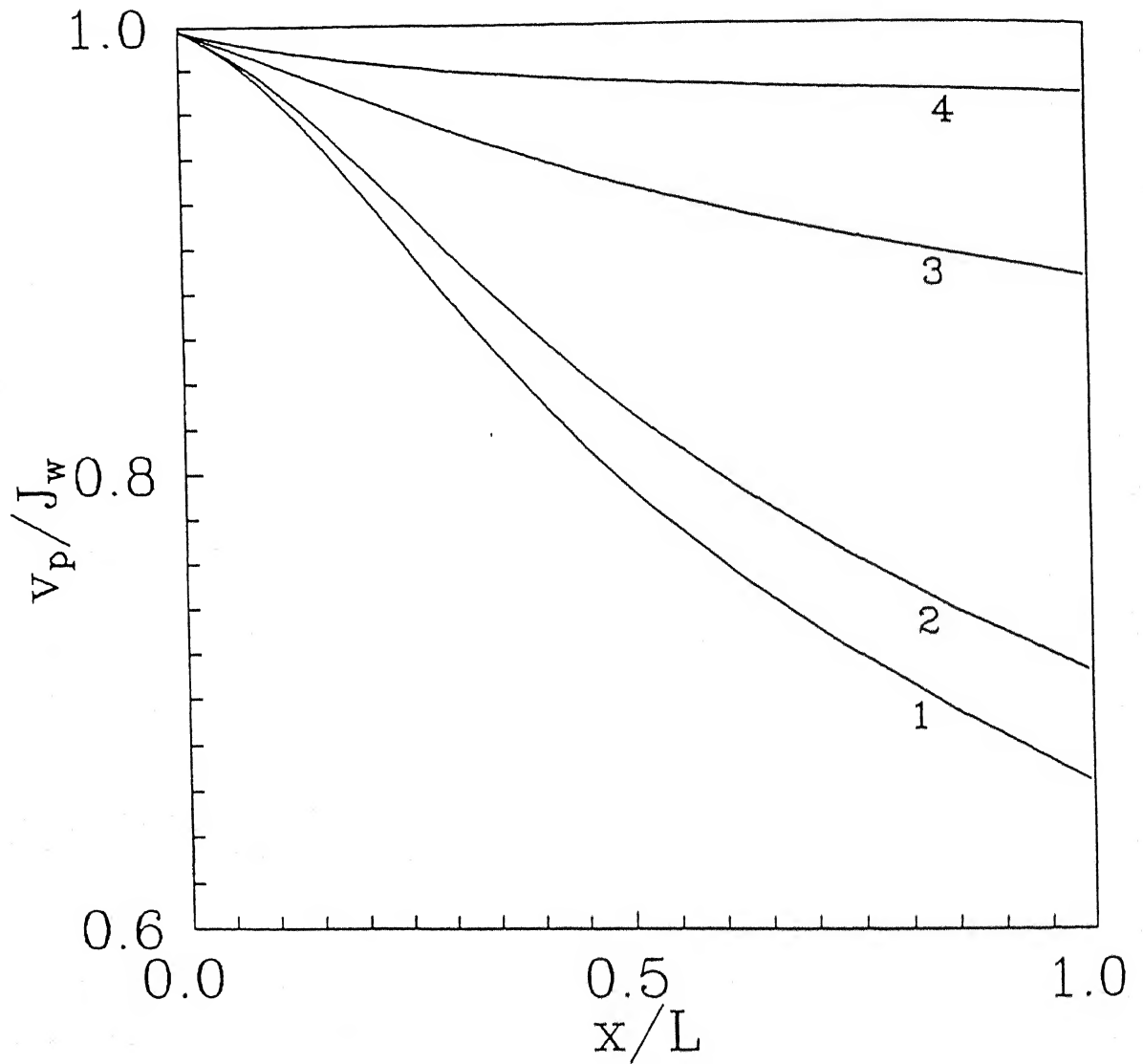


Figure 3.43: Variation of dimensionless permeate flux with channel length at constant diffusivity in a cross flow system. Simulations are performed using solution properties of Dextran T-20. Operating conditions and membrane properties are same as Fig (3.41). Curve 1: $R_r = 1.0$; 2: $R_r = 0.99$; 3: $R_r = 0.95$; $R_r = 0.90$.

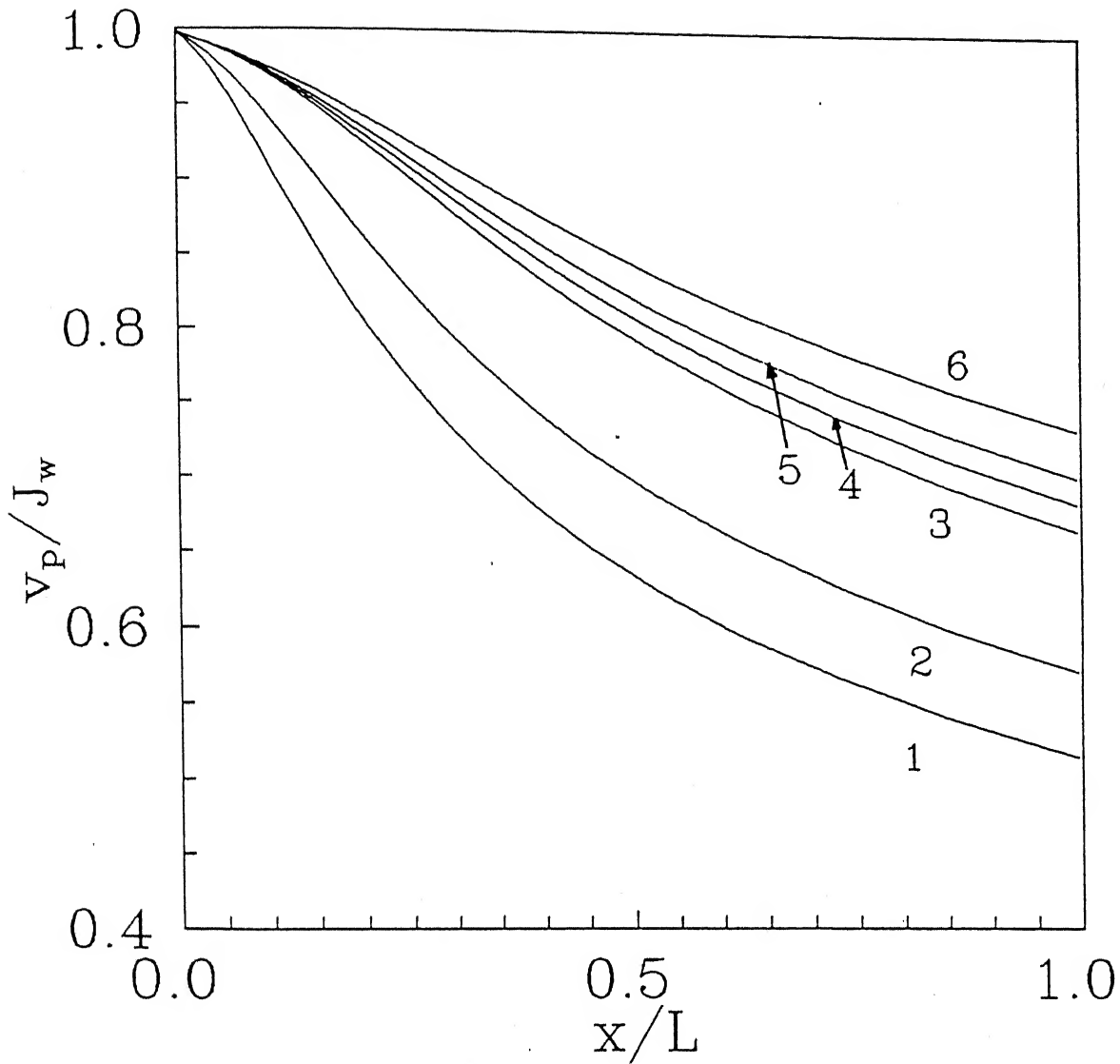


Figure 3.44: Variation of dimensionless flux with channel length in a cross flow system at constant ($R_r=1.0$). Simulations are done with the solution properties of Dextran T-20. Operating conditions and membrane properties correspond to those of Fig. (3.41). For curves 1 to 3, $K = 0$. Curve 1: $D_\infty = 6.75 \times 10^{-11} \text{ m}^2/\text{s}$; 2: $D_\infty = 8.00 \times 10^{-11} \text{ m}^2/\text{s}$; 3: $D_\infty = 10.34 \times 10^{-11} \text{ m}^2/\text{s}$; K is varied for curves 4 to 6. Curve 4: $K = 0.5 \times 10^{-3} \text{ m}^3/\text{kg}$; 5: $K = 1.0 \times 10^{-3} \text{ m}^3/\text{kg}$; 6: $K = 2.0 \times 10^{-3} \text{ m}^3/\text{kg}$.

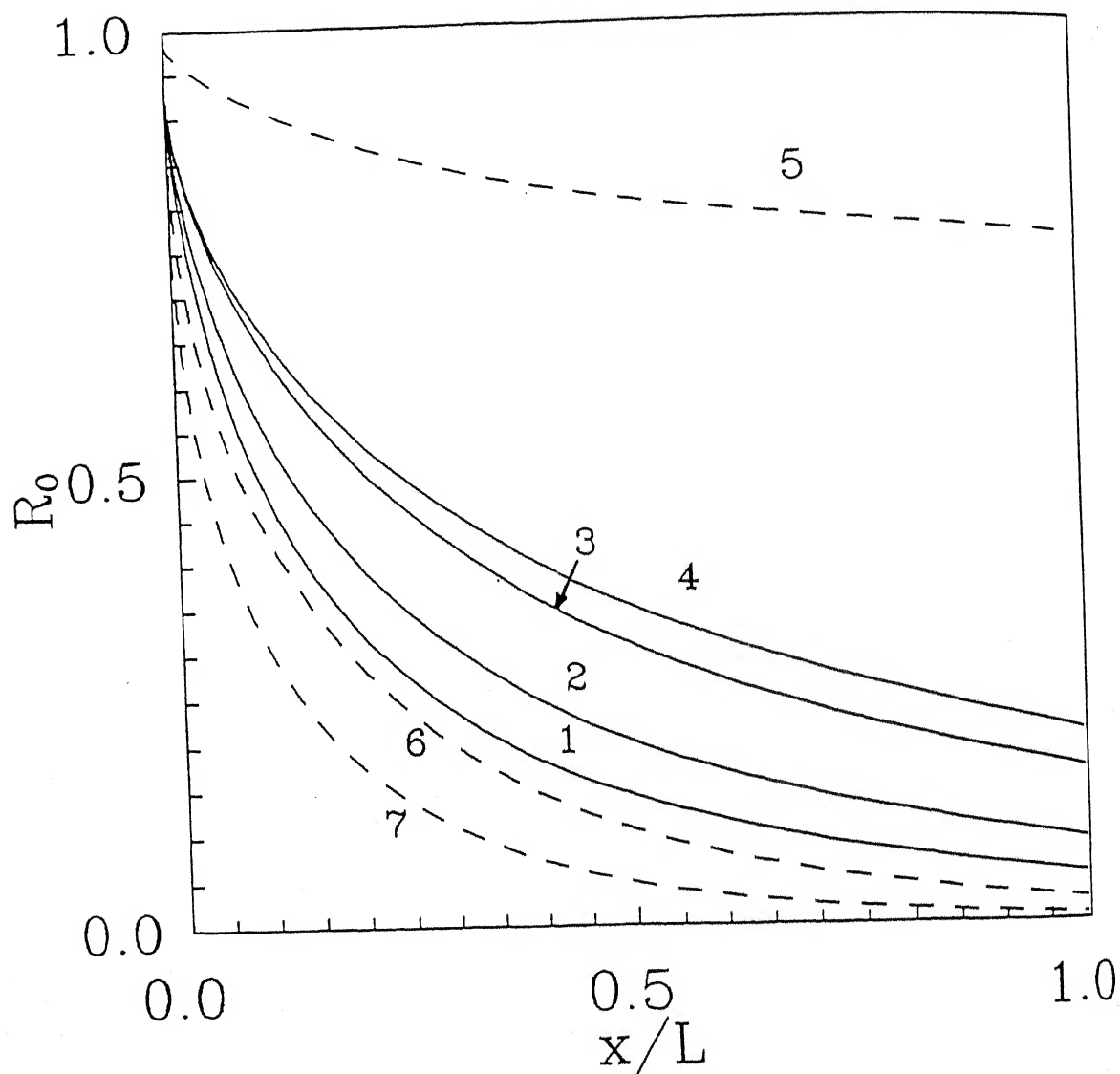


Figure 3.45: Variation of observed rejection with channel length in a cross flow system. Simulations are carried out using the solution properties of Dextran T-20. Operating conditions and membrane properties correspond to those of Fig. (3.41). Curves 1 to 4 are drawn at constant R_r (1.0) and 5 to 7 are drawn at constant value of D_∞ (10.34×10^{-11}). Curve 1: $D_\infty = 6.75 \times 10^{-11} \text{m}^2/\text{s}$; 2: $D_\infty = 8.00 \times 10^{-11} \text{m}^2/\text{s}$; 3: $D_\infty = 10.34 \times 10^{-11} \text{m}^2/\text{s}$ and $K = 0$; 4: $D_\infty = 10.34 \times 10^{-11} \text{m}^2/\text{s}$ and $K = 2.0 \times 10^{-3} \text{m}^3/\text{kg}$; 5: $R_r = 0.99$; 6: $R_r = 0.95$; 7: $R_r = 0.90$.

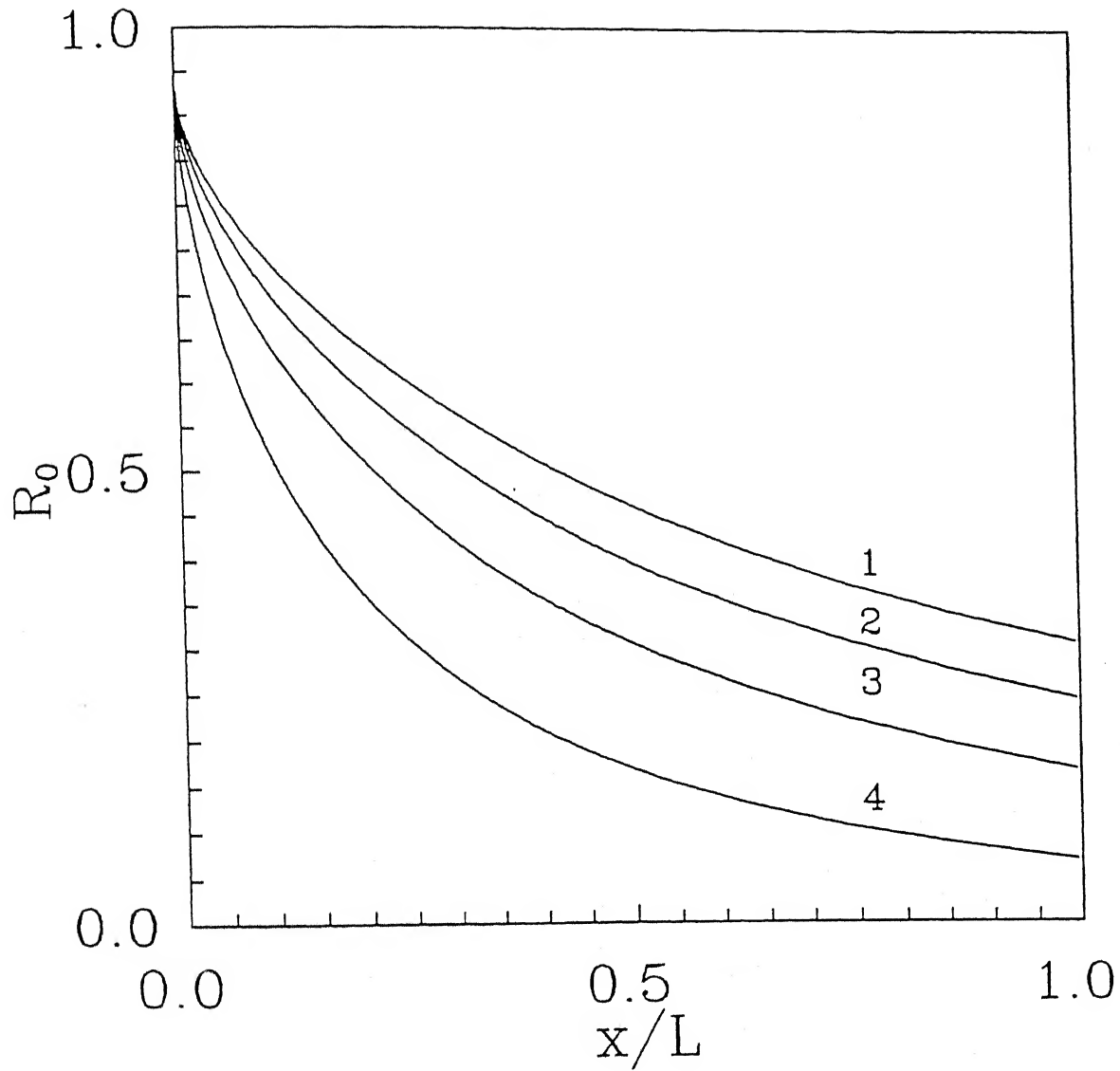


Figure 3.46: Variation of observed rejection with channel length in a cross flow system. Simulations are performed using the solution properties of Dextran T-20. Operating conditions and membrane properties correspond to those of Fig. (3.41). Curve 1: $Re = 2000$; 2: $Re = 1500$; 3: $Re = 1000$; 4: $Re = 500$.

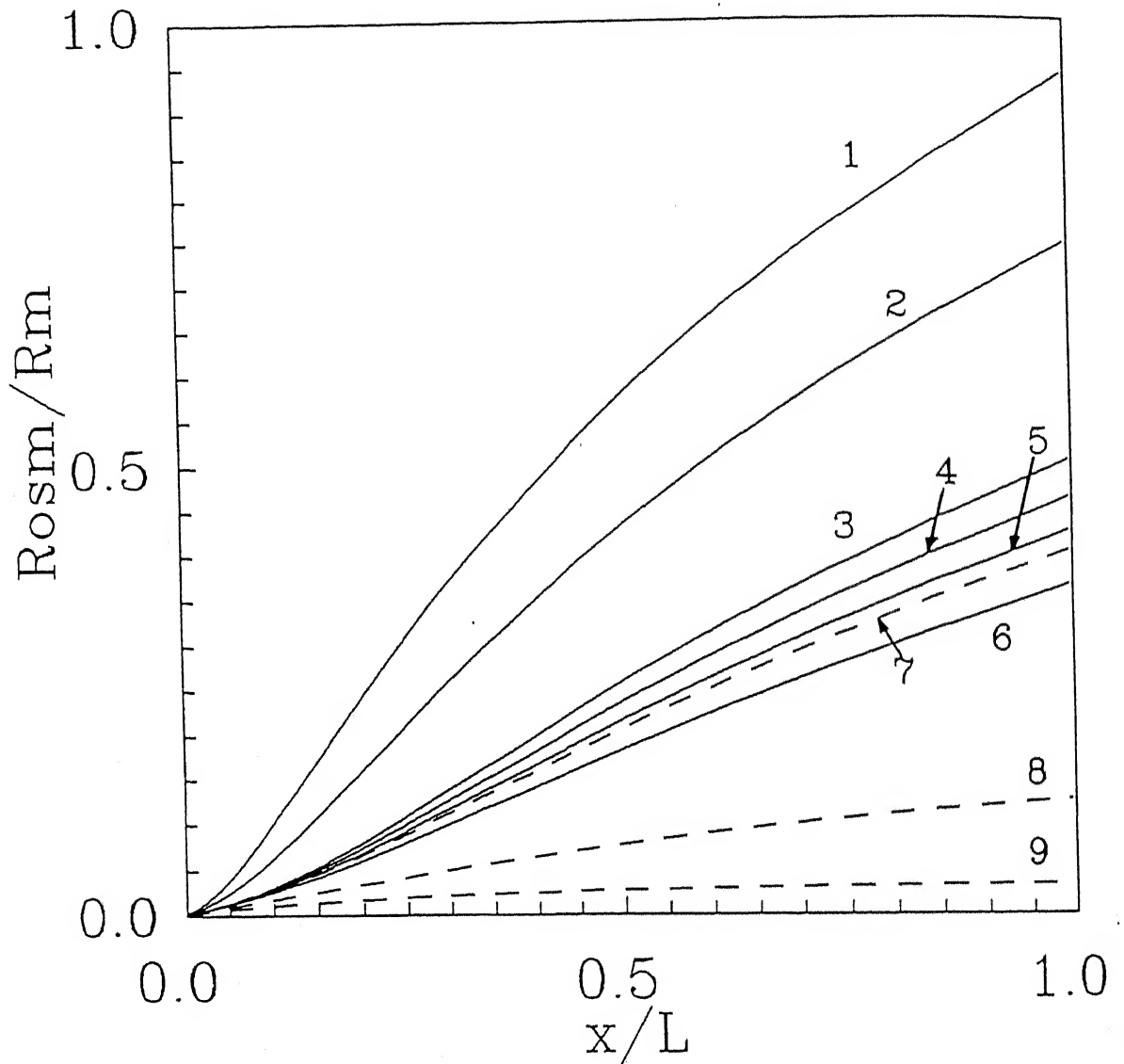


Figure 3.47: Variation of osmotic pressure resistance with channel length in a cross flow UF system. Simulations are performed with the solution properties of Dextran T-20. Operating conditions and membrane properties correspond to those of Fig. (3.41). Solid lines are for constant R_r (1.0) and discontinuous lines are for constant D_∞ ($10.34 \times 10^{-11} \text{m}^2/\text{s}$). $K = 0$ for curves 1 to 3 and K is varied for curves 4 to 6. Curve 1: $D_\infty = 6.75 \times 10^{-11} \text{m}^2/\text{s}$; 2: $D_\infty = 8.00 \times 10^{-11} \text{m}^2/\text{s}$; 3: $D_\infty = 10.34 \times 10^{-11} \text{m}^2/\text{s}$. $D_\infty = 10.34 \times 10^{-11} \text{m}^2/\text{s}$ for curves 4 to 9. Curve 4: $K = 0.5 \times 10^{-3} \text{m}^3/\text{kg}$; 5: $K = 1.0 \times 10^{-3} \text{m}^3/\text{kg}$; 6: $K = 2.0 \times 10^{-3} \text{m}^3/\text{kg}$; 7: $R_r = 0.99$; 8: $R_r = 0.95$; 9: $R_r = 0.90$.

Incomplete solute rejection governs the variations of flux decline and observed rejection significantly. Consequently, estimates of R_r , which is required as an input parameter in GIM or DS as discussed above, should be very accurate. A pore level modeling of solute transport including hydrodynamics [165, 170] and intermolecular interactions [264, 265] is a theoretical guide for prediction of R_r . Unfortunately, in such approaches, there are too many unknown parameters that are difficult to estimate independently. The use of GIM appears to be promising in estimating R_r for a membrane-solute combination. The GIM should be computationally much more efficient for parameter estimation by fitting experimental data compared to the problem of parameter estimation using partial differential equations. The use of parameter estimation using GIM of course extends to other unknown parameters as well, *e.g.* diffusivity, R_{osm} , *etc.*

The parametric study also indicates that a proper choice of membrane and other operating variables may lead to obtain a desirable flux and permeate quality for a given solute-solvent system. In addition to independent estimates of the variations of diffusivity and osmotic pressure with solute concentration, the intrinsic rejection also needs to be accurately known in order to predict the permeate flux and the observed solute rejection correctly. Earlier works suggest two routes of independent determination of the intrinsic rejection, namely, using a pore level model and using the velocity variation technique that requires UF experiments [112]. A complete predictive model for UF can then be constructed by coupling the transport equations in the external boundary layer as developed here and the model for permeate transport within the membrane pores.

Comparison of GIM with experimental results

The simplicity of GIM in comparison with DS and its remarkable accuracy to predict fluxes facilitates fitting of experimental data (particularly, flux decline data) to obtain estimates of various solution properties. While DS may be used for such types of parameter estimations, the resulting computations will generally be prohibitively large. In contrast, GIM can be used very efficiently for optimization purposes. In

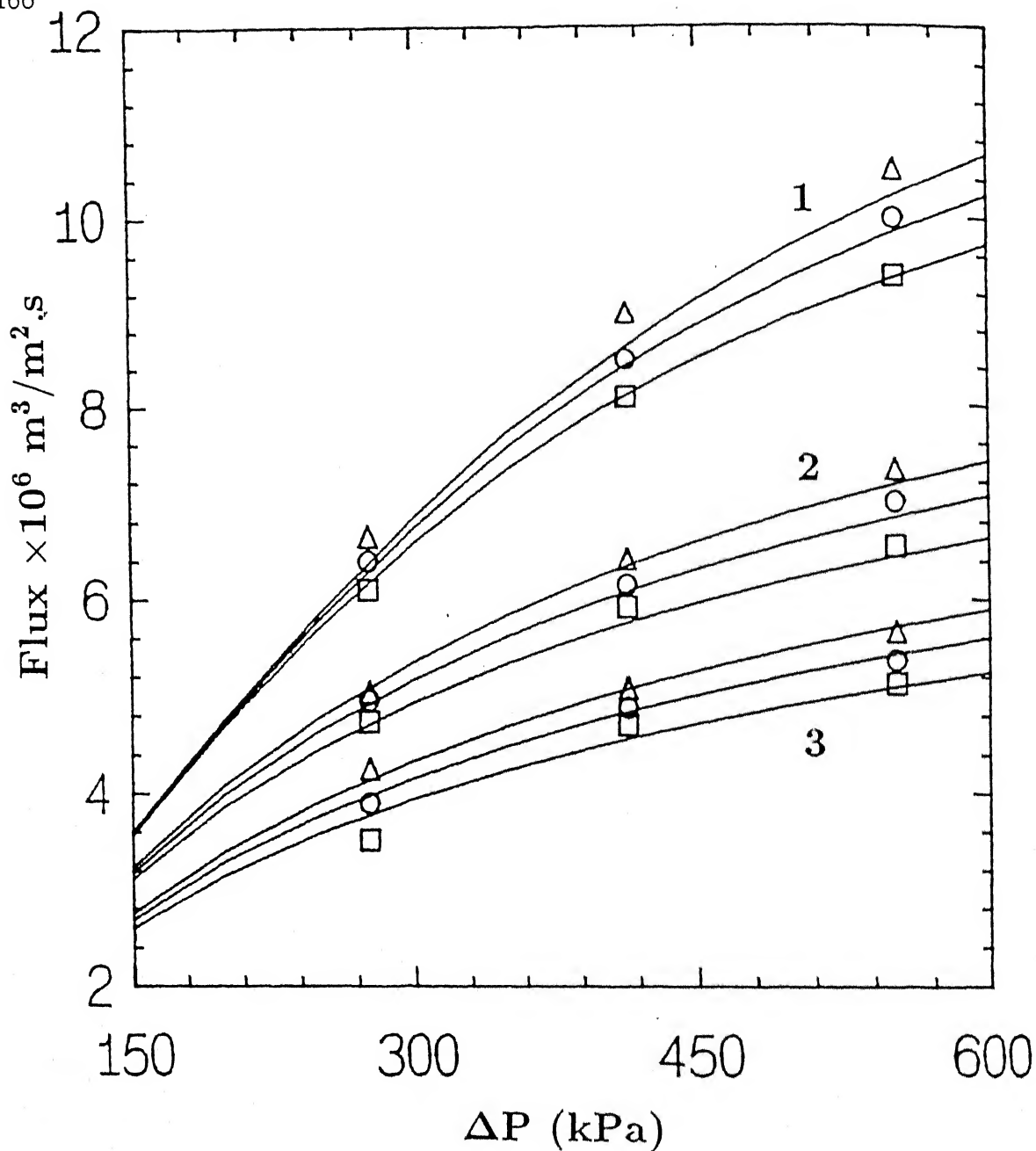


Figure 3.48: Variation of average permeate flux with ΔP during UF of dextran (T-20) in a cross flow cell. The curves represent the predictions using GIM and symbols represent the experimental fluxes. 1: $c_0 = 10 \text{ kg/m}^3$; 2: $c_0 = 30 \text{ kg/m}^3$; 3: $c_0 = 50 \text{ kg/m}^3$. For each set, the three curves from top to bottom correspond to the cross flow velocities 0.46, 0.38, 0.31 m/s, respectively. Δ — $u_0 = 0.46 \text{ m/s}$; \circ — $u_0 = 0.38 \text{ m/s}$; \square — $u_0 = 0.31 \text{ m/s}$.

what follows, the prediction of GIM with experimental fluxes and estimation of the diffusivity variation with concentration based on cross flow UF flux data is performed.

The linear dependence of the diffusivity on concentration, given by Eq.(3.114) with K as an unknown was used in GIM and the entire model was used to fit K on the basis of experimental runs (with all possible combinations of the operating conditions) in cross flow UF. Least square minimization resulted in the estimation of K which was found to be $1.0 \times 10^{-3} \text{ m}^3/\text{kg}$. The average permeate flux predicted by the GIM using this value of K are compared with the experimental V_p for cross flow UF of Dextran T-20 in Fig. (3.48), which plots the variation of the average permeate flux against the operating pressure at different feed concentrations and cross flow velocities. The maximum deviation between the experimental flux and the model result is about 10%. This establishes that the variation of D with concentration is indeed quite small as was also shown by Wijmans *et al.* [154], and may not be as significant as shown by Lebrun *et al.* [255].

3.4.5 Conclusions

The general integral method (GIM) presented in this work, can predict the flux decline and rejection behaviour simultaneously in a UF process with a proper choice of concentration profile. Apart from being less computation intensive, it gives as accurate predictions as detailed numerical solution. For low polarization UF, GIM is more accurate compared to other simplified solution schemes in a cross flow UF system. Whereas, at high polarization other simplified schemes also become competitive, especially for longer channel length. In unstirred batch cell, all the simplified models are equally good because membrane surface concentration reaches a constant value within a short period of time.

GIM is also capable to incorporate the variation of diffusivity with solute concentration. Being less computation intensive, GIM may be useful to estimate several parameters (R_r , diffusivity, R_{osm} , etc.) involved in a UF process.

Chapter 4

Estimation of Mass Transfer Coefficient with Suction

In the earlier chapter, prediction of flux decline and retention characteristics during UF in different flow configurations and under influence of various flux reducing factors were investigated. These prediction methods were based on the detailed solution of the mass, momentum and continuity balance equations in the boundary layer. Usefulness of detailed mathematical treatments for prediction of flux and retention was observed to be quite inadequate for industrial purposes due to their inherent complications. Simple film theory is still widely accepted as a design equation for continuous filtration processes. Limitations of standard film theory, based on the mass transfer coefficient, which is estimated from heat and mass transfer analogies will be evident in the subsequent sections. Effect of suction (by the porous membrane) on mass transfer coefficient is one of the most important aspects where the standard correlations are unable to achieve the results. The present chapter is fully devoted to quantify the effects of suction on mass transfer coefficients in different flow regimes and different flow configurations. First section of this chapter deals with development of Sherwood number relations to estimate the mass transfer coefficient for laminar flow regime. Performance of the developed relations in terms of prediction of permeate flux is also explored. Further, a semi-empirical route is adopted to develop correlations for mass transfer coefficients in turbulent flow

regime in different configurations. This method is looked into detail in the second section of this chapter.

4.1 Theoretical estimation of mass transfer coefficient for laminar flow

In this section, the Sherwood number relations for laminar flow regime in different flow configurations, (rectangular cross flow system, tubular and radial modules) are derived starting from first principles.

4.1.1 Introduction

Design of pressure driven membrane separation processes like reverse osmosis (RO) and ultrafiltration (UF) are generally based on the mass transfer coefficient (k) for the relevant flow configurations and flow regimes. The mass transfer coefficients used for such purposes are usually derived from the correlations obtained from heat – mass transfer analogies. The major drawbacks for the use of such Sherwood number correlations with regard to RO/UF are: (a) they are derived for flow through a non-porous conduit; hence, the effect of suction cannot be considered; (b) changes in properties like viscosity and density due to concentration polarization near the membrane surface can not be taken into consideration; (c) it is tacitly assumed that the concentration boundary layer is fully developed over most of the channel length which may not be the case for RO/UF; (d) the osmotic pressure build up near the membrane surface cannot be considered in such approaches; and, finally, (e) the mass transfer coefficient is assumed to be independent of pressure which may not be valid for RO/UF operations.

Therefore the use of standard correlations lead to an inaccurate estimation of the mass transfer coefficient and hence incorrect prediction of permeate flux. One way to avoid this is to perform a detailed simulation solving relevant momentum and solute mass balance equations with pertinent boundary conditions [108, 112, 113,

243]. But such methods may not be very attractive from a designer's point of view owing to their extensive computational effort and complications.

The mass transfer correlations for membrane separation processes have been reviewed in detail [26, 27]. It was concluded in both of the reviews that the present correlations need to be modified in light of their limitations discussed earlier. In fact it was suggested that mass transfer correlations should be developed based on experimental techniques namely, the velocity variation technique or osmotic pressure model [26, 27]. Each technique has its own disadvantages which have been discussed in detail previously [26, 27].

Another alternative method which has been quite successfully employed in our earlier work [217–220] on UF, includes the development of a second correlation for concentration polarization in terms of polarized layer resistance along with a standard mass transfer correlation like the Leveque correlation for laminar flow in a channel or Colton's correlation in a stirred cell [243]. But such approaches are solute and system specific. In addition it is difficult to work with two correlations simultaneously.

The role of suction in mass transfer through porous membranes is very important. It has been identified earlier [26, 27] that the effect of suction on mass transfer coefficient is two fold. Firstly, it enhances the mass transfer from the surface to the bulk; and, secondly, it stabilizes the laminar flow condition in the conduit by delaying the laminar to turbulent transition (typically, critical Reynolds number is shifted from 2100 to 4000 in the presence of suction [26]).

Therefore it seemed to be possible that a generalized mass transfer relation may be obtained theoretically for laminar flow from first principles. The present work aims to develop a generalized mass transfer relation including the effects of suction over a developing concentration boundary layer. Such relations can be coupled with the osmotic pressure model to predict permeate flux for osmotic pressure governed UF and also for RO. Further, the theoretical work is extended to include all

the flow modules usually encountered in membrane separation processes, namely, rectangular channel, tubular and radial cross flow configurations.

4.1.2 Theory

In this section an attempt has been made to develop a generalized mass transfer coefficient relation from the basic approach of solving simultaneously the governing solute mass and momentum balance equations along with the boundary conditions.

The flow configuration in a closed conduit is shown in Fig. (3.1). Fig. (4.1) depicts the flow geometry of a radial cross flow cell. The fluid is allowed to flow tangentially over the membrane surface. The upper boundary of the channel is impervious for the rectangular and radial cells. The permeate flux is a function of the channel length for the rectangular and tubular modules and for a radial module it is function of radius of the cell. The concentration boundary layer is developing over the effective length of the membrane.

Assumptions made in this model are: (a) the flow is steady; (b) diffusion along the membrane is negligible compared to convection in the same direction; (c) flow is laminar and fully developed; (d) permeate velocity is small enough compared to the feed velocity, keeping the parabolic velocity profile in the channel undistorted for rectangular and tubular modules; (e) concentration at the membrane surface is constant; and, (f) physical properties of the solution are constant.

With the above assumptions, the solute mass balance equation over a differential element in the conduit gives,

$$V \nabla c = \nabla (D \nabla c) \quad (4.1)$$

where, the velocity vector V is the resultant of the axial velocity, u , and the transverse velocity component, v . Under the assumption of no permanent (irreversible) adsorption of the solute on the membrane surface, which may be possible with an efficient cross flow system and a non-adsorbing membrane, the expression for nor-

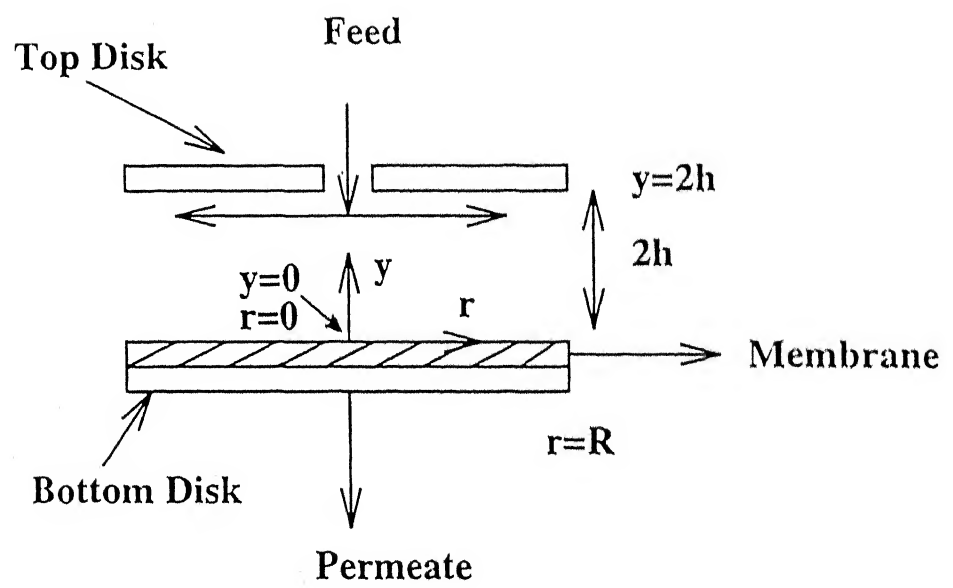


Figure 4.1: Schematic of the flow configuration in a radial cross flow cell

mal velocity component v can be approximated within the concentration boundary layer as given by Eq. (3.4).

The initial conditions of Eq.(4.1) for rectangular and tubular modules, may be expressed as,

$$c = c_0 \text{ at } x = 0 \quad (4.2)$$

and, for the radial cross flow cell

$$c = c_0 \text{ at } r = 0 \quad (4.3)$$

The assumption of constant solute concentration at the membrane surface results in the boundary condition as given by Eq.(3.5). Solute mass balance at the membrane surface results, the following boundary condition as,

$$v_p c_m R_r + D \frac{\partial c}{\partial y} = 0 \text{ at } y = 0 \quad (4.4)$$

where, R_r is the intrinsic rejection of the solute by the membrane which may be assumed to be constant for a membrane-solute system [112, 239].

Finally, in the bulk, solute concentration is constant beyond the concentration boundary layer and hence boundary condition expressed by Eq. (3.7) can be used.

From this point onwards, estimation of the mass transfer coefficient for different flow modules is presented separately.

4.1.2.1 Flow through a rectangular cell

The solute mass balance equation for flow through a rectangular channel under the assumptions stated earlier may be written in the form as given by Eq. (3.1).

A similarity solution for Eq. (3.1) is obtained by defining a dimensionless variable (lumped parameter) (η), as given by Eq. (3.8). Dimensionless concentration (c^*) can be expressed by Eq. (3.9). In terms of c^* and η , Eq.(3.1) becomes an ordinary differential equation of second order as expressed by Eq. (3.10). The axial velocity

profile within the boundary layer may be taken as, Eq. (3.3). For constant physical properties and channel geometry, $v_p x^{\frac{1}{3}} = \text{constant}$. Thus, a non-dimensional form of this can be defined as,

$$v_p \left[\frac{hx}{u_0 D^2} \right]^{\frac{1}{3}} = A_1 \quad (4.5)$$

Therefore, Eq.(3.10) becomes,

$$\frac{d^2 c^*}{d\eta^2} = -(\eta^2 + A_1) \frac{dc^*}{d\eta} \quad (4.6)$$

and the transformed boundary conditions become,

$$c^* = 1 \text{ at } \eta = \infty \quad (4.7)$$

$$\frac{dc^*}{d\eta} + A_1 R_r c^* = 0 \text{ at } \eta = 0 \quad (4.8)$$

The solution of Eq.(4.6) along with the boundary conditions Eqs.(4.7 and 4.8) can be written as,

$$c^*(\eta) = K_1 \int_0^\eta \exp\left(-\frac{\eta^3}{3} - A_1 \eta\right) d\eta + K_2 \quad (4.9)$$

where,

$$K_1 = -\frac{A_1 R_r}{1 - A_1 R_r I_1} \quad (4.10)$$

$$K_2 = \frac{1}{1 - A_1 R_r I_1} \quad (4.11)$$

and,

$$I_1 = \int_0^\infty \exp\left(-\frac{\eta^3}{3} - A_1 \eta\right) d\eta \quad (4.12)$$

Average flux over the membrane length can be obtained from Eq.(4.5) as,

$$V_p = \frac{1}{L} \int_0^L v_p(x) dx = 1.5 \left(\frac{u_0 D^2}{hL} \right)^{\frac{1}{3}} A_1 \quad (4.13)$$

Now, for a rectangular channel the equivalent hydraulic diameter can be defined by,

$$d_e = 4h \quad (4.14)$$

Therefore, A_1 can be expressed from Eqs.(4.13 and 4.14) in terms of $Pe_w = \frac{V_p d_e}{D}$ as,

$$A_1 = 0.42 \lambda_1 \quad (4.15)$$

where, $\lambda_1 = Pe_w / (ReScd_e/L)^{1/3}$, $Re = \rho u_0 d_e / \mu$ and $Sc = \mu / (\rho D)$. Hence, the integral I_1 given by Eq.(4.12) can be rewritten as,

$$I_1 = \int_0^\infty \exp \left[-\frac{\eta^3}{3} - 0.42\lambda_1\eta \right] d\eta \quad (4.16)$$

Now, the mass transfer coefficient, k , is defined and obtained from a solute mass balance at the membrane surface as,

$$k(c_m - c_0) = -D \left(\frac{dc}{dy} \right)_{y=0} \quad (4.17)$$

In terms of non-dimensional forms of c and y , the above equation can be represented by,

$$k(c_m^* - 1) = -D \left(\frac{u_0}{hxD} \right)^{1/3} \left(\frac{dc^*}{d\eta} \right)_{\eta=0} \quad (4.18)$$

Substituting values of c_m^* and $\frac{dc^*}{d\eta}$ at $\eta = 0$ from Eq.(4.9), we have,

$$k(K_2 - 1) = -D \left(\frac{u_0}{hxD} \right)^{1/3} K_1 \quad (4.19)$$

or,

$$k(x) = \frac{1}{I_1} \left(\frac{u_0 D^2}{hx} \right)^{1/3} \quad (4.20)$$

Expressing the mass transfer coefficient, k , in terms of the Sherwood number (kd_e/D) as a function of dimensionless channel length, $x^*(x/L)$, we can write,

$$Sh(x^*) = \frac{4^{1/3}}{I_1} (ReScd_e/L)^{1/3} x^{*-1/3} \quad (4.21)$$

and the average Sherwood number over length L can be expressed as,

$$\begin{aligned} \overline{Sh} &= \int_0^1 Sh(x^*) dx^* \\ &= 2.381 \frac{(ReScd_e/L)^{1/3}}{I_1} \end{aligned} \quad (4.22)$$

where I_1 is given by Eq.(4.16).

4.1.2.2 Flow through a tubular module

For steady flow through a tubular module under the previously mentioned assumptions, the solute mass balance equation can be written as,

$$u \frac{\partial c}{\partial x} - v_p \frac{\partial c}{\partial r} = \frac{D}{r} \frac{\partial}{\partial r} \left(r \frac{\partial c}{\partial r} \right) \quad (4.23)$$

Considering a thin concentration boundary layer adjacent to the wall, the curvature effects may be neglected and the problem may be treated as though the wall were flat. If the distance from the wall may be denoted as $y = R - r$; the fluid may be regarded as being confined between a flat mass transfer surface extending from $y = 0$ to $y = \infty$. Therefore the solute mass balance equation (Eq.(4.23)) can again be expressed by Eq.(3.1).

The fully developed velocity profile in a tube can be described by,

$$u = 2u_0 \left[1 - \left(\frac{r}{R} \right)^2 \right] \quad (4.24)$$

In the concentration boundary layer near the wall, the above expression for the velocity profile may be expressed as,

$$u = 2u_0 \left[1 - \left(\frac{R - y}{R} \right)^2 \right] \quad (4.25)$$

Neglecting higher order terms (y^2/R^2) for the thin concentration boundary layer, the axial velocity profile may be approximated as,

$$u = 4u_0 \frac{y}{R} \quad (4.26)$$

The similarity parameter chosen in this case is,

$$\phi = y \left(\frac{u_0}{x D d} \right)^{1/3} \quad (4.27)$$

In terms c^* and ϕ the solute mass balance equation (Eq.(4.23)) can be expressed in the following form,

$$\frac{d^2 c^*}{d\phi^2} = - \left(\frac{8}{3} \phi^2 + A_2 \phi \right) \frac{dc^*}{d\eta} \quad (4.28)$$

where,

$$A_2 = v_p \left(\frac{xD}{u_0 d^2} \right)^{1/3} \quad (4.29)$$

Average flux over the length of the module can be defined by Eq.(4.13). Expressing average flux in terms of $Pe_w(V_p d/D)$, A_2 can be written as,

$$A_2 = \frac{2}{3} \lambda_2 \quad (4.30)$$

where, $\lambda_2 = Pe_w / (ReScd/L)^{1/3}$. The initial and boundary conditions in terms of c^* and ϕ remain the same as Eqs.(4.2), (3.5), (4.4) and (3.7)). The solution of Eq.(4.28) with the boundary conditions provides the concentration profile in the tubular module,

$$c^*(\phi) = K_3 \int_0^\phi \exp\left(-\frac{8\phi^3}{9} - A_2\phi\right) d\phi + K_4 \quad (4.31)$$

where,

$$K_3 = -\frac{A_2 R_r}{1 - A_2 R_r I_2} \quad (4.32)$$

$$K_4 = \frac{1}{1 - A_2 R_r I_2} \quad (4.33)$$

and,

$$I_2 = \int_0^\infty \exp\left(-\frac{8\phi^3}{9} - \frac{2}{3}\lambda_2\phi\right) d\phi \quad (4.34)$$

Proceeding exactly as in the case of rectangular channel, the Sherwood number profile as a function of the module length can be obtained from,

$$Sh(x^*) = \frac{1}{I_2} (ReScd/L)^{1/3} x^{*-1/3} \quad (4.35)$$

and average Sherwood number over the module length can be expressed as,

$$\overline{Sh} = \frac{1.5}{I_2} (ReScd/L)^{1/3} \quad (4.36)$$

4.1.2.3 Flow through a radial cross flow cell

The geometry in a radial cross flow cell is best represented in an axisymmetric cylindrical coordinate system, where, r is the radial and y is the transverse direction (Fig. 4.1). However, for convenience, we assume a two dimensional cartesian coordinate system, where the radial direction r is not a radial coordinate but a cartesian axis. Such simplifications make the model equations simpler and do not alter the results to any significant extent. Therefore, the steady state solute mass balance equation within the concentration boundary layer can be written in the following form,

$$u \frac{\partial c}{\partial r} - v_p \frac{\partial c}{\partial y} = D \frac{\partial^2 c}{\partial y^2} \quad (4.37)$$

The radial velocity profile within the boundary layer, can be expressed [4] as,

$$u(r, y) = \frac{3Qy}{4\pi r h^2} \quad (4.38)$$

where, Q is the average volumetric flow rate given by $Q = 4\pi R h u_0$ and u_0 is the average velocity in the conduit.

The similarity parameter in this case may be chosen as,

$$\xi = y \left(\frac{Q}{\pi D h^2 r^2} \right)^{1/3} \quad (4.39)$$

In terms of c^* and ξ Eq.(4.37) can be written in the following form,

$$\frac{d^2 c^*}{d\xi^2} = - \left(\frac{\xi^2}{2} + A_3 \xi \right) \frac{dc^*}{d\xi} \quad (4.40)$$

Where,

$$A_3 = \frac{v_p}{D} \left(\frac{\pi h^2 D}{Q} \right)^{1/3} r^{2/3} \quad (4.41)$$

Average flux over the membrane radius can be defined as,

$$V_p = \frac{2}{R^2} \int_0^R v_p(r) r dr \quad (4.42)$$

Expressing average flux in terms of $Pe_w(V_p h/D)$, A_3 can be written as,

$$A_3 = 0.42 \lambda_3 \quad (4.43)$$

where, $\lambda_3 = Pe_w / (ReSch/R)^{1/3}$, $Re = \rho u_0 h / \mu$ and $Sc = \mu / (\rho D)$. The boundary conditions in terms of c^* and ξ remain the same as Eqs. (4.3), (3.5), (4.4) and (3.7)). The solution of Eq. (4.40) results in the following concentration profile,

$$c^*(\xi) = K_5 \int_0^\xi \exp\left(-\frac{\xi^3}{6} - A_3 \xi\right) d\xi + K_6 \quad (4.44)$$

where,

$$K_5 = -\frac{A_3 R_r}{1 - A_3 R_r I_3} \quad (4.45)$$

$$K_6 = \frac{1}{1 - A_3 R_r I_3} \quad (4.46)$$

and,

$$I_3 = \int_0^\infty \exp\left(-\frac{\xi^3}{6} - 0.42\lambda_3 \xi\right) d\xi \quad (4.47)$$

Proceeding exactly as in the case of rectangular channel, the Sherwood number profile as a function of channel radius can be obtained as,

$$Sh(r^*) = \frac{4^{1/3}}{I_3} (ReSch/R)^{1/3} r^{*-2/3} \quad (4.48)$$

and average Sherwood number over the channel radius can be expressed by,

$$\overline{Sh} = \frac{2.381}{I_3} (ReSch/R)^{1/3} \quad (4.49)$$

In the next section, the integrals I_1 to I_3 are examined for different domains of suction (Pe_w).

Case 1: No Suction; $Pe_w = 0$

For the rectangular cross flow cell, the integral I_1 takes the following form when there is no suction,

$$\begin{aligned} I_1 &= \int_0^\infty \exp\left(-\frac{\eta^3}{3}\right) d\eta \\ &= 3^{-2/3} \Gamma(1/3) \\ &= 1.2879 \end{aligned} \quad (4.50)$$

The corresponding expression for \overline{Sh} is,

$$\overline{Sh} = 1.85 (ReScd_e/L)^{1/3} \quad (4.51)$$

which is identical to the Leveque solution [5,6] for heat transfer in a non-porous channel.

Similarly, for a tubular module, the average Sherwood number may be obtained from Eq.(4.36), for $Pe_w = 0$,

$$\overline{Sh} = 1.62 (ReScd/L)^{1/3} \quad (4.52)$$

This expression for average Sherwood number is again identical to the Leveque solution [238] for heat transfer in a non-porous tube.

For a radial cross flow cell, the average Sherwood number may be obtained from Eq.(4.49) as,

$$\overline{Sh} = 1.47 (ReSch/R)^{1/3} \quad (4.53)$$

Case 2: RO/UF System

For a typical RO/UF system, $\lambda_{1,2,3}$ vary from very low values up to 10. The behaviour of the integrals $1/I_{1,2,3}$ in this range of $\lambda_{1,2,3}$ dictates the dependence of average Sherwood number on suction (i.e. Pe_w). To visualize the variation of $1/I_{1,2,3}$ (given by Eqs. (4.16), (4.34), (4.47)) for this range, $1/I_{1,2,3}$ is evaluated for $\lambda_{1,2,3}$ varying from 0 to 10 by numerical integration and is presented in Fig. (4.2). In Fig. (4.2) the symbols represent the numerically integrated values and the lines represent the best fit data. From this figure, it may be observed that the variation of $1/I_{1,2,3}$ with $\lambda_{1,2,3}$ is not linear. In all the cases, the correlation coefficients are more than 0.9999. Therefore the average Sherwood numbers for different flow geometries can be represented by the following equations,

rectangular cross flow cell:

$$\overline{Sh} = 1.85(ReScd_e/L)^{1/3} [1.0 + 0.32\lambda_1 + 0.02\lambda_1^2 - 8.05 \times 10^{-4}\lambda_1^3] \quad (4.54)$$

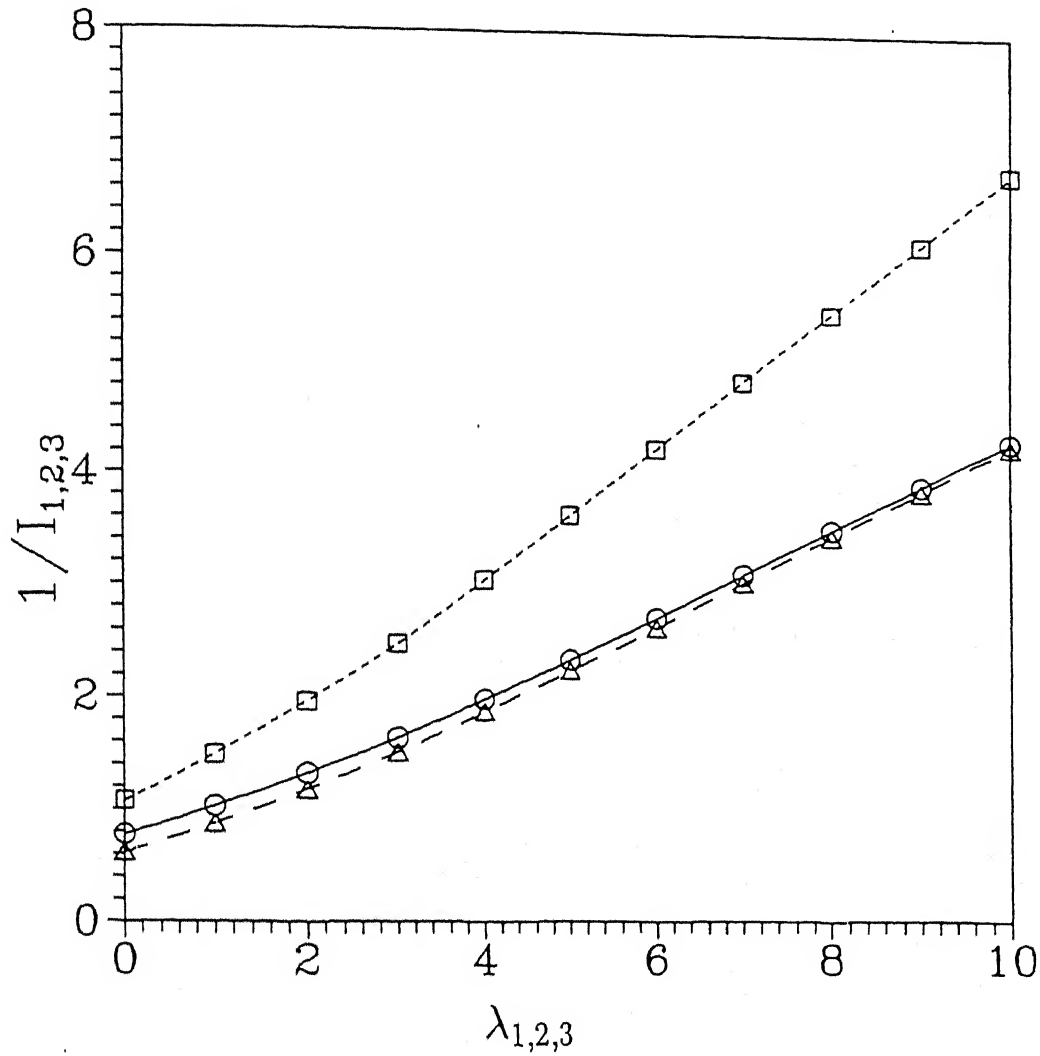


Figure 4.2: Variation of $1/I_{1,2,3}$ with $\lambda_{1,2,3}$. Solid line is for rectangular cell (Eq. (4.54)), dotted line is for tubular module (Eq. (4.55)) and long dashed line is for radial cross flow cell (Eq.(4.56)). Symbols represent the numerically integrated values, obtained from Eq.(4.16) (circle), Eq.(4.34) (box) and Eq.(4.47) (triangle)

tubular module:

$$\overline{Sh} = 1.62(ReScd/L)^{1/3} [1.0 + 0.37\lambda_2 + 0.03\lambda_2^2 - 1.05 \times 10^{-3}\lambda_2^3] \quad (4.55)$$

radial cross flow cell:

$$\overline{Sh} = 1.467(ReSch/R)^{1/3} [1.0 + 0.41\lambda_3 + 0.03\lambda_3^2 - 1.25 \times 10^{-3}\lambda_3^3] \quad (4.56)$$

4.1.2.4 Application of Sherwood number relations in RO and UF for prediction of flux:

In an osmotic pressure controlled membrane separation process, permeate flux can simply be expressed by the phenomenological equation, Eq. (3.20). Osmotic pressure of the solution can be expressed as a function of solute concentration as,

$$\pi = \alpha_1 c + \alpha_2 c^2 + \alpha_3 c^3 \quad (4.57)$$

In terms of Pe_w , Eq.(3.20) may be written as,

$$Pe_w = B_1(1.0 - \Delta\pi/\Delta P) \quad (4.58)$$

where, $B_1 = L_p \Delta P d_e / D$; it may be noted that for a tubular and radial cross flow module, d_e in the relation of B_1 should be replaced by d and h , respectively.

Now, the average solvent flux through the membrane is given as,

$$V_p(c_m - c_p) = -D \left(\frac{\partial c}{\partial y} \right)_{y=0} \quad (4.59)$$

In terms of average Sherwood number and non-dimensional flux (Pe_w), from Eq.(4.17) and Eq.(4.59), one can obtain,

$$Pe_w = \frac{\overline{Sh}}{R_r} (1 - c_0/c_m) \quad (4.60)$$

The expressions of \overline{Sh} for different flow configurations are presented in Eqs. ((4.54), (4.55), (4.56)). Therefore, a simultaneous solution of Eqs.(3.20), (4.58) and (4.60),

provides the predicted value of Pe_w and hence, permeate flux. However, it may be noted here that apart from the operating conditions (ΔP , u_0 , c_0), the characteristic retention for solute-membrane system (R_r) is required to predict the permeate flux. Generally, this characteristic retention parameter is obtained from a separate set of experiments.

4.1.3 Results and Discussions

In this section, several implications of the Sherwood number relations developed are examined. The typical value of the group ($ReScd_e/L$) for the rectangular cell (or ($ReScd/L$) for the tubular and ($ReSch/R$) for radial cross flow cell) varies from 10^3 to 10^6 in membrane separation processes. Corresponding permeate fluxes, in terms of the suction parameter (Pe_w) can be in the range 1 to 500. Sherwood number profiles along the channel length for a rectangular cell for different operating conditions are shown in Fig. (4.3). Similar profiles for tubular and radial modules are depicted in Figs. (4.4) and (4.5), respectively. Such profiles were generated from Eq.(4.21), Eq.(4.35) and Eq.(4.48), where the integrals I_1 , I_2 and I_3 were evaluated numerically. In these figures, the suction parameter Pe_w varies from 0 to 300; solid lines are for $ReScd_e/L$ (or $ReScd/L$ or $ReSch/R$) $=10^3$ and dashed lines are for $ReScd_e/L$ (or $ReScd/L$ or $ReSch/R$) $=10^5$. It can be observed from the figures that Sherwood number decreases sharply near the entrance and then gradually for the rest of the conduit. Local Sherwood number increases with an increase in suction (as Pe_w increases). This leads to increased mass transfer from the surface to the bulk and coincides with the qualitative description of the effects of suction on mass transfer coefficient by Gekas and Hallstrom [27]. At the higher ($ReScd_e/L$), the Sherwood number is larger for the same suction. For the same solute and system geometry, an increase in Re increases forced convection and, consequently, the growth of the concentration boundary layer is minimized and so that the Sherwood number increases.

Now for the description of a realistic mass transfer operation in a conduit, it is con-

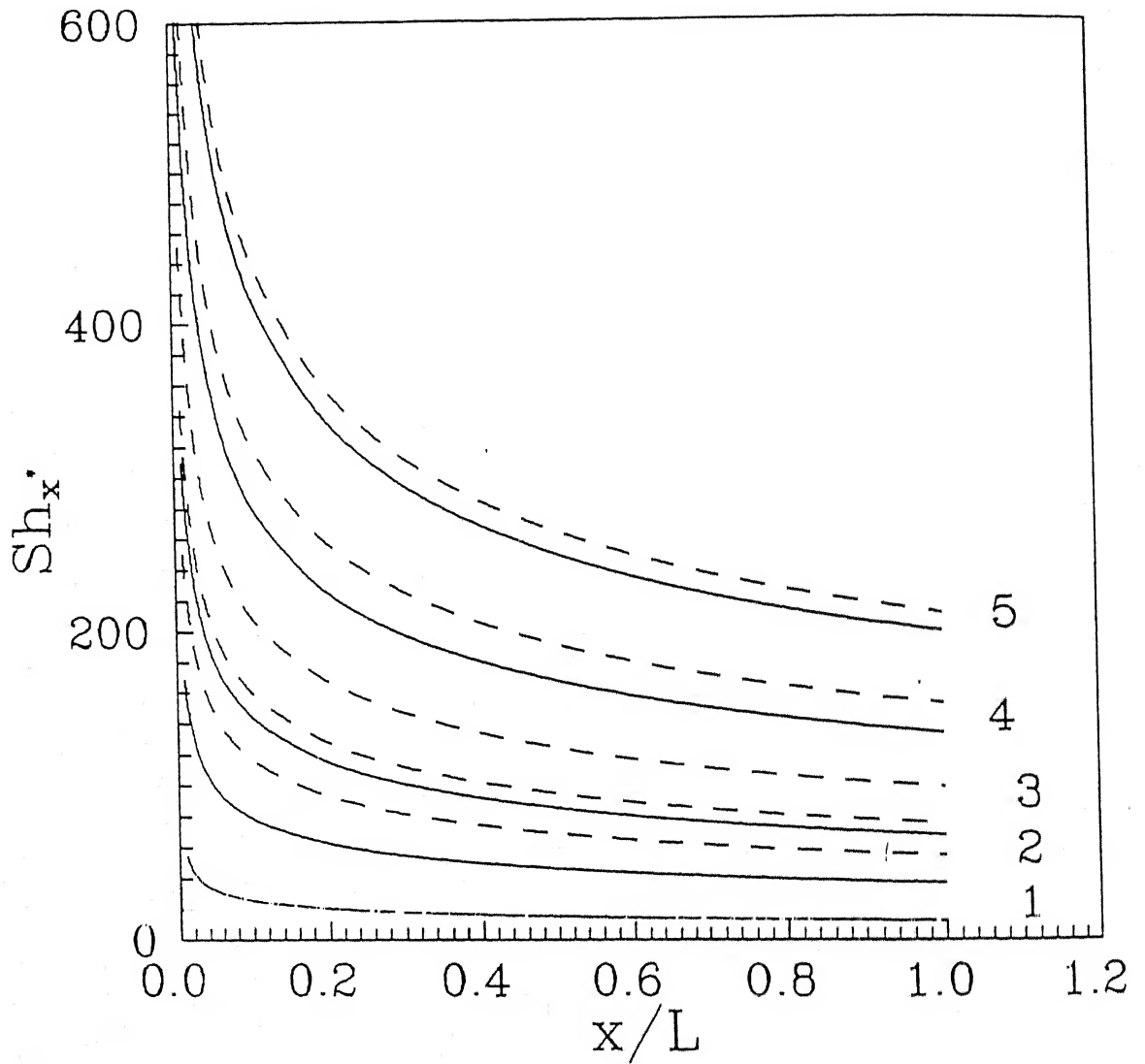


Figure 4.3: Variation of local Sherwood number along the channel length for different values of suction, for a rectangular cross flow cell. 1: $Pe_w = 0$; 2: $Pe_w = 50$; 3: $Pe_w = 100$; 4: $Pe_w = 200$; 5: $Pe_w = 300$. Solid lines are for $ReScd_e/L = 10^3$ and dashed lines are for $ReScd_e/L = 10^5$

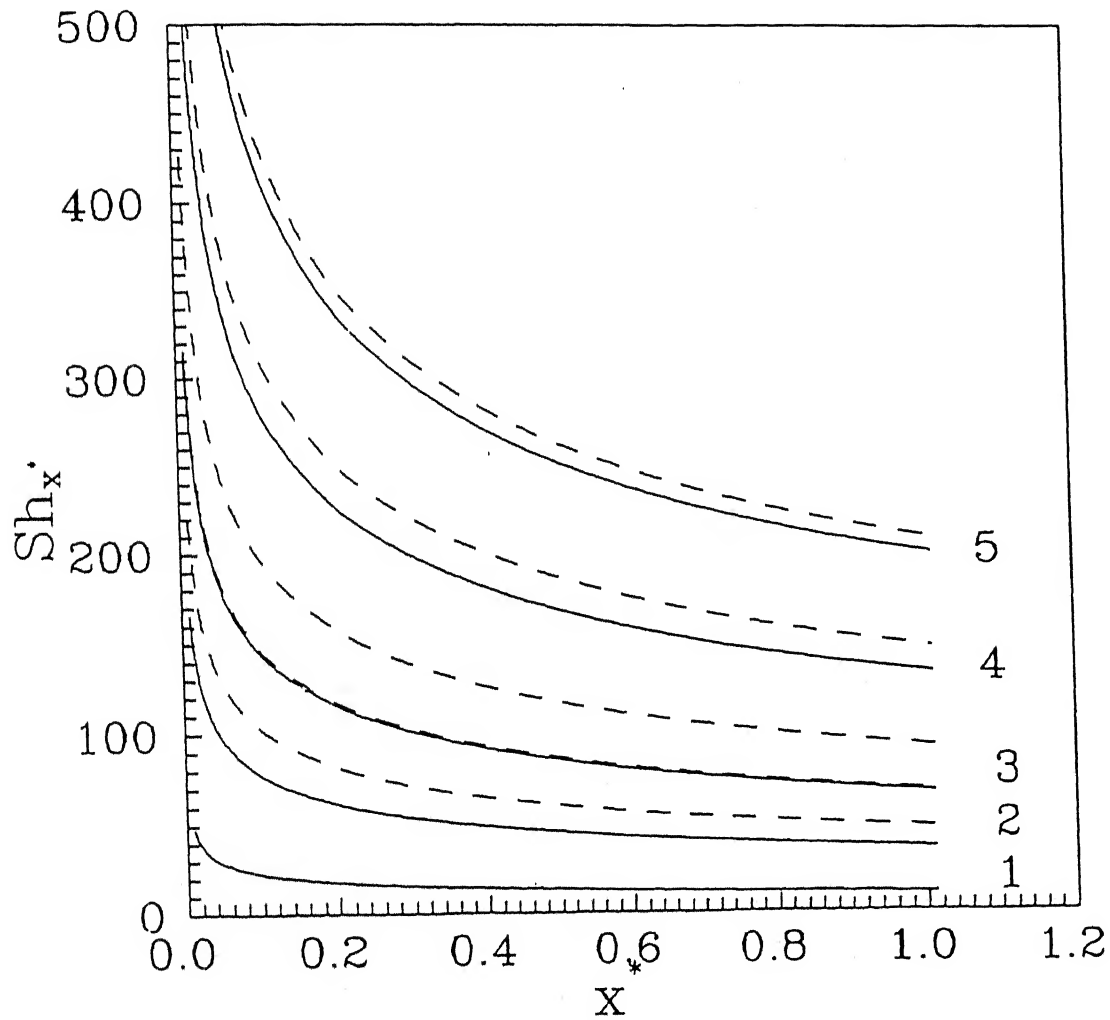


Figure 4.4: Variation of local Sherwood number along the module length for different values of suction, for a tubular module. 1: $Pe_w = 0$; 2: $Pe_w = 50$; 3: $Pe_w = 100$; 4: $Pe_w = 200$; 5: $Pe_w = 300$. Solid lines are for $ReScd/L = 10^3$ and dashed lines are for $ReScd/L = 10^5$

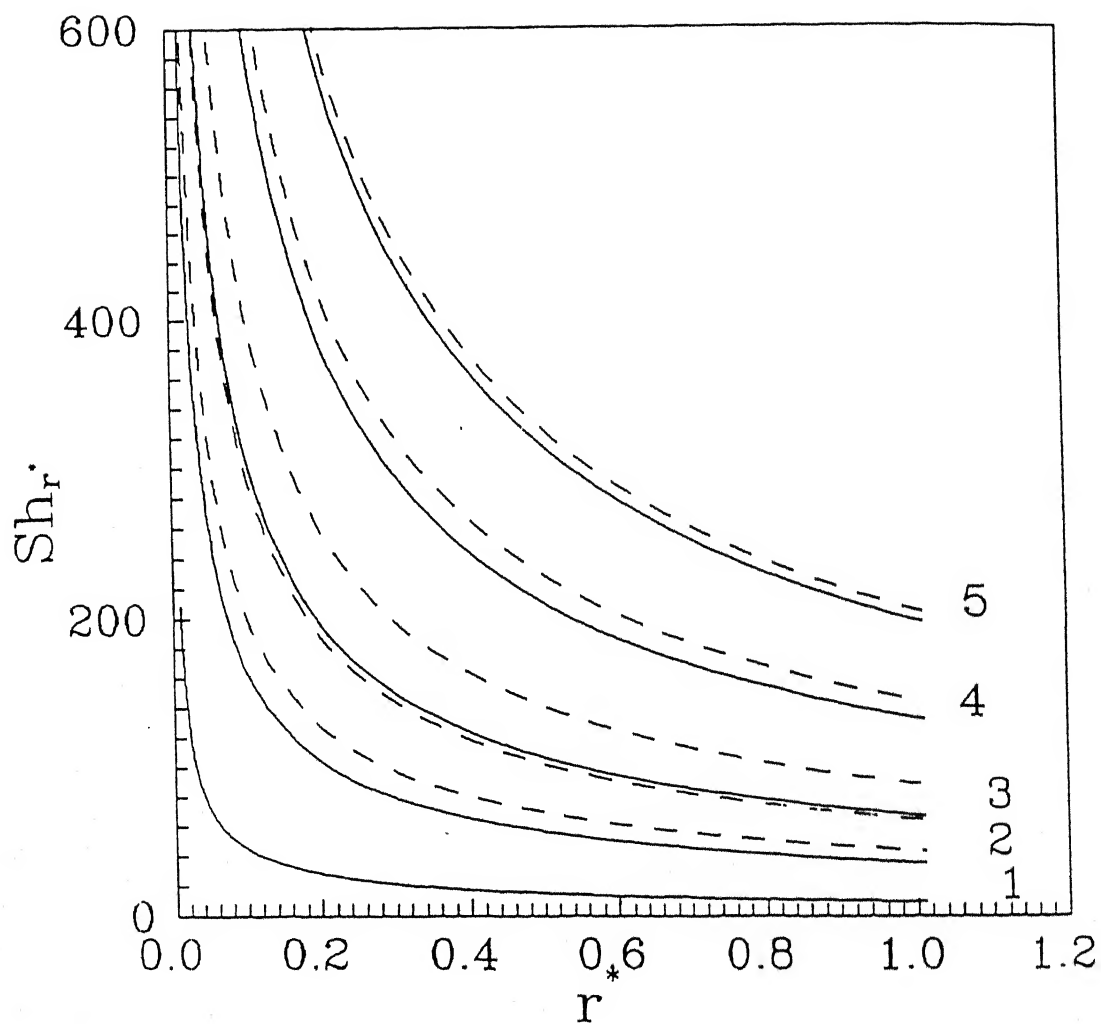


Figure 4.5: Variation of local Sherwood number along the channel radius for different values of suction, for a radial cross flow cell. 1: $Pe_w = 0$; 2: $Pe_w = 50$; 3: $Pe_w = 100$; 4: $Pe_w = 200$; 5: $Pe_w = 300$. Solid lines are for $ReSch/R = 10^3$ and dashed lines are for $ReSch/R = 10^5$

venient to work with an average mass transfer coefficient and an average Sherwood number relationship. The effects of suction on the average Sherwood number as estimated from Eqs.(4.54), (4.55) and (4.56) can be compared to the average Sherwood number with no suction (the standard Leveque equation Eqs.((4.51), (4.52) and (4.53)) for the different operating conditions and flow geometries. The ratio of \overline{Sh} with suction to that without suction versus Pe_w for different values of $ReScd_e/L$ for a rectangular cell is plotted in Fig. (4.6). For a realistic UF system, $ReScd_e/L$ is of the order of 10^5 to 10^6 . When $ReScd_e/L$ is 10^5 , a Pe_w of the order of 500 results in about a 6 fold increase in the average Sherwood number compared to that given by Leveque equation where the enhancement factor is about 3 for $ReScd_e/L = 10^6$. The effects of suction on the average Sherwood number for a tubular module is presented in Fig. (4.7). In this case, the effects of suction are even greater. When $ReScd/L = 10^5$, the enhancement factor is approximately 7 while for $ReScd/L = 10^6$ it is about 3.5 for $Pe_w = 500$. The ratio of Sherwood number with and without suction for a radial cross flow cell is presented in Fig. (4.8). From the figure, it can be observed that the enhancement ratio is 7.7 for $ReSch/R = 10^5$ and 3.8 for $ReSch/R = 10^6$ for $Pe_w = 500$. Hence, the effect of suction on Sherwood number increases for rectangular, tubular and radial modules. Therefore, it can be concluded that there exists a significant effect of suction on Sherwood number and hence, on mass transfer.

The proposed Sherwood number relations can also be used to predict the permeate flux in RO and UF. For RO in a rectangular channel, Eq.(4.54) mass transfer coefficient along with Eq.(4.60) for the osmotic pressure and Eq.(4.58) were solved iteratively using the Newton–Raphson technique. The experimental data of Merten et al. [266] were used for this purpose and the simulations were carried out for different channel dimensions (L/d_e). The predicted change in Pe_w with Re is shown in Fig. (4.9). The figure indicates very close agreement between the predicted and experimental Pe_w (experimental data correspond to $L/d_e = 16.56$). Interestingly, the agreement is excellent up to $Re = 2620$. It was expected that laminar to turbulence transition

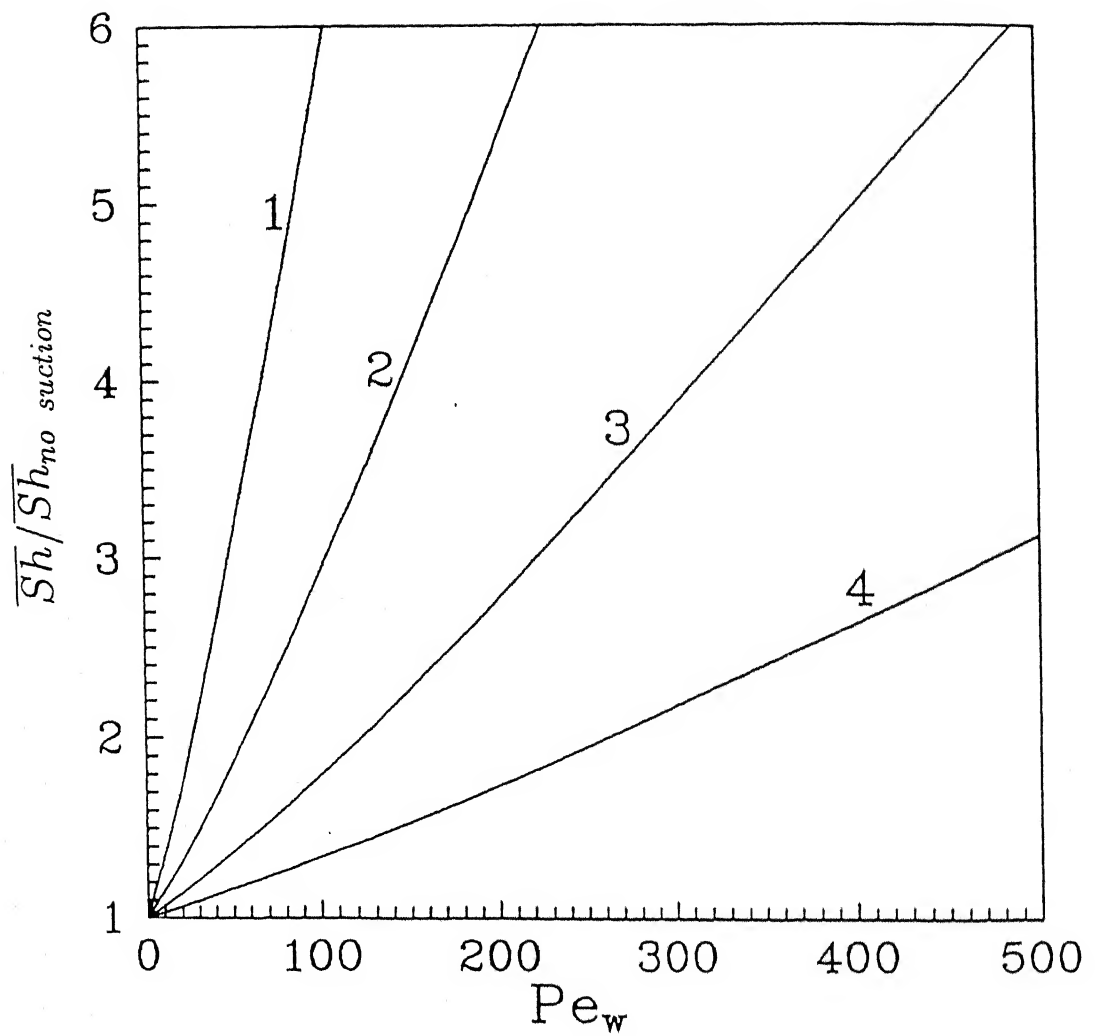


Figure 4.6: Variation of $\overline{Sh}/\overline{Sh}_{no\ suction}$ with Pe_w for different $ReScd_e/L$ in a rectangular cell. 1: $ReScd_e/L = 10^3$; 2: $ReScd_e/L = 10^4$; 3: $ReScd_e/L = 10^5$; 4: $ReScd_e/L = 10^6$

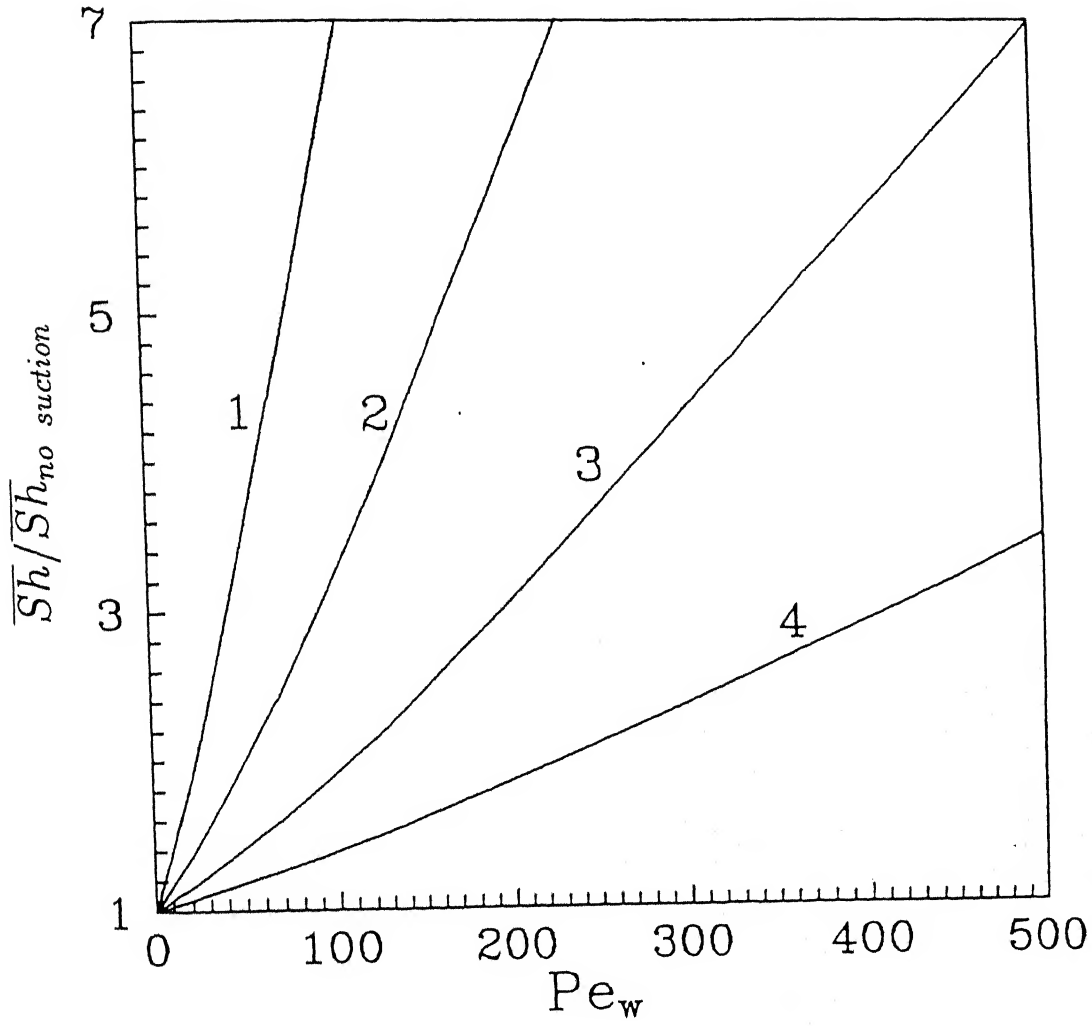


Figure 4.7: Variation of $\overline{Sh}/\overline{Sh}_{no\ suction}$ with Pe_w for different $ReScd_e/L$ in a tubular module. 1: $ReScd/L = 10^3$; 2: $ReScd/L = 10^4$; 3: $ReScd/L = 10^5$; 4: $ReScd/L = 10^6$.

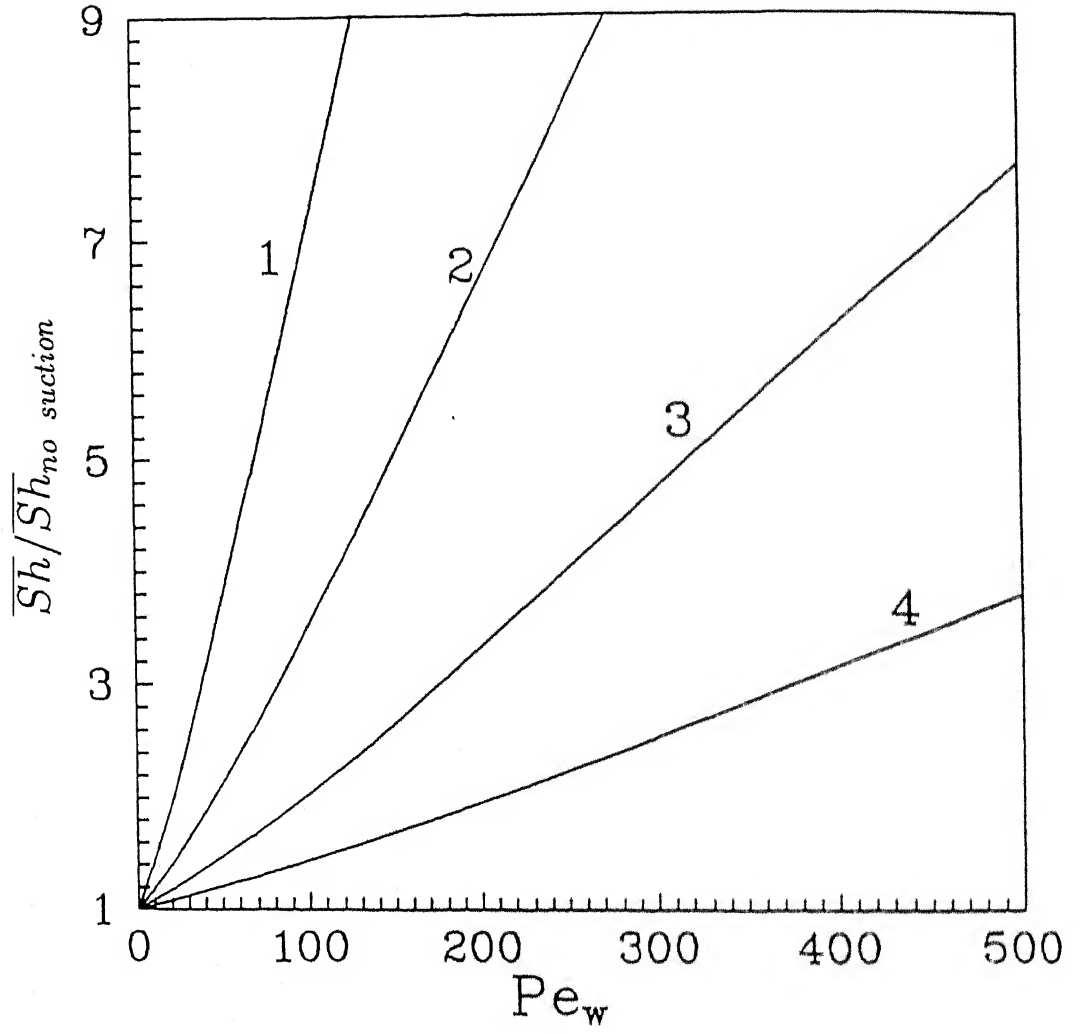


Figure 4.8: Variation of $\overline{Sh}/\overline{Sh}_{no\ suction}$ with Pe_w for different $ReSch/R$ in a radial cross flow cell. 1: $ReSch/R = 10^3$; 2: $ReSch/R = 10^4$; 3: $ReSch/R = 10^5$; 4: $ReSch/R = 10^6$.

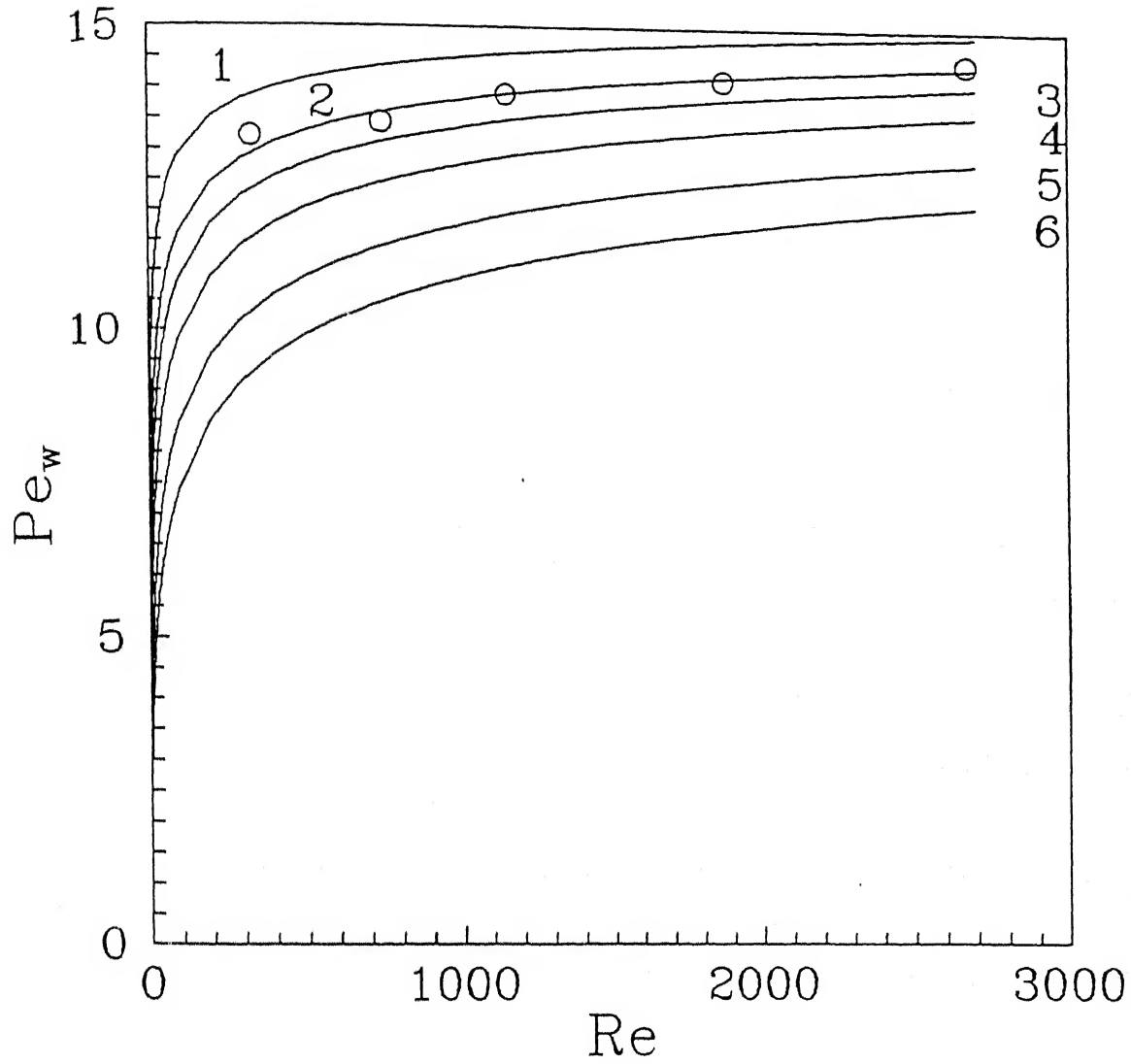


Figure 4.9: Variation of dimensionless flux (Pe_w) with Re for RO system. Solid lines are predicted flux and symbols are the experimental data of Merten et al. [266]. 1: $L/d_e = 5.0$; 2: $L/d_e = 16.56$; 3: $L/d_e = 30.0$; 4: $L/d_e = 60.0$; 5: $L/d_e = 150.0$; 6: $L/d_e = 300.0$.

would occur in the range 2000–2200. But, suction has stabilized the boundary layer leading to a delay in the onset of turbulent flow [27].

The prediction of flux in UF was carried out for dextran and PEG solutions in the rectangular cross flow cell. The mass transfer coefficient in this case was evaluated using Eq.(4.54). This equation along with the osmotic pressure model Eq.(4.58) and Eq.(4.60) was solved as described earlier to obtain the permeate flux. The experimental data of our earlier work (section 3.1) are considered for comparison with the predicted values. Intrinsic retention (R_r) for dextran was taken as 1.0 and that for PEG was 0.9. The experimental and predicted values of the permeate flux for dextran for all the operating conditions are shown in Fig. (4.10). The figure indicates an excellent matching of the two. For PEG at all the operating conditions, the predicted and experimental flux values are plotted in Fig. (4.11). The figure reveals a close agreement between the experimental and calculated flux values. The maximum deviation between the values is $\pm 10\%$.

The comparison of predicted and experimental permeate flux for ultrafiltration of PEG 6K in a radial cross flow cell was also carried out. In this case, the average mass transfer coefficient was evaluated from Eq.(4.56). As mentioned earlier, the osmotic pressure model Eq.(4.58), along with Eqs.(4.56) and (4.60) was solved iteratively. The experimental data for UF of PEG are obtained from Ganguly [267] for comparison with the predicted results. The value of R_r was taken as 0.88 [267]. The comparison between experimental and predicted permeate flux is presented in the non-dimensional (i.e. in terms of Pe_w) form in Fig. (4.12) for all the experimental conditions. Most of the predicted values lie within $\pm 10\%$ of the experimental data. Therefore, the Sherwood number relationships developed in this work for different flow geometries include the effects of suction and can be used for an accurate prediction of permeate flux in both cross flow RO and UF.

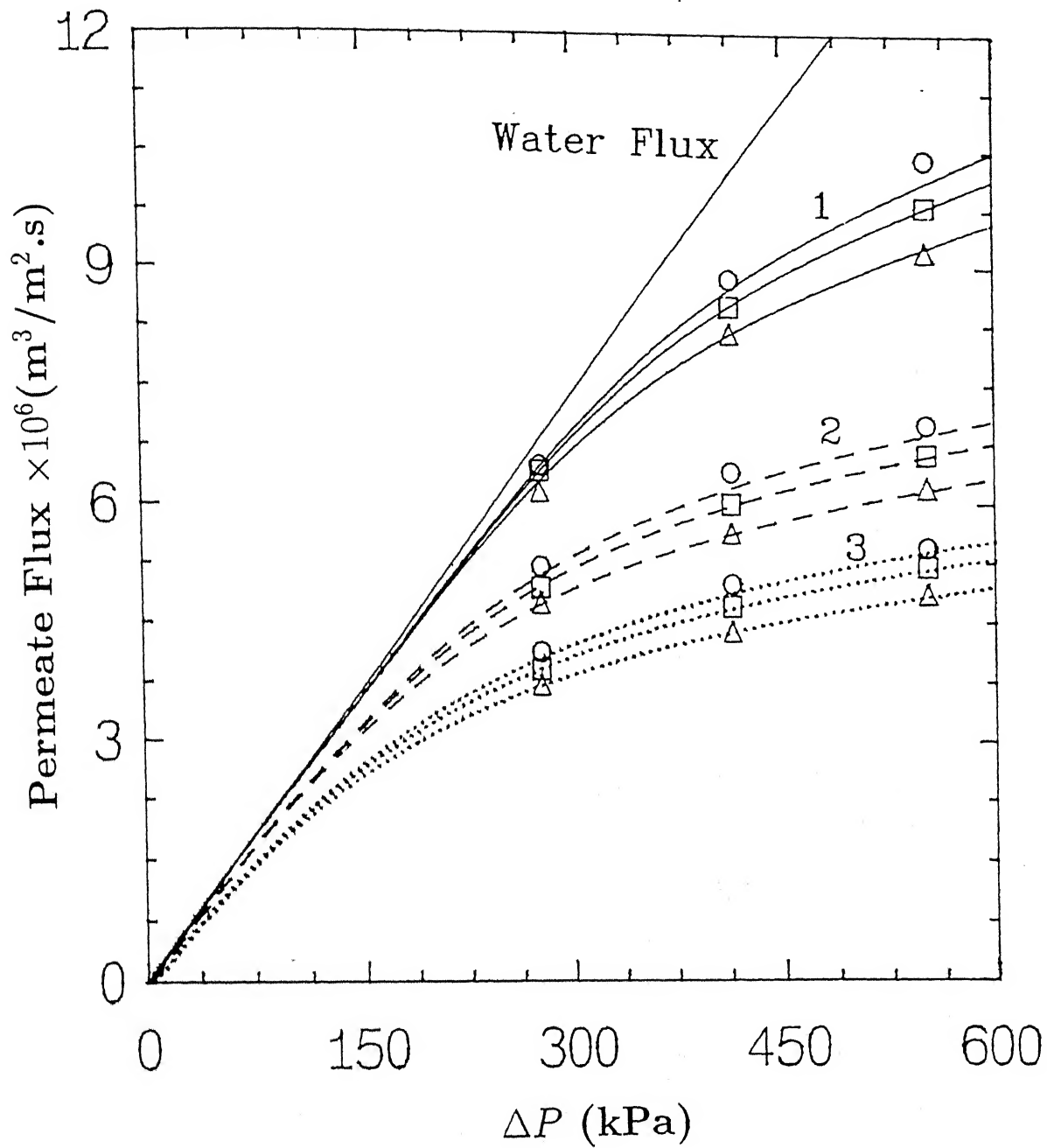


Figure 4.10: Variation of permeate flux with pressure for UF of dextran (T-20). 1: $c_0 = 10$ kg/m³; 2: $c_0 = 30$ kg/m³; 3: $c_0 = 50$ kg/m³. Symbols represent as, open circle, $u_0 = 0.44$ m/s; box, $u_0 = 0.38$ m/s and triangle, $u_0 = 0.30$ m/s. Curves are the predicted values of permeate flux.

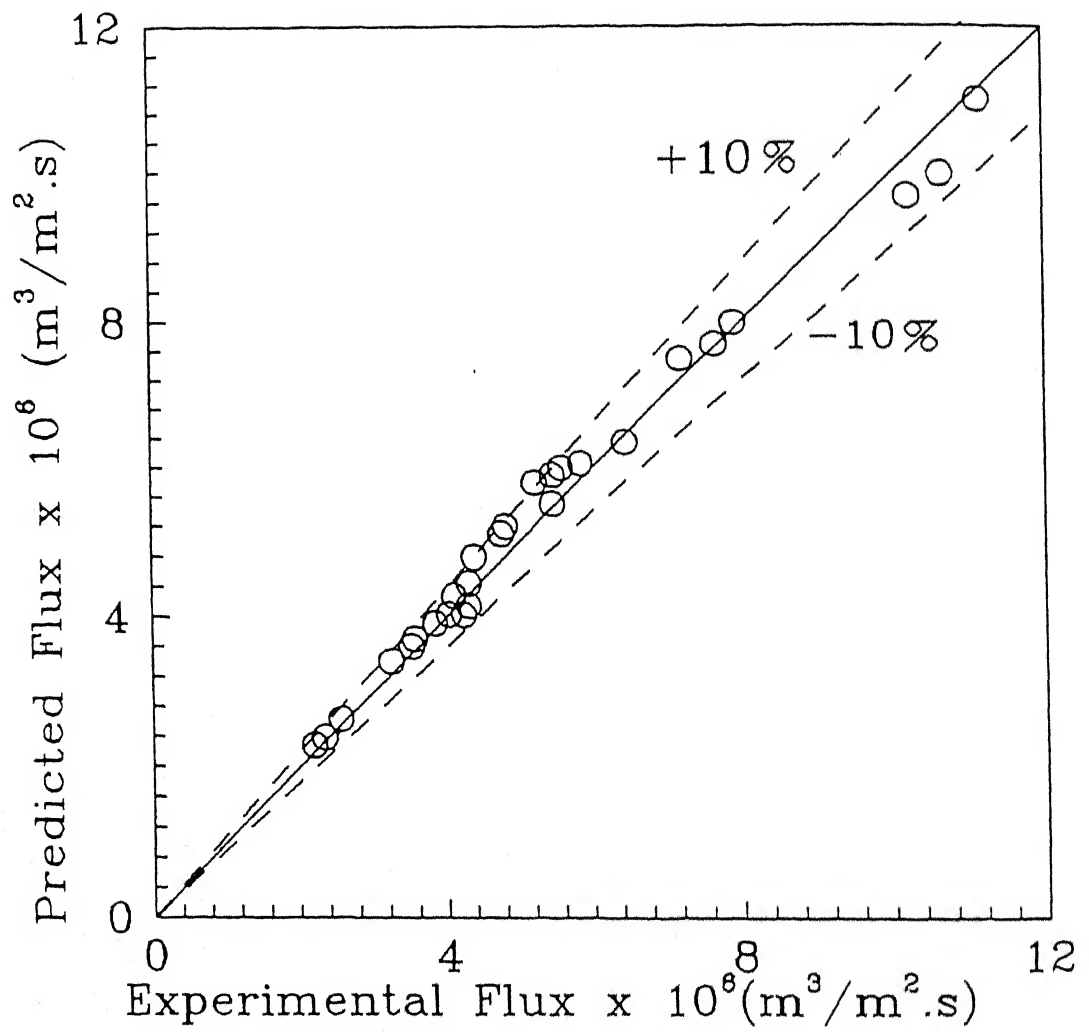


Figure 4.11: Fitting between predicted and experimental permeate flux for UF of PEG 6K in a rectangular channel. Dashed lines are for $\pm 10\%$ deviations.

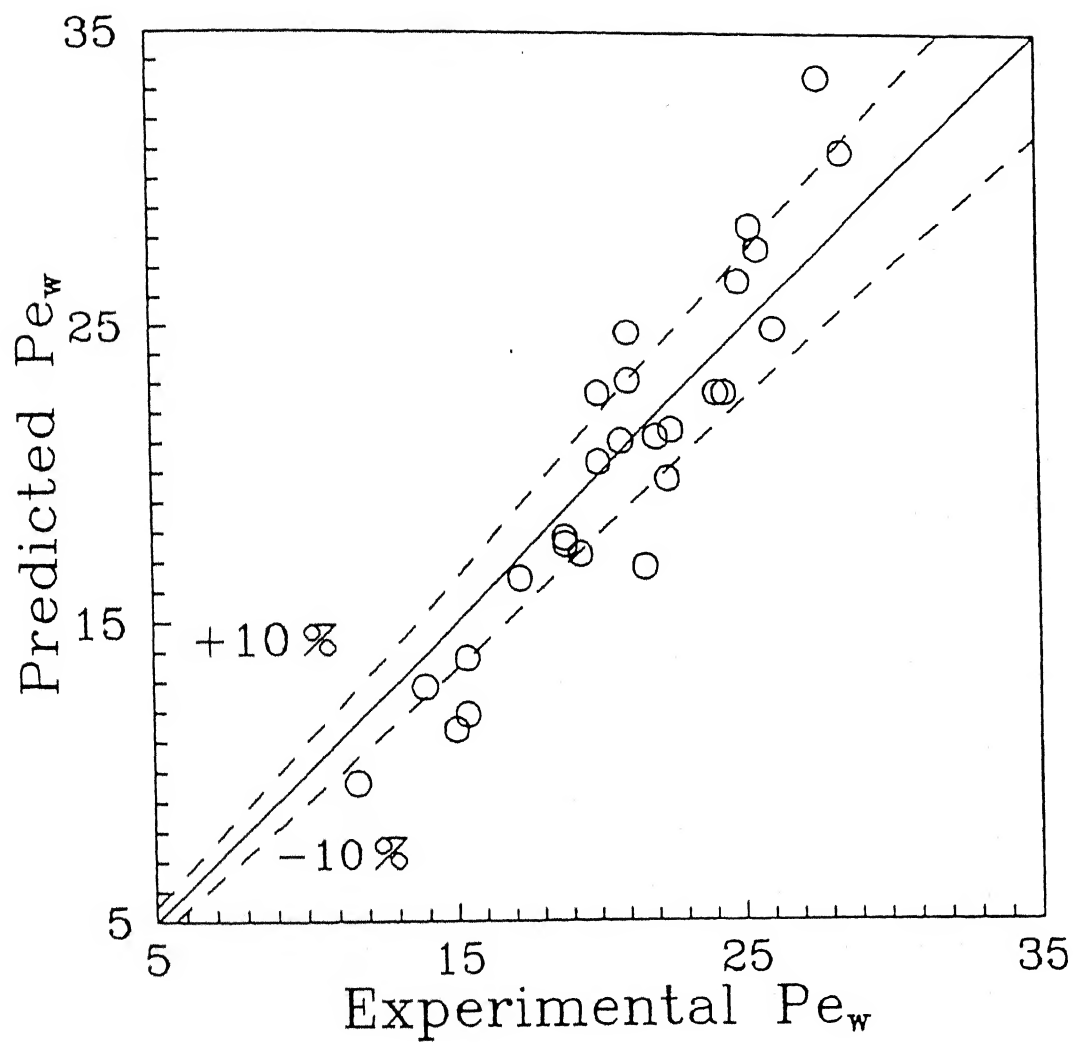


Figure 4.12: Fitting between predicted and experimental permeate flux for UF of PEG 6K in a radial cross flow cell. Dashed lines are for $\pm 10\%$ deviations.

4.1.4 Conclusions

General Sherwood number relations for cross flow RO and UF including the effects of suction for different flow geometries were obtained from first principles. Suction through the porous membrane had a significant effect on the mass transfer coefficient. The proposed Sherwood number relations were used to predict mass transfer coefficient and, in turn, the permeate flux for both RO and UF. The simple relations developed in this work to quantify the effects of suction on mass transfer coefficient should be of immense help to the process and design engineers.

4.2 Development of Correlations for Mass Transfer Coefficient in Ultrafiltration Systems

In the preceding section of this chapter, derivations of Sherwood number relations were carried out under laminar flow regime. This approach was not extended to turbulent flow regime due to the inadequacy as well as complications of the pertinent theories of turbulence. Therefore, in this section, correlations are developed for estimation of mass transfer coefficient via a semi-empirical route for different configurations and for turbulent as well as laminar flow regimes.

4.2.1 Introduction

Film theory is a classical and the most widely accepted theory for designing of ultrafiltrative system. This requires the accurate estimation of mass transfer coefficient. The limitations associated with the existing Sherwood number correlations which are derived from the heat and mass transfer analogies for flow through a non-porous conduit have been extensively discussed in the previous section. It also seems possible that a generalized mass transfer correlation for a UF system may be arrived at if the theoretical understanding of the polarization mechanism can be properly incorporated in the mass transfer correlation using appropriate dimensionless groups or numbers.

The present section aims at the development of such generalized mass transfer correlations and may be viewed as a modification of the existing Sherwood correlations for the non-porous channels or ducts which incorporates the effects of suction and concentration polarization.

4.2.2 Theory

The following general theoretical development pertains to three different UF modules; namely, the rectangular, radial cross flow and the stirred batch cell. Details about each type of module are presented elsewhere [113, 123, 243].

The phenomenological flux expression for the osmotic pressure controlled UF, including irreversible solute adsorption, is:

$$v_p = \frac{\Delta P - \Delta \pi}{\mu(R_m + R_a)} \quad (4.61)$$

where the osmotic pressure difference across the membrane, $\Delta \pi (= \pi_m - \pi_p)$, can be evaluated if the concentration dependence of the osmotic pressure is available. The resistance due to irreversible fouling (R_a), can be experimentally determined by the measurement of water flux before and after the experiment. A common form of expressing the concentration dependence of osmotic pressure in the case of macromolecular solutions is the virial expression, given by Eq. (4.57). The osmotic pressure dependence on solute concentration for a particular feed solution is characterized by the coefficients ' α_i ' which can be ascertained independently by means of experiments or by using appropriate theories [243].

The simplest solution of the steady-state 1-dimensional formulation is the classical film theory, expressed by Eq. (3.27), which considers the transport across a stagnant film of thickness δ . The usual approach for designing a UF process involves the simultaneous solution of Eqs. (4.61) and (3.27) to obtain the membrane surface concentration (c_m), and hence the permeate flux (v_p). This requires an accurate estimate of the mass transfer coefficient (k). It is a lumped parameter that includes the effects of all the deviations for flow through the membrane on the mass transport across the film, and is normally obtained using a correlation of the form:

$$Sh = a_0 Re^m Sc^n \quad (4.62)$$

where $Sh = kd_h/D$.

It is clearly evident that the correlations of the form given in Eq. (4.62) are only applicable for non-porous ducts, and do not include the effects of the wall suction and concentration polarization that should play an important role in governing the mass transfer behaviour in any UF system. Therefore, these correlations need generalization to be applicable for a UF system.

The differential solute mass balance in the steady-state 2-dimensional flow can be represented in each of these cells, using a Cartesian system, is given by Eq. (3.1). The non-dimensionalization of Eq. (3.1) using the dimensionless quantities $c^* = c/c_0$, $u^* = u/u_0$, $x^* = x/L$, $y^* = y/h$ and $Pe = v_p h/D$ results in the following governing equation containing the well known dimensionless numbers:

$$\left(Re Sc \frac{h}{L} \right) u^* \frac{\partial c^*}{\partial x^*} - Pe_{test} \frac{\partial c^*}{\partial y^*} = \frac{\partial^2 c^*}{\partial y^{*2}} \quad (4.63)$$

For laminar flow in a radial cross flow configuration, the dimensionless group $(Re Sc h/L)$ is replaced by $(Re Sc h/R)$. In the case of turbulent flow in a stirred cell, the pertinent non-dimensional groups are Re , Sc and $Pe(v_p R/D)$. These dimensionless groups play a very important role in governing the transport phenomena in a UF system.

Therefore, a suitable generalization of the existing form of the correlation will be to include another dimensionless term, Pe_{test} , that incorporates the effects of wall suction and concentration polarization. This can be done by using a correlation of the form:

$$Sh = a Re^{\beta_1} (Pe_{test})^{\beta_2} Sc^{\beta_3} \quad (4.64)$$

where Pe_{test} is a dimensionless group which accounts for the deviations from the non-porous system. In a membrane process, the dimensionless quantity Pe_{test} includes wall suction, changes in properties due to polarization, effect of pressure, changes in the properties of the membrane (it may be reversible fouling during the experiments), *etc.* Such correlations will be extremely useful in scaling up the UF operation to full plant size. If the effective filtration area of the full plant is known, the extent of concentration polarization in it can be estimated using the proposed correlation, and the flux decline data obtained from the experimental UF cell.

The general expressions developed so far are now used for correlating the flux behaviour using different flow configurations and solute-membrane pairs under various operating conditions. Experimental data developed in our laboratory, as well as those from literature for different flow geometries and for different solutes

over a wide range of operating conditions, have been fitted in a model described by Eq. (4.64) by the least-squares technique. A detailed statistical analysis was performed to test the adequacy of the model along with the estimate of the model parameters.

For fitting of the model based on the observations, two questions generally arise; first, whether all the terms are significant enough to be included in the model; second, how adequate the model is, or is there any systematic lack of fit [268]. The first question can be answered by computing the confidence limits or carrying out t -test on regression parameters. In t -test, we test the null hypothesis (H_0), i.e. the parameter β_k is equal to an expected value b_k (often 0), against an alternate hypothesis (H_1), i.e. the parameter β_k differs significantly from b_k . The relevant test statistic is:

$$t = \frac{\beta_k - b_k}{SE(\beta_k)} \quad (4.65)$$

If $|t_{obs}|$ is larger than $t_{\alpha/2}$ for the pertinent degrees of freedom, then the null hypothesis (H_0) is rejected. This implies that the effect of the parameter is significant and the relevant variable should be included in the model.

The confidence interval for β_k is bounded by the values that just produce a significant result at the desired probability level. Thus, $(1 - \alpha)$ confidence limits for β are given by $\beta_k \pm t_{\alpha/2} \times SE(\beta_k)$.

The second question regarding the adequacy of the model can be answered through analysis of variance (ANOVA) between the observed and modeled population. In this case, the null and alternate hypotheses are, respectively, $H_0 : \sigma_1^2 = \sigma_2^2$ and $H_1 : \sigma_1^2 \neq \sigma_2^2$. If $F_{obs} < F_{tab,\alpha}$ then, H_0 is accepted at α level of significance. This implies that the variance between the observed and fitted population may be equal, i.e., the model is adequate. Along with these statistical tests the correlation coefficients between the model and observed data were also computed.

4.2.3 Experimental Data

In our laboratory, experiments were performed with three types of UF devices, namely, the cross-flow rectangular channel, radial flow, and stirred batch cell (see

[113, 123, 242]). Experiments on the cross flow systems were performed for the laminar flow regime, while the stirred cell experiments were carried out under turbulent flow conditions. In all devices, a continuous mode of operation was maintained by recycling the permeate and retentate to the feed chamber in order to keep the feed concentration constant. Crossflow rates were measured by rotameters, while the permeate rate was obtained by measuring the volume permeated against time. Experimental data [9, 115, 122] were also used to develop the correlations. The characteristic features of the experiments are given in Table 4.1.

Experimental permeate fluxes (v_p) and permeate concentrations (c_p) were used to determine the mass transfer coefficient from the phenomenological and the film theory expressions (Eqs. (4.61) and (4.64), respectively). In addition, computations for the velocity variation method were also performed using the experimental data.

4.2.4 Results and Discussion

4.2.4.1 Experimental determination of mass transfer coefficient

(a) Osmotic pressure method

The mass transfer coefficient is determined experimentally from UF experiments in different flow geometries and regimes using Eqs. (4.61) and (4.64). The physical properties of the macromolecular solutions required for this purpose are the density, viscosity, diffusivity, and the osmotic pressure. Correlations for density and viscosity variations with solute concentration for PEG 6K, BL and PVP 10K were developed in our laboratory and are available elsewhere [123, 242]. The density and viscosity of dextran and BSA solutions are obtained from [144]. Diffusivity of the solutes are obtained from various sources [19, 27, 115]. The osmotic pressure dependence on solute concentration were obtained as virial expansions of solute concentration. For PEG and BL, the osmotic pressure was determined using Flory's equation [123], while experimental correlations were used for dextran, BSA and PVP [19, 115, 238].

Table 4.1: The characteristic features of the experimental data.

Ref.	Cell geometry, flow condition & dimension (cm)	Membrane	Solute	Pressure, (kPa)
[9]	Rectangular cross flow; Laminar 48×7.62×.38	UM10 (Amicon)	BSA(69K)	70-275
[122]	Rectangular cross flow; Laminar 10×4×0.1	930 (DDS)	Dextran (T-20)	500-2000
[115]	Rectangular cross flow; Turbulent 10×6×0.59	Polysulfone	Dextran (T-70)	200-600
[219]	Stirred cell; Turbulent 6.2(dia)	Spectra Por Type C(5K)	PEG(6K)	275-690
[220]	Stirred cell; Turbulent 6.2(dia)	Spectra por Type C(5K)	PEG(6K), BL	550-830
This work	Rectangular cross flow; Laminar 32×6×0.15	Permionics (1K)	PEG(6K), Dextran(T-20),BL	275-550
[242]	Stirred cell; Turbulent 6.2(dia)	Permionics (1K)	PVP(10K)	550-830
[113]	Radial cross flow; Laminar 6.0(dia) ×0.30	Spectra por Type C(5K)	PEG(6K)	550-830

Table 4.2: Hydraulic resistances for different membranes.

Reference	Type of membrane	R_m (m ⁻¹)
[9]	UM 10 (AMICON)	1.38×10^{13}
[122]	930 (DDS)	6.12×10^{13}
This work, [242]	Permionics (1K)	4.06×10^{13}
[115]	Polysulfone	6.94×10^{12}
[27, 219, 219]	Spectra por C (5K)	1.78×10^{13}

Different types of membranes were used in the UF experiments, all of which exhibited high solute rejection. The hydraulic resistance (R_m) of these membranes are listed in Table 4.2.

Using the given permeability and osmotic pressure data for a particular solute, the membrane surface concentration (c_m) is first estimated from Eqs. (4.61) and (4.57). Substitution of c_m and the experimental v_p in Eq. (4.64) gives the experimental mass transfer coefficient (k_{exp}).

The osmotic pressure model [26] is solute and UF system specific. In addition, the approach has other inherent assumptions like those of constant solution properties (diffusivity, density, viscosity, etc.) in the polarized layer, which may lead to erroneous estimation of the mass transfer coefficient. Nevertheless, it is perhaps the only method that accounts for the role of the osmotic pressure in governing the mass transfer during UF and RO processes explicitly.

(b) Velocity variation technique

The mass transfer coefficient is also determined experimentally using this technique for the different flow geometries. One problem associated with the implementation of this technique seems to be the poor reproducibility of the data and the relatively large number of data points required for obtaining statistically significant estimates of the mass transfer coefficient.

Table 4.3: Mass transfer coefficients for PEG 6K in a stirred cell under turbulent flow condition using different techniques.

ΔP (kPa)	c_0 (kg/m ³)	ω (rad/s)	k_{exp} $\times 10^6$ (m/s)	k_{corr} $\times 10^6$ (m/s)	k_{vv} $\times 10^6$ (m/s)	k_C $\times 10^6$ (m/s)
827	70	55.50	11.95	11.4	6.21	18.7
		47.12	9.82	9.50	5.45	16.6
		34.03	8.22	7.56	4.20	12.6

The mass transfer coefficient is determined by this technique using the following relationship:

$$\ln \frac{1 - R_0}{R_0} = \frac{v_p}{k} + \ln \frac{1 - R_r}{R_r} \quad (4.66)$$

where $k \propto u^{n_1}$. In this case, n_1 is a prefixed exponent, obtained from the standard correlations corresponding to the flow geometry and regime. From the slope of the plot of $[\ln(1 - R_0)/R_0]$ versus $[v_p/u^{n_1}]$, the mass transfer coefficient is obtained. Some sample results using the velocity variation method are presented in Table 4.3. Also shown in Table 4.3 are the corresponding mass transfer coefficients determined using the osmotic pressure method. It is seen that irrespective of operating conditions and flow regimes used, the velocity variation yields lower values of k compared to the osmotic pressure method. We based the development of the mass transfer correlation using the data obtained from the osmotic pressure method. This is primarily because of several inherent drawbacks of the velocity variation method, which are: (i) requirement of a large number of data points in order to get reliable predictions; (ii) incapability of showing the variation of k with pressure; (iii) inapplicability for perfectly rejecting membranes; (iv) the experimental errors involved in the measurement of the flux and observed rejection.

In addition to the above limitations, the velocity variation technique totally de-

depends on the exponent value of Reynolds number, obtained from conventional correlation. It also seems incongruous that in several earlier applications, the so called 'best fit' lines are not really the best fits obtainable from regression analyses. These straight line fits were biased by the requirement that all such lines should have the same slope [26]. The uncertainties involved in this technique have also been discussed in detail earlier [26].

4.2.4.2 Development of the mass transfer correlations based on the standard solutes

Incorporating the dimensionless number Pe_{test} , the resulting Sherwood number correlation is developed from the experimental observations of the steady-state permeate flux for the laminar and turbulent flow regimes. The development of the correlation for each of these regimes is described below.

Laminar flow: Rectangular cross flow system

The correlation for the laminar flow regime ($Re < 2000$) for the case of cross-flow UF in a rectangular channel using the solutes described in Table 4.1 are carried out using the least-squares technique. The model which qualifies all the statistical tests (mentioned earlier) is selected. The resultant correlation is in the form:

$$Sh = a(Re Sc \frac{h}{L})^{\beta_1} (Pe_{test})^{\beta_2} \quad (4.67)$$

where h is the half channel height; L is the length of the channel. The values of the constants with the statistical analyses are presented in Table 4.4. In Fig. (4.13), Pe_{test} has been plotted against $[Sh_{exp}/(Re Sc h/L)^{\beta_1}]$. This shows that there is a significant effect of Pe_{test} on the experimental Sherwood number. The high correlation coefficient (0.99) indicates that the correlation fits very well with the experimental data.

Radial cross flow system

In the case of a radial flow cell, the correlation was tested for the UF of PEG solutions. In this case, the characteristic cell dimension is represented by the radius

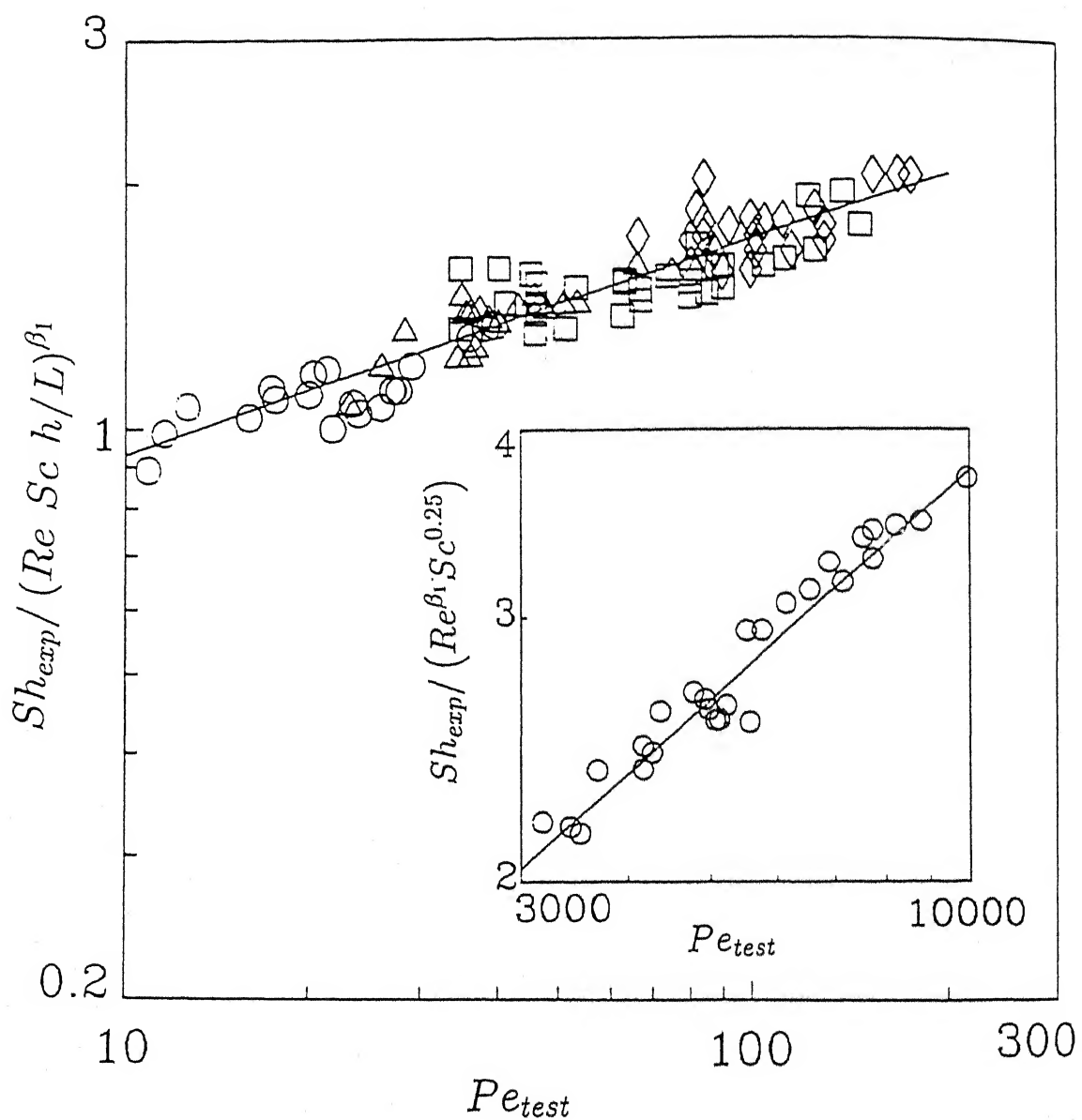


Figure 4.13: Variation of Sh_{exp} with Pe_{test} under laminar and turbulent (inset) flow domain in a rectangular channel. \circ PEG 6K (this work); \square Dextran T20 [122]; \triangle Dextran T20; \diamond BSA [9]; \circ dextran T70 [115] (inset); Solid lines are Eq. (4.67) and Eq. (4.69) (inset).

of the cell (R) instead of L . The resultant correlation has the same form as Eq. (4.67). In this case, it has been observed that the coefficient β_2 does not satisfy the t test (the effect of the group Pe_{test} is insignificant). Consequently, the Sh correlation in this case takes the following form:

$$Sh = a(Re Sc \frac{h}{R})^{\beta_1} \quad (4.68)$$

The estimates of the parameters and the corresponding statistical analyses are given in Table 4.4.

Turbulent flow: Rectangular cross flow system

The correlation for the turbulent regime in a rectangular cross flow geometry is developed using experimental data presented elsewhere [115]. The Reynolds number is defined based on the hydraulic diameter of the cell. The basic form of the correlation is given as:

$$Sh = aRe^{\beta_1} Pe_{test}^{\beta_2} Sc^{0.25} \quad (4.69)$$

The exponent of Sc is kept at the value prescribed by Diessler's eq. [26]. It has also been observed by many workers that the exponent of Sc does not change significantly from that given by the standard correlation [27]. The estimated parameters with the statistical analysis is presented in Table 4.4. This correlation also yields a very high correlation coefficient (0.99). Fig. (4.13) (inset) shows the variation of Pe_{test} with $Sh/Re^{\beta_1} Sc^{0.25}$. This indicates that there is a significant influence of Pe_{test} on Sh_{exp} .

Stirred Cell

The correlation for stirred cell UF under turbulent condition is developed using the experimental data for PEG and PVP [123, 242]. The general form of such correlation is given as:

$$Sh = aRe^{\beta_1} Pe_{test}^{\beta_2} Sc^{0.33} \quad (4.70)$$

The Reynolds number is modified as:

$$Re = \frac{\omega R^2}{\nu} \quad (4.71)$$

Table 4.4: Estimation and statistical results for the different correlations developed.

Parameter	Estimates	95% confidence limit	$ t_{obs} $	F_{obs}	r
Laminar flow in rectangular cross flow system					
a	0.51 ± 0.028	0.51 ± 0.067	12.15	0.234	0.99
β_1	0.32 ± 0.056	0.32 ± 0.133	57.10		
β_2	0.26 ± 0.02	0.26 ± 0.048	22.41		
Turbulent flow in rectangular cross flow system					
a	0.035 ± 0.007	0.035 ± 0.017	16.26	1.91	0.99
β_1	0.35 ± 0.028	0.35 ± 0.069	12.29		
β_2	0.51 ± 0.037	0.51 ± 0.09	13.84		
Laminar flow in radial cross flow system					
a	1.05 ± 0.005	1.05 ± 0.012	2.75	0.05	0.96
β_1	0.38 ± 0.038	0.38 ± 0.095	10.27		
Turbulent flow in a stirred cell					
a	0.03 ± 0.015	0.03 ± 0.036	6.00	0.77	0.93
β_1	0.66 ± 0.085	0.66 ± 0.20	7.83		
β_2	0.16 ± 0.06	0.16 ± 0.14	2.58		
Laminar flow in a rectangular cell (BL)					
a	0.44 ± 0.08	0.44 ± 0.19	3.97	0.42	0.99
β_1	0.12 ± 0.025	0.12 ± 0.061	4.89		
β_2	0.71 ± 0.011	0.71 ± 0.027	65.05		
Turbulent flow in a stirred cell (BL)					
a	0.007 ± 0.001	0.007 ± 0.002	4.03	0.042	0.94
β_1	0.69 ± 0.092	0.69 ± 0.23	3.41		
β_2	0.20 ± 0.08	0.20 ± 0.197	2.86		

The exponent of Sc was kept at 0.33 as suggested by Colton's correlation [24] because it varies over a small range between 0.33 and 0.35 for high Sc (> 1000) [27]. The estimates of the parameters with the statistical analyses are given in Table 4.4. Pe_{test} has been plotted against the quantity $[Sh_{exp}/Re^{\beta_1}Sc^{0.33}]$ in Fig. (4.14). This shows that there is a significant effect of the Pe_{test} on the Sh_{exp} .

4.2.4.3 Development of the mass transfer correlations for black liquor

Experiments on BL were carried out in a rectangular channel under laminar flow conditions, as well as in a stirred cell under turbulent flow conditions [220]. The correlations for laminar and turbulent conditions were given by Eq. (4.67) and (4.70), respectively. The parameters and relevant statistical test results are presented in Table 4.4. The dependence of Pe_{test} on Sh_{exp} are given in Fig. (4.15) for laminar and turbulent (inset) flow conditions. It can be observed that the exponent of Pe_{test} for BL is higher (0.71) compared to that of the standard solute (0.26) in the laminar flow regime. This indicates that the complexities arising from the presence of a membrane (*e.g.* effect of pressure, polarization, change of properties, *etc.*) are more prominent for a complex industrial effluent like BL. For such an effluent, the influence of Re is not very significant (exponent of Re is 0.12 compared to 0.32 for standard solutes). However, the effect of Pe_{test} is approximately similar under turbulent flow (the value of the exponent is 0.20 compared to 0.16 for the standard solutes). This reveals that under turbulent flow, polarization and related problems are less severe for BL. However, the exponent of Re is very similar 0.69 compared to 0.66 for standard solutes). Therefore, such empirical correlations will be more useful for the treatment of multicomponent complex industrial fluid mixtures.

The statistical analyses regarding the correlations are presented in Table 4.4. Tabulated values of t and F statistics were taken from Box and Hunter [268], corresponding to the respective degrees of freedom. From Table 4.4, it can be seen that the experimental t values (t_{obs}) are larger than the t -values at 5% level of significance ($t_{tab,0.05}$). This indicates that the non-dimensional groups associated with these pa-

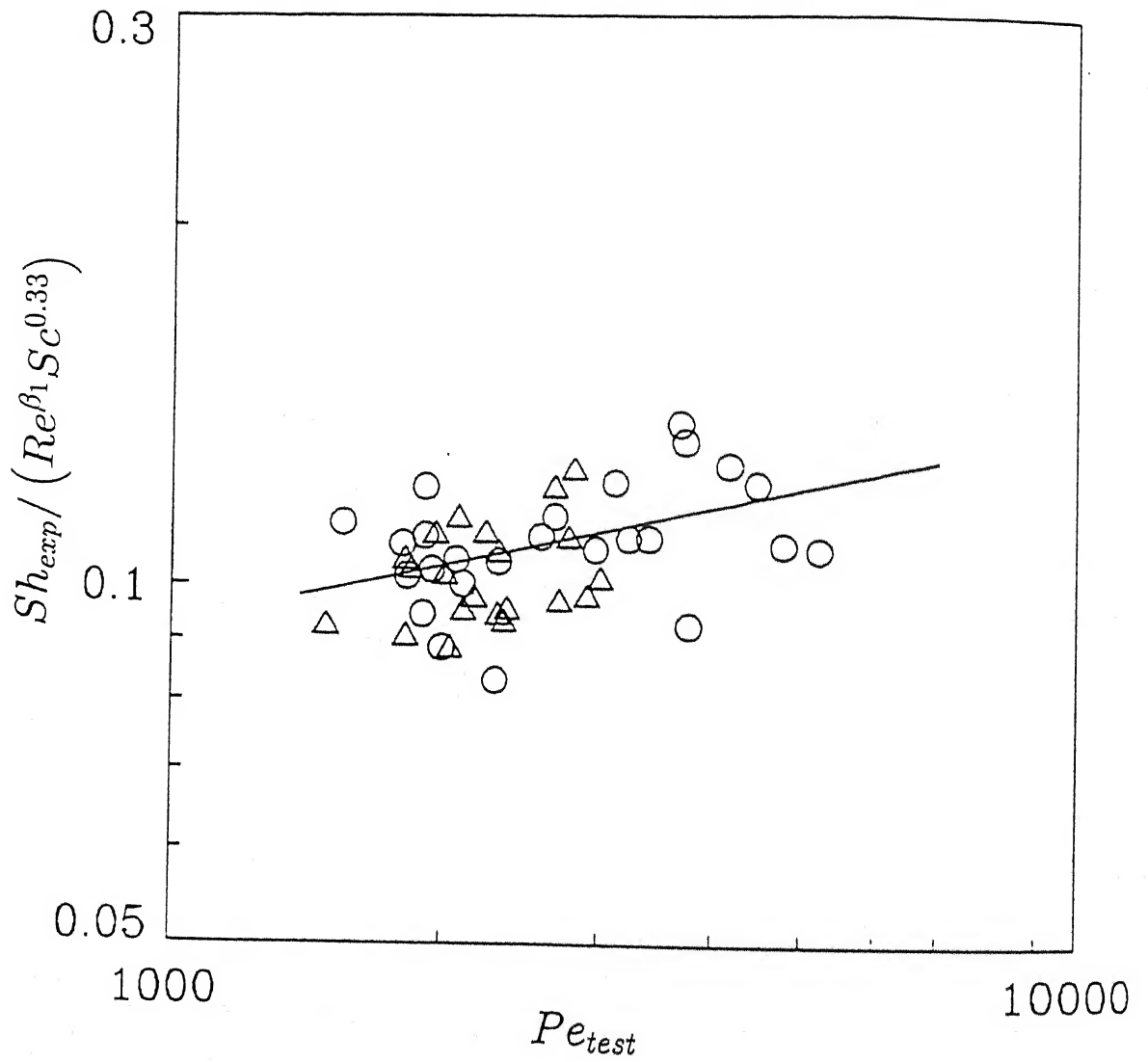


Figure 4.14: Variation of Sh_{exp} with Pe_{test} under turbulent flow domain in a stirred cell. \circ PEG 6K [220]; \triangle PVP 10K [242]; solid line is Eq. (4.70).

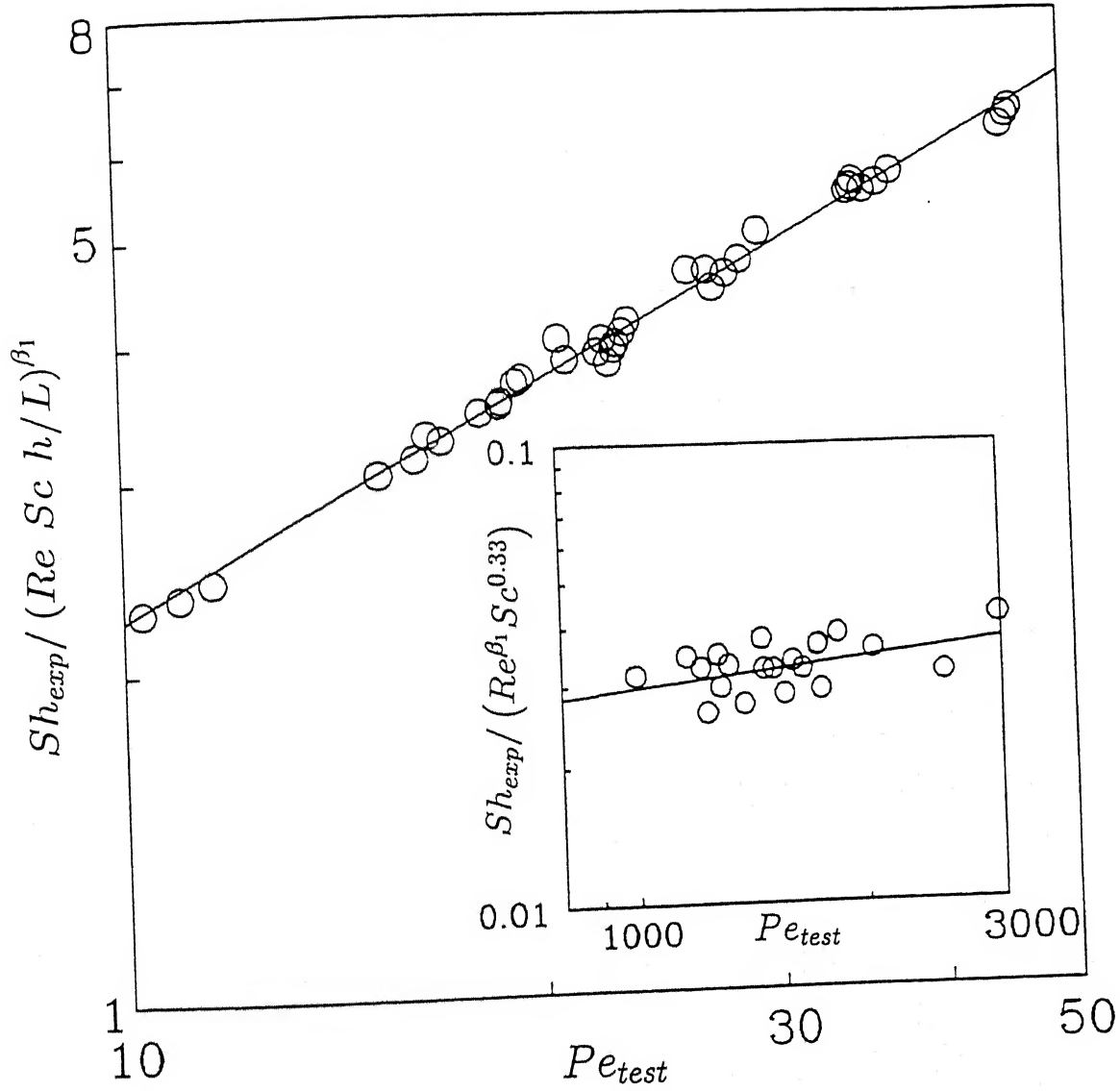


Figure 4.15: Variation of Pe_{test} for BL under laminar flow in a rectangular channel and turbulent flow in a stirred cell (inset). \circ experimental data; Solid lines are Eqs. (4.67) and (4.70) (inset) for BL.

rameters have significant influence on the developed model. The F values at 5% significance level ($F_{tab,0.05}$) are much larger than the observed F values. Therefore, the developed correlations are adequate to explain the experimental observations. Moreover, very high correlation coefficient values indicate remarkably good fit of the experimental data.

The above correlations under laminar and turbulent regimes were also compared with the standard correlations which are generally used in these cases. Under laminar regimes, the Leveque equation applies in rectangular and radial cross flow systems, while the correlations developed by Diessler [26] and Colton [24] for rectangular and stirred cells, respectively are widely used under turbulent regimes.

We compared the values of Sh obtained using the present correlation with those given by the standard correlations for different flow geometries and flow regimes. The standard correlation for laminar cross-flow in a rectangular channel is the Leveque equation [26]:

$$Sh = 1.18(Re Sc \frac{h}{L})^{0.33} \quad (4.72)$$

For laminar cross-flow in a radial cell, Eq. (4.72) holds but L is replaced by R and Re is based on channel half height h .

For turbulent cross-flow in a rectangular channel, the standard correlation is Diessler's equation [26]:

$$Sh = 0.023 Re^{0.875} Sc^{0.25} \quad (4.73)$$

where Re is based on the equivalent diameter d_h .

The standard correlation for turbulent flow in a stirred cell is Colton's correlation [24]:

$$Sh = 0.0443 Re^{0.8} Sc^{0.33} \quad (4.74)$$

The ratio, (Sh_{std}/Sh_{exp}) for different values of Pe for both laminar and turbulent regimes have been plotted in Fig. (4.16). The ratio decreases with increasing Pe , and the decrease is gradual for high Pe for a given Re . For a given Re , higher Pe can be attained by operating at lower feed concentrations or operating at higher pressure, or using a membrane with larger pore sizes. Fig. (4.16) shows that

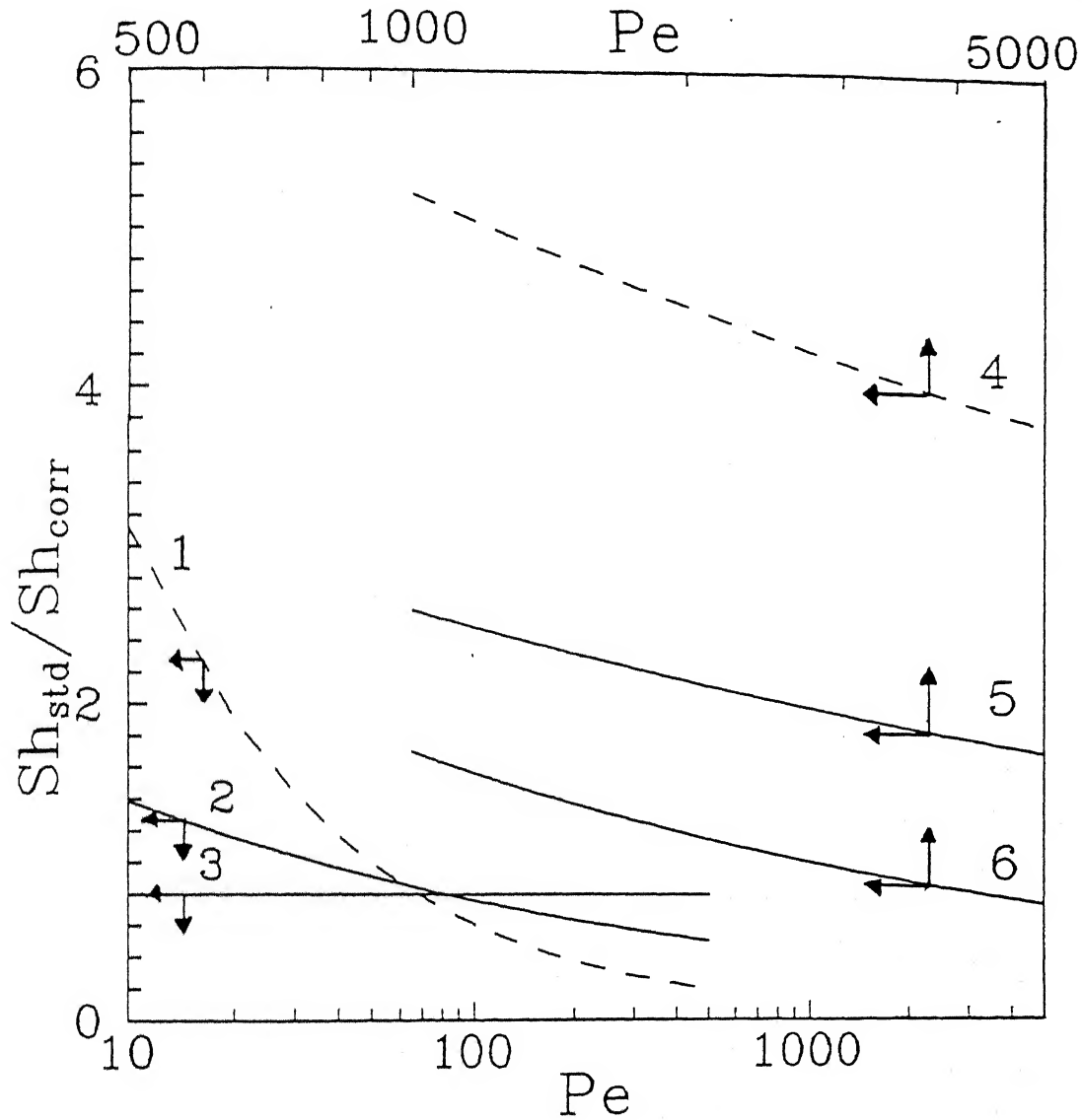


Figure 4.16: Variation of Sh_{std}/Sh_{corr} with Pe for different solutes and flow regimes. Solid lines are for standard solutes and dashed lines are for BL. Curve 1: BL under laminar conditions in a rectangular channel, $Re = 500$. 2: Standard solutes under laminar conditions in a rectangular channel, $Re = 500$. 3: Standard solutes in a radial cross flow cell, $Re = 500$. 4: BL under turbulent conditions in a stirred cell, $Re = 50,000$. 5: Standard solutes under turbulent conditions in a stirred cell, $Re = 50,000$. 6: Standard solutes under turbulent conditions in a rectangular channel, $Re = 5,000$.

the standard correlations deviate from the presently developed correlations quite significantly (which also means that the former also deviate from the experimental Sh values). Moreover, the constancy of this ratio at high Pe corroborates the attainment of limiting flux at higher pressure for constant hydrodynamic conditions. It can also be noted from Fig. (4.16) that for radial cross flow cell, the ratio does not vary with Pe_{test} but the standard Leveque correlation [26] always underpredicts mass transfer coefficient (curve 3). Fig. (4.16) also shows that this ratio for BL under laminar regime is quite high for $Pe \leq 50$ (curve 1) which signifies that the standard correlation overpredicts the mass transfer coefficient considerably under such conditions. However for higher Pe , the standard correlation underpredicts k . For turbulent regime in a stirred cell, the standard correlation always overpredicts k .

4.2.5 Conclusions

A modification of the existing Sherwood correlations for the UF systems has been made by including the effects of wall suction and concentration polarization in terms of an additional dimensionless number; namely, the Peclet number based on the test cell flux. In the present form, the modified correlation is applicable for osmotic pressure governed UF. The widely used existing correlations developed from heat and mass transfer analogies may grossly over/underpredict the mass transfer coefficient in UF systems and may lead to inefficient designs. The present forms of the correlations are suitable for UF systems.

Chapter 5

Applied aspects

Earlier chapters deal with the development of suitable theories for prediction of permeate flux and retention of an ultrafiltrative system. In this chapter, possible application and development of membrane separation processes for treatment of practical effluent are investigated. The aim of working on this topic has already been stated in chapter 1. Further, while dealing with BL in the earlier chapters, the curiosity to address the process development studies for membrane based technology for processing BL motivated to take up this work. Therefore, The first section of this chapter, aims at the process development and implications of membrane separation processes in context to recovery of water and inorganics from kraft black liquor.

5.1 Recovery of Water with Inorganic Chemicals from Kraft Black Liquor by Pressure Carbonation in Combination with Membrane Separation Processes

5.1.1 Introduction

Recovery of valuable inorganic compounds from black liquor (BL) is an integral part of the kraft pulping process. In the conventional process, BL (with 150–160 kg/m³ total dissolved solids) is concentrated to 600–650 kg/m³ and then incinerated. The molten inorganic chemicals are then causticized to recover around 85% of sodium

hydroxide. This process involves huge loss of water during the concentration step in multiple effect evaporators. Also, organics burnt during incineration cause environmental pollution. Apart from this, the equipment incurs high capital investment and energy cost. For small scale paper industries, black liquor concentration varies from 10 to 80 kg/m³ total dissolved solids (tds). Sometimes, instead of processing, this BL is discarded as it is, therefore, causing more pollution problems, lower efficiency of the adopted process and higher capital investment owing to the loss of valuable inorganics.

In kraft pulping, organics in BL are present mainly in the form of colloidal particles of alkali lignin [269]. Sodium compounds are present in free form to a lesser extent and most of them are bound with phenolic hydroxyl groups in the phenyl propane units which are a building block of lignin [269]. To achieve higher sodium recovery, sodium bound with alkali lignin should be separated. Pressure carbonation is one such process which lowers pH of the solution, frees the bound alkali and lignin is precipitated [221, 269]. Pressure carbonation, facilitated by absorption of carbon dioxide under stirring, was studied by Panda [270] to separate silica from green liquor. To control pH and reaction rate to a certain extent, dilute carbon dioxide mixed with air was employed [271]. Basu [272] studied carbonation of BL to produce modified green liquor; causticization of produced liquor was studied extensively.

Membrane separation processes are used in the pulp and paper industry for different purposes. Most of the applications are still in the laboratory stage. Ultrafiltration (UF) has been applied to remove suspended solids in white liquor [203]. Concentration of spent liquors and bleach plant effluents by reverse osmosis (RO) were extensively studied by Wiley and coworkers [205–207]. Jonsson and Wimmerstedt [203] reported concentration of spent sulfite liquor from around 150 to 250 kg/m³ (tds) by RO. Separation of alkali lignin i.e. fractionation of BL by UF was also studied [202–204]. Bhattacharya and coworkers [137, 216–220] carried out experimental studies and modeling of BL ultrafiltration in stirred and unstirred batch cells.

Among the membrane separation processes, electrodialysis has been widely studied to recover sodium compounds from BL. Radhamohan and Basu [273] reported more than 90% sodium recovery of 110–120 kg/m³ (tds) BL in a batch electrodialyzer but at the expense of severe membrane fouling, low current efficiency and higher power consumption. Mishra et al. [226, 227] studied BL treatment by batch and continuous electrodialysis. They also observed high recovery but at the cost of higher energy consumption and lower current efficiency. Moreover, BL used was of very dilute concentration less than 50 kg/m³ (tds). Roychowdhury [274] observed only 30–35% sodium recovery for a 50 kg/m³ (tds) feed BL by continuous electrodialysis. He also observed severe fouling of the membrane at higher concentrations. Apart from this, electrodialysis is a slow process and it may be difficult to operate in a continuous mode in a running plant.

Several extensive research activities were undertaken to recover inorganics and water or fractionate BL solutions. Every effort was associated with its own shortcomings. Hence, industries are reluctant to implement them. Attempts have also been made in our laboratory [137, 216–220, 226, 227, 274] to treat BL. This work is a continuity of the research efforts for a better treatment of BL.

The present work has been undertaken in the direction of developing a technology for recovery of water with the inorganic chemicals from BL. The suggested three-steps process is of carbonation of BL followed by UF and nanofiltration (NF). The pressure carbonation was used to separate organics (lignin) from inorganics where, inorganics get converted into carbonate salts. The resultant solution was treated by an open UF membrane in cross flow geometry at a low pressure to separate higher molecular weight fractions of lignin in BL. Hence, the permeate of UF may contain almost total sodium compounds and lower molecular weight fractions of lignin. The permeate of UF is then subjected to NF which rejects almost all of the organic molecules and passes water with inorganic salts which are mainly sodium carbonate salt. Further, cross flow UF (CFUF) improves the permeate flux and reduces concentration polarization [24]. The suggested three-steps process study

is an attempt for the eventual replacement of multiple effect evaporators and the incinerator in the conventional kraft recovery process. This study takes care of 50 to 90 kg/m³ (tds) of feed BL solutions which is realistic for small scale paper industries. The kinetics for BL carbonation as a function of time was also studied.

5.1.2 Experimental

5.1.2.1 Materials

Asymmetric cellulose acetate membrane, used for ultrafiltration, was obtained from *Permionics (India) Ltd.* was of 1000 molecular weight cut off (MWCO). For NF, a thin film composite (TFC) membrane of cellulose acetate was used, supplied by *Hydranautics India Ltd.*, was of 500 MWCO as specified by the manufacturer. The membranes were anisotropic, hydrophilic and of flat rectangular sheet type with an operating pH range of 2–12. The membrane was supported on a porous sheet. BL was procured from *Central Pulp Mills, Surat* and was diluted with distilled water for different concentrations in terms of tds.

5.1.2.2 Apparatus

Carbonation

A cylindrical pressure vessel of 800 ml (fitted with a pressure gauge) capacity was used for carbonation with the help of a carbon dioxide gas cylinder. A stirrer was attached to it to provide stirring. Stirrer speed was measured with the help of a stroboscope.

Membrane separation

For membrane separation, a rectangular cross flow cell was used. It was cast in gun metal and to avoid corrosion, nickel plating was done. The cell was of 0.4 m in length and 0.06 m in width. A neoprene rubber gasket of width 0.01 m was placed inside the cell. The channel height was determined by the thickness of the gasket which was 1.5 mm. In order to allow the flow to be fully developed in the channel, a minimum length was required from the entrance. Depending on the maximum

Reynolds number used, it was determined to be 0.05 m. Hence, the entrance length of 0.05 m was kept blank with a plastic sheet. Therefore, effective membrane area, after deducting gasket width, became $0.33 \text{ m} \times 0.04 \text{ m}$. The cross flow cell was connected to a reciprocating pump of capacity 5 liter/min. An *Elico* pH meter (model no. LI-120) was used to measure pH of the solutions.

5.1.2.3 Analysis

The black liquor analysis is given in Table 3.1. The major inorganic contents for different sample streams were calculated by pH metric triple titration method [236]. Total dissolved solids in black liquor was determined gravimetrically by evaporating the sample in an oven at $105 \pm 3^\circ\text{C}$.

5.1.2.4 Experimental design

Carbonation

It was observed that during carbonation for lower concentrations, pH drops very fast with time. Hence, a little higher concentration (119 kg/m^3) of BL was chosen for study of the carbonation of BL. BL of this concentration was subjected to carbonation for different contact times. At the end of each run the carbonated solution was analyzed. It was observed that pH reached a steady value for a contact time of 15 minutes. Therefore, to ensure complete carbonation, BL solution was carbonated for half an hour, at 206 kPa, 30°C and at a stirrer speed 180 rpm, in order to prepare the feed solutions for UF and NF runs. for preparation of the feed carbonated solution for the runs of UF and NF, BL solution was carbonated for half an hour. Carbonation was carried out at 206 kPa and 30°C and at a stirrer speed of 180 rpm. To get around 2.0 liter solution carbonized, the solution was treated with carbon dioxide in batches. The concentrations of feed BL solutions, before carbonation, chosen for the membrane separations were varied as 55, 73 and 90 kg/m^3 .

Membrane separation

The operating pressure for all UF runs was chosen as 689 kPa and that for NF was

1723 kPa. The recirculation flow rate for both UF and NF were chosen as $2.22 \times 10^{-5} \text{ m}^3/\text{s}$. To observe the effectiveness of different schemes (as described in results), experiments were carried out as scheme C, B, A, in that order.

5.1.2.5 Procedure

First, a solution of fixed concentration of BL was prepared. It was carbonized in the pressure vessel in batches. Membranes were compacted at 824 kPa (for UF) and at 1895 kPa (for NF) which are higher than the highest operating pressure at $2.22 \times 10^{-5} \text{ m}^3/\text{s}$ for six hours with distilled water. At the same flow rate, water flux was measured at four different pressures to determine the membrane permeability. For scheme C, BL was directly treated by NF. Feed tank was filled with 2.5 – 3.0 liter feed solution and the pump was made operative. Instantaneous pressure difference was reached (within 10 seconds). Cumulative volume of permeate was measured as function of time at fixed operating conditions. This was continued till steady state flux value was reached. Steady state flux was attained within 25 minutes. However, the run was continued for 1 hour. For scheme B, carbonated BL was subjected to NF and the run was taken as described previously. For scheme A, carbonated BL was first treated by UF. UF runs were very long, ranging from 12 to 16 hours to collect sufficient volume (around 3 liters) of permeate to carry out subsequent NF runs. Samples were collected from all the streams for analysis. All the experiments were carried out between 26°C and 31°C . Hence, all properties and data were corrected and calculated at 30°C . After each run, feed tank and the set up including the membrane was washed by recirculating distilled water at the lowest pressure and highest flow rates for nearly 30 minutes. After that the membrane permeability was checked. Above procedure was followed for different feed concentrations. The schematic diagram of the experimental set up is shown in Fig. (3.3).

5.1.3 Results and discussions

5.1.3.1 Selection of feed solution concentration

Depending on the type of alkaline pulping, capacity of the industry and raw materials used, paper mills produce black liquors of different compositions and concentrations. The concentration of BL from brown stock washers in bigger mills is around 150 kg/m^3 and that for smaller mills is $10\text{--}80 \text{ kg/m}^3$ (total dissolved solids content).

For the treatment of BL by asymmetric membranes, selection of feed concentration is very important. At higher concentrations, osmotic pressure of BL increases, therefore, permeate flux decreases to a large extent. Hence, at higher concentrations, low flux poses difficulties for comparative studies. Further, viscosity of BL also increases at higher concentrations and handling of the concentrated liquor by ordinary pumps becomes difficult.

BL is composed of a large number of macromolecular solutes of different molecular weights. During the ultrafiltration operation, solutes of lower molecular weight clog the pores, therefore, reuse of the membrane becomes difficult. For all these reasons, an intermediate range of concentrations of BL in terms of tds were chosen as ($\sim 50, 70$ and 90 kg/m^3) to study its effect on flux, rejection of the organics and recovery of the inorganics. Hence, this study may be more relevant for small scale paper industries. From this on, concentration mentioned in the text is total dissolved solids (tds).

5.1.3.2 Carbonation of BL

The inorganic constituents of BL are basically sodium compounds (NaOH , Na_2S , Na_2CO_3 , Na_2SO_4 , etc.). In the liquor, some of them are present in the free form, but most of the sodium is bound with the phenolic hydroxyl group of colloidal alkali lignin. The building block of lignin is the phenyl propane unit. Basic structural groups which are supposed to form lignin [199] are shown in Fig. (5.1). Lignin is

formed as a 3-dimensional polymeric structure with these basic units bound together by ether and carbon-carbon bonds.

In BL solutions, phenolic hydroxyl groups of lignin are present in the form of $\text{O}^- \text{Na}^+$ groups. These charged colloidal lignin particles are stable at pH greater than 7. As carbon dioxide is passed, pH of the solution decreases and $\text{O}^- \text{Na}^+$ bonds break; therefore, lignins get precipitated and Na goes into the solution. After sufficient treatment with CO_2 , almost all of the sodium compounds get converted to Na_2CO_3 and lignin gets settled in the fragmented form. In general, mass transfer in terms of absorption rate of CO_2 in the solution can be enhanced by applying higher pressure and stirring [25]. For a 119 kg/m^3 BL solution, the decrease of pH with time is shown in Fig. (5.2). As time proceeds, sodium hydroxide as well as sodium sulfide (after hydrolysis) is converted to Na_2CO_3 . The drop of activity of BL solution which is defined as the ratio of active alkali ($\text{Na}_2\text{S} + \text{NaOH}$) as Na_2O to the total titratable alkali ($\text{Na}_2\text{S} + \text{NaOH} + \text{Na}_2\text{CO}_3$) as Na_2O with time is shown in Fig. (5.3).

However, treatment of BL by CO_2 is advantageous for subsequent membrane separation processes. Cellulose acetate membranes used in the experiments were amenable to the degradation at high alkalinity ($\text{pH} > 12$) or high acidity ($\text{pH} < 2$). Consequently, direct treatment of BL which has a $\text{pH} \sim 11.5$ may shorten the membrane life. In this context, the present approach is more advantageous because after carbonation BL has a $\text{pH} \sim 7.5$, which causes less damage to the membranes during UF and NF. As already mentioned, carbonation of BL results fragmentation of lignin molecules [221]. It was observed in the experiments that this fragmentation is associated with an increase in inhomogeneity of the solution. This experimental observation was more pronounced at higher concentrations [272]; however, this effect was not studied.

5.1.3.3 Kinetics of carbonation of BL

To study the kinetics of carbonation of BL, pH and composition of the carbonated liquor were analyzed for different contact times. Since, almost complete carboniza-

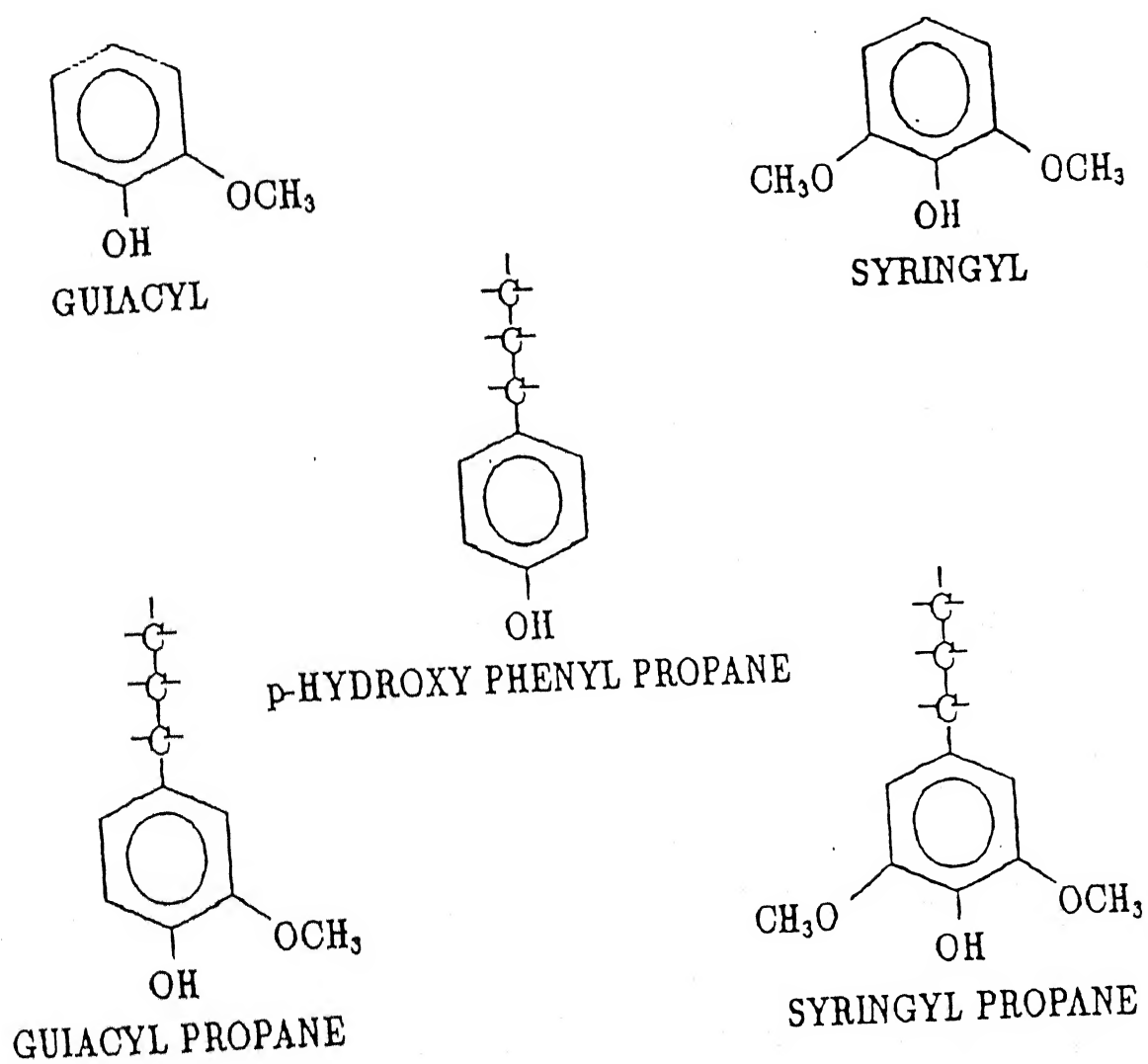


Figure 5.1: Basic Units of lignin

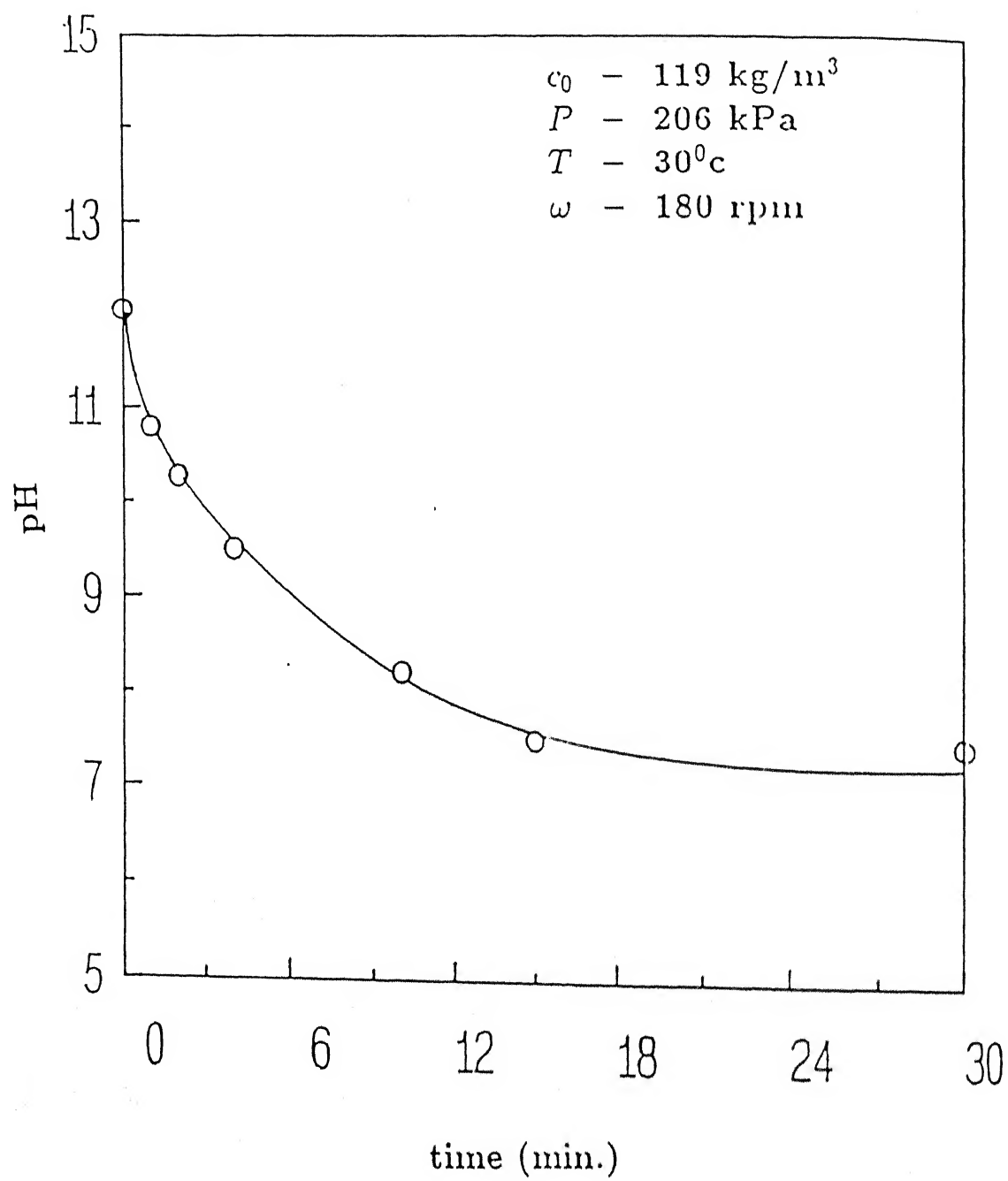


Figure 5.2: Variation of pH with time

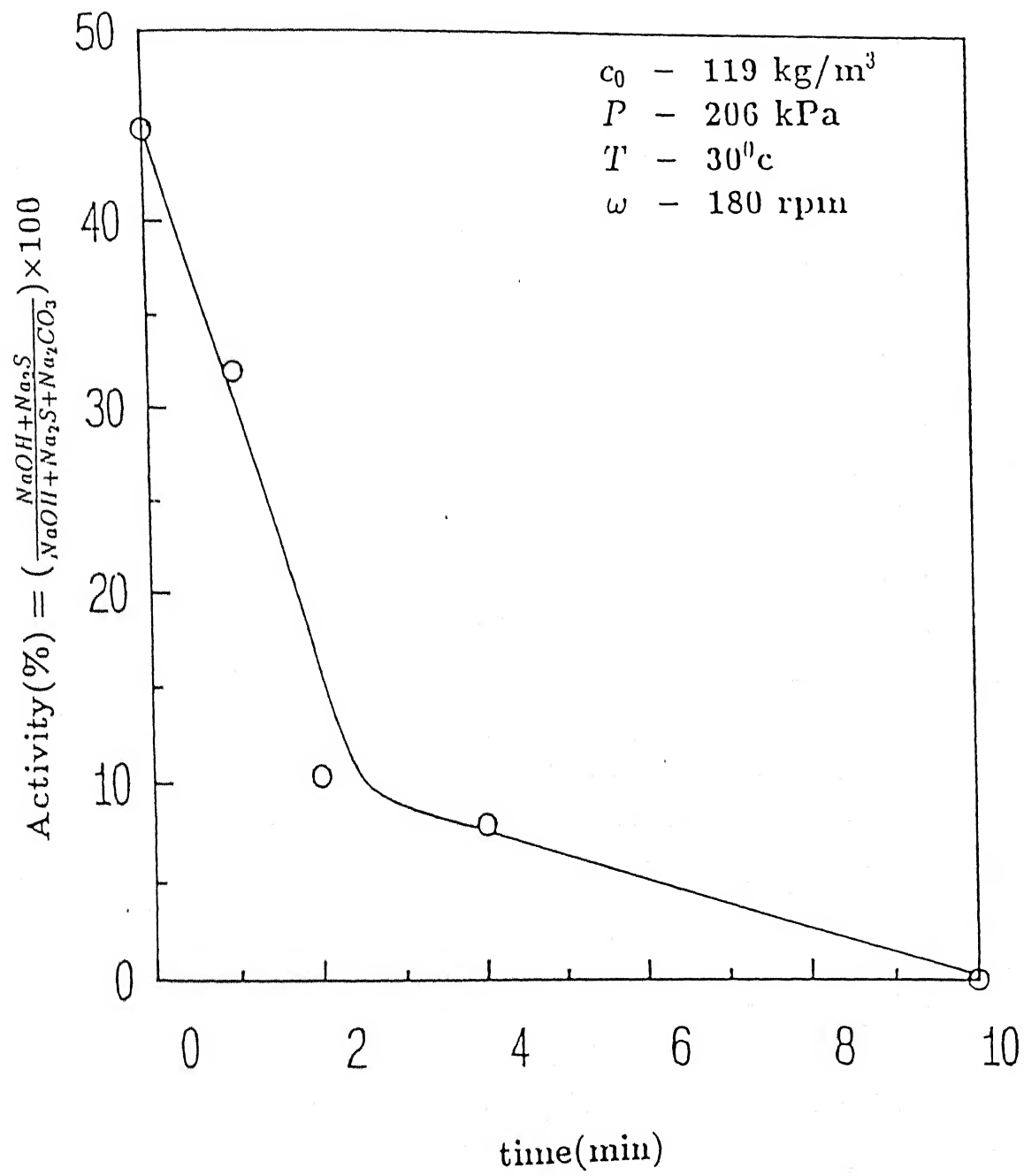


Figure 5.3: Variation of activity with time

tion could be achieved within a short period of time (within 2 minutes) for lower feed concentrations, a comparatively higher feed concentration of 119 kg/m^3 was chosen to study the kinetics. Fig. (5.2) depicts the decrease of pH with time. A constant value of 7.5 was reached for a contact time of 15 minutes.

The uptake of CO_2 by the active alkali to form sodium carbonate was determined by titrametric analysis for different contact times. Details of which are provided in the experimental section. The results have been plotted in Fig. (5.4) which shows rapid conversion of the active alkali into Na_2CO_3 initially followed by a more gradual conversion after about 3 minutes. A regression analysis of the experimental data was performed and the kinetics was described by the following correlation, with a correlation coefficient 0.99,

$$\frac{c}{c_0} = \exp(-0.505 t) \quad (5.1)$$

Here, c is the concentration of the active alkali compounds present at any time t and c_0 is that of the feed solution. The striking simplicity of the above correlation is remarkable because the first order kinetics described by it actually represents a complex set of reactions. The alkali (Na^+) present in the BL exists in two forms, namely free alkali (NaOH , Na_2S , etc.) and bound alkali in the form of alkali lignins. During carbonation, both free and bound sodium ions take part in the reactions, therefore, actual mechanism for the conversion of alkali compounds in the carbonate form is very complicated. However, the suggested correlation (Eq. (5.1)) enables one to circumvent this difficulty and it provides us the important data of the concentration of active alkali during carbonation.

5.1.3.4 Treatment of carbonated BL by membrane separations

Selection of schemes

Three different schemes of membrane separation processes for BL treatment were considered which are shown schematically in Fig. (5.5). First, carbonated BL was passed through a leaky UF membrane and the permeate of this was then subjected to NF process, as shown in scheme A. In scheme B, carbonated BL was treated by

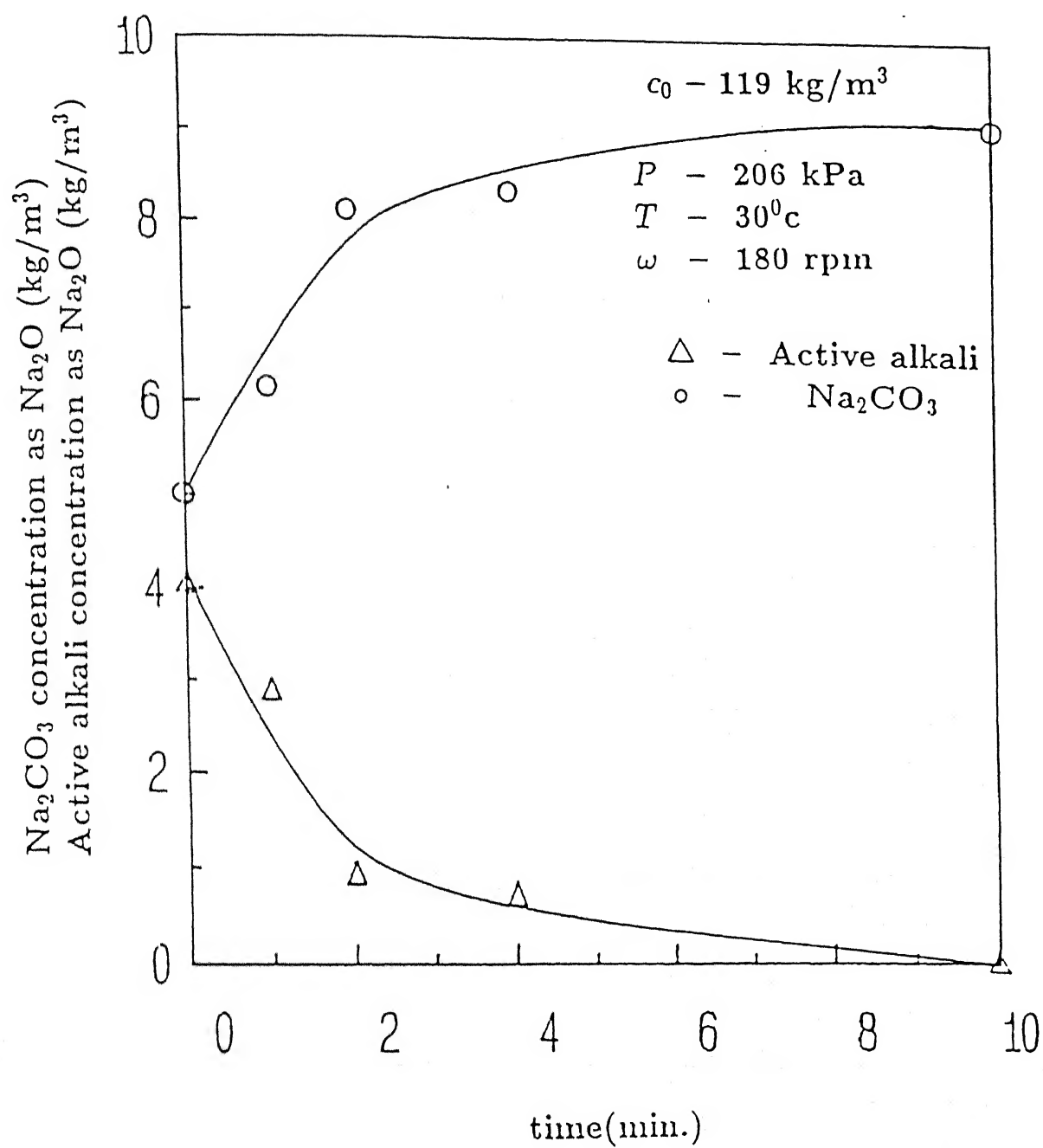


Figure 5.4: Change of concentration of active alkali and sodium carbonate with time

NF membrane to observe the effect of UF step in scheme A. In scheme C, BL was directly subjected to NF to demonstrate the significance of the carbonation step. The comparison between these schemes were done in terms of inorganic recovery, permeate flux and quality of the product permeate.

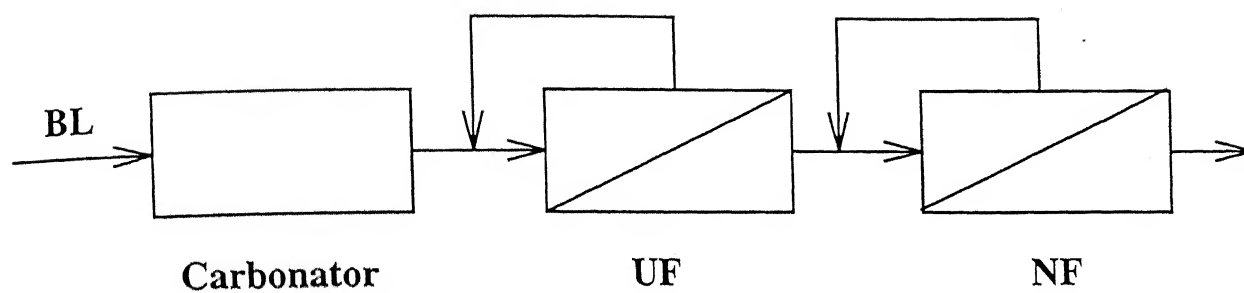
Recovery of inorganics

The variation of recovery of the inorganics with feed concentrations for different schemes is shown in Fig. (5.6). Scheme A shows the maximum recovery followed by schemes B and C, in that order. The lowest recovery in scheme C may be explained due to the retainment of bound alkali whereas in schemes A and B the carbonation procedure converts the bound alkali into sodium carbonate, resulting in a higher recovery of the inorganics. When carbonated BL is treated by NF (scheme B), membrane surface is polarized by low as well as high molecular weight fractions of lignin. Some of the pores on the membrane surface may also get clogged; even pore mouths, in some cases may get blocked. This phenomenon is considerably reduced by separation of higher molecular weight fractions of lignin fragments by UF as shown in scheme A. Therefore, during subsequent NF less hindrance is offered to the passage of the inorganic solutes and solvent through the membrane.

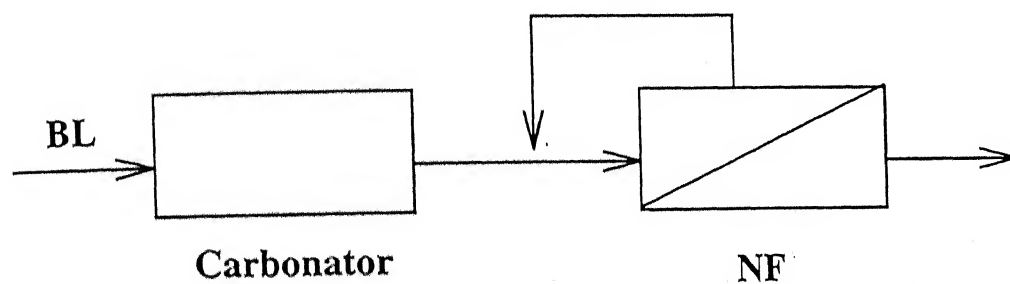
At feed concentration of 90 kg/m^3 , recovery in scheme C is 25%; at the same concentration, recovery in scheme B is 74.4% which is almost 200% more than scheme C. At these conditions, recovery in scheme A is 78% which is 4.7% more than B and 214% more than C. Therefore, as far as recovery of the inorganics is concerned, scheme A is more promising. From Fig. (5.6), it is obvious that recovery increases as feed concentration increases. At higher feed concentrations, more inorganic salts are present in the solution and hence, recovery increases as more solutes pass through the membrane.

Permeate flux

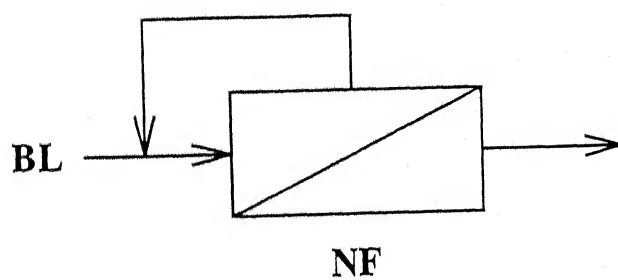
In any membrane separation process, permeate flux is of utmost importance. It is one of the influencing parameters which determines the performance of the separation process. Steady state NF permeate flux is plotted against the feed concentration



Scheme A



Scheme B



Scheme C

Figure 5.5: Different schemes which were studied

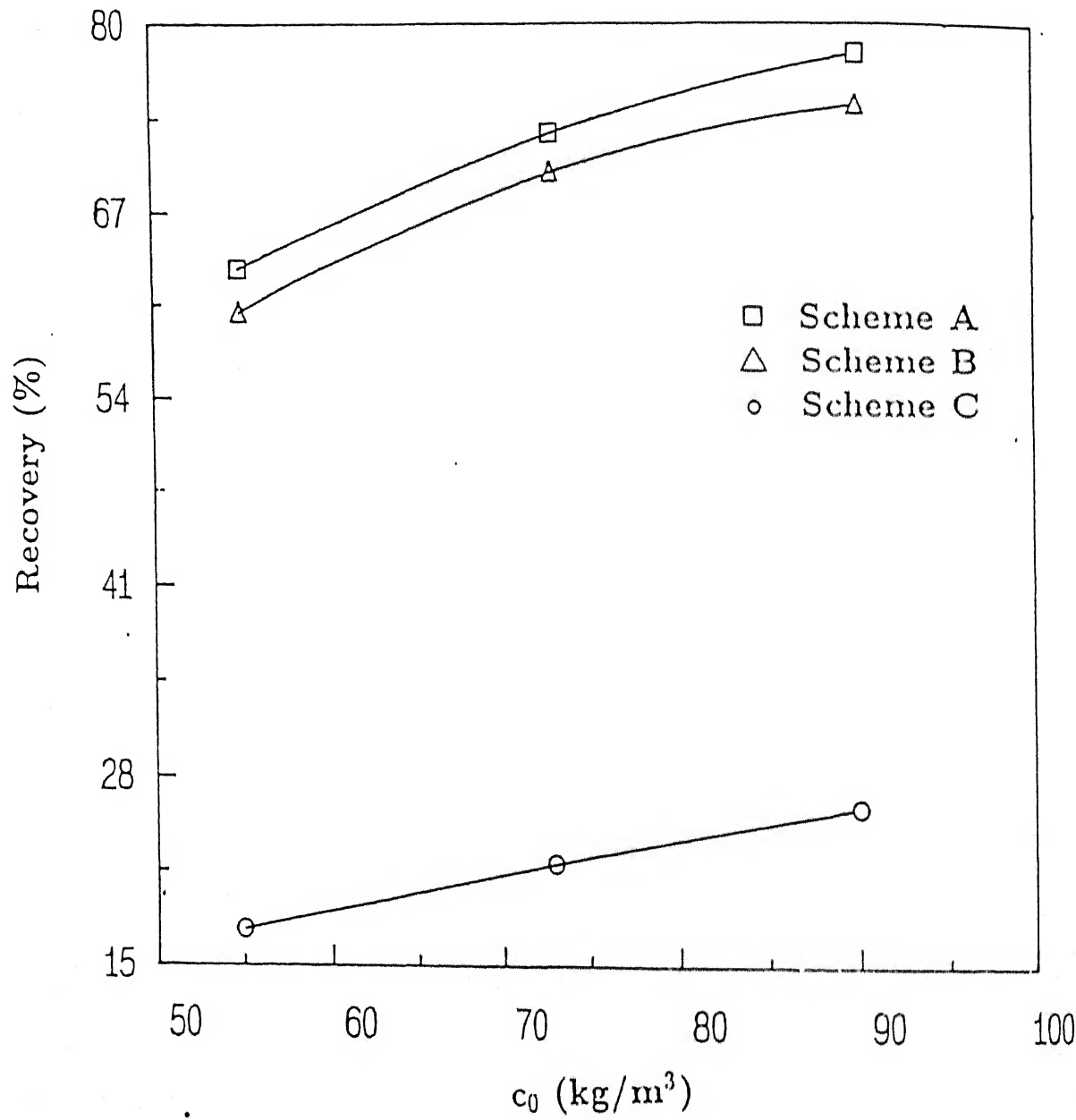


Figure 5.6: Variation of inorganic recovery with time

in Fig. (5.7). Here, scheme C gives the highest flux compared to the other schemes but at the cost of the minimum recovery of inorganic salts. Obviously, this is not advantageous, as inorganic recovery is of prime importance to the pulp industry. Lower flux of the carbonated solution can be attributed to the presence of carbonate salts and fragmented lignins which increase the osmotic pressure of the feed considerably, thereby, reducing the driving force.

This phenomenon can be explained by the phenomenological equation, Eq. (3.20). Π can be expressed for dilute solution of salts as,

$$\Pi = \frac{RTc}{M_w} \quad (5.2)$$

For salts, molecular weight is generally very small compared to the macromolecular or colloidal particles. Hence, osmotic pressure of the salt solution is very high. Osmotic pressure is further increased by increase of concentration. So, available driving force gets reduced and flux decreases. This also explains the reason for the decrease of flux at higher feed concentrations. Thus, osmotic pressure of the carbonated solution is higher with the release of the bound sodium salts in the solution. This results in reduced flux in schemes A and B. Also, smaller fragments of lignin may get adsorbed reversibly on the membrane surface and clog the pores to a larger extent than the solution without carbonation. In scheme A, the large molecular weight fractions of lignin are removed by preliminary UF. The permeate from UF is then subjected to NF, whereas in scheme B, the intermediate fractionation of higher molecular weight fractions of lignin is not performed. Therefore, the feed solution in NF step is more concentrated in scheme B compared to scheme A. Consequently, flux in scheme B is lower than that in scheme A. For example, at feed concentration 90 kg/m³, flux in scheme C is 4.53×10^{-7} m³/m².s (1.63 l/m².h) and that in B and A are 1.28×10^{-7} m³/m².s (0.46 l/m².h) and 2.43×10^{-7} m³/m².s (0.88 l/m².h), respectively. Therefore, considering both flux and recovery, scheme A is the best among the three schemes. Further, after taking each run, membrane permeability was checked and that was found virtually constant. This proves there was no permanent adsorption on the membrane surface and the adsorption or polarization during operation was

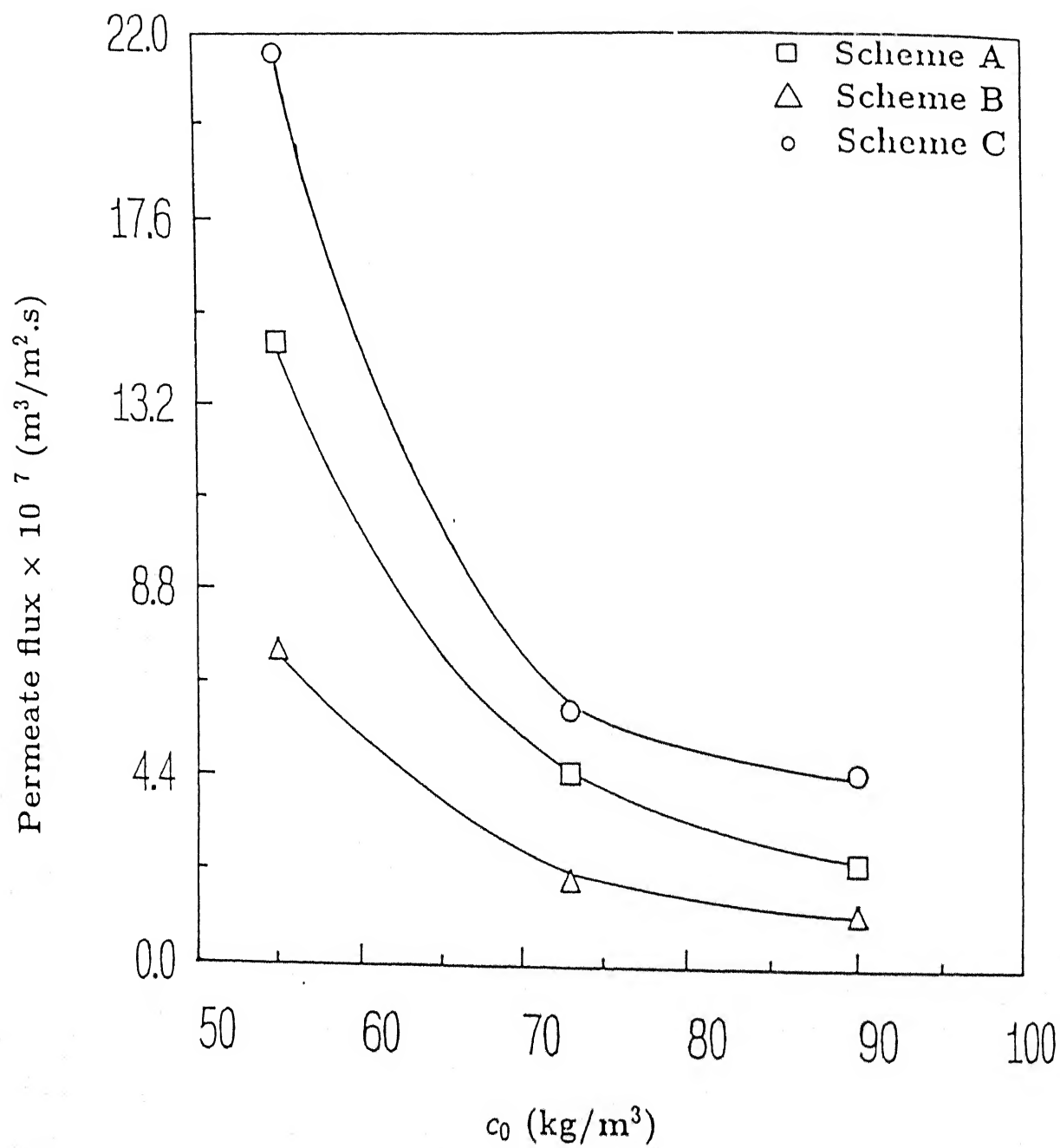


Figure 5.7: Steady state NF permeate flux for different schemes versus feed concentration

purely reversible in nature. Due to the high flow rate of the pump in the cross flow apparatus, the washings of the membranes were very efficient which restored the permeability to its original status.

Flux decline with time

In pressure driven membrane separation process, decline of flux is a major problem. As the separation process progresses, solutes start accumulating on the membrane surface, thus forming a boundary layer. This build up of solutes offers an extra resistance to the flow through the membrane. This is termed as concentration polarization. Increase in concentration also increases osmotic pressure of the solution, thus lowering the effective driving force. There may be formation of a gel layer on the membrane surface, the thickness of which increases with time. This type of fouling is generally reversible in nature. Apart from this, there may be solute adsorption on the membrane surface (pore mouths are blocked), adsorption inside the pores (pores are blocked partially) or clogging of the pores. These types of hindrances may be either reversible (removable after washing of the membrane) or irreversible (not removable even after washing) in nature. All these resistances can simply be put in the form of resistance in series model,

$$v_p = \frac{\Delta P - \Delta \Pi}{\mu(R_m + R_{bl} + R_g + R_{ad})} \quad (5.3)$$

where, R_m is the hydraulic resistance of the membrane, R_{bl} is the resistance in the boundary layer, R_g is the resistance in the gel layer and R_{ad} is the adsorptive resistance.

BL, a polydispersed liquid having solutes of wide molecular weight range of 1000–100,000 is susceptible to severe polarization during the membrane operation. Several theories have been put forward to understand, quantify and control of the concentration polarization [9, 11, 24, 150]. One way to reduce concentration polarization is to allow feed solution to flow tangentially over the membrane surface, known as the cross flow ultrafiltration. This causes reduction in the growth of the boundary layer near the surface and increase in back diffusion from the surface to the bulk of the solution. Hence, permeate flux increases significantly. In the presence

of the

resistances mentioned above, the permeate flux declines with time and eventually reaches a steady state value.

Flux decline with time for all the schemes are shown in Figs. (5.8), (5.9) and (5.10) for feed concentrations 55, 73 and 90 kg/m³, respectively. Since, UF membrane has larger pore sizes, its flux is always higher but it decreases because of the concentration polarization. The decline in flux is gradual for scheme B and C in all the cases, whereas that for scheme A is rapid. This is because, in scheme A, membrane polarization is minimized and the steady state is attained quickly. For example, in Fig. (5.8), for scheme A, steady state flux is reached within 10 minutes whereas, for scheme B and C, it was 25 and 20 minutes, respectively. Flux prediction of such behaviours have already been attempted [9, 20, 40, 44]. It is interesting to note that the flux decline (Figs. 5.8, 5.9 and 5.10) is more gradual in NF runs than that in UF experiments. This suggests that besides concentration polarization, there exists some reversible fouling (pore blocking) of the membrane during the operation. But, this fouling of the membrane is not permanent because it is observed that the membrane permeability remains unchanged after washing of the membrane.

Quality of the product permeate of NF

Quality of the NF permeate can be specified in terms of total dissolved solids (tds) rejection. Rejections, in membrane terminology are of two types, namely, observed and real rejection. However, in this study only observed rejection is considered. Rejection of tds versus feed concentration for different schemes is shown in Fig. (5.11). Here, scheme C shows the minimum and A shows the maximum rejection. The permeate having low tds content consists mainly of low molecular weight organic colouring compounds. The quality of the permeate was also observed from the colour of the final permeate i.e. of NF. The colour of the permeate in scheme C was yellow, that in B was light yellow and that in A was almost white with a slight yellowish tinge which indicates the permeate in scheme C contains the maximum amount of the organics and that in scheme A contains minimum amount of the

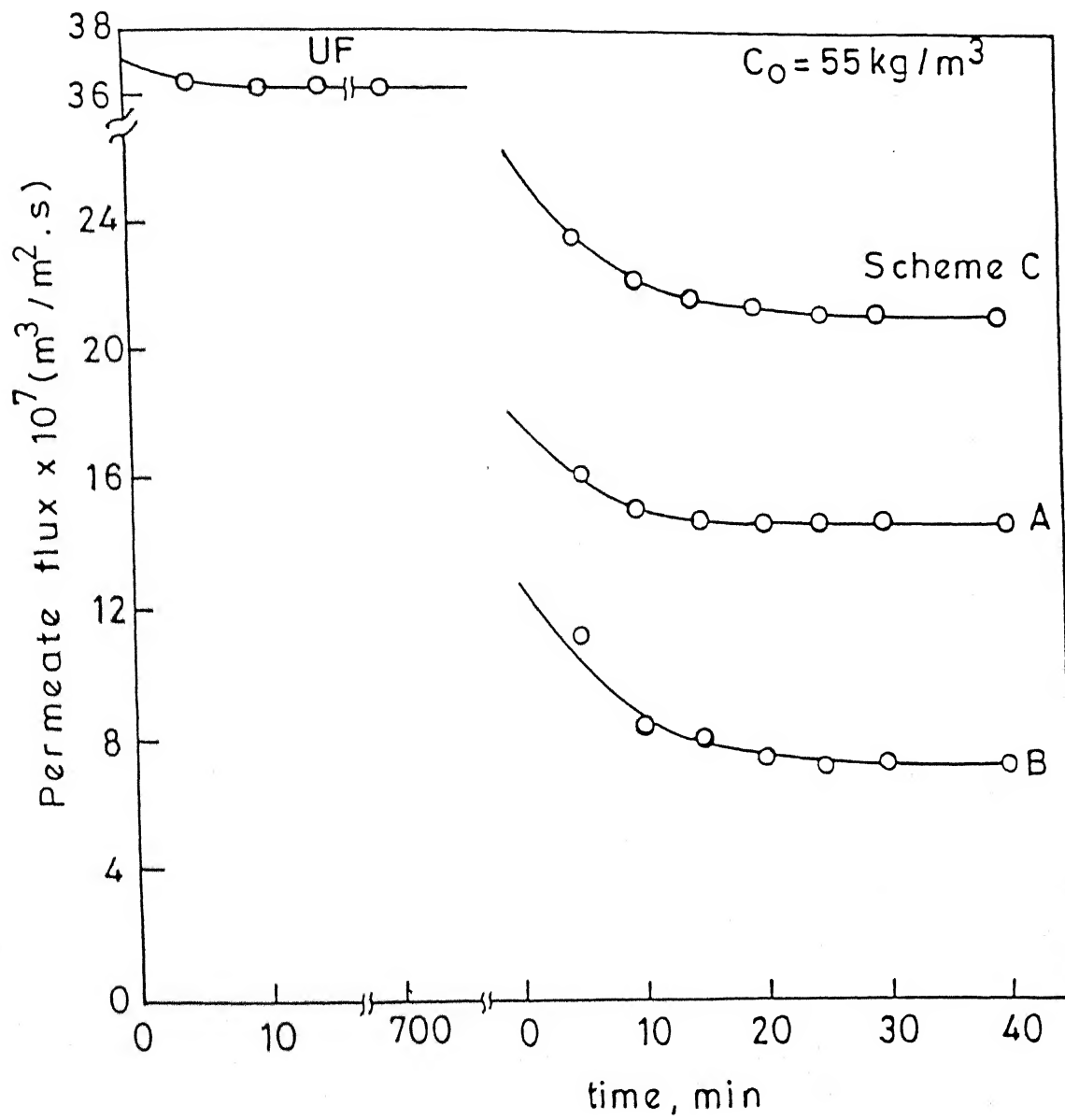


Figure 5.8: Flux decline with time for 55 kg/m^3 BL for different schemes

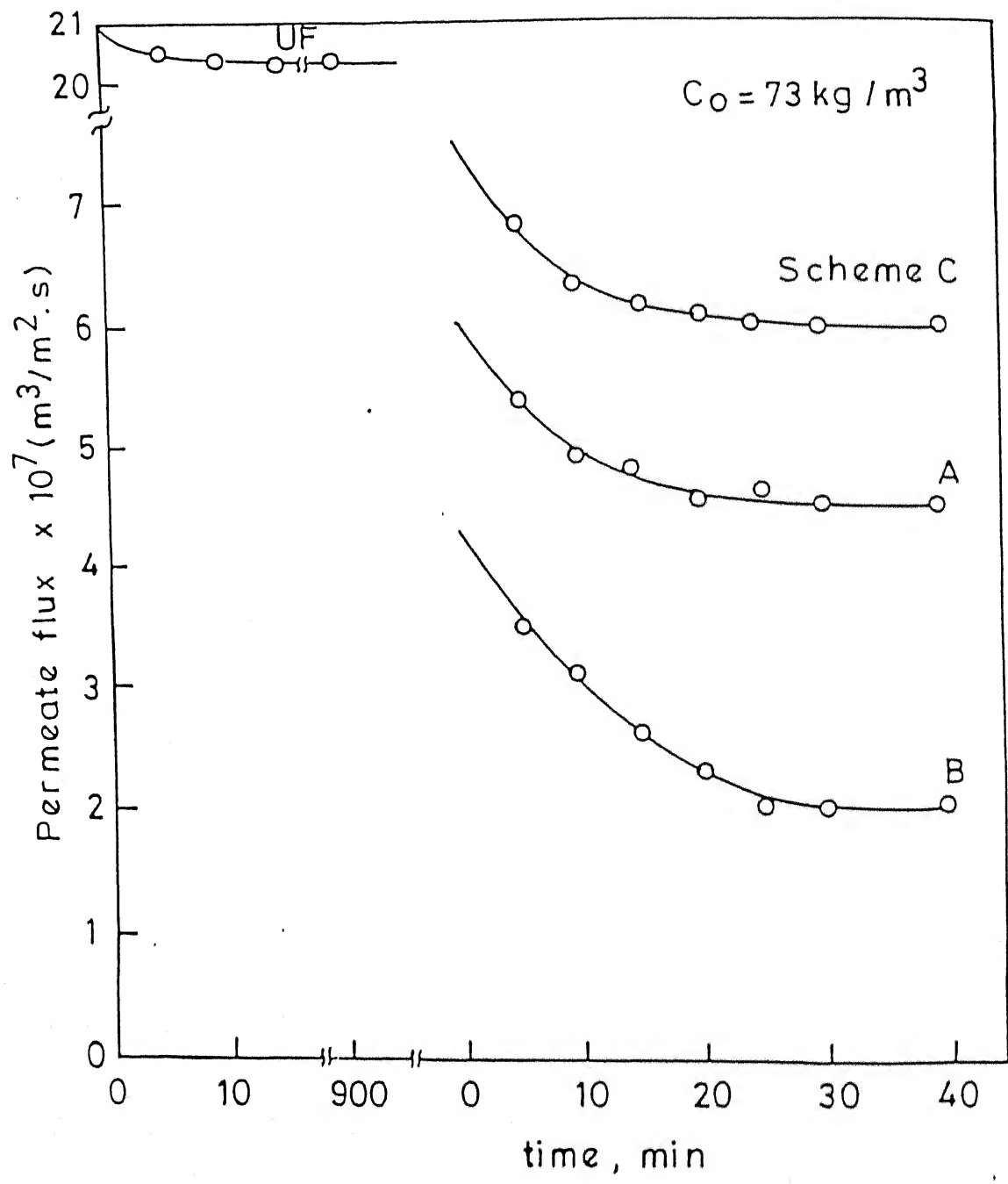


Figure 5.9: Flux decline with time for 73 kg/m³ BL for different schemes

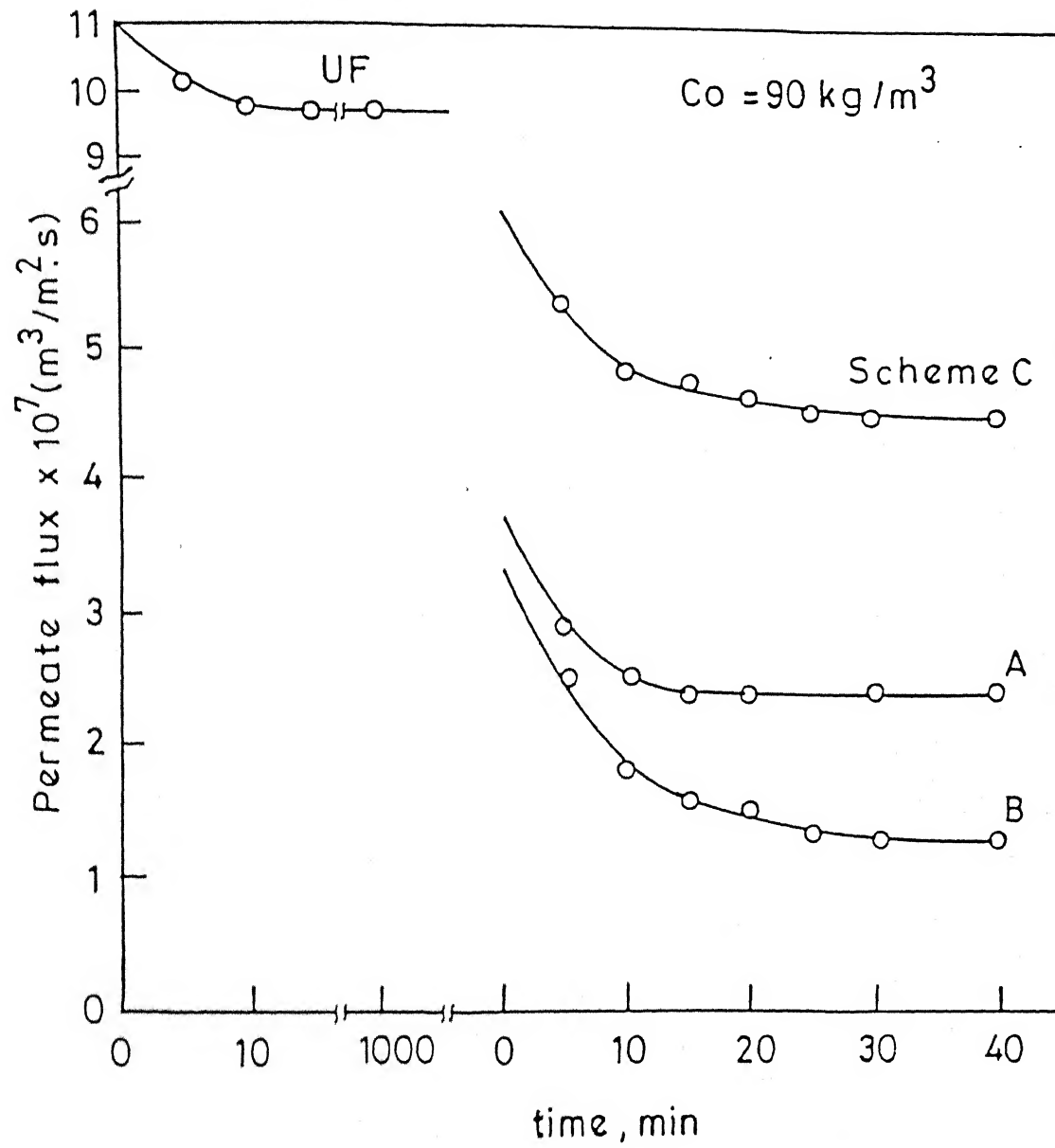


Figure 5.10: Flux decline with time for 90 kg/m^3 BL for different schemes

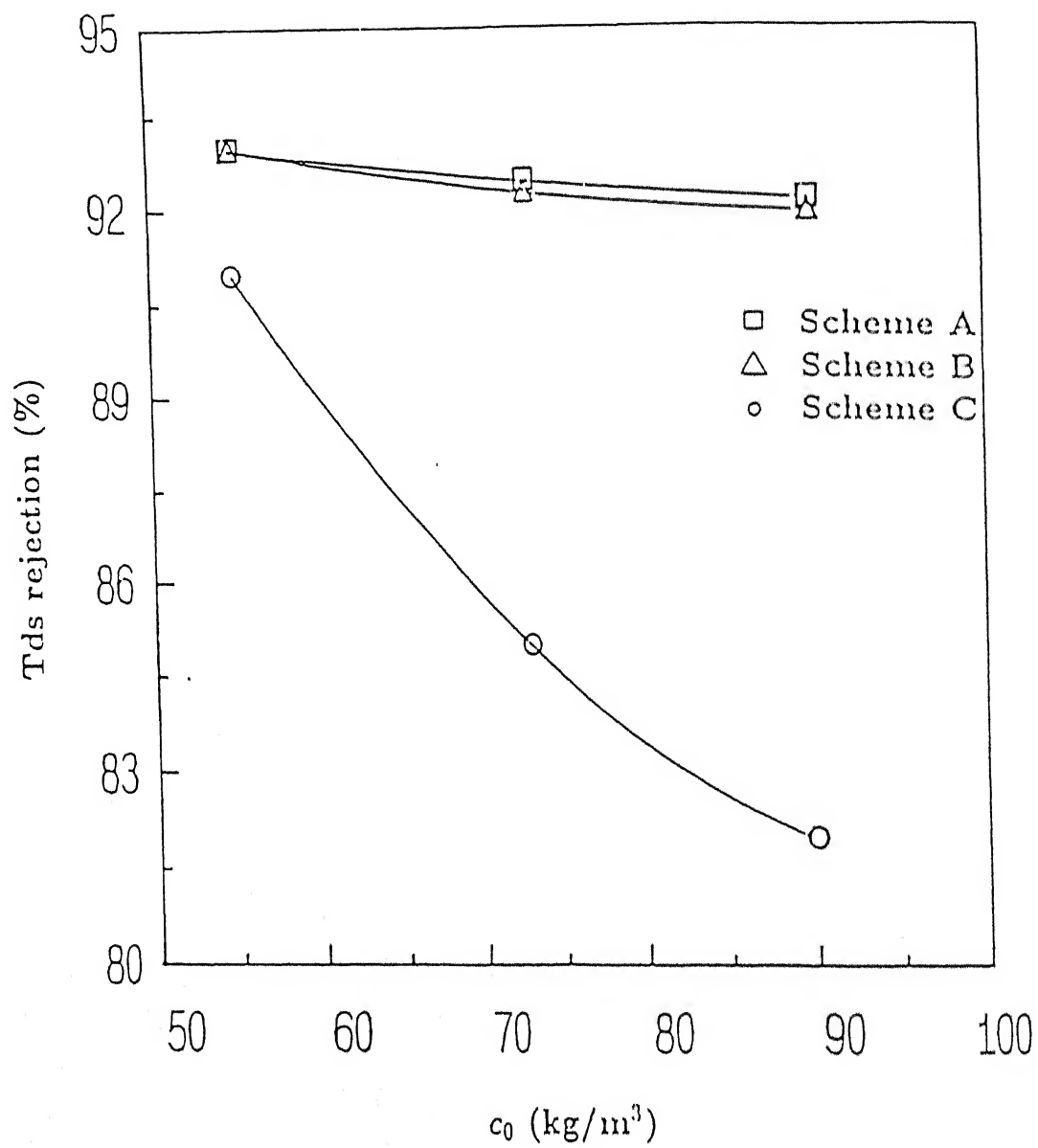


Figure 5.11: Variation of tds rejection with feed concentration for different schemes

organics. The colour of the permeate of UF, in scheme A, was observed to be black.

To summarize the overall performances of the three schemes are shown schematically in Fig. (5.12). It shows that the flux is less in scheme A compared to that in C whereas, recovery of the inorganics and rejection of the organics are maximum in scheme A.

The enhancement of the permeate flux in any membrane separation process is a major research interest in various membrane research laboratories. Although, increase in applied pressure seems to be logical to increase the driving force and therefore flux but this leads to more concentration polarization due to the osmotic pressure build up. Therefore, introduction of turbulence [216] or turbulent promoters like spacers [9] reduces the concentration polarization to a significant extent. Studies on pressure pulsation [11] may prove significant increase in permeate flux. Negative transmembrane pressure pulsing also results in an increase in flux in presence of irreversible membrane fouling as well as reversible concentration polarization [81]. Using such techniques, the permeate flux in scheme A can be improved to make the process economically viable.

Causticization and colour removal

The final permeate can be treated in a conventional causticizer with lime, so that all sodium carbonate get converted to sodium hydroxide. The trace amount of colour in the permeate can also be removed by adsorption of colouring compounds by lime which was confirmed by the author's earlier work [275, 276]. The causticized permeate can then be recycled back to the digester.

Energy consumption

In an attempt to illustrate the viability of scheme A, a simple energy consumption calculation for carbonation under stirring and membrane separations was carried out. The calculations are simple presentations of energy consumption and should not be taken as a complete illustration of the process calculations. It was observed that energy consumed in carbonation is insignificant compared to the pumping energies in the membrane modules. Energy consumption for scheme A is around

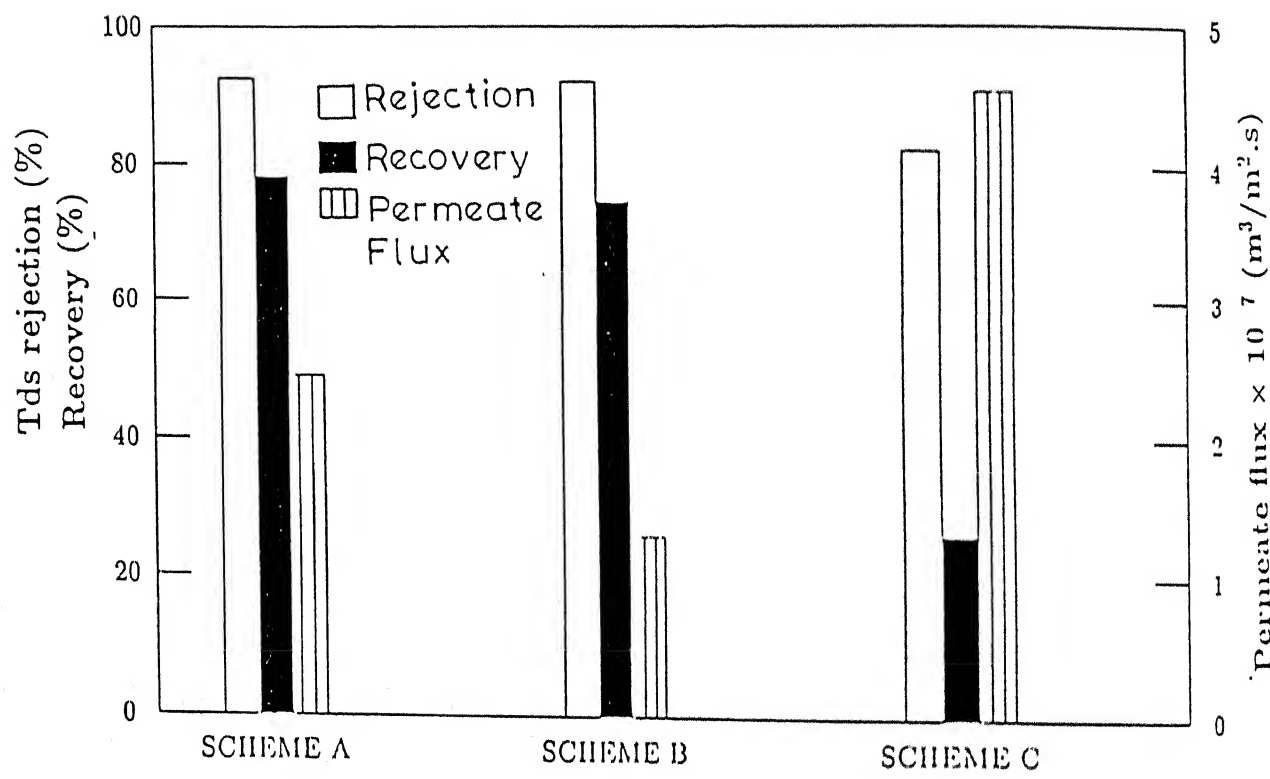


Figure 5.12: Performance of different schemes

300 kJ/kg and that for B and C is around 280 kJ/kg.

5.1.4 Conclusions

From the present study, it can be concluded that carbonation of BL with membrane separation may be a possible route to recover water with inorganics without destroying the organics. The process outlined here may replace expensive as well as polluting equipment, used in the conventional kraft process plant.

Carbonation of BL helps in releasing bound alkali chemicals to the bulk. Study of the carbonation of BL reveals that the overall decay of concentration of active alkali obeys a first order type rate law. This may help to estimate time required to attain an extent of carbonation.

Carbonation followed by UF and NF proved to be better than carbonation with RO or direct NF of BL. Scheme A shows better results in terms of inorganic recovery and permeate quality. Inorganics recovery can further be increased by choosing a suitable NF membrane with pores slightly bigger than the one used in this study. This should enhance permeate flux at the expense of slight permeate quality (tds may increase).

5.2 Removal of phenol by micelle enhanced ultrafiltration

Separation of trace amount of phenol from an aqueous stream by solubilizing it in surfactant micelles and subsequently separating them using an ultrafiltration membrane are discussed in this section.

5.2.1 Introduction

One of the most long standing problems confronting chemical engineers and separation scientists is the removal of toxic organic solutes present in trace quantity from aqueous streams. Membrane separation processes while attracting in principle, are not found to be desirable when being employed directly. Membranes, capable of passing water and rejecting organic solutes are simply not available due to their incompatibility. Extensive research is being carried out world wide to develop membranes, particularly inorganic membranes, to fulfill this inadequacy. However, much success is yet to come. Fixed bed adsorption is the most conventional process for such separations but the process neither selective nor energy efficient. Other alternate processes such as distillation or solvent extraction are apparently even more unattractive.

Micellar enhanced ultrafiltration (MEUF) is a recently developed technique to remove dissolved organic solutes from waste streams. In this process [228, 277], surfactant is added to the aqueous stream. The surfactants form aggregates of about 50-150 molecules called micelles. The organic solutes tend to solubilize in the interior of the micelles. Some selectivity of solute absorption is possible because of the extent of solubilization that depends not only on the structure of the solubilizate but also that of the surfactant. The micellar solution is filtered through a membrane capable of rejecting micelles. The solubilizate, therefore, is also rejected. The process is versatile enough to include separation of hydrocarbons, recovery and removal of organic acids and amines, and separation and concentration of metal ions [229-232].

Hence, addition of surfactants above its critical micelle concentration (CMC) to water leads to the formation of micelles; organic pollutants are solubilized within the micelle interior and can be removed from the solution by ultrafiltration. A schematic version of MEUF process is shown in Fig. (5.13).

In theory, the concentration of solute and surfactant in the permeate stream should be equal or less than the unsolubilized solute and free surfactant concentration in the retentate. Both these concentrations can be very low, resulting in more or less surfactant free permeate. The retentate stream contains the solubilized solute and the surfactant (in micellar form) in very high concentrations. Therefore, it may be less expensive to dispose off or to treat for the recovery of solute and surfactant. Since, the surfactant and solute generally have vastly different physical properties, they can also be separated [278].

The selection of surfactant is an important criterion in designing separation processes based on MEUF. The binding of hydrophobic solutes to both ionic and nonionic micelles was considered and was shown to be a function of the molecular structure of the surfactants, the concentration of the surfactant and the electrolytic composition of the water [278].

Much works have been carried out in this direction. Several models have been proposed to predict and to provide understanding behind the movement and attachment between the solute and the micelles [139, 229–232]. Markels et al. [279] have recently studied micellar ultrafiltration in an unstirred batch cell at constant flux and in cross flow system [280]. In the former, they have developed an unsteady and in the later, a steady mass-transfer model to describe UF of micellar solution and observed an excellent corroboration between experiments and prediction. The models are able to describe quantitative characterization of the intrinsic membrane rejection properties for both surfactant monomer and micelles, and support the physics at the membrane surface (presumed in the models) which may be useful for the study of MEUF.

In MEUF, it may be assumed that once the solute comes to the surface of the micelles,

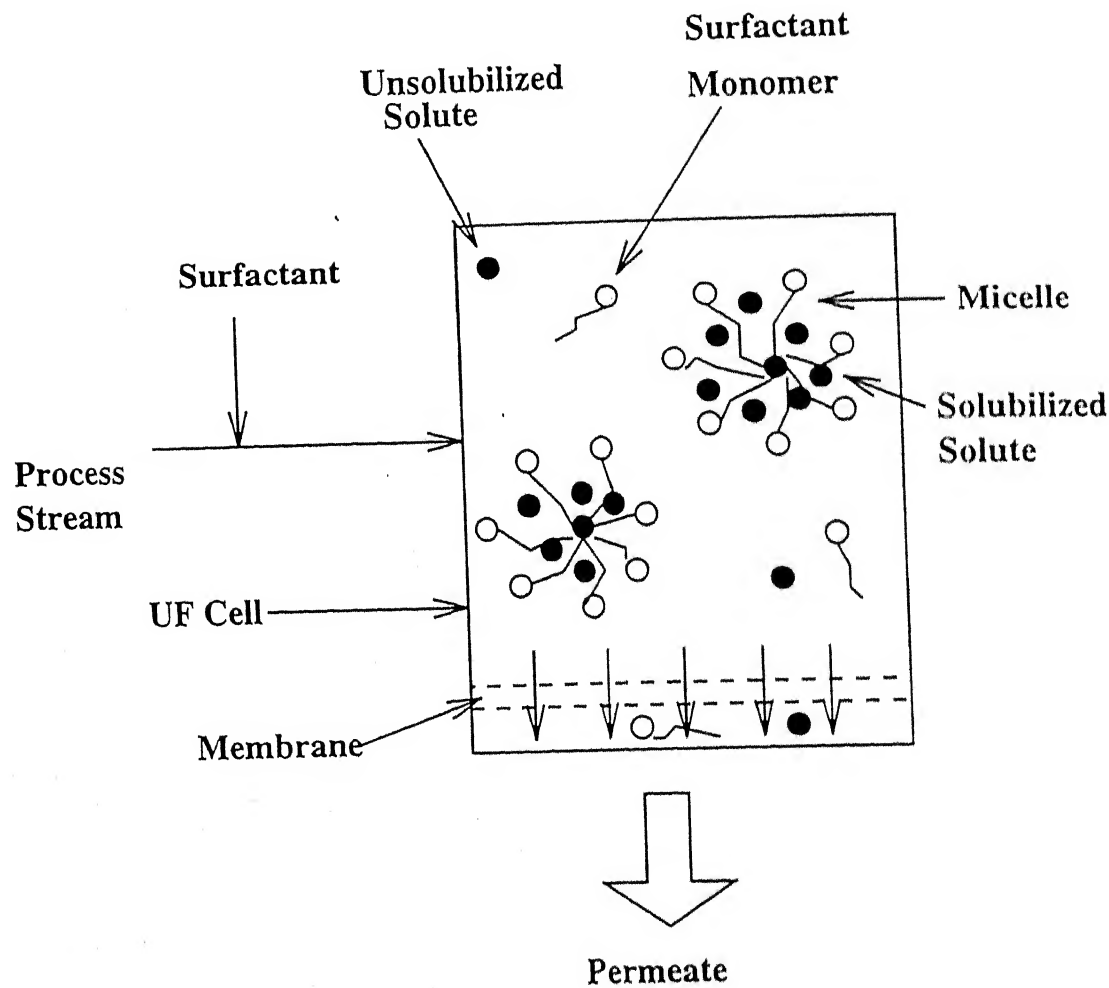


Figure 5.13: Schematic of a typical MEUF process

it moves towards the center of the micelle [281, 282]. Such assumption may allow us to incorporate the mass transfer phenomena for the transport of the solute within the micelles. The present work has been undertaken to study the consumption of organic solute within the micelle and subsequent UF of the resultant solution.

Thus the major broad objectives of the present work is, (1) to carry out an experimental study using different concentrations of a particular organic solute (phenol in water) using different concentrations of surfactant (cetyl pyridinium chloride, cpc) in a stirred and unstirred batch cell at different operating conditions, and (2) to formulate a mathematical description using mass-transfer phenomena for transport of solute from the surface to the interior of the micelle.

5.2.2 Experimental

5.2.2.1 Materials:

Asymmetric cellulose acetate membrane was used for the experiments. The membrane was supplied by Permionics India Ltd., Boroda. It was hydrophilic, anisotropic and compatible in a pH range of 2 to 12. The membrane was approximately 1000 molecular weight cut-off. The water permeability of the membrane was estimated to about $2.3 \times 10^{-11} m^3/N.s.$

Cationic surfactant, Cetyl Pyridinium Chloride was of purity 99.9% obtained from Sigma Chemicals, USA. The organic solute, phenol, was procured from Ranbaxy Laboratories Ltd., India. The surfactant was used as, supplied, without any treatment. All the solutions were prepared using distilled water.

5.2.2.2 Apparatus

The batch cell used was fabricated indigenously. The material of construction was stainless steel. The cell volume was 350 ml. The cell could withstand maximum

1000 kPa pressure. The cell was pressurized using an air compressor of the make, K F Neuberger, Germany. The stirrer speed was measured using a tachometer of the model type-630, Toshniwal, India.

5.2.2.3 Analysis

The concentrations of all the streams were measured using UV spectrophotometer (model Shimadzu, 160). Concentration of CPC was measured at a wavelength of 259 nm and that of phenol at 270 nm. The composition of the mixed stream was measured using a standard procedure as described in the literature [283]. The critical micelle concentration (CMC) of CPC was found to be 0.3 kg/m^3 which confirms the literature cited value [279, 282]. The determination of CMC was carried out by conductivity measurement using a Systronix (model 304) conductivity meter. The shape of the CPC micelles were considered to be spherical, with average aggregation number of about 136 [284]. The hydrodynamic radius of the micelle was reported as 2.5 nm [279].

5.2.2.4 Design of experiments:

Experiments were designed such that the effects of three major independent variables i.e. bulk concentration, pressure differential and stirrer speed, can be properly understood on flux and rejection. During experiments, two variable are held constant while the third was varied to get an exact picture of dependence. The levels of concentration for CPC were chosen as 10.2, 20.4 and 30.6 kg/m^3 ; the pressure was varied as 207, 345 and 483 kPa; and the stirrer speeds were 210, 300, 400 and 540 rpm.

5.2.2.5 Procedure:

Firstly, a fresh membrane was placed on the porous support at the bottom of the cell. The cell was then assembled. The cell was pressurized with distilled water for at least 2 hours at 620 kPa (the pressure was higher than the highest operating pressure) for compacting the membrane. Water flux was continuously measured during this period. Constancy of water flux suggested no further compaction of the membrane. The constant water flux was noted down to calculate membrane permeability. The feed solution was prepared by adding measured amount of surfactant and phenol in half liter of distilled water. The solution was kept under slight stirring for about fifteen minutes; during this time period, the solution became clear. The cell was then filled up with the feed solution. The stirrer speed (for required rpm, for the stirred cell) was adjusted by regulating the voltage supply through a variac. The cell was pressurized to the level of the operating pressure with the help of an air compressor. Cumulative volume of permeate over time was collected in a measuring cylinder to measure flux. Permeate concentrations of surfactant and organic solute were calculated from absorption values using UV spectrophotometer, as mentioned earlier. After each run, the whole cell was rinsed thoroughly with distilled water. The membrane was washed and rinsed with distilled water for at least one hour to remove any deposition. The water permeability of the membrane was measured before the next run. This procedure was repeated for each set of operating conditions. All the experiments were conducted at room temperature ($30 \pm 2^\circ\text{C}$).

5.2.3 Results and Discussions:

This section has been designed into two parts. The first one, consists of the permeate flux and rejection characteristics of the micellar solution in both stirred and unstirred batch cells with respect to the membrane, used in this study. The second part deals with the consumption of phenol in the micelles, distribution of phenol concentration within the micelles and finally, determination of the equilibrium parameter which

dictates the dependence of consumption on the operating conditions.

5.2.3.1 Permeate flux and rejection characteristics of micellar solution for the membrane

For ultrafiltration of micellar solution in an unstirred batch cell, the flux was observed to be almost invariant with time. This trend is shown in Fig. (5.14). It can clearly be observed from the figure that the permeate flux was higher for higher operating pressure for a fixed bulk concentration. For example, for a solution of 10.2 kg/m^3 bulk concentration, permeate flux was observed $4.08 \text{ m}^3/\text{m}^2\text{s}$ at 207 kPa; whereas, flux increases to $5.12 \text{ m}^3/\text{m}^2\text{s}$ for pressure at 345 kPa. For a fixed operating conditions, the spherical micelles, deposit on the membrane surface forming a loosely packed porous layer, the thickness of which grows with time. However, from the experimental observations of the flux data over time suggests that the resistance offered by this growing layer to the transport of the solvent is negligibly small. In an osmo-UF system, the flux can simply be related to the pressure according to Eq. (3.20). Therefore, with increase in pressure, the effective driving force for the transport of the solvent is more for a fixed feed concentration. Hence, permeate flux increases with pressure.

The effect of stirring on the permeate flux for a fixed operating pressure is presented in Fig. (5.15). It is evident from this figure that for a particular operating pressure and feed concentration, flux increase with increase in stirrer speed. Also, for a fixed stirrer speed, flux decreases with increase in bulk concentration. Under stirring, the positions of the micelles on the membrane surface get disturbed; therefore, the fraction of exposed surface area of the membrane to the permeating solution is more. It is more prominent at higher turbulence (higher rpm). This leads to the increase in permeate flux with increase in stirrer speed. With increase in bulk concentration, osmotic pressure of the solution increases; therefore, the effective pressure gradient decreases. Hence, flux decreases with concentration which is clear from Eq. (3.20).

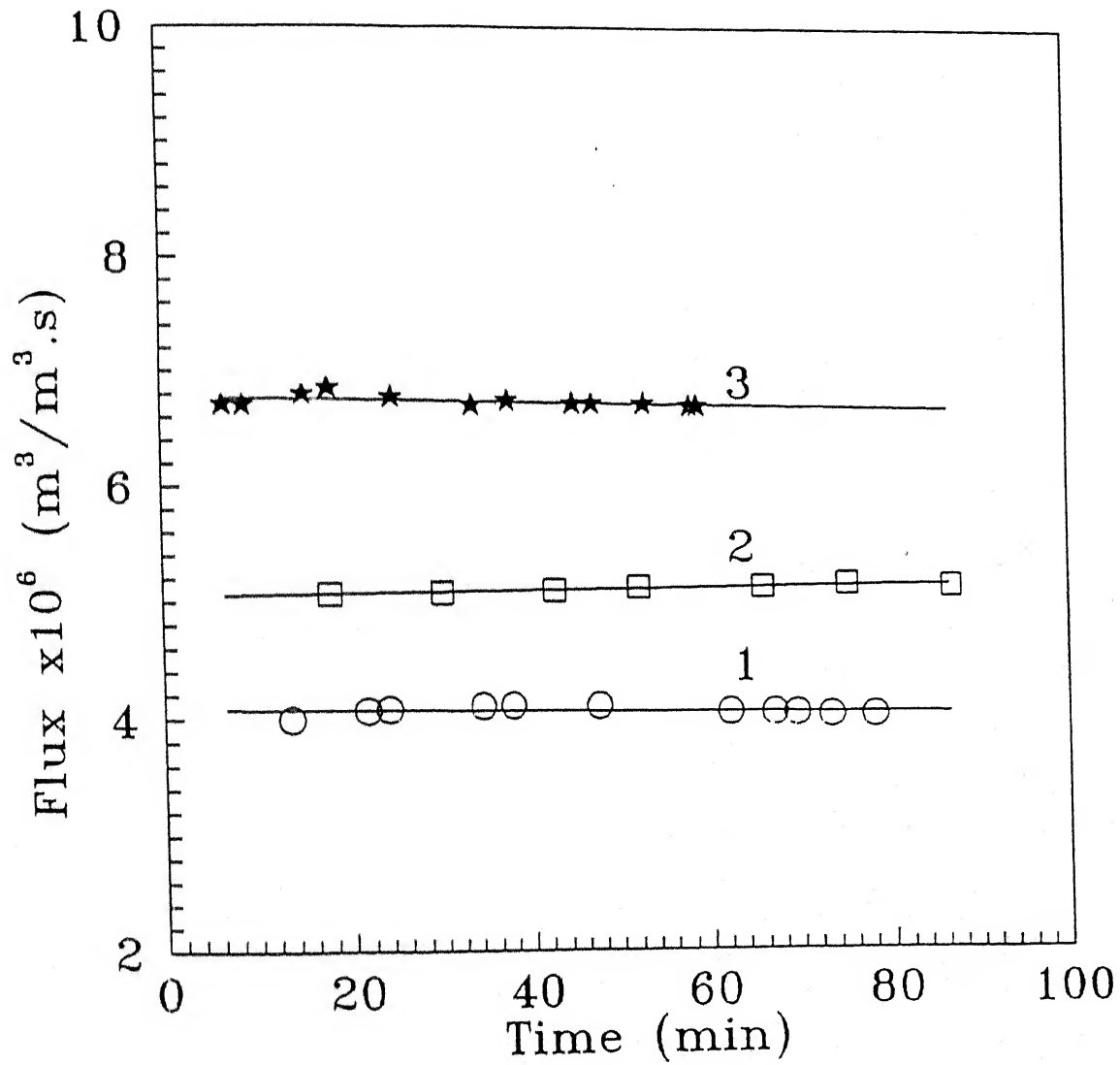


Figure 5.14: Variation of permeate flux with time for CPC solution in unstirred batch cell for $c_0 = 10.2 \text{ kg/m}^3$; 1: $\Delta P = 207 \text{ kPa}$; 2: $\Delta P = 345 \text{ kPa}$; 3: $\Delta P = 483 \text{ kPa}$; symbols are for experimental data.

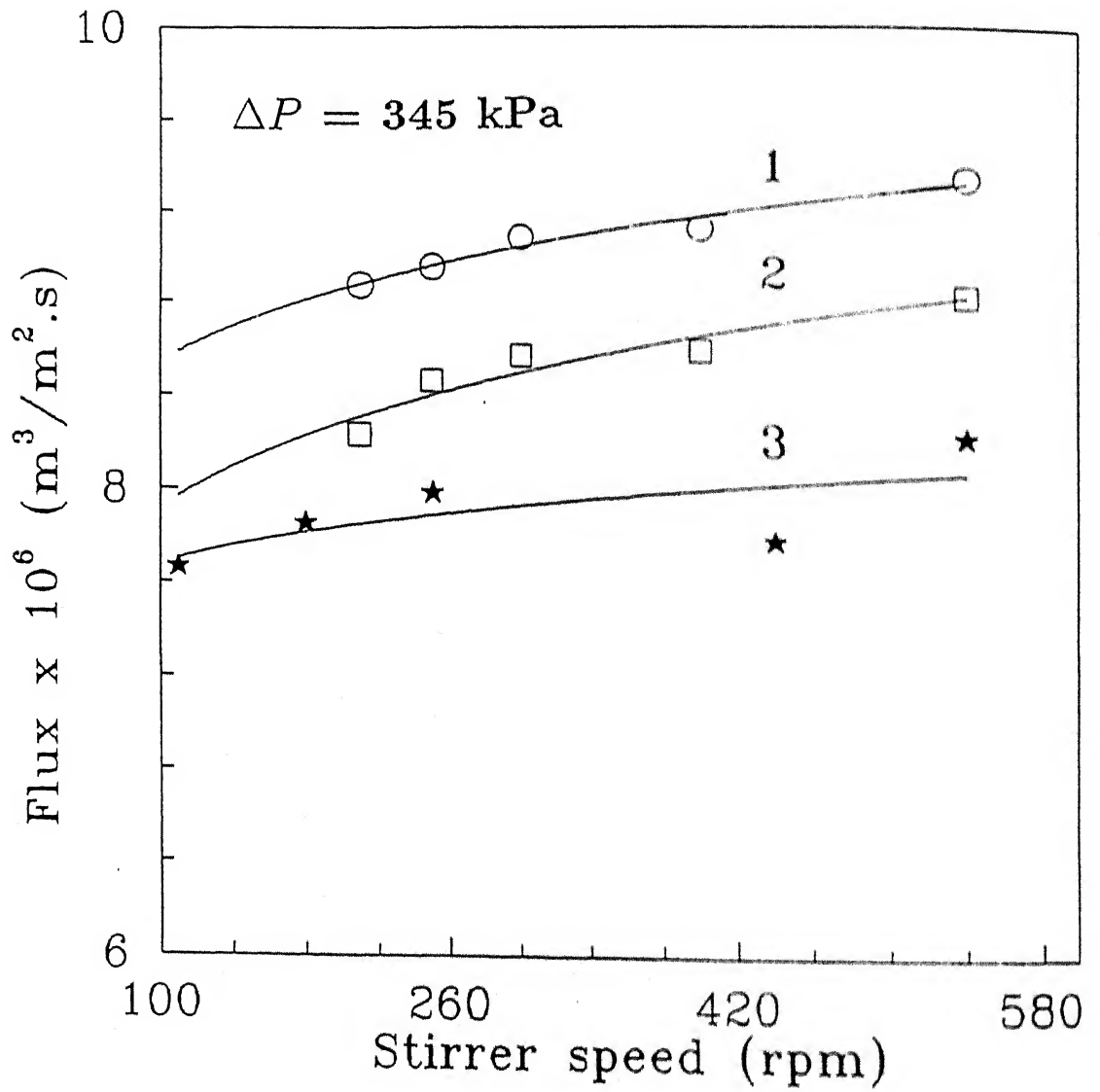


Figure 5.15: Variation of permeate flux with stirrer speed for CPC solution in stirred batch cell. 1: $c_0 = 10.2 \text{ kg/m}^3$; 2: $c_0 = 20.4 \text{ kg/m}^3$; 3: $c_0 = 30.6 \text{ kg/m}^3$; symbols are for experimental data.

From the earlier discussions, it may be stated that stirring increases permeate flux considerably for a fixed operating conditions. This is described in Fig. (5.16). This figure summarizes the comparison of permeate flux for different feed concentrations at 345 kPa pressure in an unstirred and stirred cell at 540 rpm. The trends indicate that stirring at 540 rpm results approximately 1.5 times increment of permeate flux. Also, flux decreases with increase in feed concentration for both the cases. These results may be explained by the earlier discussions.

The permeate concentration of the surfactant for different feed concentrations is shown in Fig. (5.17), under both stirred and unstirred conditions. It may be observed that permeate concentration increases with increase in feed concentration. Also, permeate concentration is more under unstirred situation for a fixed operating conditions. Under unstirred conditions, permeate concentration increases exponentially with the bulk concentration. Whereas, in stirred cell, there is a negligible increase in permeate concentration upto a feed concentration 200 mM; beyond this, permeate concentration increases rapidly. The dynamic behaviour of the micelles on the membrane surface is described in Fig. (5.18) for both flow conditions of the cells. Micelles occupy more or less a fixed location on the membrane surface under unstirred conditions (Fig. 5.18a). This leads to a local concentration gradient between feed and permeate sides which is more prominent at higher bulk concentrations. Due to this concentration gradient, surfactant monomers diffuse at a faster rate to the permeate side, resulting higher concentration. The corresponding situation under stirring is described in Fig. (5.18b). In this case, there is no permanent positions of the micelles on the membrane surface. The micelles are in continuous, random motion. This minimizes the probability of building up of the concentration gradient across the membrane unlike unstirred cell. However, it is observed from the experiments (Fig. 5.17) that this is valid upto 200 mM feed concentration; beyond which the effect of stirring is not felt due to enormous increase in the number concentration of micelles.

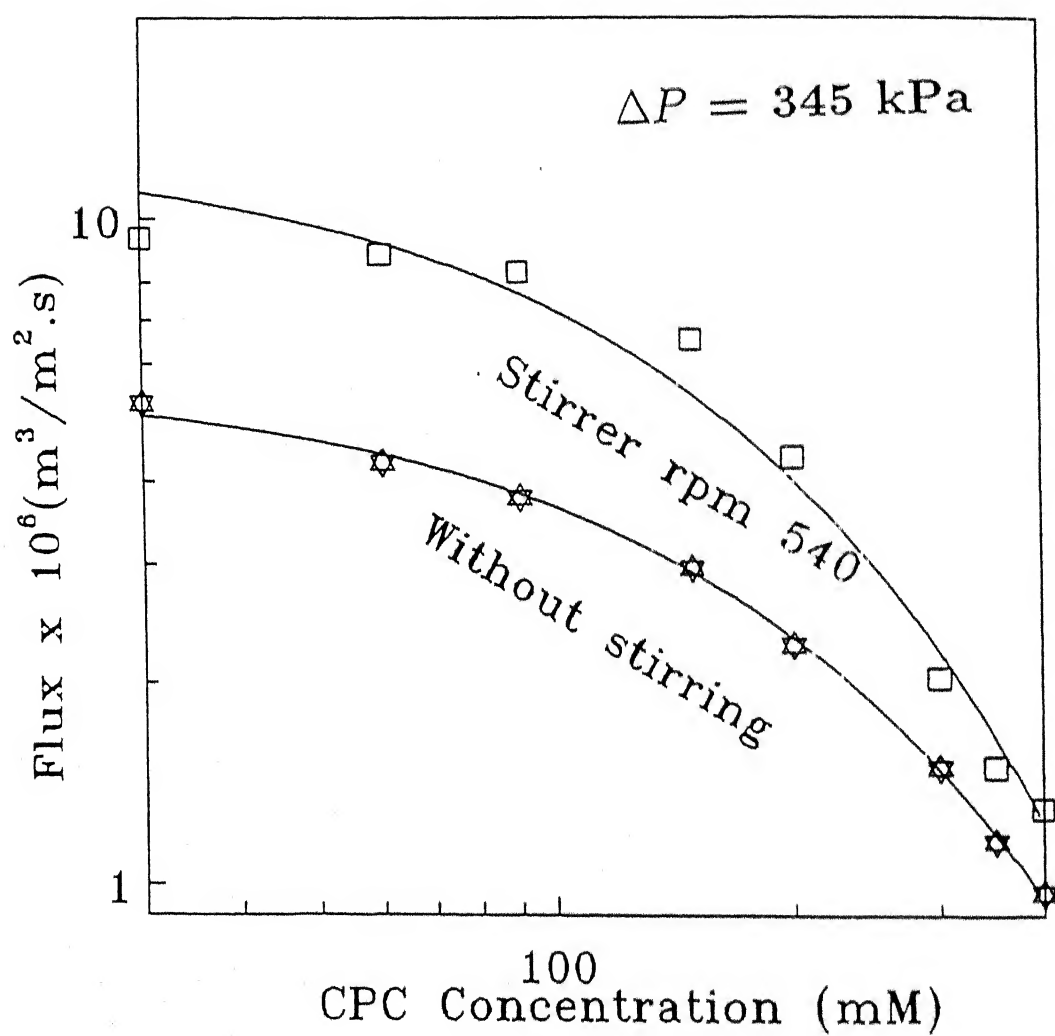


Figure 5.16: Comparison of permeate flux with concentration between stirred and unstirred batch UF; symbols are for experimental data.

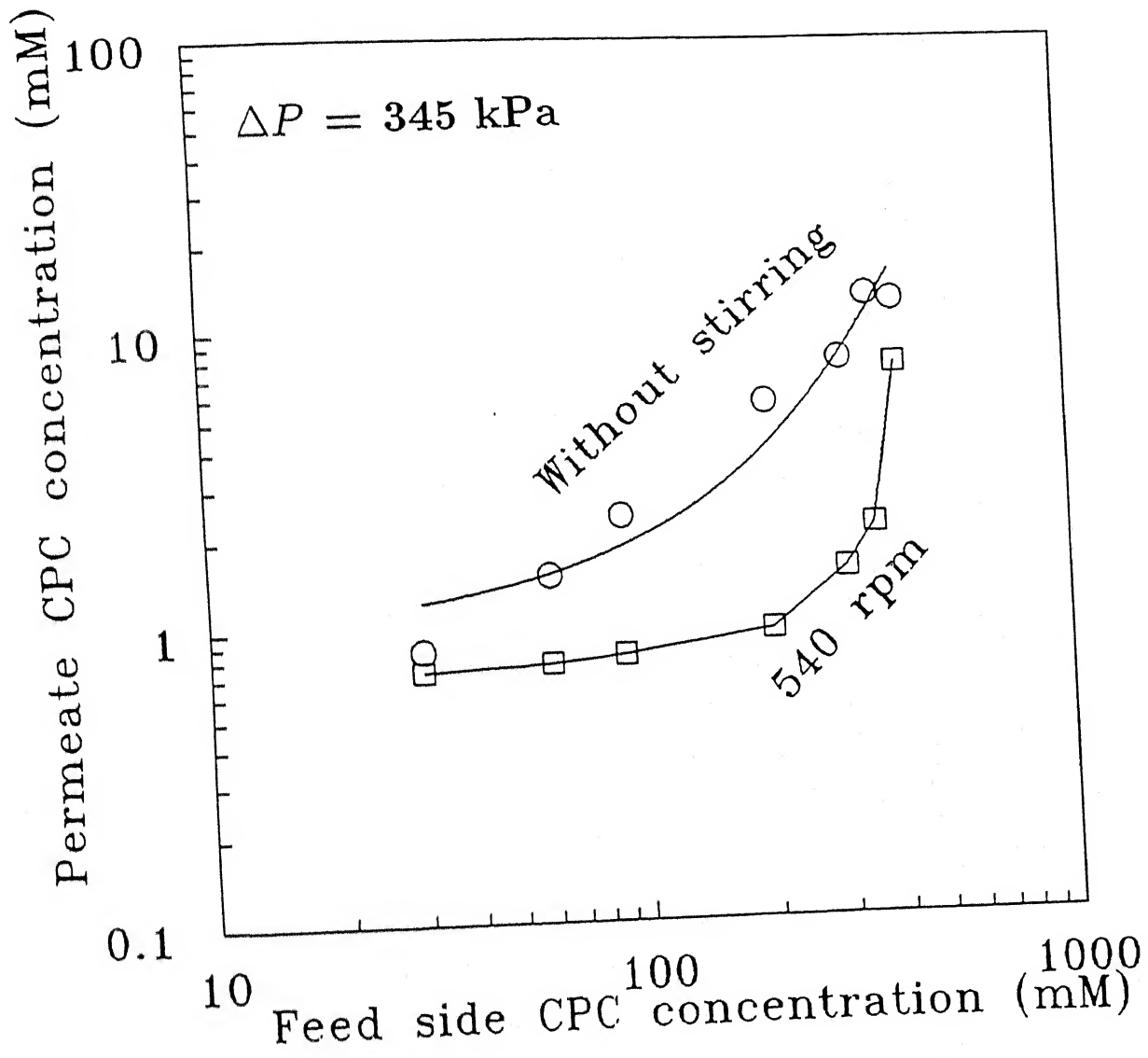


Figure 5.17: Comparison of permeate concentration with feed concentration between stirred and unstirred batch UF ; symbols are for experimental data.

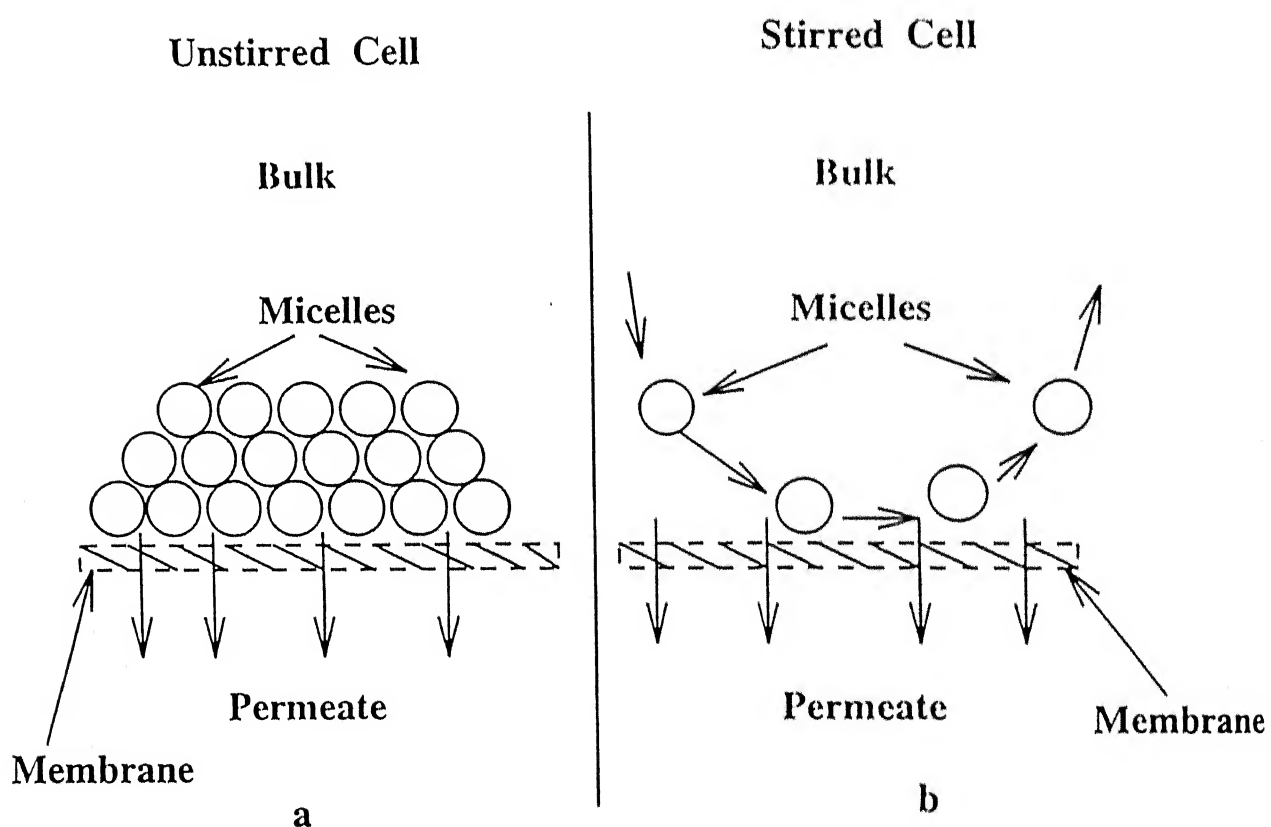


Figure 5.18: Schematic of micelle deposition on the membrane surface. (a): Unstirred cell; (b): Stirred cell.

5.2.3.2 Consumption of phenol within the micelles

In aqueous medium, ionic surfactants produce charged micelles with polar head groups aligning towards the bulk of the solution and apolar tail groups aligning away from the solution. This arrangement makes a polar and a non-polar environment outside and inside of the micelle, respectively. Charged pollutants of counter ions get adsorbed on the micelle surface and non-polar solutes get solubilized within the hydrophobic interior of the micelle.

The present work deals with the solubilization of phenol within the CPC micelles. It may be assumed that the unsolubilized phenol in the bulk passes freely through the membrane. Therefore, phenol concentration in the permeate stream gives the concentration of the unsolubilized phenol in the bulk [228]. In unstirred cell, the variation of phenol consumption with feed CPC to phenol ratio for different operating pressures is presented in Fig. (5.19). The figure reveals two interesting trends. Firstly, for a particular pressure, percentage consumption of phenol increases rapidly and then gradually (eventually reaching a plateau) with increase in CPC to phenol ratio in the bulk. Secondly, for a particular combination of CPC and phenol, percentage consumption increases with decrease in pressure. With increase in feed side CPC concentration, the number of micelles in the solution increases. This enhances the net consumption of phenol. At higher concentrations, the feed solution starts getting saturated by the micelles. Therefore, the phenol consumption attains almost a constant value at higher CPC to phenol ratio. With increase in pressure, the micelles become more compact and hence, the solute holding capacity of the micelles decrease [282]. This leads to decrease in consumption at higher pressure. From the figure, it may be observed that the phenol consumption is optimum at CPC to phenol ratio in the feed, around 30. Interestingly, this optimal value of CPC to phenol ratio is independent of the operating pressure.

For proper understanding of the extent of solubilization of the solute in a micelle, the solute distribution in the micelle phase should be investigated. The solute is

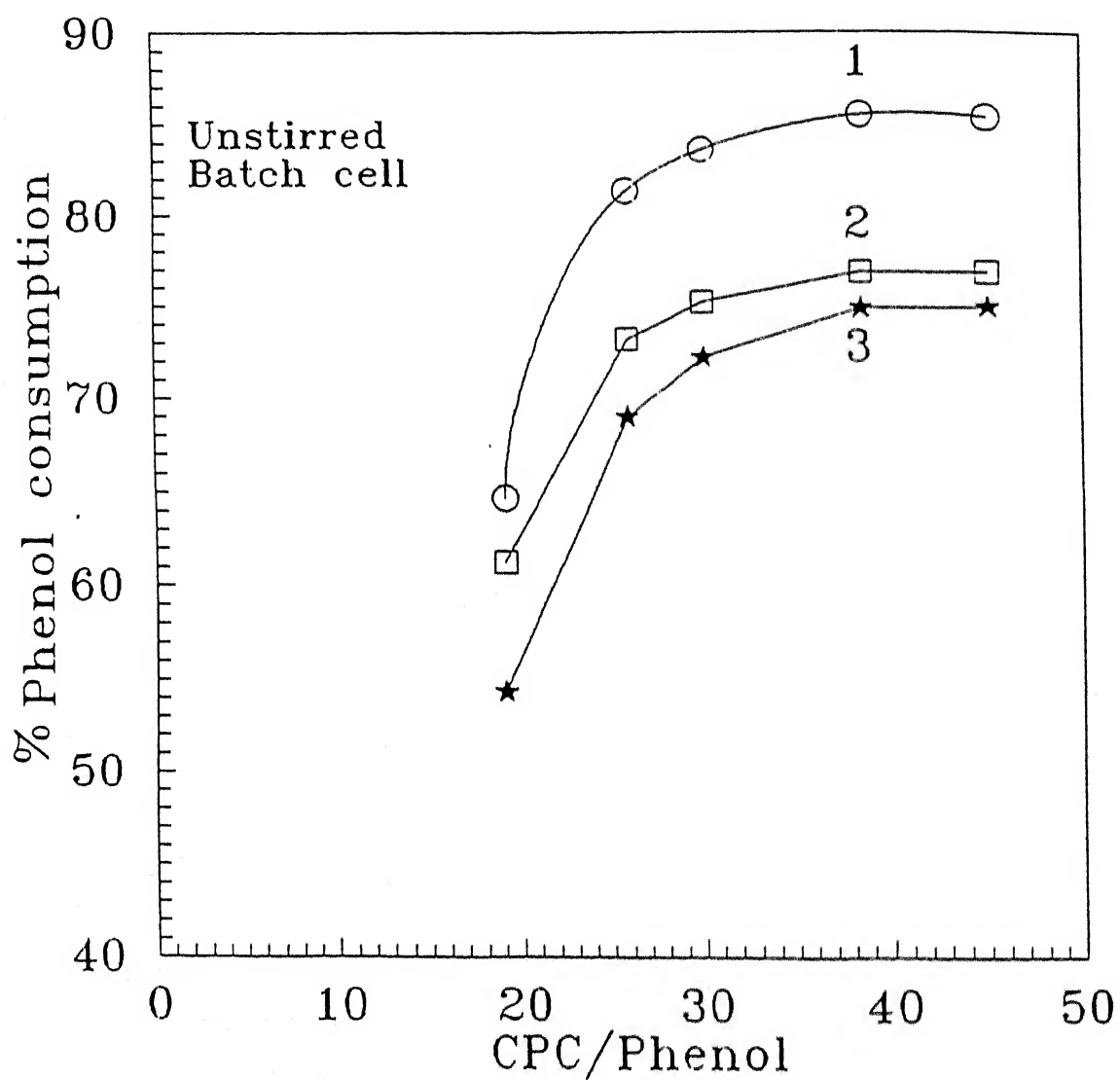


Figure 5.19: Variation of phenol consumption with CPC to phenol ratio in the bulk. 1: $\Delta P = 207$ kPa; 2: $\Delta P = 345$ kPa; 3: $\Delta P = 483$ kPa ; symbols are for experimental data.

distributed between the bulk aqueous phase and micelle phase through an equilibrium parameter which may be a function of the operating conditions; namely, initial and unsolubilized solute concentration, pressure, extent of micellization, etc. So, we attempt a simplified mathematical description of the solute distribution within a spherical micelle.

The relevant assumptions taken in this study to have a realistic description of solute distribution are as follows: (a) Time averaged aggregation number of the micelle is constant and it is 136 in the present case [284]; (b) The diffusion of solute is only due to polar and nonpolar interactions; (c) Diffused solute front advances like the reaction front similar to a gas-solid reaction as in unreacted core model [285]; (d) Physical properties of the micelles and the solute are constant; (e) Distribution of solute in stern layer is negligible. Since, both cationic and anionic surfactants have a strong affinity for water, the head groups may get spaced out to attain maximum solvation by water. Therefore, stern layer may be assumed to be polar in nature; (f) No reaction between surfactant and solute molecules; (g) The time scale of diffusion of solute is of the order of nano seconds [282]; (h) Solute distribution is symmetrical with respect to θ and ϕ coordinate as in Fig. (5.20).

The diffusion controlled solute mass balance equation at steady state in spherical polar coordinate with the above assumptions can be written as:

$$D \left[\frac{1}{r^2} \frac{\partial}{\partial r} \left(r^2 \frac{\partial c}{\partial r} \right) \right] = 0 \quad (5.4)$$

The solution of Eq.(5.4) can be expressed as,

$$c(r) = -\frac{K_1}{r} + K_2 \quad (5.5)$$

In order to solve Eq.(5.5), two boundary conditions should be specified to evaluate K_1 , and K_2 . At $r = R$ i.e. on micelle phase boundary (neglecting the Stern layer thickness), the solute concentration is in equilibrium with the unsolubilized free phenol concentration in the bulk phase. If c_p is the free phenol concentration in the bulk phase (which is also equal to permeate concentration of phenol) and c_s is the

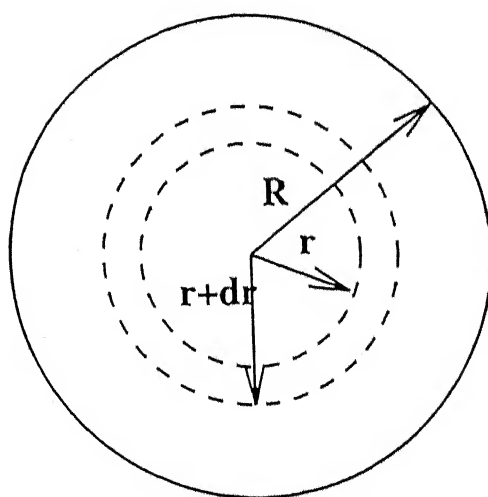


Figure 5.20: Distribution of organic solute in the micelle phase.

phenol concentration in the micelle phase at $r = R$ and the system is in equilibrium, then we can write,

$$c_s = Hc_p \quad (5.6)$$

where, H is the equilibrium parameter. Within the micelle, organic solute tends to move towards the hydrophobic core, like the transport under a potential field. Therefore, at the center of the micelle, we can fix the following boundary condition,

$$c = \text{finite at } r = 0 \quad (5.7)$$

The physical boundary condition given by Eq.(5.7) forces K_1 in Eq.(5.5) to be zero for a bounded solution. Therefore, Eq.(5.5) becomes,

$$c(r) = K_2 \quad (5.8)$$

Hence, solute is uniformly distributed throughout the micelle. Using the boundary condition given by, Eq.(5.6),

$$c(R) = K_2 = c_s = Hc_p \quad (5.9)$$

Therefore, the average solute concentration in the micelle can be expressed as,

$$\bar{c} = K_2 = c_s = Hc_p \quad (5.10)$$

5.2.3.3 Analysis of the results:

The solute mass balance for a unit volume can be written as,

$$c_o = c_p + \Phi_s \bar{c} \quad (5.11)$$

Substituting the value of \bar{c} from Eq.(5.10) into Eq.(5.11), we can obtain,

$$c_o - c_p = \Phi_s Hc_p \quad (5.12)$$

and hence,

$$H = \frac{1}{\Phi_s} \left(\frac{c_o}{c_p} - 1 \right) \quad (5.13)$$

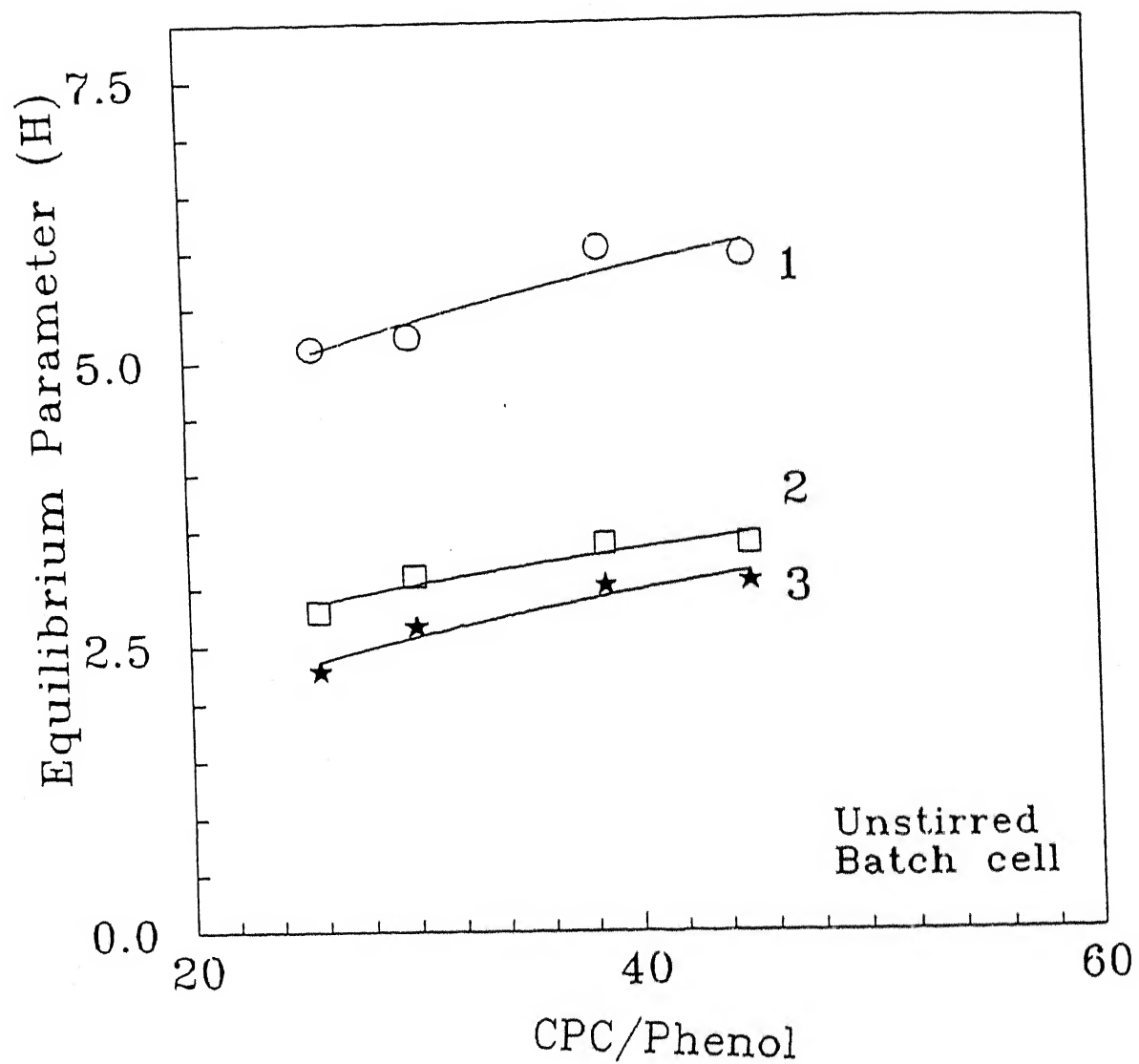


Figure 5.21: Variation of equilibrium parameter with CPC to phenol ratio for different pressure in unstirred batch cell. 1: $\Delta P = 207$ kPa; 2: $\Delta P = 345$ kPa; 3: $\Delta P = 483$ kPa ; symbols are for experimental data.

From Eq.(5.13), it is obvious that the equilibrium parameter H is a function of feed and unsolubilized phenol concentrations and extent of micellization. In a pressure driven membrane separation process, H should be a function of pressure. This is shown in Fig. (5.21). The figure indicates that H decreases as pressure increases. This is explained by reduction of solute consumption capacity of micelles at higher pressures as discussed earlier. For a given feed CPC to phenol ratio and operating pressure, H can be evaluated from Fig. (5.21) and using that H value, one can easily obtain c_p , i.e. unsolubilized (or permeate) phenol concentration from Eq.(5.13). Therefore, H may be considered as a true reflection of the efficiency for MEUF processes.

The solubilization of a partially charged organic solute like phenol in a charged micelle is a complex phenomena owing to polar, non-polar interactions. The micellar shape and size as well as interior configuration of surfactant monomers in the micelle affect the solubilization. The present work, therefore, provides a simplistic analysis for an overall quantitative description of MEUF process.

5.2.4 Conclusions

Constant flux was observed during an experimental run under a fixed applied pressure and bulk CPC concentrations, suggesting negligible effects of concentration polarization. Increase in pressure increases the monomer concentration in the permeate side. Stirring during MEUF improves permeate flux. However, the effect of stirring was limited upto 200 mM CPC concentration at 540 rpm. Increase in pressure decreases the solute containing capacity of the micelles. Maximum solute consumption within micelles was also observed to be controlled by a optimum surfactant/solute ratio (30). Theoretical development of the concentration profile within micelle suggested that there is a uniform distribution of the solute throughout the micelle. A simple design criterion for determination of the efficiency of MEUF process is outlined by obtaining a relationship between operating conditions and equilibrium parameter (H).

Chapter 6

General conclusions and recommendations

In a topic like studies on flux and retention characteristics during UF, several aspects of concentration polarization could have been addressed with proper theoretical perspectives alongwith experimental observations. Incorporation of different flux decline mechanisms are essential from a designer's point of view. In light of this, among some of the major aspects of the studies on consequences of concentration polarization, following may be listed and categorized into:

- (i) osmotic pressure controlled, gel layer controlled as well as osmotic and gel layer transition controlled UF process studies;
- (ii) incorporation of wide variations of properties with concentration and solute environment (since it is well known that macromolecular solutions are highly non-ideal) for accurate predictions of concentration polarization. These property variations are essentially due to interactions between the molecules;
- (iii) solute-membrane interactions affecting the rejection, thereby affecting the extent of concentration polarization [180]; hence, the role of surface interactions during UF;
- (iv) development of predictive models to provide more physical significance to the existing simple models generally developed with the specific adjustable parameters which lack physical significance. Further, these existing models may vary with the operating conditions, nature of the solutes and the membranes;

(v) to simplify, yet accurate, predictive models and solution techniques (theoretical or semi-empirical) for efficient design of UF process to cover various consequences of concentration polarization;

and, (v) finally, development of closer predictive models for better design of units using industrial effluents - essentially specific design case-studies.

The present work, however, could attempt some of the above major aspects. Modeling of concentration polarization for osmotic pressure controlled mechanism under the framework of boundary layer theory is addressed for the purpose of characterization of flux and retention behaviour of solutes. Comparisons of existing boundary layer solutions as well as development of several new techniques of such problems, have been successfully attempted in chapter 3. Performances of these solutions were evaluated in terms of their simplicities and accuracies. In particular, the developed generalized integral method can predict the flux decline and retention behaviour simultaneously with a proper choice of concentration profile. Apart from being less computational intensive, it gives as accurate solution as that obtained by detailed numerical techniques. However, inclusion of solute adsorption aspect by the membrane, where adsorption may occur during the process, would have given a closer picture of flux decline during UF.

In any membrane processes, it is observed that the flux decline is rapid initially and gradual later on. A semi-empirical approach to model such realistic situation has also been addressed. However, the approach presented is limited by the accuracies involved in the experimental determination of variations of properties with concentrations. Hence, more sophisticated experimentations are desired for the development of such models.

In an important attempt, a two component model for prediction of flux and retention was developed. Such models are useful for gel layer controlled UF. However, this method can only be successful for known compositions and physical properties of the feed solution. Further, such models can be close predictive once the exact study of partition coefficient was carried out between permeating and non-permeating

solutes.

Modified Sherwood number relations were obtained from first principles for different modules incorporating effects of suction in laminar flow regime. However, this theoretical approach could not be extended to turbulent flow regime due to complications of existing theories of turbulence. Therefore, a semi-empirical approach was adopted to obtain modified Sherwood number relations in turbulent as well as in laminar flows. Modifications of these Sherwood number relations, incorporating the effects of property variations, would further make the relations more complete.

The final major aspect of concentration polarization on flux and retention behaviour is to attempt case studies. Recovery of water and inorganic chemicals from kraft BL using membrane separation processes was successfully attempted. The process outlined (section 5.1), may replace expensive as well as polluting equipment used in the conventional kraft processing plant. Carbonation of BL, in particular, helped in releasing bound alkali chemicals to the bulk. Further, in another attempt, removal of phenol from aqueous streams through micellar enhanced UF was investigated. However, detailed experimentations and their implications are necessary to develop a full-proof technology in this context.

Appendix A

Membrane characteristics

Water permeabilities of the low rejecting membrane was $2.46 \times 10^{-11} \text{ m}^3/\text{N.s}$ and that of the high rejecting membrane was $6.56 \times 10^{-12} \text{ m}^3/\text{N.s}$. Further, rejection characteristics for both the membranes were evaluated with five standard solutes at a concentration 0.5 % (w/v) under 550 kPa and at a high turbulence (500 rpm) in a batch cell. The solutes used to characterize the membranes were a) glycerol (molecular weight 92), obtained from *Ranbaxy Laboratories Ltd., India*, b) dextrose (molecular weight 180), obtained from *Saravai Chemicals, Boroda*, c) sucrose (molecular weight 342), obtained from *BDH Chemicals, England*, d) PEG (molecular weight 600), obtained from *Hopkins Willams Ltd., England*, e) PEG (molecular weight 4000), obtained from *Fluka, Germany*. The characteristic solute rejection curves for both the membranes are presented in Fig. (A.1).

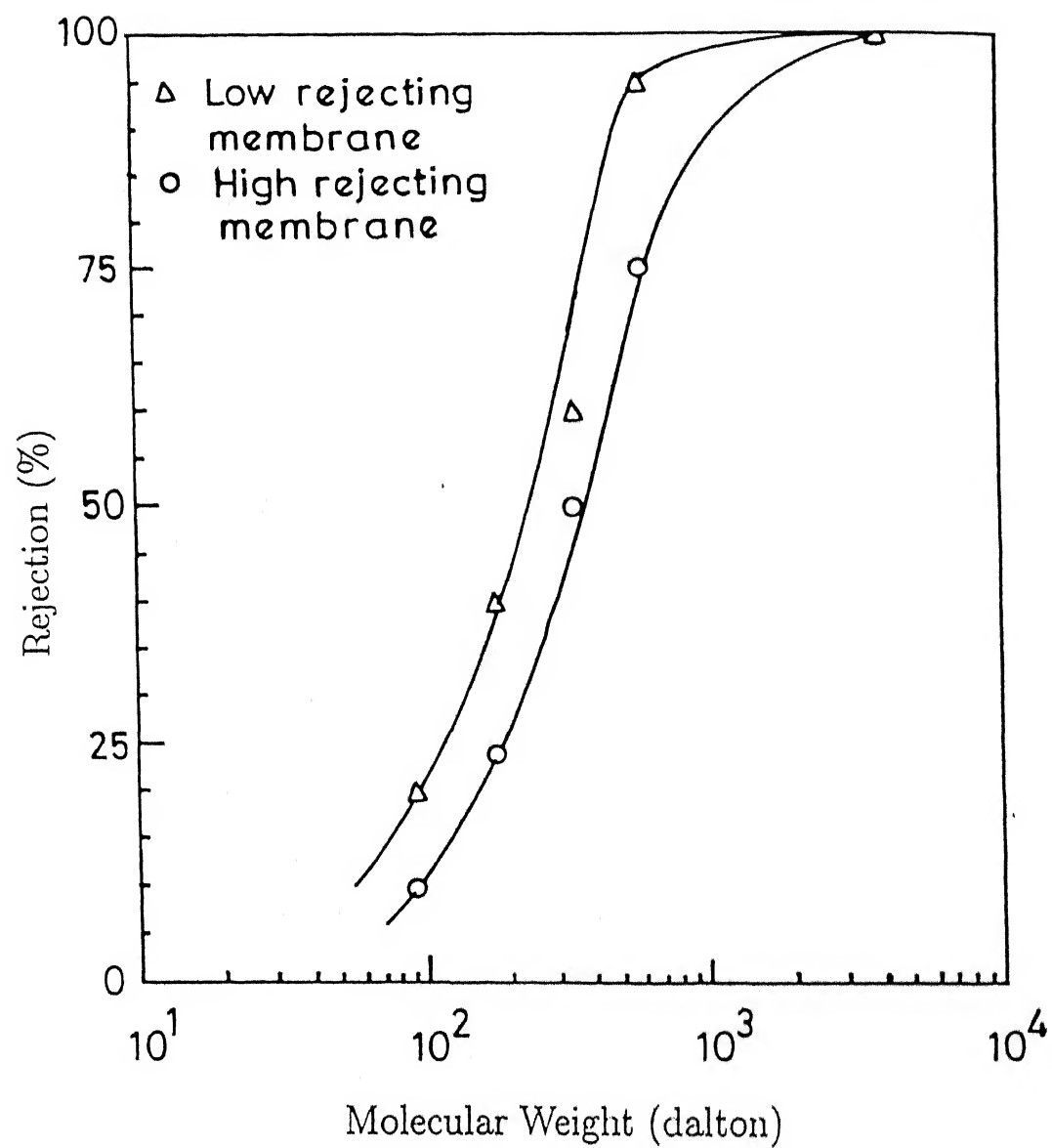


Figure A.1: Rejection curves for the membranes

Appendix B

Physical properties of the solutes

B.1 Viscosity

Viscosities of different solutes were measured in the laboratory and were correlated as polynomial function of concentration.

PEG 6000

$$\mu = 0.85 + 0.145c + 0.027c^2 - 4.276 \times 10^{-3}c^3 + 2.840 \times 10^{-4}c^4 \quad (\text{B.1})$$

BL

$$\mu = 0.85 + 0.062c - 1.117 \times 10^{-2}c^2 + 1.98 \times 10^{-3}c^3 \quad (\text{B.2})$$

where, c is in gm of solutes in 100 ml of solution, μ is in cp.

PVP 10000

$$\mu = 8.5 \times 10^{-4} - 2.5135 \times 10^{-6}c + 1.4447 \times 10^{-7}c^2 \quad (\text{B.3})$$

PEG 4000

$$\mu = 8.5 \times 10^{-4} + 8.9751 \times 10^{-6}c - 5.9031 \times 10^{-9}c^2 \quad (\text{B.4})$$

where, c is in kg/m³ and μ is in Pa-s.

B.2 Density

Densities of different solutions were measured in the laboratory and were correlated as polynomial function of concentration.

PEG 6000

$$\rho = 0.995 + 0.278 \times 10^{-4}c - 0.982 \times 10^{-8}c^2 \quad (\text{B.5})$$

BL

$$\rho = 0.995 + 0.438 \times 10^{-4}c + 0.398 \times 10^{-5}c^2 \quad (\text{B.6})$$

PVP 10000

$$\rho = 0.995 + 6.34 \times 10^{-5}c + 6.84 \times 10^{-7}c^2 \quad (\text{B.7})$$

PEG 4000

$$\rho = 0.995 + 1.096 \times 10^{-4}c + 3.84 \times 10^{-7}c^2 \quad (\text{B.8})$$

where, c is in gm of solutes in 100 ml of solution and ρ is in gm/ml.

Density and viscosity for dextran were obtained from Gill et al. [144].

B.3 Diffusivity

The diffusion coefficients of the PEG 6000, 4000, PVP 10,000 and BL were obtained from the empirical equation for a polymeric solution [286]. Diffusivity of dextran (T20), sucrose and PVA were obtained from the literature. The values of diffusivities for different solutes are listed in Table B.1.

B.4 Osmotic pressure

The data of experimental osmotic pressures at different concentrations for PVP and sucrose solutions were taken from the literature [238, 287] and fitted in the following correlations (with correlation coefficient more than 0.99), for PVP,

$$\pi = (89.642c + 1.46c^2 + 0.0158c^3) \quad (\text{B.9})$$

and for sucrose,

$$\pi = 3.77 \times 10^3 c + 38.79c^2 - 0.04c^3 \quad (\text{B.10})$$

where, π is in Pa and c is in Kg/m³.

Table B.1: Diffusion coefficients of different solutes

Solute	Diffusivity $\times 10^{10} m^2/s$
PEG 6K [286]	1.50788
PEG 4K [286]	1.726
PVP 10K [286]	1.272
BL [286]	2.43143
Dextran T20 [255]	0.675
PVA 52K [254]	0.28
Sucrose [287]	5.24

Osmotic pressure for dextran was obtained from the correlation developed by Wijmans et al. [154], which is given as,

$$\pi = (0.375c + 7.52c^2 + 76.4c^3) \times 10^5 \quad (\text{B.11})$$

where, π is in Pa and c is in gm/ml.

Osmotic pressure for PEG and BL were calculated from Flory's Eq. [257] as,

$$\pi = -\left(\frac{RT}{V_1}\right)\left[\ln\gamma_1 + \left(1 - \frac{1}{x}\right)\gamma_2 + x_1\gamma_2^2\right] \quad (\text{B.12})$$

where, $x = (v_2M_2)/(v_1M_1)$. v_1 and v_2 are the specific volumes and M_1 and M_2 are the molecular weights of the solvent and the polymer, respectively. γ_1 and γ_2 are concentration dependent terms described by, $\gamma_2 = c/\rho_2$ and $\gamma_1 = 1 - \gamma_2$.

Here, c is concentration and ρ_2 is the density of the polymer in the amorphous state; x_1 in the above is a parameter depending upon the nature of the polymer-solvent interaction. The relevant values of the parameters for PEG and BL were obtained from [113].

Bibliography

- [1] M. Cheryan, Ultrafiltration Handbook, Technomic Publishing Co., Lancaster, PA, 1986.
- [2] R. Rautenbach and R. Albrecht, Membrane Processes, John Wiley and Sons, NY, 1986.
- [3] G. Belfort, Synthetic Membrane Processes, Academic Press, NY, 1984.
- [4] P. Aptel and M. Clifton, Ultrafiltration, in P. M. Bungay, H. K. Lonsdale and M. N. de Pinho, Eds., Synthetic Membranes: Science, Engineering and Applications, D. Riedel Publishing Co., Dordrecht, Holland, 1986.
- [5] A. S. Michaels, Fifteen years of ultrafiltration: Problems and future promises of an adolescent technology, In A. R. Cooper, Ed., Ultrafiltration Membranes and Applications, Plenum Press, NY, 1980.
- [6] G. B. vanden Berg and C. A. Smolders, Flux decline in ultrafiltration process, Desalination, 77 (1990) 101.
- [7] A. S. Michaels, New separation technique for chemical process industry, Chem. Eng. Prog., 64 (1968) 32.
- [8] R. H. Davis and S. A. Birdsell, Hydrodynamic model and experiments from cross flow microfiltration, Chem. Eng. Commun., 49 (1987) 217.

- [9] R. F. Probstein, J. S. Shen, and W. F. Leung, Ultrafiltration of macromolecular solutions at high polarization in laminar channel flow, *Desalination*, 24 (1978) 1.
- [10] D. G. Thomas, Forced convection mass transfer in hyperfiltration at high fluxes, *Ind. Eng. Chem. Fundam.*, 12 (1973) 396.
- [11] S. Illias and R. Govind, Potential applications of pulsed flow for increasing concentration polarization in ultrafiltration, *Sep Sci. Technol.*, 25 (1990) 1307.
- [12] J. A. Howell, R. W. Field and D. Wu, Yeast cell microfiltration: Flux enhancement in baffled and pulsatile flow systems, *J. Membrane Sci.*, 80 (1993) 59.
- [13] V. G. J. Rodgers and R. E. Sparks, Effect of transmembrane pressure pulsing on concentration polarization, *J. Membrane Sci.*, 68 (1992) 149.
- [14] C. C. Hermann, High frequency excitation and vibration studies on hyperfiltration membranes, *Desalination*, 42 (1982) 329.
- [15] H. B. Winzeler and G. Belfort, Enhanced performance for pressure-driven membrane processes: The argument for fluid instabilities, *J. Membrane Sci.*, 80 (1993) 35.
- [16] G. Belfort, Fluid mechanics in membrane filtration: Recent developments, *J. Membrane Sci.*, 40 (1989) 123.
- [17] F. F. Stengaard, Characteristics and performance of new types of ultrafiltration membranes with chemically modified surfaces, *Desalination*, 70 (1988) 207.
- [18] S. N. Jagannadh and H. S. Muralidhara, Electrokinetics method to control membrane fouling, *Ind. Eng. Chem. Res.*, 35 (1996) 1133.
- [19] D. R. Trettin and M. R. Doshi, Pressure Independent Ultrafiltration - is it Gel Limited or Osmotic Pressure Limited?. In A. F. Turbak, editor, *Synthetic Membranes Vol II: Hyper and Ultrafiltration Uses*, ACS Symp. Ser. no. 154, 1981.

- [20] J. S. Shen and R. F. Probstein, On the prediction of limiting flux in laminar ultrafiltration of macromolecular solutes, *Ind. Eng. Chem. Fundam.*, 16 (1977) 459.
- [21] E. Mathiasson, The role of macromolecular adsorption in fouling of ultrafiltration membranes, *J. Membrane Sci.*, 16 (1983) 23.
- [22] M. Abdul Mazid, Separation and fractionation of macromolecular solutions by ultrafiltration, *Sep. Sci. Technol.*, 23 (1988) 2191.
- [23] V. Gekas and B. Hallstrom, Microfiltration membranes: Crossflow transport mechanisms and fouling studies, *Desalination*, 77 (1990) 175.
- [24] W. F. Blatt, A. Dravid, A. S. Michaels, and L. Nelson, Solute polarization and cake formation in membrane ultrafiltration: causes, consequences and control techniques, in *Membrane science and technology*, Flinn, J. E. (Ed.), Plenum press, New York, (1970) 47.
- [25] R. E. Treybal, *Mass Transfer Operations*, McGraw-Hill, NY, 1985.
- [26] G. B. vanden Berg, Racz, I. G. and C. A. Smolders, Mass transfer coefficients in cross flow ultrafiltration, *J. Membrane Sci.*, 47 (1989) 25.
- [27] V. Gekas and B. Hallstrom, Mass transfer in the membrane concentration polarization layer under turbulent cross flow. I. Critical literature review and adaptation of existing Sherwood correlations to membrane operations, *J. Membrane Sci.*, 80 (1987) 153.
- [28] H. K. Lonsdale, The growth of membrane technology, *J. Membrane Sci.*, 10 (1982) 81.
- [29] B. S. Parekh (Ed.), *Reverse Osmosis Technology: Application for high purity water production*, Mercel Dekker, NY, 1988.

- [30] S. Bruin, A. Kikkert, J. A. G. Weldring and J. Hiddink, Overview of concentration polarization in ultrafiltration, *Desalination*, 35 (1980) 223.
- [31] E. Mathiasson and B. Sivik, Concentration polarization and fouling, *Desalination*, 35 (1980) 59.
- [32] S. P. Palecek and A. L. Zydney, Intermolecular electrostatic interactions and their effects on flux and protein deposition during protein filtration, *Biotechnol. Prog.*, 10 (1994) 207.
- [33] P. Aimar, S. Baklouti and V. Sanchez, Membrane - solute interactions: Influence on pure solvent transfer during ultrafiltration, *J. Membrane Sci.*, 29 (1986) 207.
- [34] C. Kleinstreuer and G. Belfort, Mathematical modeling of fluid flow and solute distribution in pressure-driven membrane modules, in G. Belfort (Ed.), *Synthetic Membrane Processes: Fundamentals and water applications*, Academic Press, NY, 1984.
- [35] G. Belfort, Fluid mechanics and cross flow filtration, in H. S. Muralidhara (Ed.), *Advances in Solid-liquid Separation*, Battele Press, Columbus, Ohio, 1986.
- [36] S. Chellam, M. R. Wiesner and C. Dawson, Laminar flow in porous ducts, *Rev. Chem. Eng.*, 11 (1995) 53.
- [37] A. S. Berman, Laminar flow in channels with porous walls, *J. Appl. Phys.*, 24 (1953) 1232.
- [38] S. W. Yuan and A. B. Finckelstein, Laminar pipe flow with injection and suction through a porous wall, *Trans ASME*, 78 (1956) 719.
- [39] P. L. T. Brian, Concentration polarization in reverse osmosis desalination with variable flux and incomplete salt rejection, *Ind. Eng. Chem. Fundam.*, 4 (1965) 439.

- [40] R. H. Davis and J. D. Sherwood, A similarity solution for steady state cross flow microfiltration, *Chem. Eng. Sci.*, 45 (1990) 3204.
- [41] L. Dresner, Boundary layer build-up in the demineralization of salt water by reverse osmosis, Oak Ridge Nat. Lab. Report, (1964) 3621.
- [42] F. Belluci and A. Pozzi, Numerical and analytical solutions for concentration polarization in hyperfiltration without axial flow, *Int. J. Heat Mass Transf.*, 18 (1975) 945.
- [43] W. N. Gill, C. Tien and D. Zeh, Boundary layer effects in reverse osmosis desalination, *Ind. Eng. Chem. Fundam.*, 5 (1966) 367.
- [44] W. F. Leung and R. F. Probstein, Low polarization in laminar ultrafiltration of macromolecular solutions, *Ind. Eng. Chem. Fundam.*, 18 (1979) 274.
- [45] S. Srinivasan, C. Tien and W. N. Gill, Simultaneous development of velocity and concentration profiles in reverse osmosis systems, *Chem. Eng. Sci.*, 22 (1967) 417.
- [46] W. G. Light, Contending with chlorine attack of reverse osmosis membranes, 5th annual membrane technology/planning conference: Business Communications Co. Inc., Norwalk, CT, 1989, 233.
- [47] A. Mirmohseni, W. E. Price, G. G. Wallace and G. G. Zhao, Adaptive membrane systems based on conductive electroactive polymers, *J. Int. Mater. Syst. Struct.*, 4 (1993) 43.
- [48] A. Mirmohseni, W. E. Price and G. G. Wallace, Electrochemically controlled transport of small charged organic molecules across conducting polymer membranes, *J. Membrane Sci.*, 100 (1995) 239.
- [49] H. Zhao, W. E. Price and G. G. Wallace, Transport of copper (II) across stand alone conducting polymer membranes, *Polymer*, 34 (1993) 16.

- [50] M. J. Steuck and N. Reading, Porous membranes having hydrophilic surface and processes, US Patent, 4,618,533, 1986.
- [51] K. J. Kim, A. G. Fane and C. J. D. Fell, The performance of ultrafiltration membranes pretreated by polymers, *Desalination*, 70 (1988) 229.
- [52] A. G. Fane, C. J. D. Fell and Kim K. J., The effect of surfactant pretreatment on ultrafiltration of proteins, *Desalination*, 53 (1985) 37.
- [53] S. Kimura and I. Jitsuhara, Transport through charged ultrafiltration membranes, *Desalination*, 46 (1983) 407.
- [54] L. E. S. Bruik, S. J. G. Elbers, J. Robbertson and P. Both, The antifouling action of polymer preadsorbed on ultrafiltration and microfiltration membranes, *J. Membrane Sci.*, 76 (1993) 281.
- [55] V. Chen, A. G. Fane and C. J. D. Fell, The use of anionic surfactants for reducing fouling of ultrafiltration membranes: Their effects and optimization, *J. Membrane Sci.*, 67 (1992) 249.
- [56] D. Poulia, V. Gekas and G. Tragardh, Interaction behavior in ultrafiltration of nonionic surfactants. Part I: Flux behavior, *J. Membrane Sci.*, 69 (1992) 251.
- [57] A. Jonsson and B. Jonsson, The influence of of nonionic and ionic surfactants on hydrophilic and hydrophobic ultrafiltration membranes, *J. Membrane Sci.*, 56 (1991) 49.
- [58] A. Higuchi, S. Mishima and J. Nakagawa, Separation of proteins by surface modified polysulfone membranes, *J. Membrane Sci.*, 57 (1991) 175.
- [59] A. Kulkarni, D. Mukherjee and W. N. Gill, Flux enhancement by hydrophilization of thin film composite reverse osmosis membranes, *J. Membrane Sci.*, 114 (1996) 39.

- [60] M. Nystrom and P. Jarvinen, Modification of polysulfone ultrafiltration membranes with UV irradiation and hydrophilicity increasing agents, *J. Membrane Sci.*, 60 (1991) 275.
- [61] P. W. Kramer, Y. S. Yeh and H. Yasuda, Low temperature plasma for the preparation of separation membranes, *J. Membrane Sci.*, 46 (1989) 1.
- [62] G. Belfort, R. H. Davis and A. L. Zydney, The behavior of suspensions and macromolecular solutions in cross flow microfiltration, *J. Membrane Sci.*, 96 (1994) 1.
- [63] A. R. DaCosta, A. G. Fane and D. E. Wiley, Ultrafiltration of whey protein solutions in spacer filled flat channels, *J. Membrane Sci.*, 76 (1993) 245.
- [64] M. R. Mackley and N. E. Sherman, Cake filtration mechanisms in steady and unsteady flows, *J. Membrane Sci.*, 77 (1993) 113.
- [65] A. R. DaCosta, A. G. Fane, C. J. D. Fell and A. C. M. Franken, Optimal channel spacer design for ultrafiltration, *J. Membrane Sci.*, 62 (1991) 275.
- [66] M. J. vander Waal and I. G. Racz, Mass transfer in corrugated plate membrane modules. I. Hyperfiltration experiments, *J. Membrane Sci.*, 40 (1989) 243.
- [67] G. M. Rios, H. Rakotoarisoa and B. T. de la Fuente, Basic transport mechanisms of ultrafiltration in presence of fluidized particles, *J. Membrane Sci.*, 34 (1987) 331.
- [68] G. Arroyo and C. Fonade, Use of intermittent jets to enhance flux in cross flow filtration, *J. Membrane Sci.*, 80 (1993) 117.
- [69] H. R. Millward, B. J. Bellhouse and G. Walker, Screw thread flow promoters: An experimental study of ultrafiltration and microfiltration performance, *J. Membrane Sci.*, 106 (1995) 269.

- [70] S. Najarian and B. J. Bellhouse, Enhanced microfiltration of bovine blood using a tubular membrane with a screw threaded insert and oscillatory flow, *J. Membrane Sci.*, 112 (1996) 249.
- [71] J. Hiddink, D. Kloosterboer and S. Bruin, Evaluation of static mixer as convection homogeneous promoters in ultrafiltration of dairy liquids, *Desalination*, 35 (1980) 149.
- [72] Z. F. Cui and K. I. T. Wright, Flux enhancement with gas sparging in downwards cross flow ultrafiltration: Performance and mechanisms, *J. Membrane Sci.*, 117 (1996) 109.
- [73] K. H. Youm, a. G. Fane and D. E. Wiley, Effects of natural convection instability on membrane performance in dead-end and cross flow ultrafiltration, *J. Membrane Sci.*, 116 (1996) 229.
- [74] E. G. Richardson and E. Tyler, The transverse velocity gradient near the mouths of pipes in which an alternating or continuous flow of air is established, *Proc. Phys. Soc. London*, 42 (1974) 1927.
- [75] T. J. Kennedy, R. L. Merson and B. J. McCoy, Improving permeating flux by pulsed reverse osmosis, *Chem. Eng. Sci.*, 29 (1974) 1927.
- [76] H. Bauser, H. Chmiel, N. Stroh and E. Walitza, Interfacial effects with microfiltration membranes, *J. Membrane Sci.*, 11 (1982) 321.
- [77] J. A. Howell and S. M. Finnigan, The effect of pulsed flow on ultrafiltration fluxes in a baffled tubular membrane system, *Desalination*, 79 (1990) 47.
- [78] S. M. Finnigan and J. A. Howell, The effect of pulsatile flow on ultrafiltration flux in a baffled tubular membrane systems, *Chem. Eng. Res. Des.*, 67 (1989) 278.
- [79] K. D. Miller, S. Weitzel and V. G. J. Rodgers, Reduction of membrane fouling in the presence of high polarization resistance, *J. Membrane Sci.*, 76 (1993) 77.

- [80] S. Najarian and B. J. Bellhouse, Effect of liquid pulsation on protein fractionation using ultrafiltration process, *J. Membrane Sci.*, 114 (1996) 245.
- [81] V. G. J. Rodgers and R. E. Sparks, Reduction of membrane fouling in ultrafiltration of binary protein mixtures, *AIChE J.*, 37 (1991) 1517.
- [82] M. Lopez-Leiva, Ultrafiltration in a rotary annular filter, PhD Thesis, Department of Food Engineering, Lund University, Sweden, 1979.
- [83] J. Leibherr, Scrfiltration in Ringspalt, PhD thesis, ETH, Zurich, Switzerland, 1978.
- [84] G. I. Taylor, Stability of a viscous liquid contained between two rotating cylinders, *Philos. Trans. R. Soc. London, Ser. A*, (1923) 223.
- [85] K. H. Kroner and V. Nissinen, Dynamic filtration of microbial suspensions using an annular rotating filter, *J. Membrane Sci*, 36 (1985) 85.
- [86] K. H. Kroner, V. Nissinen and H. Ziegler, Improved dynamic filtration of microbial suspensions, *Bio/Technology*, 5 (1987) 921.
- [87] J. Murkes and C. G. Carlsson, Cross flow filtration. Theory and Practice, Wiley, NY, 1988.
- [88] H. B. Winzeler, Membrane Filtration mit hoher Trennleistung und minimalem Energiebedarf, *Chimia*, 44 (1990) 288.
- [89] K. Y. Chung, R. Bates and G. Belfort, Dean vortices with wall flux in a curved channel membrane system. 4. Effect of vortices on permeation fluxes of suspensions in microporous membrane, *J. Membrane Sci.*, 81 (1993) 139.
- [90] G. Belfort, P. Mikulasek, J. M. Pimbley and K. Y. Chung, Diagnosis of membrane fouling using a rotating annular filter. 2. Dilute particle suspensions of known particle size, *J. Membrane Sci.*, 77 (1992) 23.

- [91] M. G. Brewster, K. Y. Chung and G. Belfort, Dean vortices with wall flux in a curved channel membrane system. 1. A new approach to membrane module design, *J. Membrane Sci.*, 81 (1993) 127.
- [92] K. Y. Chung, W. A. Edelstein and G. Belfort, Dean vortices with wall flux in a curved membrane system. 6. Two dimensional magnetic resonance imaging of the velocity field in a curved impermeable slit, *J. Membrane Sci.*, 81 (1993) 151.
- [93] K. Y. Chung, W. A. Edelstein and G. Belfort, Dean vortices in a curved channel membrane system. 5. Three dimensional magnetic resonance imaging and numerical analysis of the velocity field in a curved impermeable tube, *AIChE J.*, 39 (1993) 1592.
- [94] W. R. Dean, Fluid motion in a curved channel, *Proc. R. Soc. London, Ser. A*, 121 (1928) 402.
- [95] P. G. Drazin and W. H. Reed, *Hydrodynamic Stability*, Cambridge Univ. Press, Cambridge, UK, 1981.
- [96] H. B. Winzeler and H. Schomberg, Membran Modul fur die Mikro und Ultrafiltration hohe permeatleistung dank sekundarsformungs Effekt. Poster presentation at the third membrane colloquium, Aachen, Germany, 1991.
- [97] J.F.G. Reis and E. N. Lightfoot, Electropolarization chromatography, *AIChE J.*, 22 (1976) 770.
- [98] J. D. Henry, L. F. Lawler, C. H. A. Kuo, A Solid/liquid separation process based on cross flow and electrofiltration, *AIChE J.*, 23 (1977) 851.
- [99] C. Mullon, J. M. Radovich, B. Behnam, A semiempirical model for electro-ultrafiltration-diafiltration, *Sep. Sci. Technol.*, 20 (1985) 63.
- [100] R. J. Wakeman and E. S. Tarleton, Modelling cross flow electro and microfiltration, *Proc. of 4 th world filtration congress*, Ostende, Belgium, 1986.

- [101] H. Yukawa, K. Shimora, A. Sude and A. Maniwa, Cross flow electro-ultrafiltration for colloidal solutions of protein, *J. Chem. Eng. Jpn.*, 16 (1983) 305.
- [102] C. W. Robinson, M. H. Siegel, A. Condemine, C. Fee, T. Z. Fahidy and B. R. Glick, Pulsed electric field cross flow ultrafiltration of bovine serum albumin, *J. Membrane Sci.*, 80 (1993) 209.
- [103] S. Lentsch, P. Aimar and J. L. Orozco, Enhanced separation of albumin-poly (ethylene) glycol by combination of ultrafiltration and electrophoresis, *J. Membrane Sci.*, 80 (1993) 221.
- [104] T. K. Sherwood and P. L. T. Brian, Salt concentration at phase boundaries in desalination by reverse osmosis, *Ind. Eng. Chem. Fundam.*, 4 (1965) 113.
- [105] D. R. Trettin and M. R. Doshi, Ultrafiltration of colloidal suspensions and macromolecular solutions in an unstirred batch cell, *Ind. Eng. Chem. Fundam.*, 20 (1981) 221.
- [106] D. R. Trettin and M. R. Doshi, Ultrafiltration in an unstirred batch cell, *Ind. Eng. Chem. Fundam.*, 19 (1980) 189.
- [107] R. Singh and L. Laurence, Influence of slip velocity at a membrane surface on ultrafiltration performance. 1. Channel flow system, *J. Heat Mass Transf.*, 22 (1979) 721.
- [108] C. Kleinstreuer and M. S. Paller, Laminar dilute suspension flows in plate and frame ultrafiltration units, *AIChE J.*, 29 (1983) 529.
- [109] M. J. Clifton, N. Abidine, P. Aptel and V. Sanchez, Growth of the polarization layer in ultrafiltration with hollow fiber membranes, *J. Membrane Sci.*, 21 (1984) 233.
- [110] R. P. Ma, C. H. Gooding and W. K. Alexander, A dynamic model for low pressure hollow fiber ultrafiltration, *AIChE J.*, 31 (1985) 1728.

- [111] R. E. Lebrun, C. R. Bouchard, A. L. Rollin, T. Matsuura and S. Sourirajan, Computer simulation of membrane separation process, *Chem. Eng. Sci.*, 44 (1989) 313.
- [112] C. R. Bouchard, P. J. Carreau, T. Matsuura and S. Sourirajan, Modeling of ultrafiltration: predictions of concentration polarization effects, *J. Membrane Sci.*, 97 (1994) 215.
- [113] S. Ganguly and P. K. Bhattacharya, Development of concentration profile and prediction of flux for ultrafiltration in a radial cross flow cell, *J. Membrane Sci.* 97 (1994) 185.
- [114] R. L. Goldsmith, Macromolecular ultrafiltration with microporous membranes, *Ind. Eng. Chem. Fundam.*, 10 (1971) 113.
- [115] J. G. Wijmans, S. Nakao, C. A. Smolders, Flux Limitations in Ultrafiltration: Osmotic Pressure Model and Gel Layer Model, *J. Membrane Sci.*, 20 (1984) 115.
- [116] V. L. Vilker, C. K. Colton and K. A. Smith, The osmotic pressure of concentrated protein solutions: Effect of concentration and pH in saline solutions of bovine serum albumin, *J. Colloid. Interf. Sci.*, 79 (1981) 548.
- [117] V. L. Vilker, C. K. Colton and K. A. Smith, Concentration polarization in protein ultrafiltration. II. Theoretical and experimental study of albumin ultrafiltered in an unstirred batch cell, *AIChE J.*, 27 (1981) 637.
- [118] W. Pusch, Osmotic pressure of T10 solution, *Desalination*, 68 (1988) 69.
- [119] O. Kedem, and A. Katchalsky, Thermodynamic Analysis of Permeability of Biological Membranes to Non-electrolytes, *Biochim. Biophys. Acta.*, 27 (1958) 229.
- [120] F. Belluci, E. Drioli and A. Pozzi, Flow regimes in an unstirred discontinuous hyperfiltration process: Comparison between theoretical and experimental results, *Desalination*, 16 (1975) 287.

- [121] H. Nabetani, M. Nakajima, A. Watanabe, S. Nakao, S. Kimura, Effects of osmotic pressure and adsorption on ultrafiltration of ovalalbumin, *AIChE J.*, 36 (1990) 907.
- [122] G. Jonsson, Boundary layer phenomena during ultrafiltration of dextran and whey protein solutions, *Desalination*, 51 (1984), 61.
- [123] S. Bhattacharjee and P. K. Bhattacharya, Flux decline behaviour with low molecular weight solutes during ultrafiltration in an unstirred batch cell, *J. Membrane Sci.* 72 (1992) 149.
- [124] Chudacek M. W., and A. G. Fane, The Dynamics of Polarization in Unstirred and Stirred Ultrafiltration, *J. Membrane Sci.*, 21 (1984) 145.
- [125] A. S. Michaels, New separation technique for CPI, *Chem. Eng. Prog.* 64 (1968) 31.
- [126] M. C. Porter, Concentration polarization with membrane ultrafiltration, *Ind. Eng. Chem. Prod. Res. Dev.*, 11 (1972) 234.
- [127] R. L. C. Flemmer, C. A. Buckley and G. R. Groves, An analysis of the performance of a spiral wound ultrafiltration membrane with a turbulence promoting net under conditions of strong pressure gradient and fouling, *Desalination*, 41 (1982) 25.
- [128] C. A. Buckley, R. L. C. Flemmer and G. R. Groves, Fouling studies and mathematical modelling of ultrafiltration of textile effluents, *Desalination*, 47 (1983) 171.
- [129] R. W. Baker and H. Strathmann, Ultrafiltration of Macromolecular Solutions with High-flux Membranes, *J. Appl. Polym. Sci.*, 14 (1970) 1197.
- [130] S. Nakao, S. Yumato and S. Kimura, Analysis of rejection characteristics of macromolecular gel layer for low molecular weight solutes in ultrafiltration, *J. Chem. Eng. Jpn.*, 15 (1982) 463.

- [131] S. Nakao and S. Kimura, Models of membrane transport phenomena and their applications for ultrafiltration data, *J. Chem. Eng. Jpn.*, 15 (1982) 200.
- [132] S. Nakao and S. Kimura, Effect of Gel Layer on Rejection and Fractionation of Different Molecular Weight Solutes by Ultrafiltration, *AIChE Symp. Ser.*, A. F. Turbak, ed., in *Synthetic Membranes*, vol. II, 1981.
- [133] S. Nakao, T. Nomura, S. Kimura, Characteristics of macromolecular gel layer formed on ultrafiltration tubular membrane, *AIChE J.*, 25(1979) 615.
- [134] S. Kimura and S. Nakao, Fouling of cellulose acetate tubular reverse osmosis modules treating the industrial water in Tokyo, *Desalination*, 17 (1975) 267.
- [135] F. Belluci and E. Drioli, Protein ultrafiltration: An experimental study. *J. Appl. Polym. Sci.*, 19 (1975) 1639
- [136] R. F. Probstein, W. F. Leung and Y. Alliance, Determination of diffusivity and gel concentration in macromolecular solutions by ultrafiltration, *J. Phys. Chem.*, 83 (1979) 1228.
- [137] C. Bhattacharjee, and P. K. Bhattacharya, Prediction of limiting flux in ultrafiltration of kraft black liquor, *J. Membrane Sci.* 72 (1992) 137.
- [138] M. Bodzek and K. Konieczney, PAN/PVC ultrafiltration membranes with treatment of amphoteric emulsion paint, *Desalination*, 80 (1991) 43.
- [139] R. B. Grieves, D. Bhattacharya, W. G. Schomp and J. L. Bewley, Membrane ultrafiltration of a non-ionic surfactant, *AIChE J.*, 19 (1973) 766.
- [140] C. Charcosset and L. Choplin, Ultrafiltration of non Newtonian fluids, *J. Membrane Sci.*, 115 (1996) 147.
- [141] J. Howell, R. Field and D. Wu, Ultrafiltration of high viscosity solutions: Theoretical developments and experimental findings, *Chem. Eng. Sci.*, 51 (1996) 1405.

- [142] M. Pritchard, R. Field and J. A. Howell, The UF of viscous fluids, *J. Membrane Sci.*, 102 (1995) 223.
- [143] P. Aimar and V. Sanchez, A novel approach to transfer limiting phenomena during ultrafiltration of macromolecules, *Ind. Eng. Chem. Fundam.*, 25 (1986) 789.
- [144] W. N. Gill, D. E. Wiley, C. J. D. Fell, A. G. Fane, Effect of viscosity on concentration polarization in ultrafiltration, *AIChE J.* 34 (9) (1988) 1563.
- [145] A. A. Kozinsky and E. N. Lightfoot, Protein ultrafiltration: A general example of boundary layer filtration, *AIChE J.* 18 (1972) 1030.
- [146] R. W. Field, A theoretical viscosity correction factor for heat transfer and friction in pipe flow, *Chem. Eng. Sci.*, 45 (1990) 1343.
- [147] P. Aimar and R. Field, Limiting flux in membrane separations: A model based on the viscosity dependency of the mass transfer coefficient, *Chem. Engg. Sci.*, 47(1992) 579.
- [148] A. G. Fane and A. G. Waters, Initial flux and rejection characteristics of partially permeable ultrafiltration membranes, *J. Appl. Polym. Sci.*, 26 (1981) 3007.
- [149] J. A. Howell and O. Velicangil, Protein ultrafiltration: Theory of membrane fouling and its treatment with immobilized proteases, in A. R. Cooper (Ed.), *Ultrafiltration Membranes and Applications*, Plenum Press, NY, 1980.
- [150] A. G. Fane, C. J. D. Fell and A. Suki, The effect of pH and ionic environment on the ultrafiltration of protein solutions with retentive membranes, *J. Membrane Sci.*, 16 (1983) 195.
- [151] H. Reihanian, C. R. Robertson and A. S. Michaels, Mechanisms of polarization and fouling of ultrafiltration membranes by protein, *J. Membrane Sci.*, 16 (1983) 237.

- [152] C. W. van Oers, M. A. G. Vorstman, W. G. H. M. Muijselaar and P. J. A. M. Kerkhof, Unsteady state flux behaviour in relation to presence of a gel layer, *J. Membrane Sci.* 73(1992) 231.
- [153] L. Song and E. Elimelech, Theory of concentration polarization in crossflow filtration, *J. Chem. Soc. Farad. Trans.*, 91 (1995) 3389.
- [154] J. G. Wijmans, S. Nakao, J. W. A. Van der Berg, F. R. Troelstra, and C. A. Smolders, Hydrodynamic resistance of concentration polarization boundary layers in ultrafiltration, *J. Membrane Sci.* 22 (1985) 117.
- [155] S. Nakao, J. G. Wijmans, and C. A. Smolders, Resistance to The Permeate Flux in Unstirred Ultrafiltration of Dissolved Macromolecular Solutions, *J. Membrane Sci.*, 26 (1986) 165.
- [156] G. B. van den Berg and C. A. Smolders, The boundary layer resistance model for unstirred ultrafiltration. A new approach. *J. Membrane Sci.*, 47 (1989) 149.
- [157] K. Persson and J. Nilsson, Fouling resistance models in microfiltration and ultrafiltration, *Desalination*, 80 (1991) 123.
- [158] K. M. Persson, G. Tragardh and P. Dejmek. Fouling behaviour of silica on four different microfiltration membranes, *J. Membrane Sci.*, 76 (1993) 51.
- [159] K. M. Persson, G. Capannelli, A. Bottino and G. Tragardh, Porosity and protein adsorption of four polymeric microfiltration membranes, *J. Membrane Sci.*, 76 (1993) 61.
- [160] K. C. Ingham, T. F. Busby, Y. Sahlestrom and F. Castino, Separation of macromolecules by ultrafiltration: Influence of protein adsorption, protein-protein interaction and concentration polarization, In A. R. Cooper, Ed., *Ultrafiltration Membranes and Applications*, Plenum Press, NY, 1980.
- [161] A. G. Fane, Factor affecting flux and rejection in ultrafiltration, *J. Sep. Proc. Tech.*, 4 (1983) 15.

- [162] M. Pouliot, Y. Pouliot, M. Britten and N. Ross, Effects of pH and ionic environments on the permeability and rejective properties of an alumina microfiltration membrane for whey proteins, *J. Membrane Sci.*, 95 (1994) 125.
- [163] E. A. Tsapiuk, M. T. Byrk, M. I. Medvedev and V. M. Kochkodan, Fractionation and concentration of lignosulfonates by ultrafiltration, *J. Membrane Sci.*, 47 (1989) 107.
- [164] D. M. Malone and J. L. Anderson, Hindered diffusion of particles through small pores, *Chem. Eng. Sci.*, 33 (1978) 1429.
- [165] T. Matsuura and S. Sourirajan, Reverse osmosis transport through capillary pores under the influence of surface forces, *Ind. Eng. Chem. Proc. Des. Dev.*, 20 (1981) 273.
- [166] B. D. Mitchell and W. M. Deen, Theoretical effects of macromolecular concentration and charge on membrane rejection coefficients, *J. Membrane Sci.* 14 (1984) 75.
- [167] B. D. Mitchell and W. M. Deen, Effect of concentration on the rejection coefficients of rigid macromolecules in track-etch membranes, *J. Colloid. Interf. Sci.*, 113 (1986) 132.
- [168] E. D. Glandt, Density distribution of hard spherical molecules inside small pore of various shapes, *J. Colloid. Interf. Sci.*, 77 (1980) 512.
- [169] A. J. Post and E. D. Glandt, Equilibrium partitioning in pores with adsorbing walls, *J. Colloid Interf. Sci.*, 108 (1985) 31.
- [170] W. M. Deen, Hindered transport of large molecules in liquid-filled pores, *AIChE J.*, 33 (1987) 1409.
- [171] S. Dumon and B. Bernier, Ultrafiltration of protein solutions on ZrO_2 membranes. The influence of surface chemistry on adsorption, *J. Membrane Sci.*, 74 (1992) 289.

- [172] D. N. Lee and R. L. Merson, Examination of cottage cheese whey by scanning electron microscopy: Relationship to membrane fouling during ultrafiltration, *J. Dairy Sci.*, 58 (1975) 1423.
- [173] A. D. Marshall, P. A. Munro and G. Tragardh, The effect of protein fouling in microfiltration and ultrafiltration on permeate flux, retention and selectivity: A literature review, *Desalination*, 90 (1993) 65.
- [174] V. Gekas and B. Hallstrom, Microfiltration membranes, cross flow transport membranes and fouling studies, 77 (1990) 195.
- [175] A. G. Fane and C. J. D. Fell, A review of fouling and fouling control in ultrafiltration, *Desalination*, 62 (1987) 117.
- [176] K. J. Kim, A. G. Fane, C. J. D. Fell and D. C. Joy, Fouling mechanisms of membranes during protein ultrafiltration, *J. Membrane Sci.*, 68 (1992) 79.
- [177] J. L. Nilsson, Protein fouling of ultrafiltration membranes: Causes and consequences, *J. Membrane Sci.*, 52 (1990) 121.
- [178] G. Jonsson, P. Pradanos and A. Hernandez, Fouling phenomena in microporous membranes. Flux decline kinetics and structural modifications, *J. Membrane Sci.*, 112 (1996) 171.
- [179] E. Drioli and F. Bellucci, Concentration polarization and solute-membrane interactions affecting pressure driven membrane processes, *Desalination*, 26 (1978) 17.
- [180] S. Bhattacharjee, Role of surface interactions in prediction of flux decline during ultrafiltration, PhD thesis, Department of Chemical Engineering, I. I. T. Kanpur, India, 1995.
- [181] G. Green and G. Belfort, Fouling of ultrafiltration membranes: Lateral migration and the particle trajectory model, *Desalination*, 35 (1980) 129.

- [182] A. L. Zydney and C. K. Colton, A Concentration polarization model for the filtrate flux in cross flow microfiltration of particulate suspensions, *Chem. Engg. Commun.*, 47 (1986) 1.
- [183] E. C. Eckstein, P. G. Bailey and A. H. Shapiro, Self-diffusion of particles in shear flow of a suspension, *J. Fluid Mech.*, 79 (1977) 191.
- [184] D. T. Leighton and A. Acrivos, Viscous resuspension, *Chem. Eng. Sci.*, 41 (1986) 1377.
- [185] D. T. Leighton and A. Acrivos, Measurement of the shear induced coefficient of self diffusion in concentrated suspensions of spheres, *J. Fluid Mech.*, 177 (1987) 109.
- [186] F. W. Altena and G. Belfort, Lateral migration of spherical particles in porous channels: Application to membrane filtration, *Chem. Eng. Sci.*, 39 (1984) 343.
- [187] F. W. Altena, R. J. Weigand and G. Belfort, Lateral migration of spherical particles in laminar porous tube flows: Application to membrane filtration, *Physiochem. Hydrodyn.*, 6 (1985) 393.
- [188] G. Belfort, R. J. Weigand and J. T. Mahar, Particulated membrane fouling and recent developments in fluid mechanics of dilute suspensions, *ACS Symp. Ser.*, 281, 1985.
- [189] R. J. Otis, F. W. Altena, J. Mahar and G. Belfort, Measurement of single spherical particle trajectories with lateral migration in a slit with one porous wall under laminar flow conditions, *Experiments Fluids*, 4 (1986) 1.
- [190] D. A. Drew, J. A. Schomberg and G. Belfort, Lateral migration of a small sphere in fast laminar flow through a membrane duct, *Chem. Eng. Sci.*, 46 (1991) 3219.
- [191] C. A. Romero and R. H. Davis, Global model of cross flow microfiltration based on hydrodynamic particle diffusion, *J. Membrane Sci.*, 39 (1988) 157.

- [192] E. F. Leonard and C. S. Vassilief, The deposition of rejected matter in membrane separation processes, *Chem. Engg. Commun.*, 30 (1984) 209.
- [193] M. R. Mackley and N. E. Sherman, Cross flow cake filtration mechanisms and kinetics, *Chem. Eng. Sci.*, 47 (1992) 3067.
- [194] W. M. Lu and S. C. Ju, Selective particle deposition in crossflow filtration, *Sep. Sci. Technol.*, 24 (1989) 512.
- [195] K. Stamatakis and C. Tien, A simple model of cross flow filtration based on particle adhesion, *AIChE J.*, 39 (1993) 1293.
- [196] M. E. O'Neill, A sphere in contact with a plane wall in slow linear shear flow, *Chem. Eng. Sci.*, 23 (1968) 1293.
- [197] S. L. Goren, The hydrodynamic force resisting the approach of a sphere to a plane permeable wall, *J. Colloid Interf. Sci.*, 69 (1979) 78.
- [198] J. D. Sherwood, The force on a sphere pulled away from a permeable half-space, *Physiochem. Hydrodyn.* 10 (1988) 3.
- [199] R. G. McDonald, *Pulping of Wood*, McGraw-Hill, New York, 1969.
- [200] M. D. Afonso and M. N. Pinho, Membrane Separation Processes in the pulp and paper industry, *Desalination*, 85 (1991) 53.
- [201] B. Chakravarti and A. S. Srivastava, Application of membrane technology for recovery of water from pulp and paper mill effluent, *Desalination*, 67 (1988) 363.
- [202] O. Olsen, Membrane technology in pulp and paper industry, *Desalination*, 35 (1980) 291.
- [203] A. S. Jonsson and R. Wimmerstedt, The application of membrane technology in the pulp and paper industry, *Desalination*, 53 (1985) 181.

- [204] D. L. Woerner and J. L. McCarthy, Ultrafiltration of kraft black liquor, AIChE Symp. Ser., 80 (1984) 25.
- [205] A. J. Wiley, A. C. F. Ammerlaan and G. A. Dubey, Application of reverse osmosis to processing of spent liquors from the pulp and paper industry, Tappi, 50 (9) (1967) 455.
- [206] A. C. F. Ammerlaan, B. F. Lucek and A. J. Wiley, Membrane processing of dilute pulping wastes by reverse osmosis, Tappi, 52 (1) (1969) 118.
- [207] A. J. Wiley, G. A. Dubey, J. M. Holderby and A. C. F. Ammerlaan, Concentration of dilute pulping water by reverse osmosis and ultrafiltration WPCF J., 42(8), part 2 (1970) R279.
- [208] A. C. F. Ammerlaan and A. J. Wiley, The engineering evaluation of reverse osmosis as a method of processing spent liquors of the pulp and paper industry, Tappi, 52 (1969) 1703.
- [209] A. J. Wiley, L. E. Dambruch, P. E. Parker and H. S. Dugal, Tappi Environ. Conf. Proc., (1978) 63.
- [210] A. J. Wiley, K. Scharpf, I. Bansal and D. Arps, Reverse osmosis concentration and spent liquor solids in press liquors from high density pulp, Tappi, 55 (1972) 1671.
- [211] I. K. Bansal and A. J. Wiley, Membrane processes for fractionation and concentration of spent sulfite liquors, Tappi, 58 (1975) 125.
- [212] P. H. Claussen, Membrane filtration of SSL for by-product recovery and pollution control, Pulp and Paper Can., 79 (1978) T81.
- [213] M. P. Drouin and M. J. Desroches, Isolation of lignin from spent kraft liquor by hyper and UF, AIChE Forest Prod. Div., 2 (1988) 58.

- [214] S. U. Lin and W. J. Detroit, Ekman Days Wood Chemistry Symposium, Stockholm, 4 (1981) 44.
- [215] M. K. Hill, Tappi Proceedings, Pulping conference, Florida, 629, 1985.
- [216] Rajnish and P. K. Bhattacharya, Ultrafiltrative solute rejection behaviour of black liquor, in: S. Sourirajan and K. Matsuura (Eds.), Reverse osmosis and Ultrafiltration, ACS Symp. Ser. 281 (1985) 313.
- [217] T. K. Poddar, R. P. Singh and P. K. Bhattacharya, Ultrafiltration flux and rejection characteristics of black liquor and polyethylene glycol, Chem. Eng. Commun., 75 (1989) 39.
- [218] S. Das Gupta and P. K. Bhattacharya, Comparative limiting flux analysis of black liquor and polyethylene glycol in ultrafiltration, Chem. Eng. Commun., 93 (1990) 193.
- [219] S. Sridhar and P. K. Bhattacharya, Limiting flux phenomena in ultrafiltration of kraft black liquor, J. Membrane Sci., 57 (1991) 187.
- [220] C. Bhattacharjee and P. K. Bhattacharya, Flux decline analysis in ultrafiltration of kraft black liquor, J. Membrane Sci., 82 (1993) 1.
- [221] A. Pearl, The Chemistry of Lignin, Merrell Dekker Inc., New York, 1967.
- [222] R. Alen, P. Patja and E. Sjostrom, Carbon dioxide precipitation of lignin from pine kraft black liquor, Tappi, 62 (1979) 108.
- [223] M. Nystrom and M. Lindstrom, Optimal removal of chlorolignin by ultrafiltration achieved by pH control, Desalination, 70 (1988) 145.
- [224] F. G. Wilde, Recovery of lignosulfonates from a calcium bisulfate pulp mill effluent by ultrafiltration, Desalination, 67 (1988) 495.
- [225] J. Li, T. O'hagan and J. M. Macleod, Using ultrafiltration to analyze the molar mass distribution of kraft lignin at pH 13, Can. J. Chem. Eng., 74 (1996) 110.

- [226] A.K. Mishra and P.K. Bhattacharya, Alkaline Black Liquor treatment by batch Electrodialysis, *Can. J. Chem. Eng.*, 62 (1984) 723.
- [227] A.K. Mishra and P.K. Bhattacharya, Continuous electrodialysis treatment of alkaline black liquor, *J. Membrane Sci.*, 33 (1987) 83.
- [228] J. F. Scamehorn, J. H. Harwell, D. T. Wasan, D. O. Shah and M. E. Ginn (Ed.), *Surfactants and chemical engineering*, Marcel Dekker Inc., New York, 1986.
- [229] R. O. Dunn, J. F. Scamehorn and S. D. Christian, Use of micelle enhanced ultrafiltration to remove dissolved organics from aqueous streams, *Sep. Sci. Technol.*, 20 (1985) 257.
- [230] L. L. Gibbs, J. F. Scamehorn and S. D. Christian, Removal of n-alcohols from aqueous streams using micellar-enhanced ultrafiltration, *J. Membrane Sci.*, 30 (1987) 67.
- [231] S. N. Bhat, G. A. Smith, E. D. Tucker, S. D. Christian and J. F. Scamehorn, Solubilization of cresols by 1-hexadecyl pyridinium chloride micelles and removal of cresols from aqueous streams by micellar-enhanced ultrafiltration, *Ind. Eng. Chem. Res.*, 26 (1987) 1217.
- [232] S. D. Christian, S. N. Bhat, E. E. Tucker, J. F. Scamehorn, and D. A. El-Sayed, Micellar enhanced ultrafiltration of chromate anion from aqueous streams, *AIChE*, 34, No. 2, (1988) 189.
- [233] A. A. Kozinsky and E. N. Lightfoot, Ultrafiltration of proteins in stagnation flow, *AIChE J.*, 17 (1971) 81.
- [234] R. F. Probstein, *Physiochemical Hydrodynamics*, Butterworths, Boston, MA, 1989.
- [235] H. Schlichting, *Boundary Layer Theory*, McGraw-Hill, 1979.

- [236] C. E. Libby (Ed.), *Pulp and Paper Science and Technology*, vol. 1, McGraw-Hill, NY, 1962.
- [237] E. A. Tsapiuk, M. T. Bryk, V. M. Kochkodan and E. E. Danilenko, Separation of aqueous solution of non ionic organic solutes by ultrafiltration, *J. Membrane Sci.*, 48 (1990) 1.
- [238] P. M. Bungay, H. K. Lonsdale and M. N. de Pinho (Eds.), *Synthetic Membranes: Science, Engineering and Applications*, D. Reidel Publishing Co., Dordrecht, 1983.
- [239] W. S. Opong and A. L. Zydney, Diffusive and convective protein transport through asymmetric membranes, *AIChE J.*, 37 (1991) 1497.
- [240] P. Pradanos, J. I. Arribas and A. Hernandez, Retention of proteins in cross flow ultrafiltration through asymmetric inorganic membranes, *AIChE J.*, 40 (1994) 1901.
- [241] P. Aimar, C. Taddei, J. Lafaille, V. Sanchez, Mass transfer limitations during ultrafiltration of cheese whey with inorganic membranes, *J. Membrane Sci.*, 38 (1988) 203.
- [242] J. M. Dias, Analysis of polarized layer resistance through secondary gel layer type in ultrafiltration, M. Tech. Thesis, Department of chemical Engg., Indian Institute of Technology, Kanpur, 1993.
- [243] S. Bhattacharjee, A. Sharma, P. K. Bhattacharya, Surface interactions in osmotic pressure controlled flux decline during ultrafiltration, *Langmuir*, 10 (1994) 4710.
- [244] R. F. Madsen, Application of ultrafiltration and reverse osmosis to cane juice, *Int. Sugar J.*, 83, (1981) 35.
- [245] G. Tragardh and V. Gekas., Membrane technology in sugar industry, *Desalination*, 69, (1988) 9.

- [246] S. Kishihara, H. Tamaki, S. Fujii, and M. Komoto, Clarification of technical sugar solutions through a dynamic membrane formed on a porous ceramic tube, *J. Membrane Sci.*, 41, (1989) 103.
- [247] G. P. Meade, *Cane Sugar Handbook*, Wiley, New York 1963.
- [248] G. Belfort and N. Nagata, Fluid mechanics and cross flow filtration: Some thoughts, *Desalination*, 53, (1985) 57.
- [249] S. Bhattacharjee, A. Sharma, and P. K. Bhattacharya, A unified model for flux prediction during batch cell ultrafiltration", *J. Membrane Sci.*, 111 (1996) 243.
- [250] H. Matsuyama, T. Shimomura, and M. Teramoto, Formation and characteristics of dynamic membrane for ultrafiltration of protein in binary protein system, *J. Membrane Sci.*, 92 (1994) 107.
- [251] V. Starov, A model and mathematical representation for membrane concentration and purification of macromolecular solutions containing low molecular weight contaminants, *J. Membrane Sci.*, 79 (1993) 241.
- [252] J. L. Gaddis, D. A. Jernigan, and H. G. Spencer, Determination of gel volume deposited on ultrafiltration membranes, *ACS Symp. Ser.*, S. Sourirajan and T. Matsuura, (Eds.), in *Reverse Osmosis and Ultrafiltration*, 1985.
- [253] S. Agarwal, Studies on flux decline phenomena in ultrafiltration of sugar cane juice for recovery of sugar, M. Tech. Thesis, Dept. of Chemical Engineering, Indian Institute of Technology, Kanpur, India, 1996.
- [254] J. Brandrup and E. H. Immergut (Eds.), *Polymer Handbook*, Wiley, New York, 1975.
- [255] L. Lebrun and G. Junter, Diffusion of dextran through microporous membrane filters, *J. Membrane Sci.*, 88 (1994) 253.

- [256] W. B. Russel, D. A. Saville and W. R. Schowalter, Colloidal Dispersions, Cambridge Univ. Press, Cambridge, 1989.
- [257] P. J. Flory, Principles of polymer chemistry, Cornell Univ. Press, Ithaca, 1953.
- [258] C. J. van Oss, K. Arnold, R. J. Good, K. Gawrish and S. Okhi, Interfacial tension and the osmotic pressure of solutions of polar polymers, J. Macromol. Sci. - Chem., A-27 (1990) 563.
- [259] B. N. Preston, W. D. Comper, A. E. Hughes, I Snook and W. van Megen, Diffusion of dextran at intermediate concentrations, J. Chem. Soc. Faraday Trans., 78 (1982) 1209.
- [260] E. M. Fahner, G. H. Grobman and K. H. Ebert, Elastic and quasielastic light scattering studies on the branching characteristics of dextrans, Macromol. Chem., 185 (1984) 2205.
- [261] G. Jonsson and C. E. Boessen, Concentration polarization in a reverse osmosis test cell, Desalination, 1 (1977) 21.
- [262] J. L. Anderson, F. Rauh and A. Morales, Particle diffusion as a function of concentration and ionic strength, J. Phys. Chem., 82 (1978) 608.
- [263] G. D. J. Phillies, G. B. Benedek and N. A. Mazer, Diffusion in protein solutions at high concentration: A study by quasielastic light scattering spectroscopy, J. Chem. Phys., 65 (1976) 1883.
- [264] J. M. A. H. Hoffman and H. N. Stein, Hydrodynamic and surface interaction forces on a particle in a pore, J. Colloid Interf. Sci., 154 (1992) 359.
- [265] S. Bhattacharjee and A. Sharma, Lifshitz-van der Waals energy of spherical particles in cylindrical pores, J. Colloid Interf. Sci., 171 (1995) 288.
- [266] U. Merten, H. K. Lonsdale and R. L. Riley, Boundary layer effects in reverse osmosis, Ind. Eng. Chem. Fundam., 3 (1964) 210.

- [267] S. Ganguly, Development of concentration profile in cross flow ultrafiltration using kraft black liquor in comparison to polyethylene glycol, M. Tech. Thesis, IIT Kanpur, 1991.
- [268] G. E. P. Box, W. G. Hunter and J. S. Hunter, Statistics for Experimenters, pp.453-505, John Wiley, New York, 1978.
- [269] K. Passinen, in proceedings of the symposium on recovery of pulping chemicals, Helsinki, 1968.
- [270] A. Panda, Removal of silica from the recovery system of alkaline pulp mills, Ind. pulp and paper, 16 (1962) 701.
- [271] H. Romantschuk and J. Mattila, Development of the carbonating stage of the tampere recovery process, Tappi J., 54 (1971) 1495.
- [272] S. Basu, Causticization and sludge sedimentation characteristics of modified green liquor, Tappi J., 57 (1974) 101.
- [273] K. Radhamohan and S. Basu, Electrodialysis in the regeneration of paper mill spent liquor, Desalination, 33 (1980) 185.
- [274] S. Roychowdhury, Cation-neutral membrane electrodialysis process studies of kraft black liquor, M. Tech thesis, Department of chemical eng., Indian Institute of Technology, Kanpur, 1991.
- [275] M. P. Gupta and P. K. Bhattacharya, Studies on colour removal from bleach plant effluent of kraft pulp mill, J. Chem. Tech. Biotechnol., 35B (1985) 23.
- [276] N. C. Shah and P. K. Bhattacharya, Bleach plant effluent treatment by fly-ash, Chemica Oggi, 3 (1988) 59.
- [277] P. S. Leung and A. R. Cooper, Ultrafiltration membranes and applications, Plenum Press, New York, 1979.

- [278] K. Kandori and R. S. Schechter, Selection of surfactants for micellar-enhanced ultrafiltration, *Sep. Sci. Technol.*, 25 (1990) 83.
- [279] J. H. Markels, S. Lynn and C. J. Radke, Micellar ultrafiltration in an unstirred batch cell at constant flux, *J. Membrane Sci.*, 86 (1994), 241.
- [280] J. H. Markels, S. Lynn and C. J. Radke, Cross flow ultrafiltration of micellar surfactant solutions, *AIChE J.*, 41 (1995) 2058.
- [281] D. N. Rubingh and P. M. Holland, *Cationic Surfactants*, Mercel Dekker Inc., New York, 1991.
- [282] J. H. Clint, *Surfactant Aggregation*, Chapman and Hall, New York, 1992.
- [283] A. I. Vogel, *A Textbook of Macro and Semimicro Quantitative Inorganic Analysis*, Longmans, London, 1955.
- [284] K. Shinoda, T. Nakagawa, B. Tamasushi and T. Isemura, *Colloidal Surfactants*, Academic Press Inc., New York, 1963.
- [285] O. Levenspiel, *Chemical Reaction Engineering*, John Wiley, New York, 1972.
- [286] T. K. Sherwood, R. L. Pigford and C. R. Wilke, *Mass Transfer*, McGraw-Hill, New York, 1975.
- [287] S. Sourirajan, *Reverse Osmosis*, Academic Press, NY, 1970.

List of publications

Publications :

Refereed articles :

1. S. De, J. M. Dias and P. K. Bhattacharya, "Short and long term flux decline analysis in ultrafiltration", *Chem. Eng. Commun.*, in press.
2. S. De and P. K. Bhattacharya, "Flux prediction of kraft black liquor in cross flow ultrafiltration using low and high rejecting membranes", *J. Membrane Sci.*, **109**, 109-123 (1996).
3. S. De and P. K. Bhattacharya, "Recovery of water with inorganic chemicals from kraft black liquor using membrane separation processes", *Tappi J.*, **79**, 103-111 (1996).
4. S. De, S. Bhattacharjee and P. K. Bhattacharya, "Development of correlations for mass transfer coefficients in ultrafiltration systems", *Devlop. Chem. & Min. Processes*, **3**, 187-206 (1995) [*Special Theme Issue: Advances on Membrane Separation and Adsorption*]

Manuscripts communicated:

1. S. De, S. Bhattacharya, P. K. Bhattacharya and A. Sharma, "Generalized integral and similarity solutions for concentration profiles for ultrafiltration", submitted to *J. Membrane Sci.*
2. S. De and P. K. Bhattacharya, "Prediction of mass transfer coefficient with suction in the application of reverse osmosis and ultrafiltration", submitted to *J. Membrane Sci.*
3. M. Syamal, S. De and P. K. Bhattacharya, "Phenol consumption by cetyl pyridinium chloride micelles in micellar enhanced ultrafiltration", submitted to *J. Membrane Sci.*
4. S. De and P. K. Bhattacharya, "Modeling of ultrafiltration process for a two component aqueous solution of low and high (gel-forming) molecular weight solutes", submitted to *AIChE J.*

Patent: Process for recovery of inorganic chemicals from kraft black liquor – Director IITK; P. K. Bhattacharya and S. De. Patent application number: 814/Del/95/1936 dated 3.5.1995.